Department of Chemical Engineering

Synthesis and Evaluation of Porous Composite Hydrogels for Tissue Engineering Applications

Chao Li

This thesis is presented for the Degree of
Doctor of Philosophy
of
Curtin University of Technology

Jan 2012

Declaration

To the best of my knowledge and belief this thesis contains no materials previously published by any other person except where due acknowledgement has been made.

This thesis contains no material which has been accepted for the award of any other degree or diploma in any university.

Signature : ……..

Date : 30 Jan 2012

Abstract

The purpose of this dissertation was to synthesize and evaluate porous poly(2-hydroxyethyl methacrylate) (PHEMA) and PHEMA composite hydrogels containing various concentrations of titanium dioxide (TiO_2) nanoparticles, silicon dioxide (SiO_2) nanoparticles, and multi-walled carbon nanotubes (CNTs) for tissue engineering applications. Eighteen PHEMA nanocomposite hydrogels and five control PHEMA hydrogels were prepared in varying concentrations of water (60-90 wt.%) via a free radical polymerization process. Four of these hydrogels were modified further with an OVICOLL® | CLEAR collagen, a mixture of type I and type III collagen, for the improvement of cell activities.

Gravimetric analysis and X-ray diffraction analysis, as well as scanning electron microscopy (SEM), were used to examine the presence of the nanoadditives contained in the hydrogel polymers. The presence of collagen also was confirmed using a Fourier transform infrared spectroscope, an ultraviolet-visible spectrophotometer and an SEM.

All hydrogels appeared opaque and exhibited various porous structures, which then were studied using a SEM. The porous structures were found to be dependent largely on the HEMA:water concentrations in the polymerisation mixtures. There was no significant difference in the porous structure for PHEMA and PHEMA composite hydrogels containing additives. The results from the polymer volume fraction study also indicated the porous structures of the resultant hydrogels.

The tensile properties of the hydrogels were examined using a SINTECH® 200/M material testing workstation. The viscoelastic properties of the hydrogels were investigated using a HAAKE MARS III Modular Advanced Rheometer System. The mechanical properties of the hydrogels, apparently, were affected by the presence of the porous structures. In general, higher tensile and elastic moduli were seen for hydrogels with less porous structures. In contrast, lower tensile and elastic moduli were seen for more porously structured hydrogels. The addition of TiO_2 particulates did not show significant influence on tensile and elastic moduli. However, the

addition of CNTs increased the viscoelastic moduli of PHEMA hydrogels, which can be attributed to their fibre characteristics. The hydrogels produced in this study have shown a great range of linear viscoelasticity and a quick recovery characteristic, dependent on the macroporous structures and the presence of the TiO_2 nanoadditives.

The delivery of a model molecule, methylene blue and three biomolecules, including prednisolone 21-hemisuccinate sodium salt, caffeine, and bovine serum albumin were carried out under static and dynamic conditions. Rheological stimulations were used for the dynamic conditions. The delivery of both single and dual molecules was investigated. It was found that increasing the frequency and the shear strain of the stimulations accelerated the relative biomolecule release under dynamic conditions. However, in comparison to the static conditions, the relative delivery of the biomolecules was slowed by the application of rheological stimulations, due to the reabsorption of the biomolecule into the hydrogel matrix under the dynamic conditions. The release profiles of the biomolecules were affected by the concentrations of the biomolecules and their molecular weights, as well as the porous structures of the hydrogels. When dual biomolecules were utilised in the system, the delivery profile of each of the biomolecules was the same as the single biomolecule delivery profile. The relative release also was dependent on the porous structures and the molecular weights.

The biomineralisation of the hydrogels was evaluated with a calcification study. The infiltration of the calcium phosphate was found to be more vigorous in a more porously structured hydrogel, and it was significantly enhanced after TiO_2 nanoparticles were incorporated. An assay indicated that PHEMA and its nanocomposite hydrogels were tolerated well by the NIH 3T3 fibroblast cells. However, the cell growth on both PHEMA and PHEMA composite hydrogels was relatively slow. The presence of collagen significantly increased numbers of viable cells on modified hydrogels in comparison to that seen on hydrogels containing no collagen molecules. This was true for two other types of cell, including green fluorescent protein-transfected 253 human melanoma cells and human mesenchymal stem cells.

In summary, porous PHEMA composite hydrogels make an excellent family of scaffolding materials for soft tissue regeneration. Their porous structures and mechanical properties can be tailor-made, simply by adjusting the chemical composition in the formulae to meet the requirements of specific applications. The bioactivities of the hydrogels also can be improved by tethering natural molecules without altering the porous structure or the mechanical properties. Biomolecules can be preloaded into the hydrogel matrices by a simple diffusion process at room temperature due to the presence of large pores. The preloaded concentrations and the subsequent delivery of these biomolecules can easily be adjusted by changing the concentrations of the stock solutions. This is highly desirable for an ideal tissue scaffold, which not only can provide interconnected pores and dictated mechanical properties, but also is capable of delivering essential signalling biomolecues for the tissue regeneration process. Therefore, these preliminary investigations of PHEMA and PHEMA composite hydrogels have demonstrated their great potential for tissue engineering applications.

Acknowledgements

I would like to thank my thesis advisor, A/Prof. Xia Lou, for her guidance, support and great patience. I am so deeply grateful for the opportunity to join her research group and conduct my PhD work under her supervision. Her vision and dedication to research have been truly inspirational. I also want to take this opportunity to thank all my dissertation committee members, including Prof. Moses Tadé and Prof. Roland De Marco.

Thanks also go to Prof. Ming Ang, the Head of Chemical Engineering, for his support and help.

I thank Dr Shaoqiong Liu and Ms Yan Li from the Institute of Bioengineering and Nanotechnology, Singapore, as well as Ms Bev Kinnear of the Molecular Immunology Group, Curtin University, for their kind help in carrying out the cellular activity assays of the collagen-modified hydrogels.

I would like to thank Prof. Choo-May Lai for allowing me to use the facilities and resources in the Department of Molecular Ophthalmology at the Lions Eye Institute (LEI). Assistance from Prof. Choo-May Lai and Ms Marisa De Pinho at LEI is appreciated very much.

Many thanks for those who provided great technical help during my laboratory work. These included Grant Cope, Kristy Blyth, Dr Peter Sheppard, Peter Chapman and Tomoko Radomirovic (Department of Chemistry, Curtin); Karen Hynes, Ann Cornell, Zero Zhang, (Department of Chemical Engineering, Curtin); Alain Delhaize (Department of Biomedical Sciences, Curtin), Angela Samec (Department of Pharmacy, Curtin); Elaine Miller, Dr Rob Hart (Discipline of Applied Physics, Curtin); Peter Duncan, Lyn Kirilak (Centre for Microscopy, Characterization and Analysis, The University of Western Australia).

The work of present and past members in the polymer research group is very much appreciated. Thanks go to Dr. Ailin Ding, Yenny, Yuli and Shuo for their friendship.

I would also like to thank undergraduate students completing projects within our group, including Elance, Yek Chuan, Tristan and Eric. I also appreciate the help I received from other PhD students including Monica and Thu Le in the Department of Chemical Engineering.

I would like to thank Dr. John Fielder for his great help in reading my thesis.

I would like to take the opportunity to say how much I appreciate my friends, including Binghui and Winie, Yun, Xiangpeng, Hongfei and Xiaomei, Yanqiang and Dr. Pengchao Si. I also want to thank friends from the Curtin Christian Union and Carmel Church. They brought great fun into my life while in Perth.

I want to acknowledge the Australian Research Council for a Discovery Project Grant (DP0557148), Curtin for its International Research Tuition Scholarship (CIRTS), and the Department of Chemical Engineering for financially supporting this project.

Finally, and most importantly, I would like to thank my parents, Guang-nian Li and Xue-ling Zhang for their love, support, encouragement and understanding. Thanks to my sister (Ya-ping Li), my bother in-law (Sheng-Li Zhang), my brother (Ming Li) and sister in-law (Qing Fang). Thanks to my lovely wife, Nina Wang, for her love and understanding. I also want to say thanks to many other relatives who have been supportive.

This thesis is dedicated to my loving parents.

Publications and Conference Presentations

Journal Publication

1. Li, C., Zheng, Y.F., Lou, X.. Enhanced calcification capacity of porous PHEMA by TiO_2 nanoparticulates, Journal of Materials Science: Materials in Medicine, 20: 2009, 2215–2222.

Full Conference Paper

2. **Li**, **C.,** Lai, C.M., De Pinho, M. and Lou, X.. Effect of TiO_2 nanoparticles on the calcification capacity of porous PHEMA hydrogels. 8th World Congress of Chemical Engineering. August 23-27, 2009. Montréal. Canada.

Conference Presentations

3. Li C., Liu, S. Q., Lou, X.. Collagen modified porous PHEMA hydrogels for tissue engineering applications. World Biomaterials Congress, 2012.
4. Li, C., Lai, C.M., De Pinho, M. and Lou, X.. Effect of TiO_2 nanoparticles on the calcification capacity of porous PHEMA hydrogels. 8th World Congress of Chemical Engineering. August 23-27, 2009. Montréal. Canada.
5. Li, C. and Lou, X.. Dynamic Mechanical Responses of PHEMA and PHEMA-TiO_2 Composite Hydrogels to the Change of Rheological Conditions. International Conference on Materials for Advanced Technologies (ICMAT) & The 2^{nd} Asian Biomaterials Congress, 25-27 June, 28 June-3 July, 2009, Singapore.
6. Lou, X., Li, C., Wang, S., Zheng, Y.F.. Preparation and Characterization of PHEMA-TiO_2 Composite Scaffolds for Bone Tissue Regeneration, 1st Asian Biomaterials Congress, 6-8 Dec, 2007, Tsukuba, Japan

Manuscripts in Preparation

7. Li, C. and Lou, X.. Dynamic Mechanical Responses of PHEMA and PHEMA-TiO_2 Composite Hydrogels to the Change of Rheological Conditions.
8. Li C., and Wang, S., Lou, X.. Delivery of Biomolecules from Porous Poly (2-hydroxyethyl methacrylate) Hydrogel under Static and Dynamic Conditions.
9. Li C., Liu, S. Q., Lou, X.. Cellular Activities of Porous Collagen-modified

Poly(2-hydroxyethyl methacrylate) (PHEMA) and PHEMA-TiO_2 Hydrogels for Tissue Engineering Application.

Contents

List of Figures

List of Tables

CHAPTER 1 INTRODUCTION

1.1. Background

Tissue Engineering is an interdisciplinary field that applies the principles of engineering and life sciences to the development of biological substitutes that restore, maintain or improve tissue function or, indeed, a whole organ (Langer and Vacanti 1993). It aims to improve treatments for tissue loss or end-stage organ failure and therefore enhances the quality of life of patients.

Tissue loss or end-stage organ failure, resulting from an injury or a disease, is a major health care problem. Every day, thousands of people of all ages are admitted to hospitals for these treatments. Estimates of the total U.S. health care costs for patients with tissue loss or end-stage organ failure exceed $400 billion annually (Langer and Vacanti 1993). These damaged or diseased human tissues or organs can be treated using donor transplants or with artificial prosthesis devices. Although these procedures have saved and improved many lives, both solutions are imperfect. There is a declining availability of donor organs and the gap continues to widen (Abouna 2001). Prosthetic replacements do not have the capacity to replicate the full function of an organ or specific tissues, and sometimes multiple operations are needed (Laurencin et al. 1999).

Tissue engineering has developed as an alternative therapy for the treatment of tissue loss or end-stage organ failure. Since the emergence of this field in the mid-1980s, tissue engineering has experienced a prodigious growth under the impetus of other principles such as cell biology and genetic engineering (Bianco and Robey 2001; Fuchs and Segre 2000; Muschler, Nakamoto, and Griffith 2004; Phillips, Gersbach, and Garcia 2007). So far, a broad range of engineered substitutes have been investigated and developed for such tissues as heart valve (Taylor, Cass, and Yacoub 2006; Simon et al. 2006; Fong et al. 2006), bladder (Pattison et al. 2005), liver (Davis and Vacanti 1996; Mayer et al. 2000), skin (Adekogbe and Ghanem 2005; Altman et al. 2003), vascular (Sarkar et al. 2006), and bone and cartilage (Hutmacher 2000, 2006; Kofron et al. 2003; Kose et al. 2003; Müller, Müller, et al. 2006).

Engineered skin replacement was one of the earlier breakthroughs of TransCyte®, a biosynthetic covering produced by Advanced Tissue Sciences Inc., approved by the Food and Drug Administration (FDA) in 1997 (Viola, Lal, and Grad 2003). Apart from success in engineering tissues, the first clinical trial of a tissue engineered organ, a bladder, was carried out by Atala and his team (Atala et al. 2006). Meanwhile, the rapid growth of replacements for such tissues as cartilage, bone, blood vessel and pancreas has reached the stage of either clinical use or approval (Place, Evans, and Stevens 2009).

Apart from the obvious benefits for human beings, tissue engineering also brings substantial financial rewards to those who succeed in translating this new technology to the clinic. In 2003, the European Commission estimated that there is a potential market range of 4 to 400 billion Euro per year for tissue engineering (Bock, Ibarreta, and Rodriguez-Cerezo 2003). According to a new report from Worldwide Markets and Emerging Technologies for Tissue Engineering and Regenerative Medicine, distributed exclusively by Life Science Intelligence, the largely untapped global market potential for tissue engineering and regenerative medicine products will exceed $118 billion by 2013 (Lichtenfeld 2010).

1.2. Tissue Engineering Approach

A tissue engineering approach involves several major steps in the curing process. Figure 1-1 illustrates a general tissue engineering procedure: (1) a small amount of ***cells*** are removed from patients; (2) the retrieved cells are screened for phenotype and their numbers are expanded; (3) cells are seeded onto a porous ***scaffold*** together with ***growth factors*** and cytokines; (4) the cell-seeded scaffold is *in intro* cultured for further increase of the cell numbers; and (5) the regenerated tissue is gained and, afterwards, implanted into the human body to replace the damaged tissues (George 2009). A clinical process in engineering a tissue does not include all these steps at all times. Whichever process is taken, cell sources, growth factors and tissue scaffolds are considered as the three most critical components in determining the success of the tissue engineering procedure (Place, Evans, and Stevens 2009).

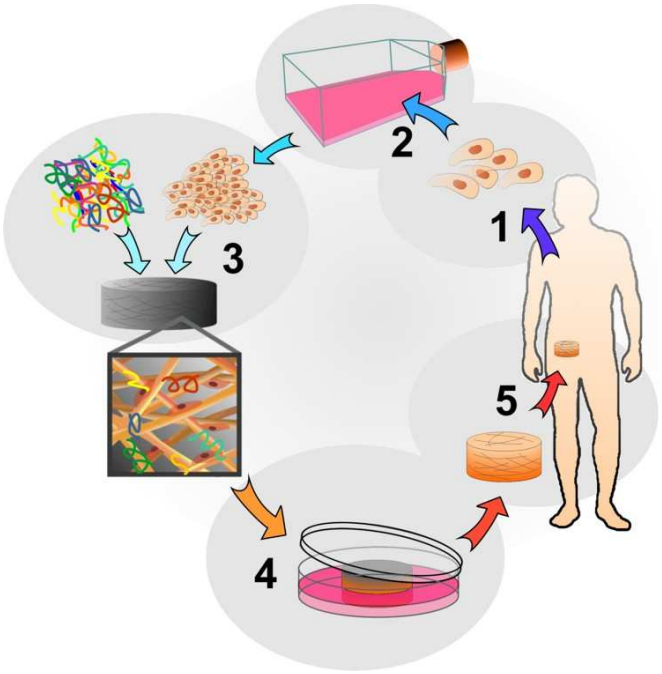

Figure 1-1 A general tissue engineering procedure (George 2009)

Cells used in tissue engineering include autologous cells (from the patient), allogenic cells (from a human donor) and xenogenic cells (from a non-human donor), named according to their sources (Heath 2000). The advantage of using autologous cells is that they produce a lower immune response after implantation, but the retrieval of these cells can be restricted by the patient's genetic disease or donor-site morbidity. Allogenic cells are relatively easier to obtain and, so far, they have been utilized in many commercial products for engineering tissues (Place, Evans, and Stevens 2009). The use of xenogenic cells in tissue engineering is controversial due to the potential of transmitting unhealthy pathogens to human beings (Griffith and Naughton 2002). Stem and progenitor cells can serve as an alternative source of cells from which the desired tissue can be derived (Heath 2000; Stappenbeck and Miyoshi 2009; Pittenger et al. 1999).

Growth factors are generally required to promote tissue regeneration, as they can induce angiogenesis, which supplies oxygen and nutrients to cells transplanted for organ substitution to maintain their biological functions (Tabata 2003). This is to say that growth factors act as signalling molecules to stimulate cell proliferation,

migration, differentiation and local tissue formation (Ma 2004). Growth factors are made of polypeptides, exhibiting molecular weights in the range of 15 kDa to 45 kDa (Salvay and Shea 2006). They can be found either as matrix bound proteins attached to the extracellular matrix (ECM) or as soluble molecules secreted by cells, or cleaved from the matrix by certain enzymes or proteases (Tayalia and Mooney 2009).

Various growth factors are available for engineering different sorts of tissue (Chen, Zhang, and Wu 2010). It should be noted that different cell types can produce the same type of growth factor, which can conversely act on these cell types with the same effect (McIntosh, Bellus, and Jab 2000). For example, epidermal growth factor, a potent mitogen for epithelial cells, is the most widely used growth factor for skin regeneration (Niall, Ryan, and O'Brien 1982). Such a growth factor also has the functionality of enhancing proliferation of mesechymal, glial and fibroblast cells (Tayalia and Mooney 2009).

The action of growth factors is typically concentration dependent. The concentration gradients of growth factors play a major role in tissue regeneration (Tayalia and Mooney 2009; Biondi et al. 2008; Gurdon and Bourillot 2001). Normally, growth factors can elicit cellular activities at a very low concentration of 10^{-9}~10^{-11}M (Gurdon and Bourillot 2001). The concentration gradients of growth factors provide a mechanism by which cells can obtain spatial and directional cues. So far, the magnitudes of the gradients to elicit the desired cellular activities are unknown (Biondi et al. 2008). The presence of growth factors plays a crucial role in the process of tissue regeneration, which depends not only on the growth factors themselves, but also on many other factors. These factors include concentration, spatial/temporal distribution, and a combination of different growth factors. In addition, growth factors have short half-lives (of the order of minutes to hours) and are rapidly degraded or cleared, thereby minimizing their biological effect (Salvay and Shea 2006). Thus, delivery systems using tissue scaffolds have been developed for administering the proper amounts of growth factors to enable regeneration. Discussion of these delivery systems can be found in Section 1.3.

Tissue scaffolds function as a reservoir to provide support for cells to adhere, migrate, proliferate and differentiate, as well as for diffusion of nutrients and growth factors

(Ma 2004). Design of a scaffold exhibiting the proper physical properties, mechanical properties, surface properties, mass transport properties and biological properties plays a prodigious role, as it affects the formation and ultimate function of the formed tissues (Drury and Mooney 2003). A few essential requirements must be considered when a tissue scaffold is constructed. Firstly, the scaffolding materials should be biocompatible, which means they should be non-immunogenic and non-toxic to the cells. Secondly, the scaffold must contain appropriate pore sizes for cell migration and nutrient transport, as well as waste removal (Cheung et al. 2007). Thirdly, the scaffold should have proper physical surface properties, including surface area, surface topography, roughness and chemical properties, including surface charge and suitable biofunctionalities. Fourthly, the scaffold must have the required mechanical integrity to maintain the predesigned tissue structure. Lastly, construction and the following sterilization procedure should be performed easily and economically.

1.3. Tissue Scaffolds and Design Parameters

A tissue scaffold should meet certain design parameters to be functional for tissue regeneration, regardless of whether the scaffolding material is from natural or synthetic resources. These parameters include biocompatibility, pore structures, surface properties, mechanical properties and transportation of biomolecules. There is detailed discussion of these parameters in the following section.

Biocompatibility

Biocompatibility is the most important consideration for designing a tissue scaffold. Williams (Williams 2008) describes biocompatibility for a tissue scaffold as follows: “The biocompatibility of a scaffold or matrix for a tissue engineering product refers to the ability to perform as substrate that will support the appropriate cellular activity, including the facilitation of molecular and mechanical signalling systems, in order to optimise tissue regeneration, without eliciting an undesirable local or systemic responses in the eventual host”. That is to say, the scaffold should not have, or have very limited, immunological toxicity throughout the healing and cellular regeneration process.

The toxic response of a polymer scaffold can be caused by the toxic chemicals, which are used in the production of the scaffold. These residual chemicals (initiators, organic solvents, stabilizers, emulsifiers, and crosslinkers) in the scaffold can be toxic to host cells (Gan, Zhang, and Guan 2009). In addition, degradation products from biodegradable scaffolds, such as poly(lactic acid) (PLA), poly(glycol acid) (PGA) and poly(lactic acid-co-glycol acid) (PLGA), could also cause toxic effects, depending on the site of implantation and the rate of degradation (Taylor et al. 1994; Ignatius and Claes 1996; Matsusue et al. 1992).

Interconnected pore structure

A tissue scaffold should have an interconnected pore structure with adequate pore sizes for cell accommodation and migration, as well as transportation of nutrients and metabolic waste (Jen, Wake, and Mikos 1996). If the pores are too small, cell migration will be very limited, resulting in the formation of a cellular capsule around the edges of the scaffold. This in turn can limit diffusion of nutrients and removal of waste resulting in necrotic regions within the construct. Conversely, if the pores are too large, there is a decrease in surface area, limiting cell adhesion (Yannas 1992). Therefore, an optimal pore size should be ensured, and this size varies from type to type according to the envisioned applications. It is suggested that a pore size of 5 µm is required for neovascularisation, 5-15 µm for fibroblast ingrowth, 20 µm for the ingrowth of hepatocytes, 20-125 µm for regeneration of adult mammalian skin, 40-100 µm for osteoid ingrowth, and 100-350 µm for regeneration of bone (Tambralli et al. 2009; Coutu, Yousefi, and Galipeau 2009). A recent work by Linnes et al. demonstrated that pores of 35 µm in diameter are ideal for soft tissue regeneration when compared to 20 and 70 µm pores (Linnes, Ratner, and Giachelli 2007). Interconnectivity of pores is also a critical factor influencing transport properties and cell transport and migration (Moore et al. 2004; Martys, Torquato, and Bentz 1994).

Mechanical properties

Controlling the mechanical properties of a scaffold is important in tissue regeneration. In general, the mechanical properties of the scaffold are dictated by the tissue into which it is implanted. Thus, the mechanical properties of the scaffold must be sufficient to withstand the patient's normal activities without collapse. A stiff

scaffold usually is needed for hard tissues, such as bone, whereas a flexible tissue scaffold is demanded in engineering elastomeric tissues, such as skin, cartilage and blood vessels. However, in designing the proper mechanical properties of the scaffold, it is not as simple as matching a single parameter such as modulus or strength, because most tissues possess complex viscoelastic, non-linear and anisotropic mechanical properties that also vary with age, site and other factors (Butler, Goldstein, and Guilak 2000).

The mechanical properties also affect the cellular activities in the scaffold. The extent of their influence is similar to that seen for chemical properties (Dado and Levenberg 2009; Mitragotri and Lahann 2009; Engler et al. 2006; Ghosh and Ingber 2007). As such, a tissue scaffold has to be designed with tissue specific mechanical properties.

Surface properties

Physical and chemical properties of a tissue scaffold play an important role in determining the cellular response to the scaffold. It is known that protein adhesion is the first event occurring on the surface of a foreign body in a biological environment. The adsorbed proteins then determine which cells respond to the material surfaces (Wilson et al. 2005). Therefore, surface parameters often are identified to relate to the protein adhesion. These include surface wettablity, surface topography, surface charge and the presence of sell-recognizable ligands.

(a) Surface wettability: The hydrophilic nature of the surface has a strong influence on protein adsorption and cell adhesion. In general, cells can effectively adhere onto polymer surfaces presenting moderate wettability with water contact angles of 40–70° (Arima and Iwata 2007). In regard to the scaffolding materials, most metals, alloys and bioceramics appear to be more or less hydrophilic (Takebe et al. 2000; Ponsonnet et al. 2003; Hallab et al. 2001), while many polymers, particular synthetic polymers, are hydrophobic in their natural state (Liu and Ma 2004).

(b) Surface topography: Cells respond to environmental features at all length scales from the macro down to the molecular (Stevens and George 2005). This is true for

the natural environment, in which ECM provides instructive cues at levels ranging from meso- and micro- through to nano-scales to maintain cell phenotype and behaviour (Ranella et al. 2010). Although the mechanism of how cells detect and respond to these nanofeatures is not yet understood (Curtis 2004), it has been proved that increasing the nanoscale roughness of the scaffold pore walls can enhance the cellular activities, including cell attachment, proliferation and expression, of matrix components (Pattison et al. 2005).

(c) Surface charge: The surface charge of a tissue scaffold has a significant influence on cell adhesion, which shows distinct differences for the positively and negatively charged surfaces of the scaffold. In general, cells are prone to adhering closely to positively charged surfaces, whereas contact occurs only at individual points on near-neutral and negatively charged surfaces, attributable to the negative charge of cell membranes (Dames et al. 1986; Shelton, Rasmussen, and Davies 1988). Thus, research has been carried out to modify the surface charge of the scaffolding materials in order to improve their interactions with cells (Choi et al. 2008; Tong and Wang 2011).

(d) Cell-recognizable ligand: Many biomacromolecules have been used to modify the surfaces of tissue scaffolds for the purpose of improving cellular activities. These biomacromolecules include collagen, gelatin, heparin, hyaluronic acid, short peptide sequences originating from cell adhesive proteins such as the Arg–Gly–Asp (RGD) or Tyr-Ile-Gly-Ser-Arg (YIGSR), and sugar moieties such as galactose or lactose (Hersel, Dahmen, and Kessler 2003; Lutolf and Hubbell 2005). Among these biomolecules, collagen has been one of the key macromolecules because of its inherent cell adhesion properties (Heinemann et al. 2008; Ma et al. 2002). More details can be found in Section1.5.3.

Transportation of molecules

The transportation of various molecules is involved in a tissue regeneration process. These molecules include growth factors, nutrients, oxygen and waste during the tissue formation process (Valentin et al. 2009; Malda et al. 2004; Malafaya et al. 2002; Biondi et al. 2008; Chen, Zhang, and Wu 2010).

There are many ways to control the supply of these molecules. For instance, growth factors simply can be added to the culture medium for in vitro tissue formation. However, controlling the distribution of the growth factors in the desired sites by time and space generally has been unsuccessful, and this has led to an explosion of work to develop growth factor delivery strategies (Quaglia 2008; Biondi et al. 2008). These strategies can be categorized into three different types: direct loading of growth factors into the scaffold matrix, addition of separate release systems to the scaffolds, and surface tethering to tissue scaffolds (Tessmar and Göpferich 2007).

The first type of delivery system is the most commonly used. In this type, growth factors can be loaded in an interspersed way and released from the scaffold after implantation. The delivery of growth factors mainly is controlled by diffusion and the physical properties of the scaffold. These parameters include pore structure, crosslinking density and the degradation rate of the scaffold. However, this delivery system can be detrimental to the stability of the growth factors and sometimes is ineffective. For example, significant amounts of growth factor might already have been eluted from the scaffold during the manufacturing process. This can happen when water is used to remove water-soluble porogens from the scaffolds. In addition, the biological activity of the useful molecules cannot always be guaranteed when special conditions such as high temperatures are used to generate the scaffolds, as seen by the melt-processing method (Tessmar and Göpferich 2007).

The growth factors also can be incorporated into microsphere carriers, which are normally developed from polymer materials (Tabata 2000). These microspheres can be formed into a tissue engineering scaffold (Nof and Shea 2002) or incorporated into a tissue scaffold, forming a composite scaffold (Ennett, Kaigler, and Mooney 2006). As such, the polymer carriers can protect the growth factors from proteolysis and delay the release process, allowing for a prolonged bioactivity *in vivo* (Malafaya et al. 2002). In addition, the release rate of the growth factors from these microspheres can be adjusted by altering the polymer used, the amount of growth factors loaded and the size of the microspheres (Mahoney and Saltzman 1996). Meanwhile, these microspheres can be modified to deliver multiple growth factors, each with distinct release profiles (Sinha and Trehan 2003).

Growth factors also can be attached covalently to the surfaces of tissue scaffolds, ideally after the completion of the scaffold construction. This covalent attachment is most commonly applied to hydrogel carriers or scaffolds with sufficient spacer groups (Tessmar and Göpferich 2007). Results have shown that covalently attached growth factors are capable of stimulating cell proliferation and retain their biological activity (Mann, Schmedlen, and West 2001; Kuhl and Griffith-Cima 1996) (Eun et al. 1998).

Several issues should be considered when growth factors are incorporated into the scaffolds. These include: (1) the loading capacity; (2) the distribution of growth factor; (3) the interactions between the growth factors and the delivery system; (4) the release kinetics; (5) the long-term stability; and (6) the economical viability (Silva et al. 2009; Zisch, Lutolf, and Hubbell 2003).

Other properties

Good processability of a tissue scaffold is required because a particular configurational shape is of importance in maintaining the functions of the scaffold (Yang, Roach, et al. 2001). This preferred configuration should be constructed easily when the scaffolding materials are employed. Amongst the various scaffolding materials, synthetic polymers have drawn considerable attention due to their excellent . Sterilization is another important issue concerning the clinical applications of a tissue scaffold (Andrews, Hunt, and Black 2007). An optimal tissue scaffold should be able to withstand the normal sterilisation conditions with minimum damage to the delicate 3D geometry and the natural characteristics of the materials (Holy et al. 2001).

1.4. Materials for Tissue Scaffold Fabrication

Various materials have been employed for tissue scaffold fabrication. These include metals and alloys, bioceramics, polymers and combinations of these materials. In general, metal, ceramics and some strong polymers are used for hard tissue regeneration, due to their high mechanical properties. In most cases, polymers are used as scaffolding materials for the regeneration of soft tissue, such as skin or

cartilage. The advantages and disadvantages of these materials are summarised briefly in the following sections.

1.4.1. Metals

Metals have been used extensively in orthopaedic tissue replacements. These materials include titanium based alloys, cobalt based alloys, stainless steel (316L), and magnesium based alloys (Dekker et al. 2005; Frosch et al. 2003; Lopez-Heredia et al. 2008; Murugan and Ramakrishna 2005; Witte et al. 2006). Metallic implants also are used in non-orthopaedic applications, such as oral and maxillofacial surgery (i.e. dental implants, craniofacial plates and screws) and cardiovascular surgery (i.e. pacemakers, artificial heart components, catheters, clips, stents and valve replacements) (Ratner et al. 2004).

An advantage of metal implants is their excellent mechanical properties, which make them the most widely applied implant material for bone grafts. These kinds of implant are used mostly in load-bearing sites. However, metal materials have an elastic modulus significantly higher than that of bone tissue (Murugan and Ramakrishna 2005). This mechanical incompatibility causes implants to be structurally stiffer than bones, which may result in stress-shielding, and eventual implant loosening and bone resorption (Spoerke et al. 2005). In addition, metallic wear debris and metal ions that are released *in vivo* from the metal implants have been found in many tissues, including the liver, spleen, lung, and even remote bone marrow of the iliac crest. The presence of these ions in tissues raises questions of biocompatibility and the possible carcinogenic effects of these implants. Moreover, the processability of metallic implants is very limited in comparison with other materials (Yang, Leong, et al. 2001).

1.4.2. Bioceramics and Bioglasses

It was first proposed for ceramics to be used in orthopaedics during the 1960s, due to their high compressive strength and hardness properties. Various bioceramics, including hydroxyapatite (HA), tricalcium phosphate (TCP), and octacalcium phosphate (OCP), have been studied as scaffolding materials for bone regeneration. Other kinds of bioinert ceramic, including $CaSiO_3$, and ZrO_2, were also investigated for tissue regeneration applications (Ni, Chang, and Chou 2006). Among these

bioceramics, HA is the most commonly used because its composition is similar to bone minerals (Karageorgiou and Kaplan 2005). In addition, HA is able to stimulate osteoconduction and further integrate into the bone without provoking an immune reaction (Ducheyne and Qiu 1999). Bioglasses are another series of ceramic materials, and the most commonly used bioglass is 45S5, consisting of 45% SiO_2, 24.5% Na_2O, 25.4% CaO and 5% P_2O_5 (Chen, Thompson, and Boccaccini 2006). Meanwhile, different compositions of bioglass also have been investigated (Jones, Ehrenfried, and Hench 2006; Jones et al. 2007).

The overall advantages of using bioceramic and bioglass materials include their excellent biocompatibility, osteoconductivity and osteoproductivity (Hench 1997). In addition, these materials do not induce local or systemic toxicity, inflammation or a foreign body response (Murugan and Ramakrishna 2005). However, scaffolds fabricated from these inorganic materials often are difficult to process into highly porous structures and are mechanically brittle (Ma 2004).

1.4.3. Polymers

Both natural and synthetic polymers have been evaluated for tissue engineering applications. Natural polymers, including proteinic polymers (collagen, gelatin, fibrin and silk fibroin) and polysaccharides (chitosan-based polymers, cellulose, alginate and glycosaminoglycans), demonstrate adequate biocompatibility. Therefore, utilization of these materials may avoid the stimulation of chronic inflammation or immunological reactions owing to their similarity to the ECM (Mano et al. 2007). Another important advantage is that some natural polymers are capable of enhancing cellular activities (Hsu et al. 2004). Mechanically, these polymers can be adjusted to be similar to the macromolecular–based tissues (soft tissues) in the human body. However, naturally derived materials provide limited versatility in designing specific properties, such as mechanical strength and degradation time. In addition, batch variations and sterilization methods are major limitations for naturally derived materials (Lee and Mooney 2001).

Synthetic polymers are a series of manufactured polymers which have been extensively used in our daily lives. Commonly used synthetic polymers in tissue

engineering include PLA, PGA, PLGA, polypropylene fumarate, poly(ethylene glycol), poly(vinylacohol), poly(acrylic acid), poly(2-hydroxyethyl methacrylate), and polycaprolactone (Rezwan et al. 2006; Place et al. 2009). The advantages of using synthetic polymers in tissue engineering include their ease of chemical synthesis on a large scale. Thus, good processability can be ensured. Synthetic polymers have better resistance to high temperature and pressure conditions than naturally derived polymers. Moreover, many synthetic polymers, such as PLGA, have gained approval from the FDA for their applications in tissue engineering, which has motivated the application of synthetic polymers in the tissue engineering area. However, a scaffold made of synthetic polymers tends to have limited bioactivity and to provide minimal biological cues to guide tissue regeneration. As such, cells do not necessarily recognize the surface of the synthetic polymers.

1.4.4. Composite Materials

For the reason that no materials can meet all essential requirements for tissue engineering applications, composite scaffolding materials have been developed, and these materials combine the properties of both the matrix materials and the reinforcement agents. The latter are used to improve the performance of the scaffold mechanically and/or biologically. The property of a composite material is dependent not only on the matrix and reinforcement materials, but also on the type, size and size distribution of the reinforcements. The volume percentages, as well as the bioactivity of the reinforcement, also are critical to the ultimate performance of the composite. Various particulates, including titanium dioxide (TiO_2), multi-walled carbon nanotubes (CNTs), silicon dioxide (SiO_2), HA, TCP and bioglass, are commonly used as bioactive reinforcing phases, while metals and polymers have been used as the matrix materials, in composite scaffolding materials (Rich et al. 2002; Liu, Slamovich, and Webster 2006; Gerhardt, Jell, and Boccaccini 2007; Torres et al. 2007; Francis et al. 2010; Madhumathi et al. 2009; Kim et al. 2006; Cabañas et al. 2009; Cao and Kuboyama 2010; Weinand et al. 2006)

1.5. Design of Thesis Work

This project aims to synthesize and evaluate porous PHEMA and PHEMA composite hydrogels for tissue engineering applications. Porous PHEMA hydrogels will be used as a matrix scaffolding material. Various additives will be used to improve the

mechanical and biological properties of the hydrogels. These include TiO_2, SiO_2, CNTs and collagen molecules.

1.5.1. Hydrogels and PHEMA

1.5.1.1. Hydrogels and the macroporous structure

Hydrogels are polymeric materials, which are capable of sustaining their three-dimensional structure after absorbing large quantities of water or biological fluids into their structure (Wichterle and Lim 1960). The presence of hydrophilic groups such as -OH, -CONH, $-CONH_2$, -COOH and $-SO_3H_3$, enable them to absorb plenty of water (Peppas and Khare 1993). The three-dimensional (3D) structure of the hydrogels is generally crosslinked through junctions or tie points, among which strong chemical linkages (covalent and ionic bonds), permanent or temporary physical entanglements, microcrystallite and weak interactions (hydrogen bonds) can be formed. In addition, due to their thermodynamic compatibility with water, these materials are soft and elastic (Brandon et al. 2009). Therefore, under mechanical stress, hydrogels can exhibit a range of responses from rapid or elastic recovery to a time-dependent recovery, making the physical properties of hydrogels similar to that of living tissue.

Hydrogels can be classified into different groups based on numerous factors, such as their source (natural or synthetic), their nature of crosslinking (chemical or physical gels), the nature of the network (homopolymer, copolymer, interpenetrating or double networks), the presence of pores (homogeneous-optically transparent or heterogeneous-optically opaque), and their biodegradability (degradable or non-degradable hydrogels) (Kopeek and Yang 2007).

Due to their unique properties, hydrogel polymers have been considered as a class of promising scaffold materials. These properties include: (1) structural similarity to ECM of many tissues in human body; (2) capacity to be processed under relatively mild conditions; (3) capability of aqueous environment to protect cells and fragile drugs (peptides, proteins, oligonuleotides and DNA); (4) advantages of delivering biomolecules in tissue engineering; (5) provision of good transport of nutrients to

cells and products from cells; and (6) ease of modification with cell adhesive ligands (Drury and Mooney 2003).

Over the past two decades, various methods have been used to produce macroporous hydrogels. These include the freeze–thaw procedure (Plieva, Galaev, and Mattiasson 2007), porogenation (Kroupová et al. 2006), microemulsion formation (Bennett et al. 1995), fibre bonding (Mikos et al. 1993), gas foaming (Kim and Mooney 1998), and electrospinning (Sill and von Recum 2008).

Macroporous structures in hydrogel networks also may form as a result of a free-radical, crosslinking copolymerization in the presence of an inert diluent, which involves the appearance of a phase separation during the polymerization process (Seidl et al. 1967; Guyot and Bartholin 1982; Okay 2000). In the progress of polymerisation, there is a stage at which polymer chains cannot absorb all the available solvent in the reaction mixture. Microspheres of polymer chains then can be formed within the separated continuous liquid phase. As the reaction further proceeds, new microspheres are generated continuously, due to the successive separations of the growing polymers. The agglomeration of the microspheres results in the formation of a heterogeneous gel that is surrounded by interconnected channels. The channels were occupied, previously, by the diluent. Thus, the reaction system consists of two continuous phases: a gel phase and a diluent phase (Figure 1-2).

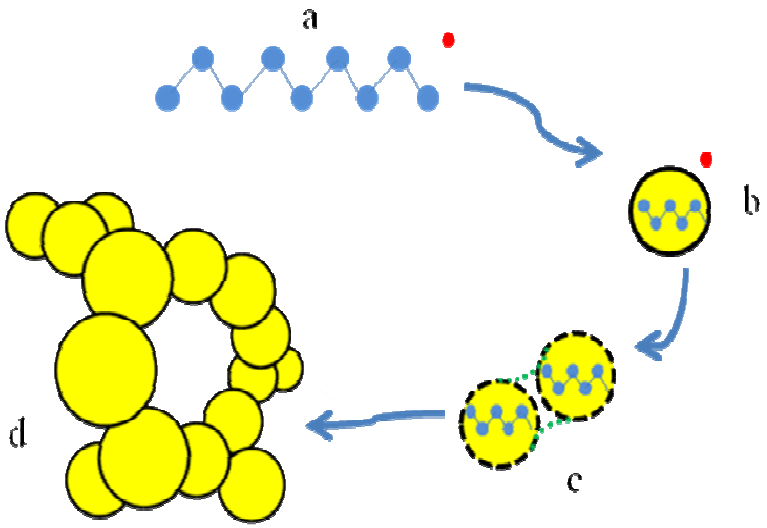

Figure 1-2 Schematic representation of the occurrence of a phase separation

(a) A growing polymer chain with free radical at one end, (b) the formation of polymer microsphere, (c) agglomeration of polymer microspheres, (d) further agglomeration leading to the separation of polymers spheres from the diluent phase

This scenario is a simplified description of a much more complex process, which involves macrosyneresis and microsyneresis processes, depending on the synthetic parameters (Seidl et al. 1967; Dusek 1971). Figure 1-3 schematically represents the mechanism of macrosyneresis and microsyneresis. Macrosyneresis relates to the deswelling of the growing network when phase separation occurs. The deswelling of the network undergoing crosslinking is transformed, progressively, into a suspension of polymer spherical particles dispersed in a liquid phase, consisting of unreacted monomer and solvent. Finally, two continuous phases co-exist and one of them is formed by loosely connected polymer spherical particles and the other by solvent. Conversely, microsyneresis relates to the segregation of solvent inside the growing network, followed by the formation of dispersed domains within the polymer matrix. When a small amount of solvent is used, pores are not interconnected. Microsyneresis can yield an interconnected pore structure for moderate amounts of solvent contents.

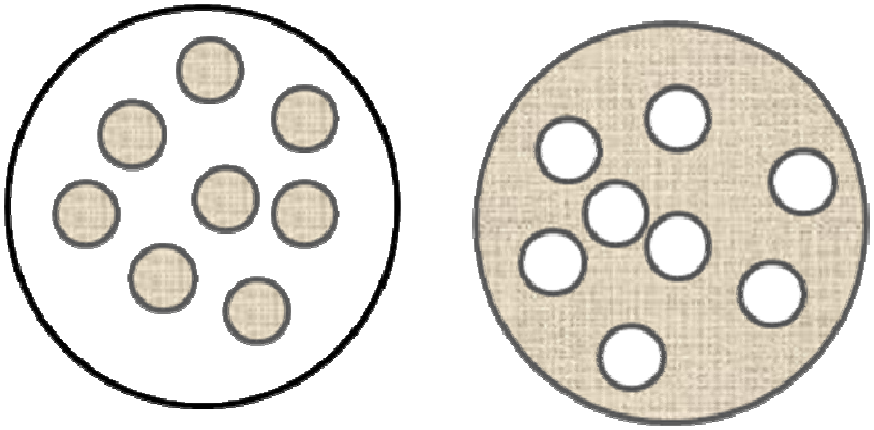

Macrosyneresis Microsyneresis

White-colored area: Liquid phase

Brown-colored area: Gel phase

Figure 1-3 Schematic representation of macrosyneresis and microsyneresis during crosslinking polymerization

Therefore, the polymerization of a polymer network in a given solvent yields a pore architecture corresponding to *macrosyneresis* (spherical, interconnected polymer particles) or *microsyneresis* (dispersed or interconnected pores in a continuous polymer matrix), depending on the solvent. It is possible to transit from *microsyneresis* to *macrosyneresis* when solvent content is beyond a certain amount.

1.5.1.2. Macroporous PHEMA Hydrogels

PHEMA is an abbreviation of poly(2-hydoxyethyl methacrylates) which is made of crosslinked polymers of 2-hydroxyethyl methacrylate (HEMA). PHEMA is well-known for its applications in vision correction devices including contact lenses and intraocular lenses (Chirila et al. 1998; Hicks et al. 2006). It swells in water without dissolution, therefore it is also termed hydrogel. Due to its successful applications for medical devices, PHEMA hydrogel has been proved to be well-tolerated by human tissues. However, these applications involve the utilisation of nonporous PHEMA hydrogels (Chirila et al. 1998; Hicks et al. 2002; Hicks et al. 1997; Hicks et al. 2006). The focus of this study is on macroporous PHEMA that could be used for other tissue engineering applications.

Macroporous PHEMA hydrogels can be manufactured via a series of methods such as bulk polymerization/porogen leaching (Stancu et al. 2007; Liu et al. 2000), fibre templating (Flynn, Dalton, and Shoichet 2003), a cryogenic technique (Savina et al.

2007), and solution polymerization (Chirila, Chen, et al. 1993; Lou, Dalton, and Chirila 2000; Lou et al. 1999; Lou et al. 2005; Lou, Wang, and Tan 2007). Among these methods, free radical polymerisation of HEMA in the presence of an initiator, a crosslinking agent and a diluent, most commonly water, is probably most convenient and cost effective. The pores and the pore structure can be altered simply by changing the monomer to diluents ratio, or initiator and crosslinking concentrations (Chirila, Chen, et al. 1993). The free radical initiators used in PHEMA polymerisation are ammonium persulphate (APS) and N,N,N',N'-tetramethylethylene diamine (TEMED). The chemical structures of the monomer and additives are shown in Table 1-1. APS, firstly, is decomposed into free radicals and this decomposition process is accelerated by TEMED. Thus, the APS molecule is left with an unpaired electron that, in turn, activates a HEMA molecule (Figure 1-4). This activated HEMA molecule can attach itself onto another HEMA molecule, thereby transferring the active unpaired electron. This continuous transferring of active unpaired electrons results in the formation of living HEMA oligomers (Figure 1-4). The chain reaction occurs until the HEMA molecule supply is exhausted (Figure 1-4). When a crosslinking agent, DVG, is added to the polymerising reaction, it links the PHEMA chains together and forms the insoluble network (Figure 1-5). Both ethyleneglycol dimethacrylate (EDMA) and 1,5-hexadiene-3,4-diol (DVG) are commonly used crosslinking agents for the preparation of macroporous PHEMA hydrogels (Clayton, Chirila, and Lou 1997).

Owing to chemical similarity, growing chains of PHEMA are very soluble within the precursor HEMA monomer. The solubility of the PHEMA chains is, however, relatively poor in water, which is used as the diluent in the present study. The previous studies confirmed that, when the water concentration is below 40-50 wt%, non-porous and transparent PHEMA form (Chirila, Constable, et al. 1993). When the water concentration is above the critical value, unfavourable thermodynamic interactions between water and the polymer network result in phase separation, which has been discussed in the previous section. Droplets of the PHEMA material effectively precipitate out of the solution, and continue to react with remaining monomers and oligomers. The droplets also join together and eventually become fixed in an interconnecting network of spherical polymer particles surrounded by

continuous channels occupied by water, which is the macroporous PHEMA hydrogels (Chirila, Constable, et al. 1993).

The channels between the droplets form interconnected pores, typically in the size range of 2-30 μm. The result is a highly heterogeneous, opaque material, with characteristics colloquially described as ‘spongy’. The term ‘phase separation sponge’ has been proposed to describe such materials as they adopt spongy characteristics exclusively due to phase separation processes (Chirila et al. 1993a). In this study, the opaque heterogeneous sponge materials will be referred to simply as the macroporous PHEMA hydrogels.

Table 1-1 Chemicals and their structures for PHEMA hydrogel preparation

Chemical name	Chemical structure
HEMA	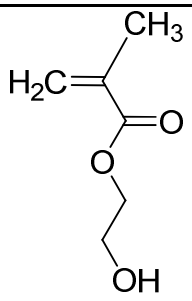
EDMA	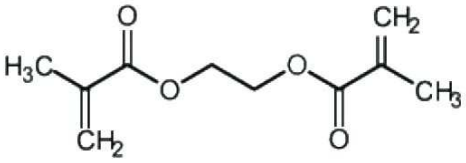
DVG	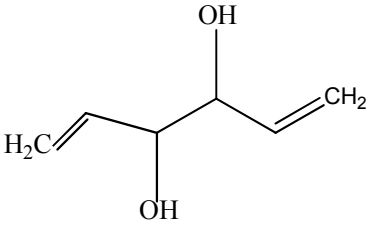
TEMED	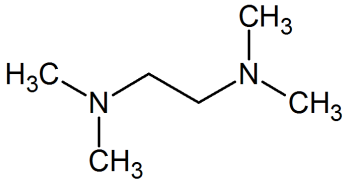

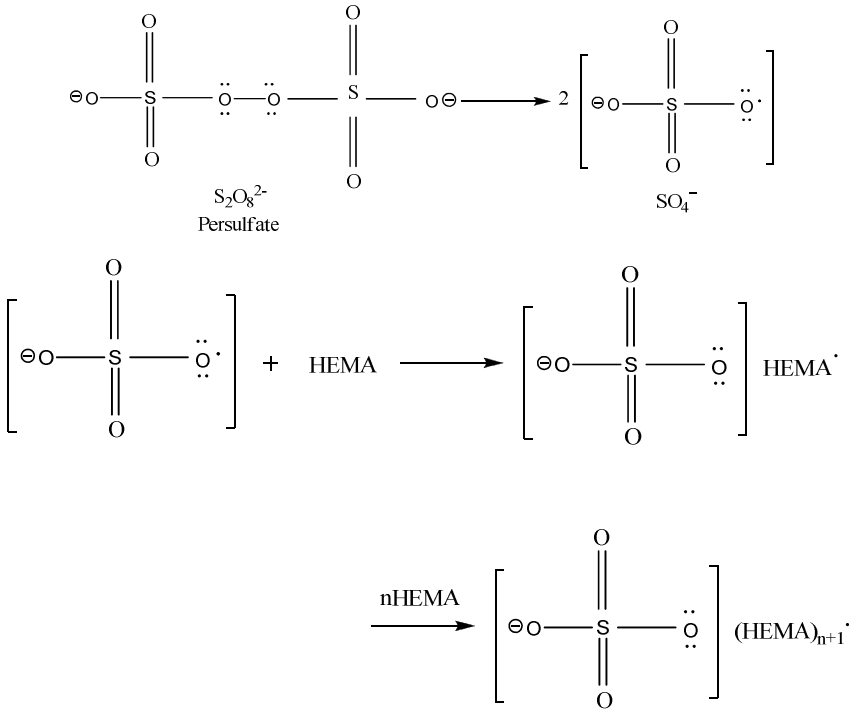

Figure 1-4 The mechanism of radical generation in the APS initiator system and the formation of oligmors of PHEMA

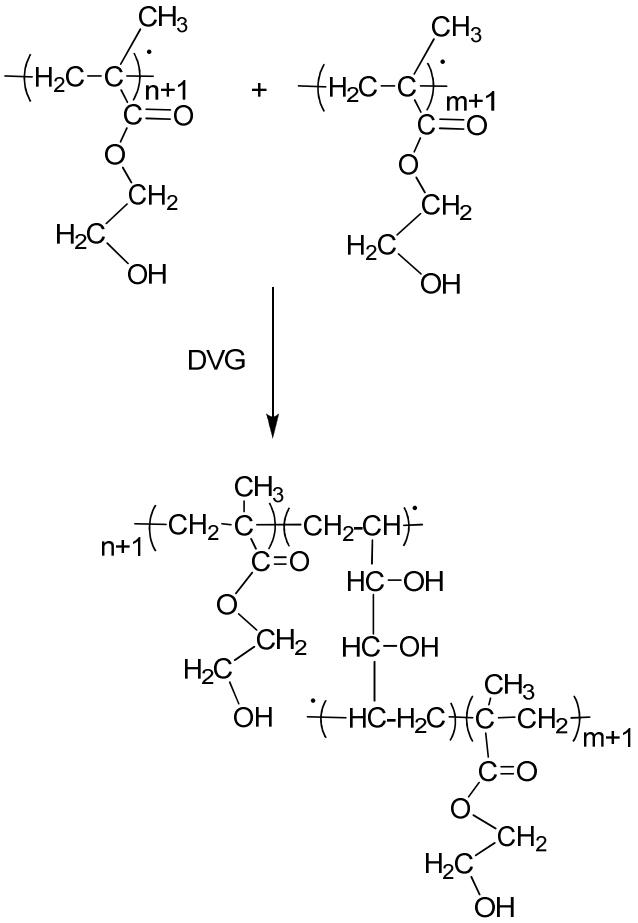

Figure 1-5 Synthetic scheme of PHEMA hydrogel using DVG as a crosslinking agent

Macroporous PHEMA hydrogels are able to encourage cell and tissue integration and have demonstrated excellent performance in a few applications such as ophthalmic implants (Crawford et al. 2002; Hicks et al. 2006; Chirila et al. 1998). They also have shown potential in applications as drug delivery systems (Lou, Munro, and Wang 2004; Lou, Wang, and Tan 2007; Wang et al. 2010). Detailed discussion on the applications of PHEMA hydrogels is undertaken in the following paragraphs.

1.5.1.3. Applications of Porous PHEMA Hydrogels

As mentioned above, successful applications of PHEMA hydrogels have been shown in contact lens and intraocular lens manufacturing (Hicks et al. 1999; Hicks et al. 2002). PHEMA hydrogels in these applications are made of nonporous structures. The use of porous PHEMA hydrogels has attracted some attention in recent years.

The application of porous PHEMA hydrogel is demonstrated in the development of an artificial cornea, AlphaCor^{TM} and an ocular socket prosthesis, in which porous PHEMA acted as a scaffold component to host the tissue in-growth to the implants so as to prevent extrusion of the devices (Chirila et al. 1998; Hicks et al. 2006).

Apart from their applications in vision correction devices, PHEMA hydrogels also have been investigated for controlled drug delivery. In general, non-porous PHEMA hydrogels are used for the diffusion of low molecular weight solutes in dense hydrogels. However, the nonporous nature of this type of hydrogel has limitations for applications such as a delivery system for biomolecules with large molecule weights. Results from our research group have shown that macroporous PHEMA hydrogels represent significant advances over the non-porous PHEMA hydrogels (Wang et al. 2010). A much higher drug loading capacity easily can be reached for macroporous PHEMA hydrogel due to the large pore volume and free space in the scaffold (Lou, Munro, and Wang 2004; Lou, Wang, and Tan 2007), whilst the release of prednisolone 21 hemisuccinate sodium salt (a small molecular weight anti-inflammatory drug) from the porous PHEMA is comparable to that from the less porous PHEMA hydrogel (Wang et al. 2010). Meanwhile, the loading of drugs can be achieved in ambient conditions through very simple means with less concern about the drug's stability (Wang et al. 2010). Moreover, macroporous PHEMA hydrogels also are suitable for delivering large molecules (proteins and growth factors) (Dziubla et al. 2001).

More recent studies have shown that PHEMA hydrogels have some potential for the regeneration of articular cartilage (Bavaresco et al. 2008), bone tissue (Song, Malathong, and Bertozzi 2005; Song, Saiz, and Bertozzi 2003), and nerve tissue (Carone and Hasenwinkel 2006). The PHEMA used in these studies also were nonporous hydrogels. In addition, use of porous PHEMA hydrogels in tissue engineering has attracted attention. Porous PHEMA hydrogels obtained from a polymerization process in the presence of water have been used to provide a stable three-dimensional scaffold for axonal regeneration in the damaged central nervous system (Plant, Harvey, and Chirila 1995; Plant, Chirila, and Harvey 1998). A channelled porously structured PHEMA hydrogel was produced using polycarolactone fibres as a template, for neural tissue engineering (Flynn, Dalton,

and Shoichet 2003). In a separate study, porous PHEMA hydrogels were prepared by a free radical polymerization of monomers in the presence of NaCl particles, for spinal cord injury (Hejcl et al. 2008).

However, like other hydrogels, PHEMA hydrogels exhibit relatively poor mechanical properties and a bioinert characteristic. Thus, we have proposed to incorporate nanoadditives and biomolecules into PHEMA hydrogels in order to improve both the mechanical and biological properties of the hydrogels for tissue engineering applications.

It is noteworthy that PHEMA is a stable polymer that is considered to be nondegradable. Biodegradable scaffolding materials most commonly are investigated for tissue engineering applications. Numerous investigations have been based on PLA, PGA and their copolymers (Holy et al. 2001; Savaiano and Webster 2004; Ma et al. 2005; Pattison et al. 2005; Gerhardt, Jell, and Boccaccini 2007; Torres et al. 2007). However, these materials exhibit a number of disadvantages. Firstly, the oligomers of these polymers are hydrophobic, which affects protein adhesion. Therefore, cell activities including cell attachment and proliferation can be much affected (Minamiguchi et al. 2008; Oh et al. 2003). Secondly, degradation products of these scaffold materials can cause toxic responses when these acidic degradation products are released abruptly, affecting cell growth and increasing inflammation in the surrounding tissue area (Martin, Winet, and Bao 1996). Last but not least, degradation can change the mechanical properties of a tissue scaffold and an autocatalyzed break down can lead to a catastrophic loss of the mechanical support from the scaffold (Atzet et al. 2008). Non-biodegradable polymers have the advantage that their properties, both chemical and mechanical, are less affected by the cellular and tissue milieu (Li et al. 2006). In addition, the fundamental understanding of the role of the scaffold biomaterial is still rather limited because of its multidisciplinary nature. Determining the ultimate success of non-degradable scaffolding materials can benefit us for a wider understanding of scaffold materials, for which various factors can be dissected (Jansen et al. 2005). Therefore, investigations of non-biodegradable materials such as polytetrafluoroethylene, polyethylmethacrylate, PHEMA and hydroxyapatite/Dacron composites in tissue

engineering also has produced much activity (Francis Suh and Matthew 2000; Kubinová et al. 2010; Kubinová, Horák, and Syková 2009).

Effort has been made to convert PHEMA to degradable hydrogel (Atzet et al. 2008; Casadio et al. 2010). However, the degradation relies on the utilization of a degradable crosslinker, including oligomeric blocks of polycaprolactone (Atzet et al. 2008), a series of dimethacrylate peptide-based crosslinking agents (Casadio et al. 2010), poly(ethylene glycol) diacrylate and N,N'-bis(methacryloyl)-L-cystine (Andac et al. 2008). Even though the crosslinker can be degraded, the resultant HEMA polymer chains remain nondegradable. Thus, our effort is focused on making porous PHEMA hydrogel bioactive so as to extend its application as an effective and permanent implanted tissue scaffold material. Non-degradable nano-additives are used for the production of composite PHEMA hydrogels. In the following sections, the nanoadditives will be introduced.

1.5.2. Titanium Dioxide (TiO_2)

TiO_2 particles (Titania) exist in different crystalline forms, including anatase, rutile and brookite. Among these structures, rutile is the most stable form and the other two can convert to rutile upon heating (Mor et al. 2006). TiO_2 has been found to be useful in such applications as photocatalysis, oxygen sensors and antimicrobial coatings (Chin, Chiang, and Fane 2006; Chung et al. 2008; Zheng, Xu, and Xu 2000). TiO_2 nanoparticles also have been found to be useful for tissue engineering, such as bone regeneration, because TiO_2 particles have an excellent capacity for inducing calcium deposition and osteoblast functions in polymers containing nano-sized titania inclusions (Liu, Slamovich, and Webster 2006; Savaiano and Webster 2004). The cytotoxicity of TiO_2 in nanoparticles or films has been investigated using different cell lines, including mouse mesenchymal stem cells and human dermal fibroblast cells (Kommireddy et al. 2005). The results indicate that TiO_2 particles are non-toxic (Carbone et al. 2006; Kommireddy et al. 2005; Kommireddy et al. 2006).

1.5.3. Carbon Nanotubes (CNTs)

Carbon nanotubes can be produced as a single tube structure (commonly called a single-walled carbon nanotube) or concentric cylinder of carbon structure (commonly referred to as a multi-walled carbon nanotube) (Harrison and Atala 2007).

Both are in cylindrical form with a diameter of several nanometres and a length greater than 100 nm, resulting in very large aspect ratios. They possess a very broad range of electronic, thermal and structural properties defined by diameter, length and twist. CNTs have the capacity to be used in cellular imaging, chemical and biological sensing, bioactive agent delivery and tissue engineering.

The toxicity (biocompatibility) of CNT has been investigated *in vitro* and *in vivo* (Firme Iii and Bandaru 2010; Chlopek et al. 2006). The results are controversial due to influences from a range of factors, including length, type of functionality, concentration, duration of exposure, method of exposure, and even the dispersant used to solubilise the nanotubes (Cui et al. 2010). Some results demonstrate that CNTs have a cytotoxic effect (Shvedova et al. 2003; Cui et al. 2005; Jia et al. 2005; Monteiro-Riviere et al. 2005; Zhang et al. 2007), whereas other results demonstrate their biocompatibility (Flahaut et al. 2006; Dumortier et al. 2006; Chen et al. 2006). Apart from the controversy about their cytotoxicity, CNTs have been reported to be capable of improving cell adhesion *in vitro,* as well as supporting other cell types, such as smooth muscle, fibroblasts and osteoblasts (MacDonald et al. 2005; Correa-Duarte et al. 2004; Supronowicz et al. 2002).

CNTs have the potential to provide essential structural reinforcement for tissue scaffolds due to their superior mechanical properties and fibre characteristics (Bhattacharyya et al. 2008; Wang and Chen 2007). It is reported that significant improvements (300%) in the dynamic mechanical properties of the composites have been observed after a small fraction (2wt%) of carbon nanotubes were incorporated into hyaluronic acid hydrogels (Bhattacharyya et al. 2008). MWNTs blended with chitosan showed significant improvement in mechanical properties compared with those of chitosan alone. Nanocomposites composed of 2% MWNT more than doubled the Young's modulus and tensile strength results compared to neat chitosan. Therefore, it has been proven that the mechanical properties of composite materials containing CNTs can be “fine-tuned” by varying the concentration of CNTs within the bulk polymers (Ceballos et al. 1999; Dang and Leong 2006; Yoshii et al. 2002) .

1.5.4. Silicon Dioxide (SiO_2)

Silicon dioxide or silica (SiO_2) is one of the most abundant compounds in the earth's crust (Park and Park 2009). Various SiO_2 nanoparticles have been used in chemical and biomedical products, such as cancer therapy, DNA delivery and enzyme immobilization (Barik, Sahu, and Swain 2008). It is one of the components of bioactive glasses, which have been widely used as additives for bone tissue regeneration scaffolds and soft tissue scaffolds (Rich et al. 2002; Francis et al. 2010; Boccaccini et al. 2010). The use of silica alone as an additive for tissue scaffolds also has been reported, due to its potential capability to induce apatite formation (Madhumathi et al. 2009; Hench 1991; Karlsson, Fröberg, and Ringbom 1989; Day et al. 2004).

1.5.5. Collagen

Collagens are a group of proteins with a characteristic molecular structure, with their fibrillar structures contributing to the extracellular matrix (Gelse, Pöschl, and Aigner 2003). So far, over 27 types of collagen have been identified and described (Myllyharju and Kivirikko 2004). The different collagen types can be recognised by the considerable complexity and diversity in their structures, their splice variants, the presence of additional, non-helical domains, their assembly and their function. The majority of collagen existing in the body is type I, which can be found in great abundance in tissues including dermis, tendon, ligaments, cornea and bone (Gelse, Pöschl, and Aigner 2003). Types II, IX and XI are found almost exclusively in cartilage tissues (Myllyharju and Kivirikko 2004). Collagen functions as a major structural component in those connective tissues (Lee and Mooney 2001). In addition, collagen molecules interact with cells to transduce molecule signals for the regulation of cell adhesion, migration, proliferation and differentiation (Malafaya, Silva, and Reis 2007). In addition, characteristics such as excellent biocompatibility, low antigenicity, the ability to be crosslinked, and tailored mechanical, degradation and water-uptake properties have enabled extensive studies of collagen for the various biomedical applications, including tissue engineering (Lee, Singla, and Lee 2001). Collagen has been used widely to modify the chemistry of scaffolds for improving cellular adhesive properties. Listed in Table 1-2 are a few examples that

have demonstrated improvements in cellular activities after modification with collagen.

Table 1-2 A summary of the methods used for surface modification using collagen

Scaffold material	Surface treatment	Collagen attachment method	Cell tested	Ref.
PLLA	Ozone oxidation to producing peroxide groups on surface	Redox-initiated coupling reaction, allowing grafting with collagen molecules	Osteoblasts	(Suh et al. 2001)
PLA	Grafting polymerization of methacrylic acid on PLLA surface to introduce -COOH groups	Chemical grafting of collagen type I using carbodimmide as coupling agent	Chondrocyte	(Ma et al. 2005)
Titanium, titanium alloy, cobalt alloy; stainless steel	Oxide techniques	Covalent coupling of collagen via a silane coupling agent and linker molecule. Collagen layer was cross-linked by carbodiimide reaction afterwards.	Human osteoblast-like cells Mysenchymal stem cells	(Müller, Abke, et al. 2006; Müller et al. 2005)
Poly(ethylene terephthalate)	Plasma treated followed by acrylic acid graft polymerization	Electrostatic adsorption of collagen onto the modified surface	Human smooth muscle cell	(Bisson et al. 2002)
PLGA (85/15)	Ammonia plasma treated	Collagen was anchored onto the modified surface	Mouse 3T3 fibroblasts	(Yang et al. 2003)
PHEMA	NA	Collagen was deposited on hydrogels by adsorption from acid solutions	Mysenchymal stem cells	(Brynda et al. 2009)

1.5.6. Research Plan and Methodology

The aim of this project is to synthesize and evaluate macroporous PHEMA and PHEMA composite hydrogels for tissue engineering applications.

Porous PHEMA hydrogels have great potential for tissue engineering applications, as has been mentioned in the above sections. These advantages include (1) macroporous PHEMA hydrogel with varying pore sizes can be formed easily by polymerization in the presence of a large amount of water; (2) the polymerization process conditions are mild and the properties of resultant hydrogels can be altered through simple chemical and/or physical processes; and (3) macroporous PHEMA hydrogels exhibit a high loading capacity for biomolecules (Wang et al. 2010; Lou, Wang, and Tan 2007; Lou, Munro, and Wang 2004) and allow the transportation of large molecules such as growth factors and other nutritional molecules. However, like other hydrogels, PHEMA hydrogels exhibit relatively poor mechanical properties and are biologically inert. Therefore, we have proposed to incorporate nanoadditives and biomolecules into PHEMA hydrogels, and to investigate the effect of these additives on the mechanical strength and the cellular activities of the composite PHEMA hydrogels.

In addition, the transportation of macromolecules is of significant importance, as cell or tissue growth requires constant provision and discharge of macromolecules such as growth factors, proteins and other nutrimental substances. For the ultimate application of any scaffolding material, investigation and understanding of the molecule diffusion properties in the porous structure of the scaffold will help in the design and fabrication of effective tissue engineering scaffolds. Therefore, evaluation of the transportation of macromolecules within the produced porous composite scaffolds also is conducted in this study.

A series of porous PHEMA and PHEMA composite hydrogels, including PHEMA-TiO_2, PHEMA-SiO_2, PHEMA-CNT, and collagen modified PHEMA and PHEMA composite hydrogels, will be fabricated. The design parameters, including pore structure and porosity, mechanical behaviour, topographic properties and cellular activities, as well as the ability for biomolecule delivery of these hydrogels, will be investigated systematically for possible applications as tissue engineering scaffolds.

In brief, porous PHEMA and PHEMA composite hydrogels will be synthesized through a free radical polymerization process in the presence of water (Li, Zheng, and Lou 2009). Various porous structures of the hydrogels will be generated by

altering of the HEMA:water ratios in the polymerization mixtures. TiO_2, SiO_2 and CNT particulates will be used as nanoadditives for composite hydrogels. Collagen will be incorporated, through chemical bonding, into selected hydrogels for the improvement of cellular activities.

The presence and the concentrations of the nanoadditives and collagen molecules will be analysed using various analytical instruments. These include Fourier transform infrared spectroscopy (FTIR), UV-Vis absorption spectroscopy (UV-Vis), scanning electron microscopy including energy-dispersive X-ray spectroscopy (SEM/EDX), X-ray diffraction (XRD), and gravimetric analysis (GA). The porous structure of the hydrogels will be examined using SEM. The polymer volume fraction also will be determined as a quantitative measure of the porosity.

Mechanical properties of PHEMA and PHEMA composite hydrogels will be studied using a SINTECH® 200/M Material Testing Workstation and a HAAKE MARS III Modular Advanced Rheometer System. The tensile behaviours, as well as the viscoelastic moduli, linear viscoelastic range and recovery properties of the hydrogels, will be investigated.

The delivery of biomolecules from selected PHEMA hydrogels also will be examined. Both single and dual delivery systems will be used in this study. Delivery of biomolecules in static and dynamic conditions will be explored. The cytotoxicity and cellular activities of the produced hydrogels will be assessed using various cell lines. The calcification capacity of the porous hydrogels also will be evaluated.

CHAPTER 2 MACROPOROUS PHEMA AND PHEMA COMPOSITE HYDROGELS: SYNTHESIS AND CHARACTERIZATION

2.1. Introduction

This chapter focuses on the synthesis and characterization of a series of macroporous poly(2-hydroxyethyl methacrylate) (PHEMA) composite hydrogels containing varying concentrations of three nanoadditives, including titanium dioxide (TiO_2), silicon dioxide (SiO_2) and multi-walled carbon nanotubes (CNTs).

As mentioned in the previous chapter, a macroporous network is critical for nutrient exchange and oxygen delivery, as well as for the long-term survival of tissue cells, when engineering various tissues. Several reported methods have increased the effective pore sizes of the PHEMA hydrogels to several micrometers (Krauch and Sanner 1968; Haldon and Lee 1972; Murphy, Skelly, and Tighe 1992). These include the application of a solid matrix that, subsequently, is dissolved or dispersed in water. This method was introduced for the production of PHEMA hydrogels (Krauch and Sanner 1968). One of the most convenient methods is to polymerize HEMA monomer in the presence of water above a critical level (reportedly 40-45 wt%) (Rosenberg, Bartl, and Leško 1960; Yasuda, Gochin, and Stone 1966; Hasa and Janáček 1967; Gouda et al. 1970; Warren and Prins 1972). During this process, a macroporous PHEMA network forms as a result of phase separation, which is caused by the presence of excessive water in the monomer mixture that exceeds the maximum swelling capacity of the final polymer (Chirila, Chen, et al. 1993). The phase separation occurs due to the thermodynamic interaction between water and the polymer network, and the formed macro-pores range from several to hundreds of micrometers (Chirila, Chen, et al. 1993; Lou, Munro, and Wang 2004).

In this current study, phase separation polymerisation also was used to create PHEMA hydrogels containing various porosities. Five water concentrations were

used, including 60, 70, 75, 80 and 90 wt% in the production of PHMEA and its composite hydrogels. Nanoparticulate TiO_2, multi-walled CNTs, and SiO_2 were incorporated into the porous structure in order to explore their effects on the mechanical behaviour and bioactivity of the hydrogel polymers. The produced hydrogels were examined via SEM examination to reveal the macrostructures. Gravimetric analysis (GA) and thermal gravimetric analysis (TGA) were carried out to quantify the real concentrations of the additives in composite hydrogels. XRD was conducted to confirm the presence of additives in the hydrogels. The polymer volume fraction also was measured in order to estimate the porosity of the hydrogels.

Cell viability (cytotoxicity) indicates the functional status of cells in the presence of compounds/materials (Ciapetti et al. 1996). The assessment can be accomplished either by directly counting the number of healthy cells or by measuring an indicator for healthy cells in cell populations (Castro-Concha, Escobedo, and Miranda-Ham 2006). In general, an increase in cell viability indicates cell growth, while a decrease in cell viability can be interpreted as the result of the toxic effects of the exposed materials. Several assays have been reported to quantify the cellular viability by measuring the indicator of the healthy cells. The assays can be categorized according to two characteristic parameters: metabolic activity or cell membrane integrity of healthy cells. The first category includes methods such as MTT, XTT and WST-1, which use a colorimetric reaction to measure the reducing potential of the cell. The second type of assay takes advantage of the ability of healthy cells with uncompromised cytoplasmic membrane integrity to exclude dyes such as trypan blue, methylene blue and evans blue (Castro-Concha, Escobedo, and Miranda-Ham 2006).

In this study, an MTT cleavage assay was used to examine the cytotoxicity of the selected hydrogel materials. The method originally was described by Mosmann for measuring cell survival/proliferation (Mosmann 1983). It is a colorimetric assay that measures the reduction of yellow MTT by mitochondrial succinate dehydrogenase. The MTT enters the cells and passes into the mitochondria where it is reduced to an insoluble, coloured (dark purple) formazan product. The cells then are solubilised with an organic solvent (eg. isopropanol) and the released, solubilised formazan reagent is measured spectrophotometrically (Peterson, Kimura, and Schubert 1997). Since a reduction of MTT can occur only in metabolically active cells, the level of

activity is a measure of the viability of the cells. The advantages of using this assay include: (a) sensitivity and reproducibility; (b) elimination of the need for radioactive compounds; (c) ease with which it can be performed and quantified; and (d) rapidity (Ferrari, Fornasiero, and Isetta 1990).

Calcium is an important element and is the most abundant mineral in the body. It interacts with phosphorus to form calcium phosphate (CaP), which is the material for bone and teeth tissue formation. The formation of CaP is a process called calcification and it occurs in many situations in the human body. The formation of CaP may cause failure of some implants (Vijayasekaran et al. 2000). However, its formation helps the osteogenesis of implants and prostheses for orthopaedic correction (Aimoli, Torres, and Beppu 2006), as well as aiding in the development of new bone tissues in their regeneration (Zhao and Chang 2004). In addition, it has been well accepted that the deposition of hydroxyapatite-like CaP onto biomaterial surfaces can facilitate direct bonding to hard tissue which, in turn, provides a favourable procedure to mimic the bone environment through the promotion of osteointegration by the osteoblast attachment and osteogenic differentiation (Yokogawa et al. 1997). Thus, many investigations have attempted to promote calcification of synthetic biomaterials for applications in orthopaedic and dental surgery.

The calcification capacity of the produced hydrogels was investigated using a simulated body fluid (SBF) containing ion concentrations similar to those in human blood plasma. Hydrogels, including group I (20HEMA-5TiO_2, 20HEMA-0.5CNT, 30HEMA-5TiO_2, and 30HEMA-5SiO_2) and group II (10HEMA-7.5TiO_2, 20HEMA, 20HEMA-7.5TiO_2, and 40HEMA-7.5TiO_2), were selected to explore the calcification capacity of porous PHEMA hydrogels. The hydrogels were incubated in the SBF and the formation of CaP was evaluated using XRD, FTIR, SEM/EDX and Alizarin Red S staining.

2.2. Experimental

2.2.1. Chemicals

Ophthalmic grade 2-hydroxyethyl methacrylate (HEMA) and ethylene dimethacrylate (EDMA) were supplied by Bimax USA. Sigma-Aldrich supplied 1,5-hexadiene-3,4-diol (DVG) and this was used as a crosslinker. Ammonium persulphate (APS) and N, N, N', N'-tetramethylethylenediamine (TEMED) were purchased from Sigma-Aldrich and used as initiators for polymerization. TiO_2 nanoparticles were obtained from Degussa AG Germany (AEROXIDE® P 25, 99.5 wt%) and Sigma-Aldrich. The average size of the particles was 21 nm. SiO_2 nanoparticles (~30 nm) were from Sigma-Aldrich. Multi-walled carbon nanotubes (CNTs, diameter 10-30 nm, length 5-15 μm) were purchased from Shenzhen Nanotech Port Co., Ltd (Shenzhen, China) with a purity of >97%. CNTs were purified by an acid solution (H_2SO_4:HNO_3=3:1) for 5 hours at 40^oC, followed by sedimentation, centrifugation and filtration prior to use. All other chemicals used were analytical grade. Alzarin Red S was from Sigma-Aldrich.

The chemicals used for the cell viability assay included 3-(4,5-Dimethylthiazol-2-yl)-2,5-diphenyltetrazolium bromide (MTT) from Sigma-Aldrich, and Dulbecco's modified Eagle's medium, fetal calf serum and penicillin/streptomycin from Gibco, USA.

An SBF solution was prepared by dissolving the reagent of 11.994g NaCl (BDH Chemicals), 0.525g $NaHCO_3$ (Aldrich), 0.336g KCl (Aldrich), 0.342g $K_2HPO_4 \cdot 3H_2O$ (Aldrich), 0.458g $MgCl_2 \cdot 6H_2O$, 60ml HCl (1 kmol/m^3, Ajax Chemicals), 0.417g $CaCl_2$ (APS Chemicals), 0.107g Na_2SO_4 (Aldrich), and 9.086g $(CH_2OH)_3CNH_2$ (Sigma-Aldrich) into 750ml Mill-Q water (Masami et al. 1994). The final ion concentrations were 1.5 times that of those in human blood plasma. The pH value of the solution was adjusted to 7.4 using 1M HCl at 37±1°C, and then the solution was transferred into a 1000ml glass volumetric flask. The beaker used for transfer was washed using Mill-Q water. The solution was added into the flask and the total volume of the solution was adjusted to 1000 ml using Mill-Q water.

2.2.2. Synthesis of Porous PHEMA Composite Hydrogels

PHEMA-TiO_2 composite hydrogels

Outlined below is the general procedure to prepare a PHEMA hydrogel containing 7.5 wt% TiO_2 using 20:80 (HEMA: water) ratio. The hydrogel is coded as 20HEMA-7.5TiO_2. TiO_2 nanoparticles (0.15 g) were dispersed in Mill-Q water (8 g) using an ultrasonic water bath for 1 hour and mechanically stirred for 30 min. HEMA monomer (2 g), crosslinking agent EDMA (20 μl), and 10 wt% APS solution and TEMED (initiators; 40 μl) were subsequently added. The mixture was injected into the space between two glass plates, separated with a silicon rubber gasket, within 5 min. The polymerization process was started at room temperature, maintained for 3 hours, followed by a thermal curing at 60^{o}C for 24 hours. Upon completion of the polymerization, the hydrogel materials were removed from the glass plates, extracted via water exchange, with sufficient deionised (DI) water, and then replaced, twice a day for at least two weeks, in order to remove residual chemicals and monomers. The effective removal of the impurities with this method has been verified from the previous reports (Chirila, Chen, et al. 1993; Brynda et al. 1985; Kwok et al. 2001).

Other PHEMA-TiO_2 composite hydrogels were prepared in the same manner as above, but with a different chemical composition in accordance with Table 2-1.

Freeze drying was applied to hydrogel samples prior to some measurements, including morphological and thermal analysis. This was conducted using a DYNAVAC freeze drier (Model FD3), shown in Figure 2-1. The hydrated hydrogel specimens were put into a Petri dish and afterwards kept in a freezer at -40°C overnight. The frozen hydrogel specimens were moved into a vacuum chamber, followed by sublimation. The vacuum chamber was connected to a condenser, and cooled to -55ºC. The process lasted for a minimum of 24 hours, ensuring a complete drying of the samples.

Figure 2-1 DYNAVAC freeze drier for treatment of hydrogel specimens

PHEMA-SiO_2 and PHEMA-CNT composite hydrogels

Composite hydrogels containing SiO_2 nanoparticles and multi-walled CNTs were prepared using the same procedure as that for the PHEMA-TiO_2 composite hydrogels. The chemical composition of these hydrogels is summarised in Table 2-1.

For the convenience of this investigation, hydrogels were fabricated in two forms including sheet and button samples. The sheet samples were polymerized in the space between two glass plates, separated with a silicon rubber gasket. The mould for casting sheet hydrogel samples is displayed in Figure 2-2 a. The button-shaped hydrogels were produced in wells of tissue culture plates consisting of 24 wells (TPP, Trasadingen, Switzerland), as displayed in Figure 2-2 b.

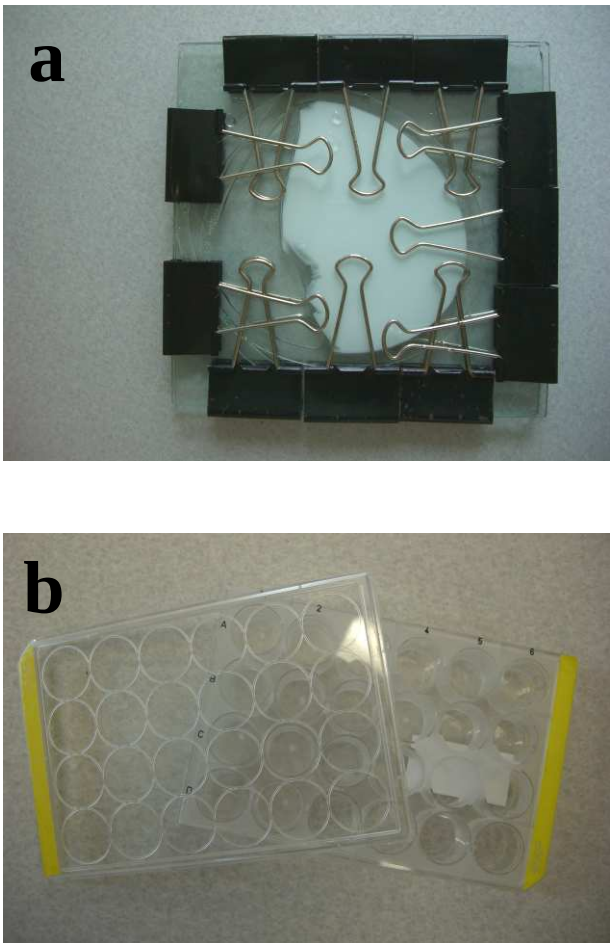

Figure 2-2 (a) A mould for casting hydrogel sheets and (b) a tissue culture plate consisting of 24 wells, for casting hydrogel buttons

2.2.3. Quantification of Additives

Gravimetric analysis was used to quantify the amounts of TiO_2 contained in the hydrogel polymers. The freeze-dried samples were crushed into fine powder and approximately 5 g of the hydrogel polymers were placed in a furnace at 450°C for four hours, ensuring complete decomposition. Pure PHEMA and the nanoparticles were used as controls. The residual polymers were weighed. The weights of the samples, before and after decomposition, were taken as W_1 and W_2 respectively. The weight loss percentage of the composite hydrogels was calculated as $100 \times W_2/(W_1-W_2)$. Three measurements were carried out for each formulation and an average weight percentage of the additive was computed. The error was presented using the STDEV.

A METTLER TOLEDO TGA/DSC instrument was used to confirm the above results using 30HEMA-7.5TiO_2 composite hydrogel. Approximately 3-5 mg of the crushed fine powder was used for the TGA analysis under nitrogen atmosphere at normal pressure. The samples were heated in alumina crucibles (70 μl) from 35 to 750^{o}C at a heating rate of 10^{o}C/min. A plain crucible containing no sample was conducted before any test in order to obtain consistent results.

2.2.4. Morphology Exmination

Morphological examination of the produced hydrogel polymers was conducted using an SEM (Zeiss 1555 VP FE-SEM, Philips XL30 SEM and Zeiss EVO 40XVP). The hydrogel specimens were freeze dried using a DYNAVAC freeze drier (Model FD3) and coated with a thin layer of carbon prior to SEM imaging. The bottom surface during the fabrication was the one that was prepared for all of these observations, to keep the results comparable.

2.2.5. Polymer Volume Fraction Measurement

The method for determining the pore size and the size distribution of a material is strongly dependant on its natural state (wet or dry). The characterization of these properties within a dry sample is relatively easy to achieve (Savina et al. 2011). Mercury intrusion porosimetry has been used most commonly, as a direct method (Sayil and Okay 2001). Another indirect method, inverse size exclusion chromatography, has been reported for the estimation of the pore size and pore size distribution of porous sorbents (DePhillips and Lenhoff 2000). However, there is no general technique to measure the pore size and size distribution of porous gels in their intact wet state (Yao and Lenhoff 2004). The direct methods for visualization of pore structure, like scanning electron microscopy (SEM), suffer from the problem of variations to pore structure being introduced during sample preparation and thus could result in erroneous estimations (Park and Hoffman 1994). Shrinkage of PHEMA has been noted commonly in previous reports (Horák, Lednick, and Bleha 1996). Environmental scanning electron microscopy (ESEM) allows the examination of the hydrated samples in their natural state and, normally, extreme care should be taken when ESEM is used for this purpose. In addition, quantitative estimation of pore size and size distribution from ESEM images also suffers from subjectivity and errors (Spiller et al. 2008).

Indirect methods commonly have been used for examining and/or quantifying the pore size of wet samples (Chalal et al. 2009; Savina et al. 2011). Calculation of the overall apparent density has been used to evaluate the porosity of various tissue scaffolds (Liu and Ma 2009; Ma and Zhang 1999; Torres et al. 2007). Solution (water or organic solutions) uptake is one of the most convenient methods to estimate the pore volume in hydrogel materials and it has been reported by many other researchers (Horák, Lednick, and Bleha 1996; Plieva et al. 2005; Yin et al. 2007). Therefore, this study uses the polymer volume fraction to estimate the porosity of PHEMA and its composite hydrogels. SEM images are used for visual examination only.

Polymer volume fraction (Φp) is defined as the ratio of the dry polymer volume to the wet volume of the same sample at its full hydration. This is a quantitative estimate of the porosity of the hydrogel, and can be determined using equations (2-1) to (2-3),

$$\Phi_p = \frac{V_p}{V_{total}} \tag{2-1}$$

$$V_p = \frac{W_{d,a} - W_{d,w}}{\rho_w} \tag{2-2}$$

$$V_{total} = \frac{W_{w,a} - W_{w,w}}{\rho_w} \tag{2-3}$$

where V_{total} represents the volume of a fully hydrated hydrogel and V_p is the volume of polymer after dehydration. Both V_{total} and V_p can be determined using the Archimedes' buoyancy principle, where the density of water (ρ_w) was taken as 1.0 mg/cm^3 in Equations (2-2) and (2-3), $W_{w,a}$ and $W_{d,a}$ represent the weight of a fully hydrated hydrogel in air and the weight of the same hydrogel in air after dehydration, and $W_{w,w}$ and $W_{d,w}$ represent the weight of a fully hydrated hydrogel in water and the weight of the same hydrogel in water after dehydration.

Measurement of these four different weights of the hydrogels was conducted using a digital balance (Analytical plus, PHAUS, NJ) (Figure 2-3). The samples were cut from each fully hydrated polymer. The free water on the specimens was quickly blotted using a wet tissue, followed by measuring $W_{w,a}$ and $W_{w,w}$. The specimens

then were dried in a convection oven (Venticell 55, MMM, Einrichtungen, Germany) for 48 hours at a temperature of 50°C. $W_{d,a}$ and $W_{d,w}$ were weighed upon completion of the drying process. Full details of the measurements can be found in the previously cited publication (Lou, Wang, and Tan 2007). Six specimens were used for each test and the average values were presented in the results. The error was presented by the STDEV.

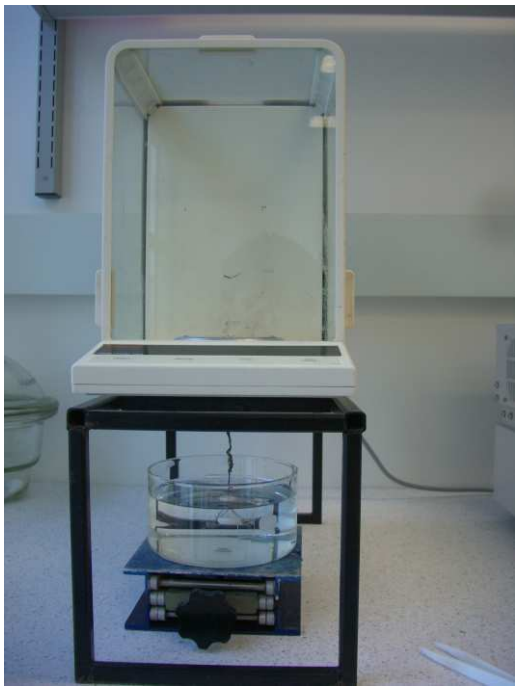

Figure 2-3 A set-up using an analytical balance for measuring weights of hydrogels in both air and water

2.2.6. Calcification Study

For each of the selected hydrogel polymers, eight specimens of disk geometry (8 mm in diameter, 1.5 mm in thickness) were put in 10 ml of 1.5 SBF solution at 37±1°C. The bottom surface of the hydrogels during the fabrication process was used for all analyses to keep the results comparable. The SBF solution was replaced with a fresh solution, weekly. Samples were retrieved at pre-designated time intervals (3, 7, 10, 14, 21 and 28 days). The formation of CaP was characterized by a series of techniques, including FTIR, Alizarin Red S staining, SEM/EDX and XRD analysis.

FTIR

An FTIR examination was carried out using a Bruker IFS 66 with a resolution of 4 cm^{-1}. The formation of CaP was confirmed using FTIR, and OPUS software was used for data analysis. The composite hydrogels were first freeze-dried and crushed into fine powders prior to the KBr disc preparation.

Alizarin Red S Staining

A small piece of calcified hydrogel sample was embedded in Tissue-Tek (O.C.T compound, ProsciTech) in a chamber and kept overnight in a freezer (Forma Scientific Inc, Marietta, USA) at -80°C. Sectional samples (10μm in thickness) were sliced using a Leica CM3050S Cryostat (Leica Microstystems, Milton, UK) at -20°C, following this standard procedure: (1) set the temperature of the cryostat at -20°C, at least 30 min prior to slicing; (2) move the frozen sample into the cryostat, followed by mounting the sample onto a sample holder using Tissue-Tek; (3) load the sample holder and make proper adjustments; (4) change the trimming thickness to 10 μm and begin trimming the sample; (5) slice sections; (6) carefully collect the section on a room temperature microscope slide; (7) keep the sections at -20°C prior to staining; and (8) clean up the chamber using 100% EtOH.

The presence of calcium in the hydrogel specimens was highlighted using a 2 wt% Alizarin Red S solution as a stain, prepared in Mill-Q water. The pH value of the solution was adjusted to 4.1~4.3 with 10 wt% ammonium hydroxide. The staining procedure followed these steps: (1) dip the slides into distilled water to remove OCT; (2) put excessive Alizarin Red Solution onto slides for 5 min; (3) shake off excess dye with care; (4) dehydrate in acetone, 10 dips; (5) wash in acetone-xylene (1:1) solution, 10 dips; and (6) clear in xylene (5 dips) and mount in permount. Eventually, the presence of calcium in the deposits was examined using an Olympus BX60 light microscopy.

SEM-EDX

The method for SEM imaging was described in Section 2.2.4. EDX analysis was carried out using a Philips XL30 with an Oxford Instruments Si-Li x-ray detector. Nickel and copper were used to calibrate the equipment. The sectional hydrogel

specimens (~0.5mm) were sliced from the bulk materials. The samples were then freeze-dried and coated with a thin layer of gold prior to the SEM imaging. The thickness of the CaP in the hydrogel samples was determined from SEM images.

XRD

XRD measurements were conducted using a Siemens D-500 powder diffractometer with Cu Kα radiation. The diffractometer was operated at 40 kV/30mA. The scanning was carried out at a step size of 0.02° and a count time of 1.5 s/step.

2.2.7. MTT Assay

The NIH 3T3 fibroblast cells were cultured in a Dulbecco's modified Eagle's medium (DMEM) containing 10% fetal calf serum (FCS) and 1% penicillin/streptomycin (Gibco, USA) at 37 °C in a humidified 5 % CO_2 incubator. Hydrogel disks (10 mm in diameter, 1.5 mm in thickness) were sterilized (autoclave: 121°C, 15 min) prior to the pre-culture with DMEM media in 24-well cell culture plates for 2 hours. Cell suspension (150 µl) with a density of 8.5×10^4 cells/ml was added to each of the hydrogels after the pre-culture media was aspirated. 200 ml of fresh media were added carefully, after 1 hour. At the desired times (Day 1, Day 3 and Day 5), 30 µl fresh MTT solution (5 mg/ml in PBS) were added to each well and the culture plates were incubated for 6 hours. The formed purple formazan was dissolved with sodium dodecyl sulfate solution (200 µl) in hydrochloric acid (pH 4.7). The culture plates were kept in the incubator overnight. The optical density of each well was measured after the hydrogels were removed from the culture plate with a spectrophotometer (Beckman, USA) at 570 nm, with background subtraction at 650 nm. Readings of a minimum of four disks were taken for each formulation. The readings from the cell culture plate (TPP, Transadingen, Switzerland) were used as a control and the reading values were normalized according to the surface area of each hydrogel. Mean ± standard deviation and the P value were calculated using one-way ANOVA with OriginPro (Version 7.5) software and the Turkey test. P values <0.05 were considered statistically significant. It should be noted that cell culture was performed on the bottom side of the hydrogels in order to obtain comparable results.

2.3. Results and Discussion

2.3.1. Synthesis of Porous PHEMA Composite Hydrogels

Eighteen composite hydrogels containing TiO_2, multi-wall CNT and SiO_2 were prepared. The hydrogels were named as follows: 10HEMA-7.5TiO_2, 20HEMA-5TiO_2, 20HEMA-7.5TiO_2, 20HEMA-10TiO_2, 25HEMA-3TiO_2, 25HEMA-7.5TiO_2, 20HEMA-12TiO_2, 30HEMA-5TiO_2, 30HEMA-7.5TiO_2, 30HEMA-10TiO_2, 40HEMA-7.5TiO_2, 20HEMA-0.5CNT, 25HEMA-0.5CNT, 20HEMA-2CNT, 30HEMA-0.5CNT, 20HEMA-5SiO_2, 30HEMA-5SiO_2, and 30HEMA-5SiO_2. Five control PHEMA hydrogels, including 10HEMA, 20HEMA, 25HEMA, 30HEMA and 40HEMA, also were synthesized. The sample codes and the chemical compositions of these hydrogel polymers are listed in Table 2-1. Numbers, including 10, 20, 25, 30 and 40, in front of HEMA, denote the percentage concentrations of HEMA monomer in relation to the total quantity of HEMA and water used in the monomer mixture. The numerical parts, including 0.5, 2, 3, 5, 7.5, 10 and 12, in front of an additive, represent the initial percentage concentrations of the additive based on the mass of HEMA in composite hydrogels. For example, a 10HEMA-7.5TiO_2 composite hydrogel material was synthesized by a mixture consisting of 10 wt% HEMA monomer, 90 wt% water and 7.5 wt% of TiO_2 nanoparticles based on HEMA content.

All hydrogels appeared to be opaque in fully-hydrated conditions, indicating a porous structure. The occurrence of the porous structure was a result of phase separation due to the presence of water during the polymerisation process (Chirila, Chen, et al. 1993; Seidl et al. 1967; Guyot and Bartholin 1982; Okay 2000). The pore sizes of the hydrogels ranged from some nanometers to micrometers, depending mainly on the HEMA:water ratios. The influence of HEMA:water ratios, and the addition of the additives, on the resultant porous structures will be displayed and discussed later.

Table 2-1 Chemical composition of PHEMA and PHEMA composite hydrogels

Sample ID	TiO_2 (g)	HEMA (g)	Water (g)	EDMA (μL)	APS (10 wt.%) (μL)	TEMED (μL)
10HEMA	-	1.0	9.0	10	20	20
10HEMA-7.5TiO_2	0.075	1.0	9.0	10	20	20
20HEMA	-	2.0	8.0	20	40	40
20HEMA-5TiO_2	0.1	2.0	8.0	20	40	40
20HEMA-7.5TiO_2	0.15	2.0	8.0	20	40	40
20HEMA-10TiO_2	0.2	2.0	8.0	20	40	40
20HEMA-0.5CNT	0.01	2.0	8.0	20	40	40
20HEMA-5SiO_2	0.1	2.0	8.0	20	40	40
25HEMA	-	2.5	7.5	25	50	50
25HEMA-3TiO_2	0.075	2.5	7.5	25	50	50
25HEMA-7.5TiO_2	0.1875	2.5	7.5	25	50	50

... cont.

Continued

Sample ID	Nanoadditives (g)	HEMA (g)	Water (g)	EDMA (µL)	APS (10 wt.%) (µL)	TEMED (µL)
25HEMA-12TiO_2	0.3	2.5	7.5	25	50	50
25HEMA-0.5CNT	0.0125	2.5	7.5	25	50	50
25HEMA-2CNT	0.05	2.5	7.5	25	50	50
30HEMA	-	3.0	7.0	30	60	60
30HEMA-5TiO_2	0.15	3.0	7.0	30	60	60
30HEMA-7.5TiO_2	0.15	3.0	7.0	30	60	60
30HEMA-10TiO_2	0.3	3.0	7.0	30	60	60
30HEMA-0.5CNT	0.015	3.0	7.0	30	60	60
30HEMA-5SiO_2	0.15	3.0	7.0	30	60	60
30HEMA-10SiO_2	0.3	3.0	7.0	30	60	60
40HEMA	-	4.0	6.0	40	80	80
40HEMA-7.5TiO_2	0.3	4.0	6.0	40	80	80

2.3.2. Contents of Nanoadditives

It is proposed that the content of the nanoadditive has an effect on the properties of a tissue scaffold. The properties include mechanical properties and cell-matrix interaction. The bioactivity also will be affected when a bioactive additive is used. Thus, it is useful to determine the real concentration of the incorporated nanoadditive. Thermal gravimetric analysis has commonly been used for this purpose and it has been applied to PHEMA composite materials as well (Huang, Chin, and Yang 2005; Nguyen et al. 2011; Silvestri et al. 2009). Table 2-2 displays the gravimetric analysis results, representing measured concentrations of the additives in the selected composite hydrogels. The results of blank PHEMA hydrogels (no additives) and the nanoparticles were used as controls. The measured concentrations of all particles are close to the incorporated values. Most of the values were lower than the theoretical concentrations of the additives, which is reasonable considering that some small particles might have been lost during the curing and extraction processes in the presence of large amounts of water. The loss of the additives is more significant in 20HEMA-10TiO_2 and 20HEMA-5SiO_2. For 20HEMA-10TiO_2, the greater amount of TiO_2 (10wt%) in the preparation might have affected the phase separation process, leading to the formation of a more porous hydrogel matrix and, therefore, a greater loss of the nanoparticles. Indeed, the polymer volume fraction of this hydrogel is smaller than that of 20HEMA-7.5TiO_2, indicating a more porous structure in 20HEMA-10TiO_2 (see Page 46, Section 2.3.3.). As for 20HEMA-5SiO_2, the extra weight loss could have been caused by the poor thermal stability of SiO_2. Weight loss of SiO_2 in a control sample was about 5% and more weight loss (7.2%) has been reported (Zhang et al. 2012). Therefore, the TA results for SiO_2 containing hydrogels indicate the minimum contents of the particles.

TGA results also confirmed the real concentration of TiO_2 in a composite hydrogel, 30HEMA-7.5TiO_2 (Figure 2-4) and demonstrated that the real concentration of the nanoparticles was 6.9 wt%, which was consistent with the results from GA.

Table 2-2 Results from GA of composite hydrogels

Sample ID	Measured concentration of the additives (wt%)	Sample ID	Measured concentration of the additives (wt%)
10HEMA	0	10HEMA-7.5TiO_2	7.8±0.1
		20HEMA-7.5TiO_2	6.8±0.2
20HEMA	0	20HEMA-10TiO_2	6.3±0.1
		20HEMA-5SiO_2	2.1±0.1
25HEMA	0	25HEMA-7.5TiO_2	6.7±1.0
		30HEMA-7.5TiO_2	6.7±0.5
30HEMA	0		
		30HEMA-5SiO_2	4.5±0.1
40HEMA	0	40HEMA-7.5TiO_2	7.0±0.1

The measurements were performed in triplicate

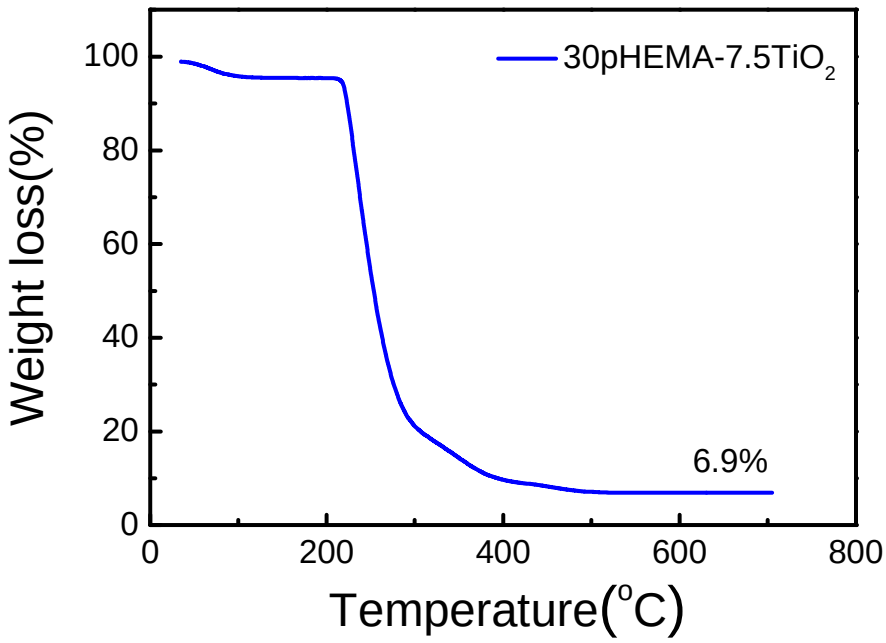

Figure 2-4 TGA curve of 30HEMA-7.5TiO_2 composite hydrogel

2.3.3. Polymer Volume Fraction

The measured polymer volume fraction (Φ_p) values of all hydrogels are summarised in Table 2-3. The higher value of Φ_p indicated a less porous structure. The results revealed that the higher the HEMA content, the less porous were the hydrogels. The incorporation of the additives increased Φ_p in most composite hydrogels, which was probably due to the higher density of the particles present in the hydrogel matrices.

Table 2-3 Polymer volume fraction of selected hydrogels

Sample ID	Polymer Volume Fraction, Φ_p (%)	Sample ID	Polymer Volume Fraction, Φ_p (%)
10HEMA	10.30±0.8	25HEMA-7.5TiO_2	21.4±4.0
10HEMA-7.5TiO_2	14.3±0.3	30HEMA	26.0±0.8
20HEMA	18.3±0.3	30HEMA-7.5TiO_2	27.0±0.0
20HEMA-5TiO_2	19.0±0.8	30HEMA-0.5CNT	27.7±0.5
20HEMA-7.5TiO_2	22.7 ±1.7	30HEMA-5SiO_2	26.7±0.3
20HEMA-10TiO_2	20.2±0.8	40HEMA	37.8±0.4
20HEMA-5SiO_2	20.9±0.5	40HEMA-7.5TiO_2	39.2±0.4
25HEMA	21.3±0.5		

Six repeats were done for each sample

2.3.4. Morphological Examination

The SEM micrographs displayed in Figures 2-5 to 2-9 provide the visible evidence to support the results received from the polymer volume fraction study. Obviously, hydrogels containing 10wt% HEMA had the most porous structures (Figure 2-5 a). The pore size became smaller once the HEMA content was increased to 20% (Figure 2-6 a). The pores in 25HEMA hydrogels were smaller (Figure 2-7 a). The pore size was dramatically reduced when the HEMA concentration was increased to 30wt% (Figure 2-8 a) and a further reduction in pores was observed in 40HEMA (Figure 2-9a). A measurement of the pore size of 20HEMA hydrogel, prepared using a similar method was 10-30 µm. However, it is suggested that the channel-like pores can

attain up to 70 µm in this hydrogel material (Chirila et al. 1993). Thus, it is a better estimation of the porosity of PHEMA hydrogels when results from polymer volume fraction and SEM images are used.

Variations in the morphology of the PHEMA hydrogels can be explained using the phase separation theory (Seidl et al. 1967; Guyot and Bartholin 1982; Okay 2000). When the polymerization process was carried out in a mixture containing a high water content (90 wt% for 10HEMA hydrogel), the monomers reacted to each other via the crosslinker until reaching a stage at which the amount of unreacted monomers was not sufficient to dissolve the growing polymer chains and the system became discontinuous, resulting in a phase separation. Thus the porous structure of the hydrogel was formed. In the solution in which less water was involved in the polymerization process (60 wt% for 40HEMA hydrogel), the phase separation was delayed due to the presence of a large amount of monomer, resulting in the formation of less porous hydrogels.

In comparison with the blank PHEMA hydrogels, the addition of the nanoparticulates had little influence on the porosity of the resultant composite hydrogels and its enhanced effect was observed for PHEMA hydrogels containing high HEMA contents, including 30 and 40% (Figure 2-8b and 2-9b). The presence of the nanoparticles was well demonstrated in most composite hydrogels.

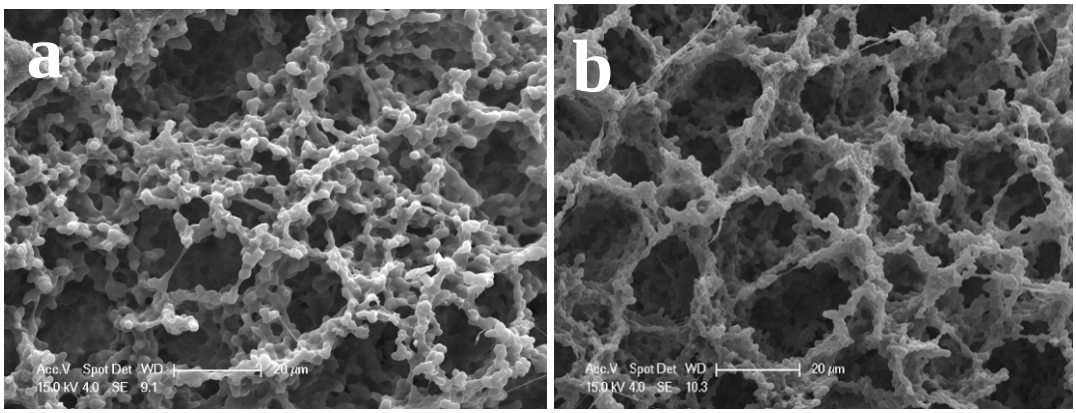

Figure 2-5 SEM micrographs of (a) 10HEMA, (b) 10HEMA-7.5TiO_2

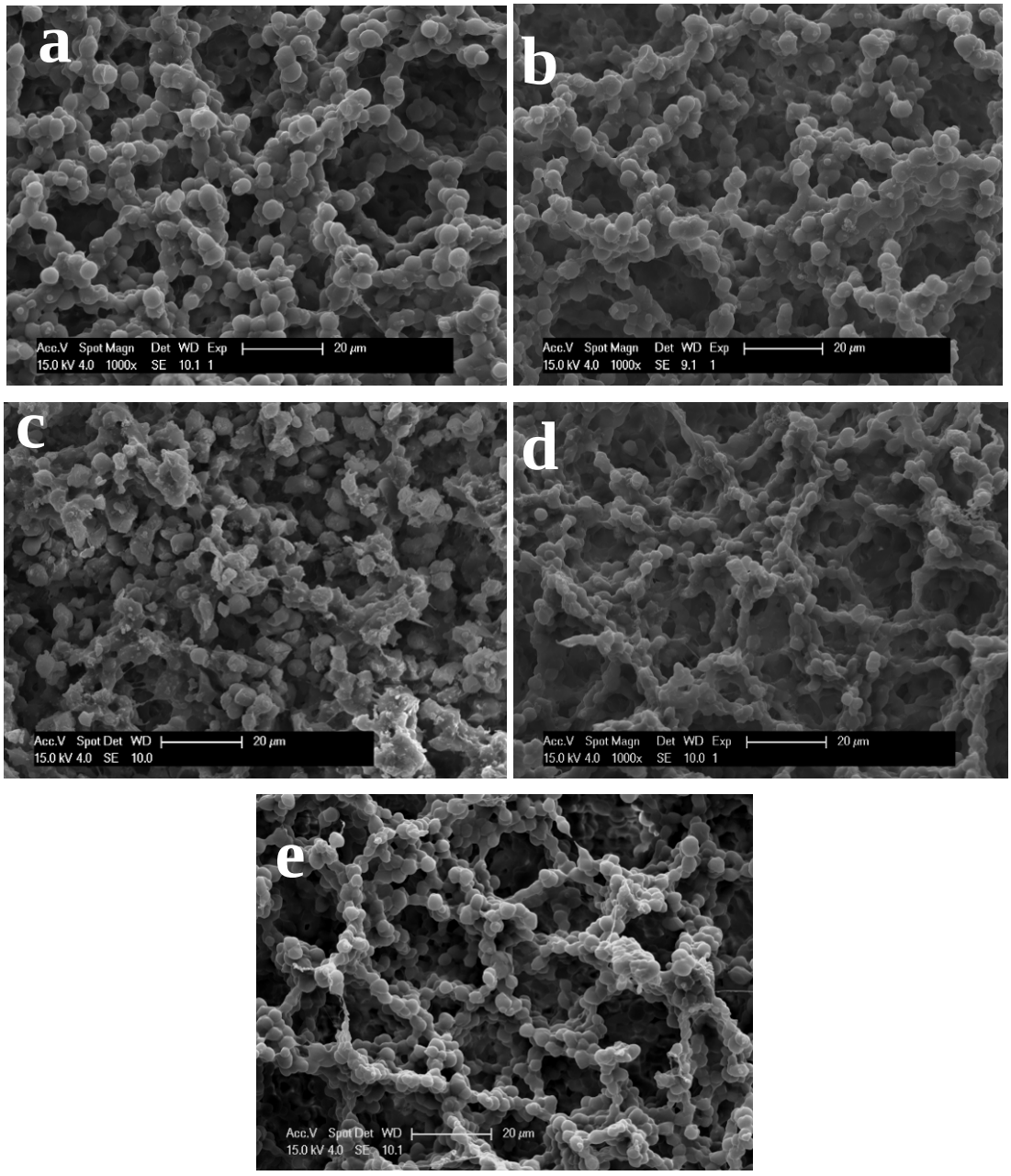

Figure 2-6 SEM micrographs of (a) 20HEMA, (b) 20HEMA-5TiO_2, (c) 20HEMA-7.5TiO_2, (d) 20HEMA-5SiO_2, and (e) 20HEMA-0.5CNT

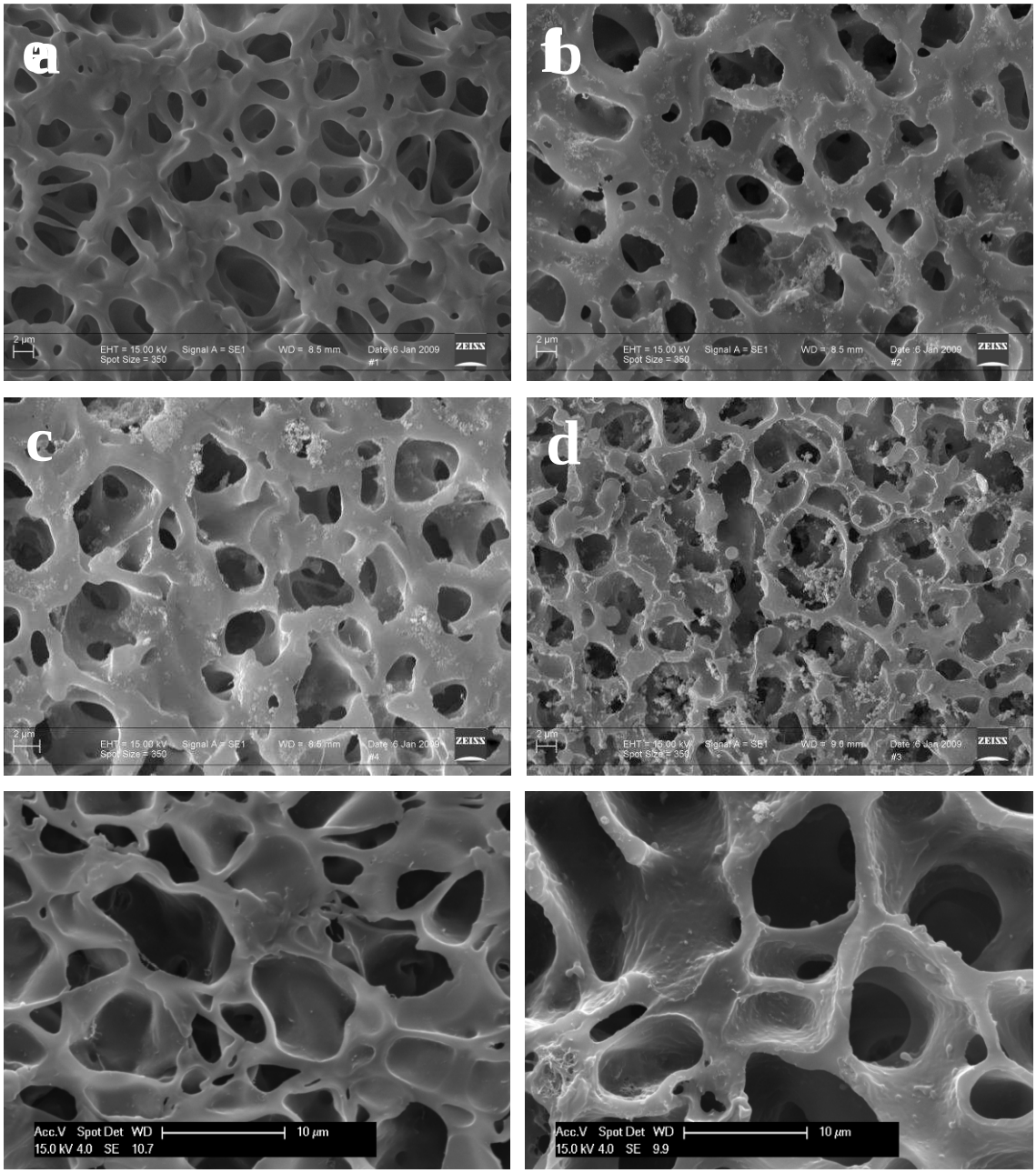

Figure 2-7 SEM micrographs (a) 25HEMA, (b) 25HEM-3TiO_2, (c) 25HEMA-7.5TiO_2, (d) 25HEMA-12TiO_2, (e) 25HEMA-0.5CNT, and (f) 25HEMA-2CNT

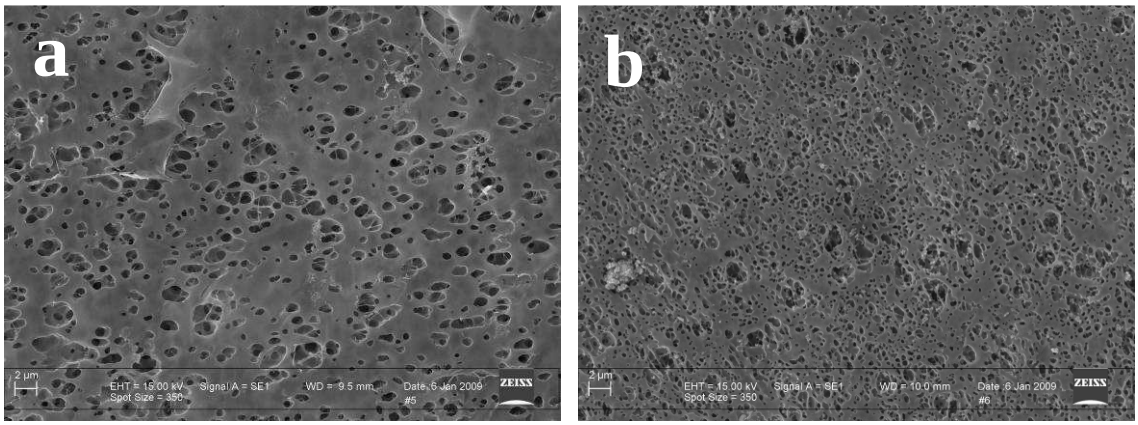

Figure 2-8 SEM micrographs of (a) 30HEMA, and (b) 30HEMA-7.5TiO_2

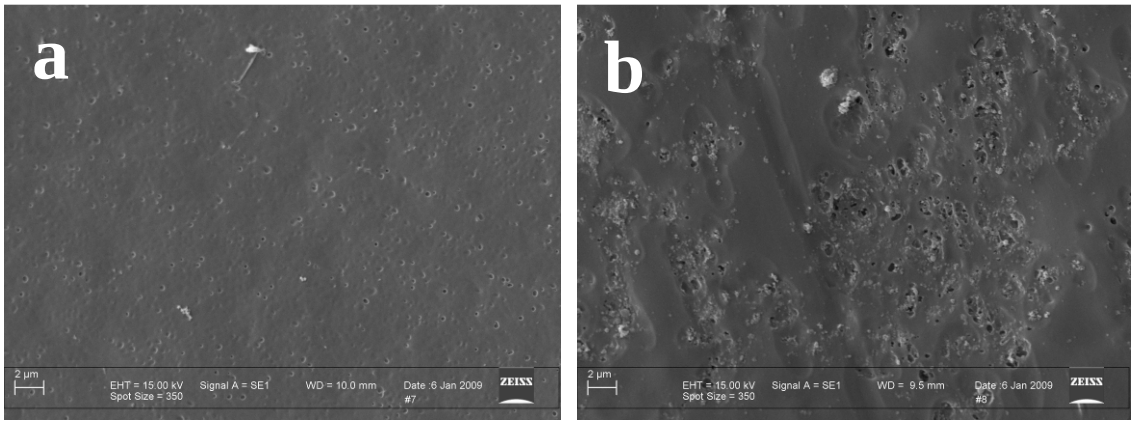

Figure 2-9 SEM micrographs of (a) 40HEMA, and (b) 40HEMA-7.5TiO_2

The distribution of TiO_2 nanoparticles in a hydrogel, namely 40HEMA-7.5TiO_2, is displayed in Figure 2-10. The composition of the nanoparticles was verified using EDX when the SEM images were taken (Image not shown due to the melting of the hydrogel under the beam). From the image in Figure 2-10 a, it can be seen that the aggregated nanoparticles were evenly distributed across the sectional surface of the hydrogel, though a decrease of TiO_2 towards the top surface of the hydrogel was seen. This is due to the gravitational sedimentation of the particles during the polymerization process. The presence of TiO_2 also was confirmed by XRD and is shown in the spectra (Figure 2-11), in which typical peaks at 25.2°, 27.4° and 48°

represent the presence of TiO_2 in the hydrogels. It can be noticed that the peak locations were shifted in different PHEMA hydrogels, which was caused by experimental error (Kishen, George, and Kumar 2006; Nakano et al. 2002).

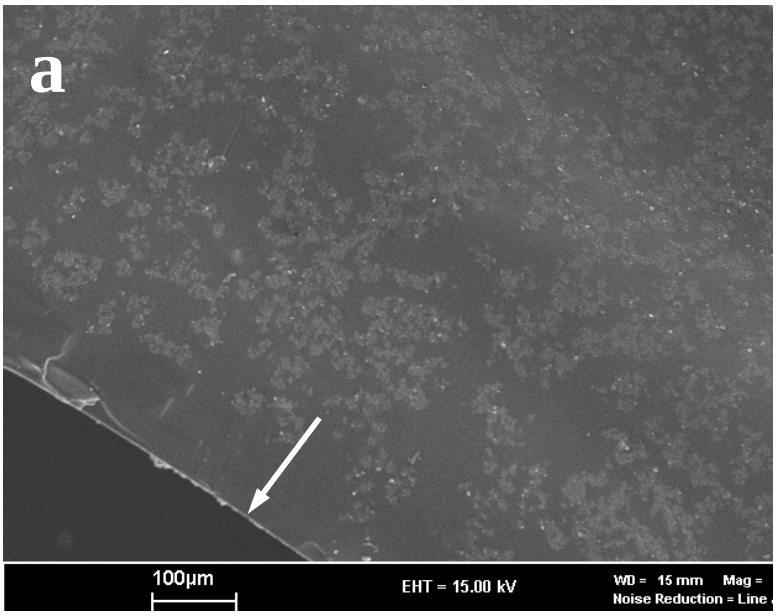

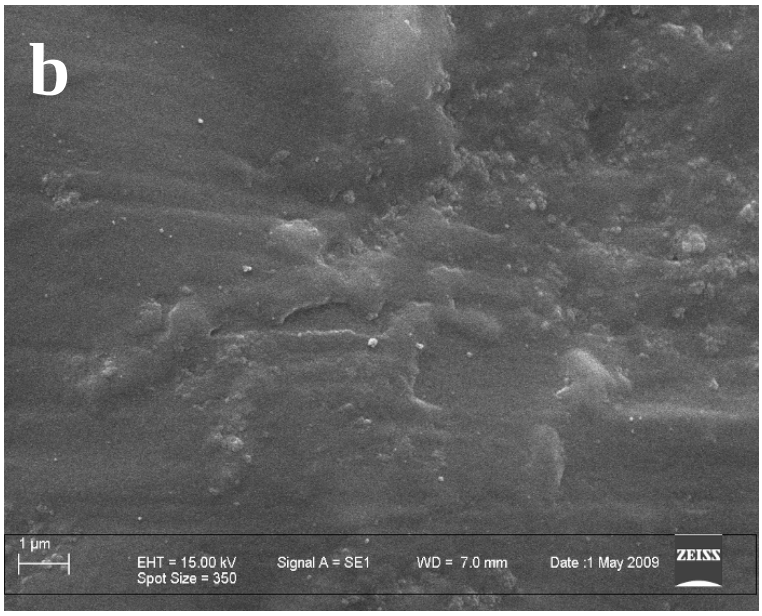

Figure 2-10 SEM micrographs of the 40HEMA-7.5TiO_2 hydrogel with different magnifications; the arrow in (a) indicates the top surface of the hydrogel

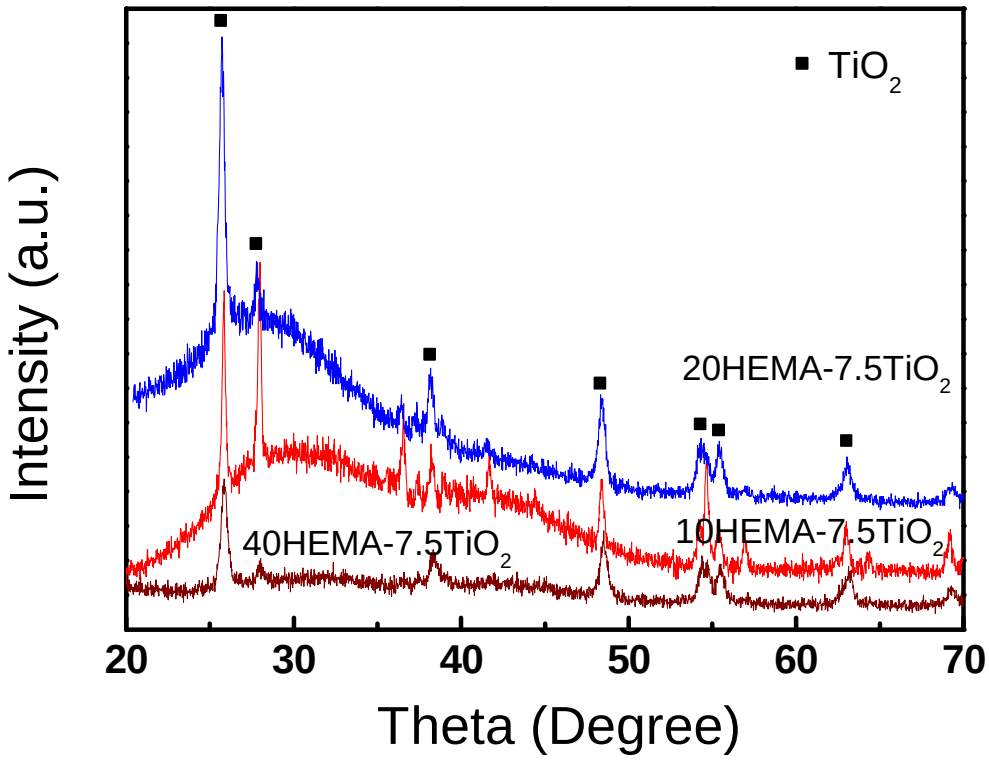

Figure 2-11 XRD spectra showing the presence of TiO_2 particles in composite hydrogels

2.3.5. Calcification Capacity of Hydrogels

Influence of nanoadditives

The CaP formation was first investigated using PHEMA composite hydrogels containing all three types of nanoadditives. These included 20HEMA-5TiO_2, 20HEMA-0.5CNT, 30HEMA-5SiO_2, and 30HEMA-5TiO_2. The formation of CaP was determined using XRD, and the deposition of hydroxyapatite-like CaP mineral was verified using typical peaks at 26° and 32° (Shi et al. 2006). This method has been reported in numerous publications (Torres et al. 2007; Miyazaki et al. 2002). The XRD results demonstrated that the formation of hydroxyapatite-like CaP was much more apparent in the hydrogels containing TiO_2 nanoparticles after 21 days incubation (Figure 2-12). A small amount of CaP was found on 20HEMA-0.5CNT and no apatite formation was observed on SiO_2 containing composite hydrogels. The capability of inducing CaP formation by TiO_2 has been demonstrated by other research groups (Gerhardt, Jell, and Boccaccini 2007; Torres et al. 2007). The fibre-

shaped structure (5-15 μm in length) of CNTs was attributed to the CaP formation on the composite hydrogel containing CNTs (Firkowska et al. 2006). However, other researchers also have reported slow growth of apatite using CNTs in the composite materials, because of their low concentration (Zhang et al. 2009). The lack of calcification in the SiO_2-containing hydrogels could be due to the low concentration silanol groups in comparison to silica gel (Li et al. 1994; Pereira, Clark, and Hench 1995). Based on these obtained results, further investigations in the following chapters will focus only on TiO_2-containing PHEMA hydrogels.

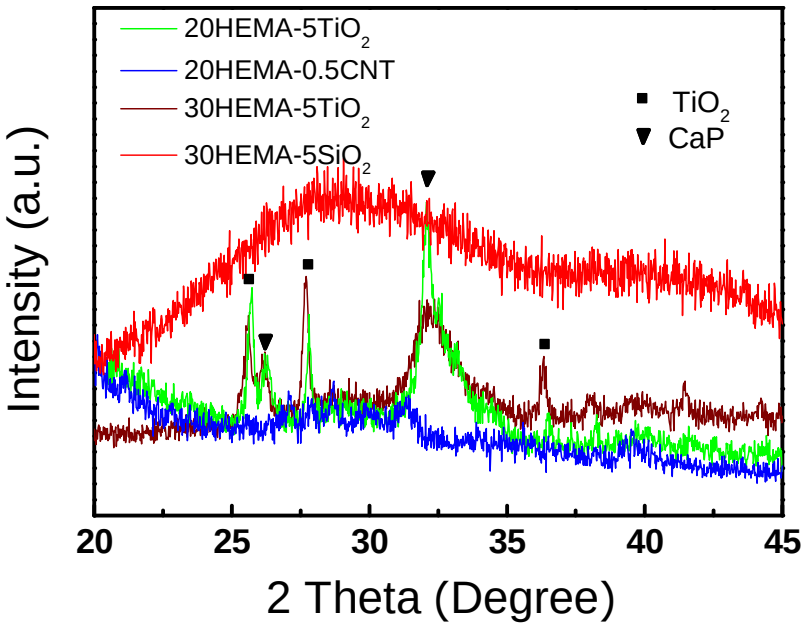

Figure 2-12 XRD spectra showing the formation of CaP on selected hydrogels after 21 days incubation in SBF solution

CaP formation on HEMA-TiO_2 composite hydrogels

10HEMA-7.5TiO_2, 20HEMA, 20HEMA-7.5TiO_2 and 40HEMA-7.5TiO_2 were selected for systematic investigation of the CaP formation. The occurrence of the CaP was confirmed by FTIR and the results from FTIR are shown in Figure 2-13. The FTIR spectrum of 10HEMA-7.5TiO_2 before incubation in SBF solution is shown in Figure 2-13a. From the spectrum, a number of peaks at 1726 cm^{-1} (ν, C=O), 1454 cm^{-1} (δ, CH_2; δ, CH_3), 1390 cm^{-1} (CH_2 twist and rock), 1160 cm^{-1} (ν_a, C-O-C), 1075 cm^{-1} (ν, C-O-C) and 750 cm^{-1} (ν, -C-O-) were determined, corresponding to

PHEMA structure (Huang, Chin, and Yang 2004, 2005; Ji et al. 2003). In comparison to the FTIR spectrum of the same material after incubation in SBF (Figure 2-13 b), strong absorbance at 564 and 603 cm^{-1} and between 1000 and 1200 cm^{-1} respectively were seen, attributed to the asymmetric bending and stretching modes of the phosphate group (Liu, Tao, and Ding 2002; Radin and Ducheyne 1992). Similar results have been reported using other types of PHEMA composite hydrogels (Costa et al. 2005).

Figure 2-14 shows the XRD spectra of CaP formed on different hydrogels, including a porous 20HEMA-7.5TiO_2 and a dense hydrogel 40HEMA-7.5TiO_2, after (a) 14 and (b) 28 days incubation in SBF respectively. Strong peaks at 32° corresponding to CaP can be observed from the spectrum of 20HEMA-7.5TiO_2 (Figure 2-14a), which indicates that much more CaP has been formed on the 20HEMA-7.5TiO_2 hydrogel in comparison to that formed on the 40HEMA-7.5TiO_2. After 28 days incubation, a peak at 32° (corresponding to hydroxyapatite-like CaP) became obvious, presenting a continuous growth of CaP on both hydrogels. Also, the continuous growth of CaP on 20HEMA-7.5TiO_2 was shown by the relatively high intensity of the CaP peak in comparison to the peaks corresponding to TiO_2 (2θ=25.2°). The relative intensity of the CaP on 20HEMA-7.5TiO_2 was still much higher than 40HEMA-7.5TiO_2 after 28 days incubation.

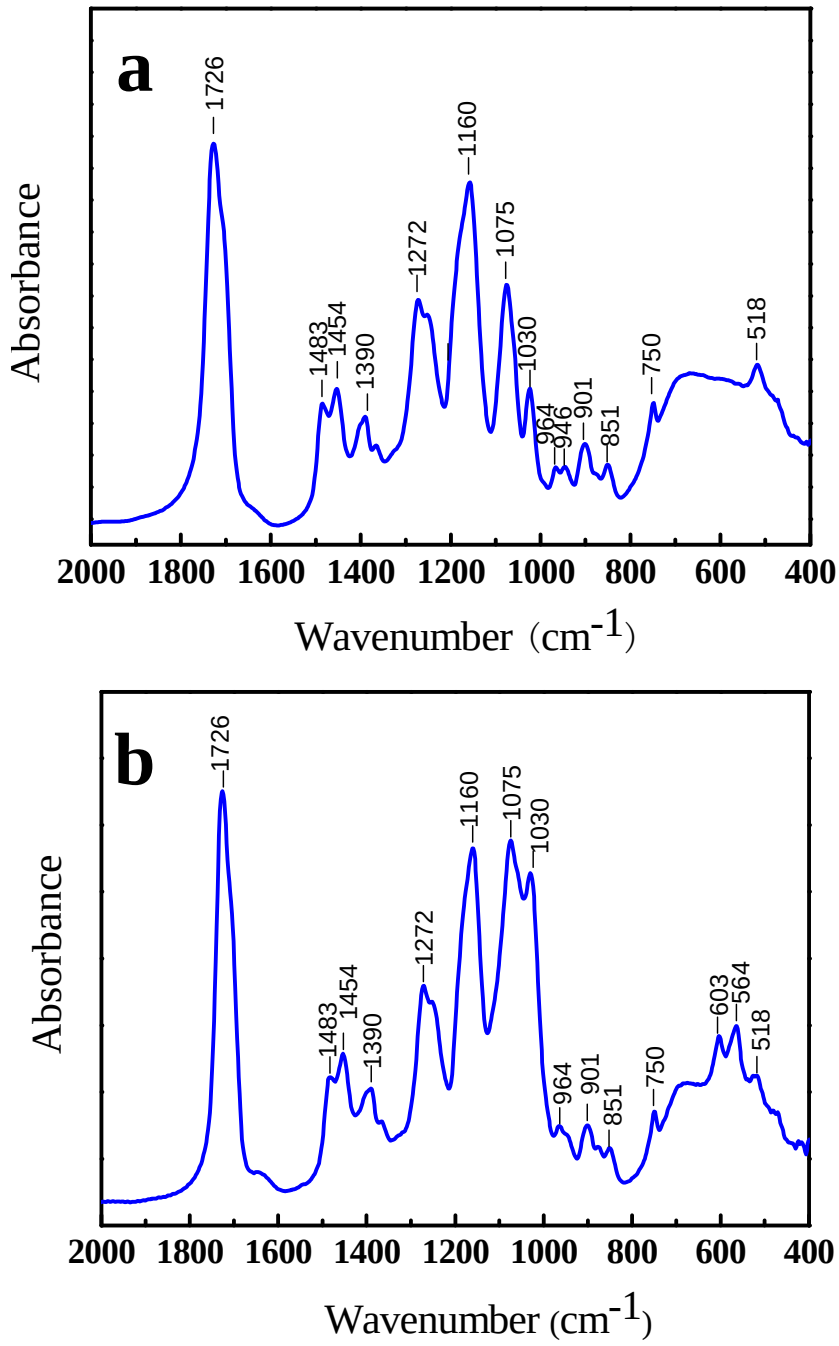

Figure 2-13 FTIR spectra of 10HEMA-7.5TiO_2 composite hydrogels (a) before and (b) after 10 days incubation in SBF

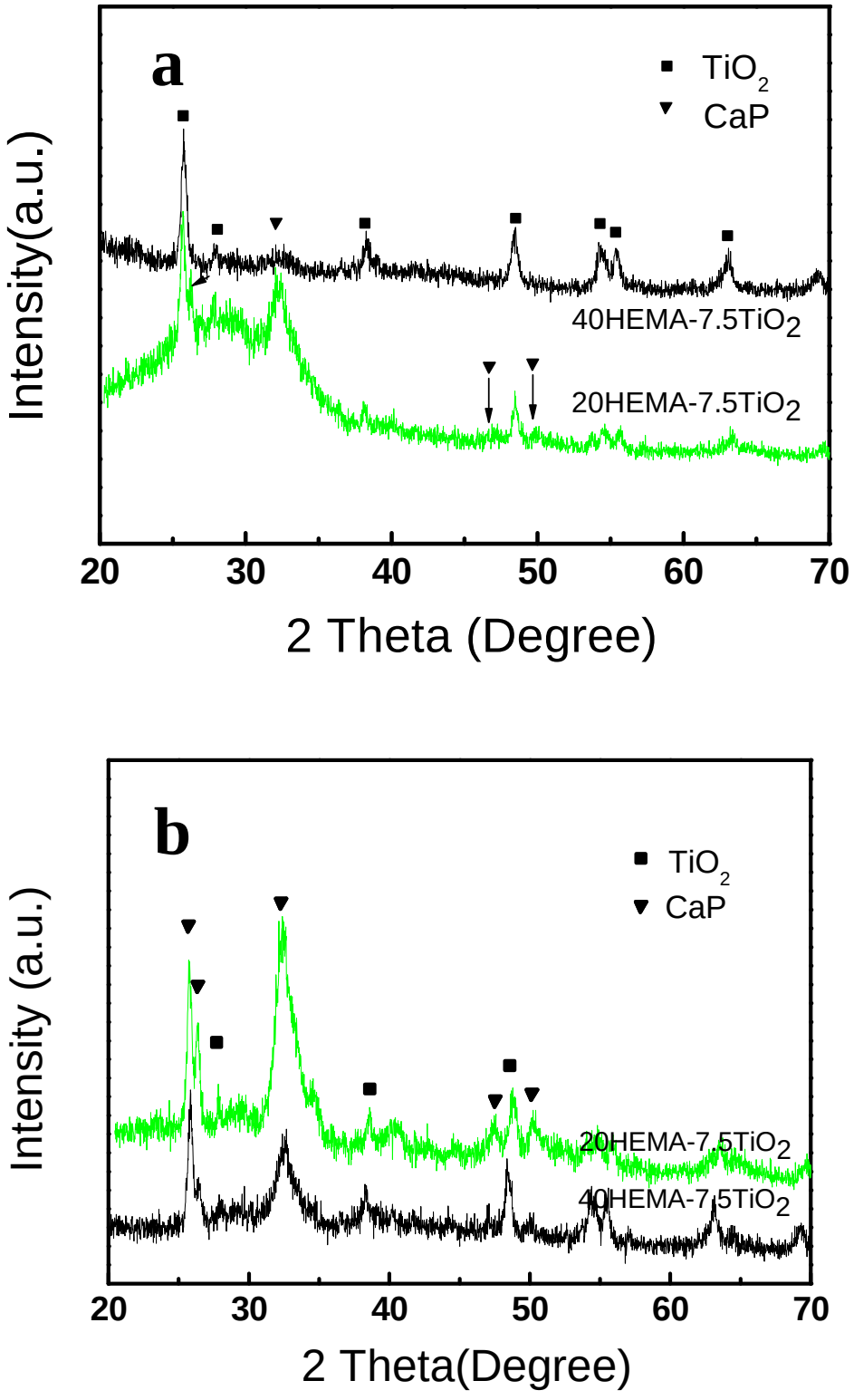

Figure 2-14 XRD spectra showing the formation of CaP on selected hydrogels after (a) 14 and (b) 28 days incubation in SBF

XRD spectra in Figure 2-15 show the growth of CaP in 20HEMA and 20HEMA-7.5TiO_2 at various time points. As can be noticed, there was no CaP formed on 20HEMA after 14 days incubation, whereas a small amount of CaP was formed on 20HEMA after 28 days incubation (Figure 2-15 a). However, strong peaks, attributed to CaP on the 20HEMA-7.5TiO_2 composite hydrogel, were found after 14 days incubation, indicating an enhancement of the calcification capability after the addition of TiO_2 nanoparticles. Continuously increasing amounts of CaP were verified, when the incubation time lasted for 28 days, by comparing the relative intensity of CaP peaks with that of TiO_2 nanoparticles (Figure 2-15 b).

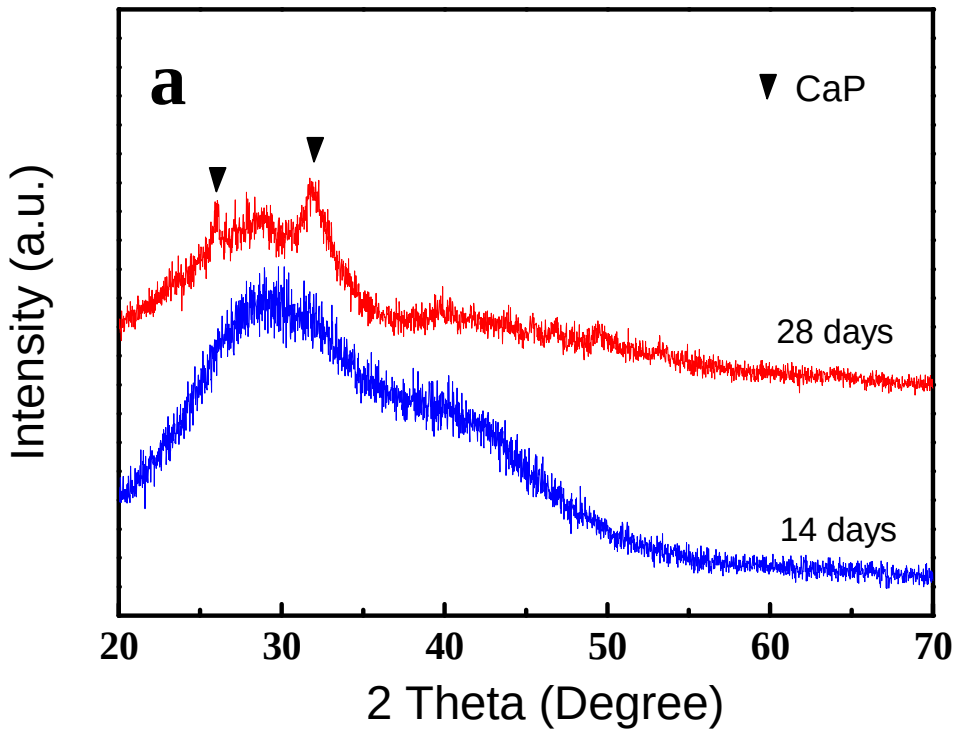

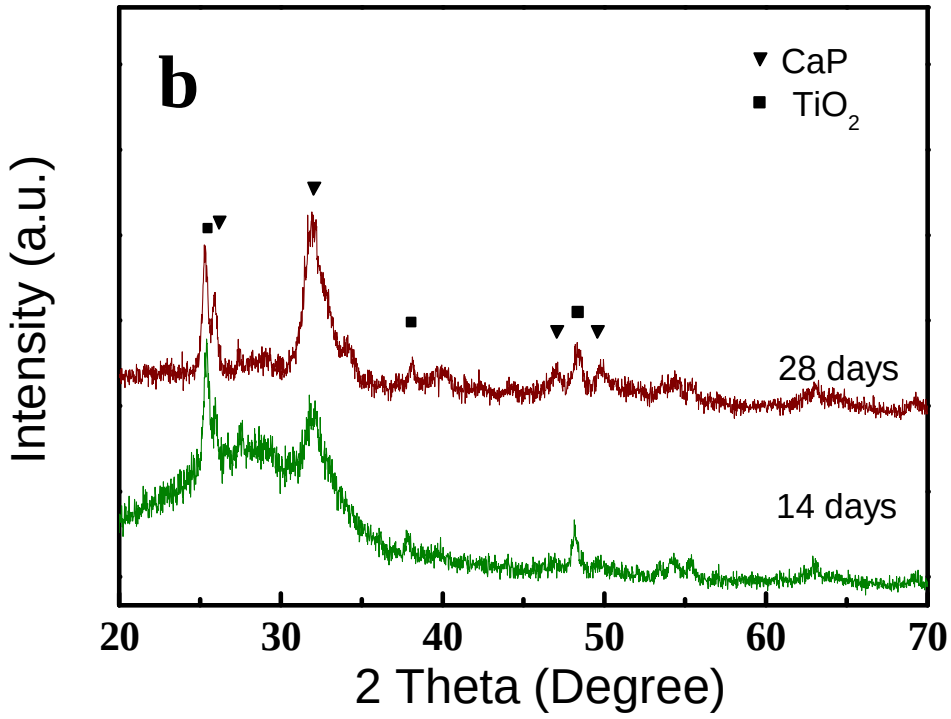

Figure 2-15 XRD spectra of (a) 20HEMA hydrogel after 14 days and 28 days incubation in SBF (b) 20HEMA-7.5TiO_2 hydrogel after 14 and 28 days incubation in SBF

SEM examination revealed CaP deposits on the composite hydrogel 20HEMA-7.5TiO_2 at as early as day 3 (Figure 2-16a). With the increase in the SBF incubation time to day 14 and 28, increased CaP formation also was observed (Figure 2-16b and 2-16c). A mixture of both singular spherical and the aggregated form of CaP was observed. This formation characteristic of CaP also has been reported on other types of PHEMA hydrogel (Zainuddin et al. 2006). On day 28, the surface of the TiO_2-containing hydrogel became fully covered with CaP.

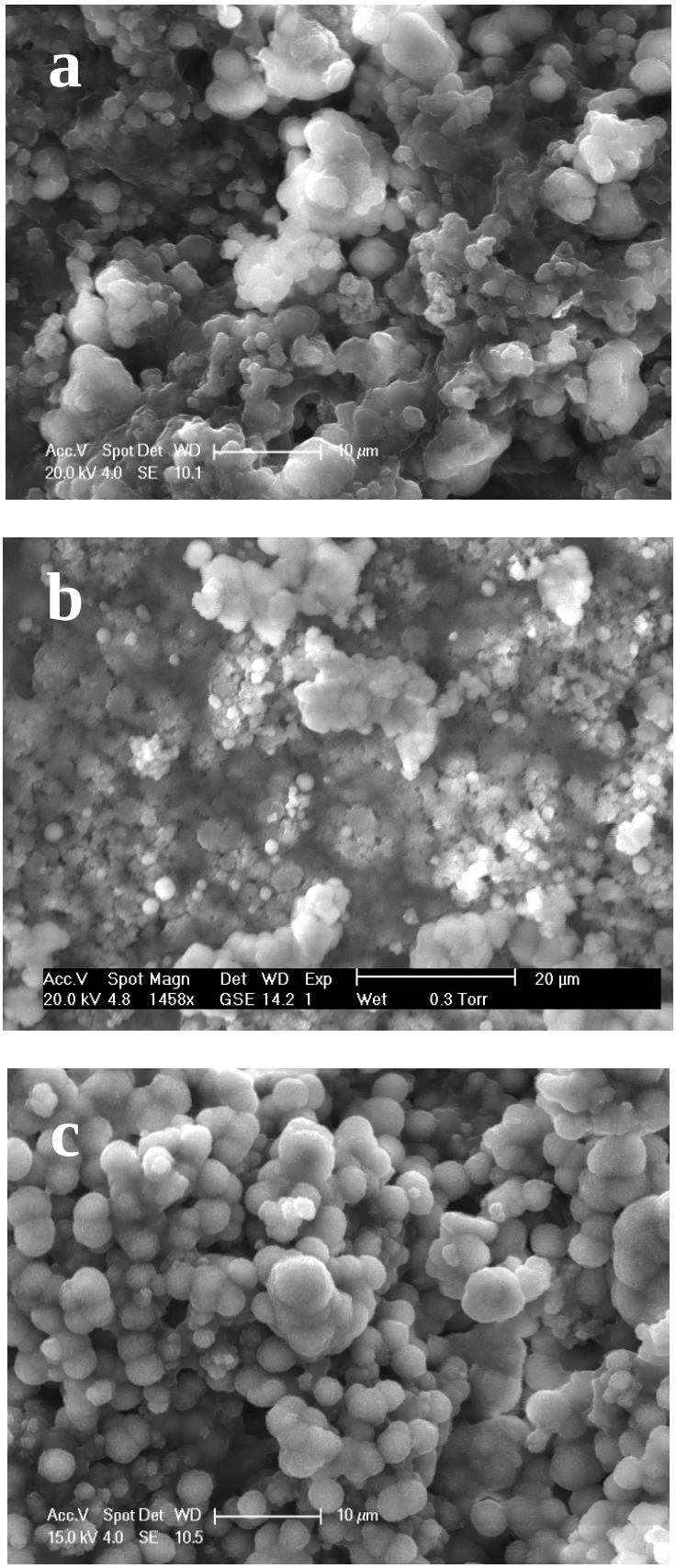

Figure 2-16 SEM micrographs of 20HEMA-7.5TiO_2 sponge after (a) 3, (b) 14, and (c) 28 days incubation in SBF

The penetration of CaP during the formation process also was examined by SEM on the cross-sections of the specimens, (see Figure 2-17). The images demonstrate that most CaP formation occurred on the surface closest to the edge of the hydrogels. Based on the micron bar of the images, the thickness of the formed CaP layer increased significantly from around 30 μm in the control 20HEMA hydrogel, to 70 μm in the 40HEMA-7.5TiO_2 composite hydrogel, and further increased to 120 μm in the most porous hydrogel, 10HEMA-7.5TiO_2.

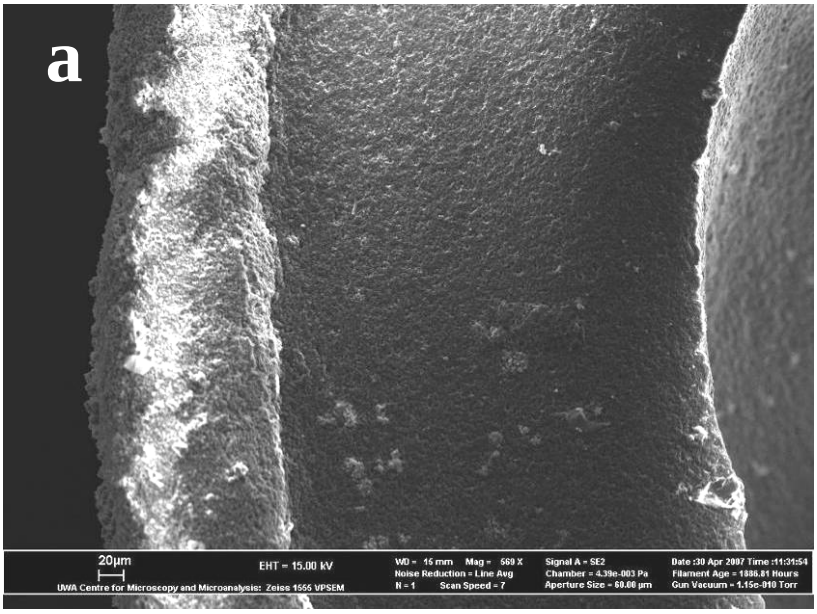

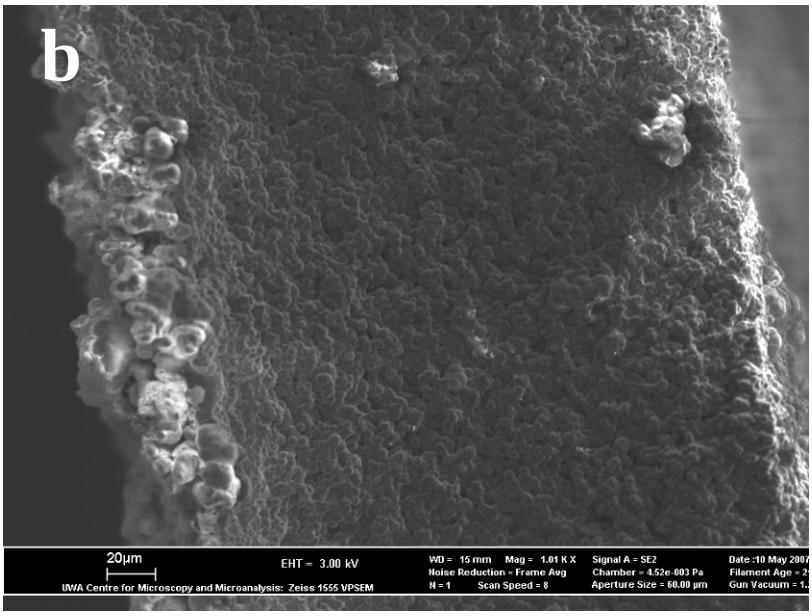

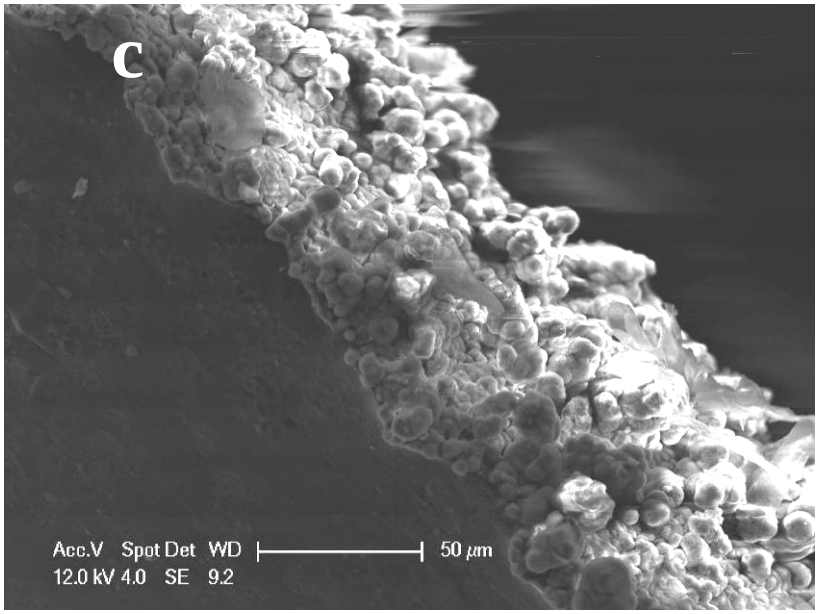

Figure 2-17 SEM micrographs showing the cross-sectional view of (a) 10HEMA-7.5TiO_2, (b) 20HEMA, and (c) 40HEMA-7.5TiO_2 composite hydrogels after 28 days incubation in SBF

The formed CaP on various hydrogel materials after 28 days incubation was stained with Alizarin Red S (Lou et al. 2005). The stained CaP layer formed on different hydrogels is shown clearly by the orange-coloured layers seen in Figure 2-18. A similar trend was found for the thickness of the CaP layer in comparison to the previous findings (Figure 2-17). The results show significant enhancement in calcification capacity in all PHEMA-TiO_2 hydrogels (Figures 2-18b to 2-18d). A limited amount of CaP was found in 20HEMA (Figure 2-18 a). Infiltration of calcium up to 800-1000 μm was observed in 10HEMA-7.5TiO_2 and 20HEMA-7.5TiO_2 (Figures 2-18b to 2-18c). Diffusion of calcium ions was less than 100 μm in 40HEMA-7.5TiO_2 (Figure 2-18d). The rapid infiltration of calcium ions must be due to the porous structure of the hydogels. These findings signify that the formation of CaP is strongly dependent on the bioactivity of TiO_2 nanoparticles.

The estimated thickness values of CaP layers using the staining method is generally greater than those from SEM images. This is understandable since the staining was carried out using fully hydrated samples whilst the samples examined by SEM were dehydrated.

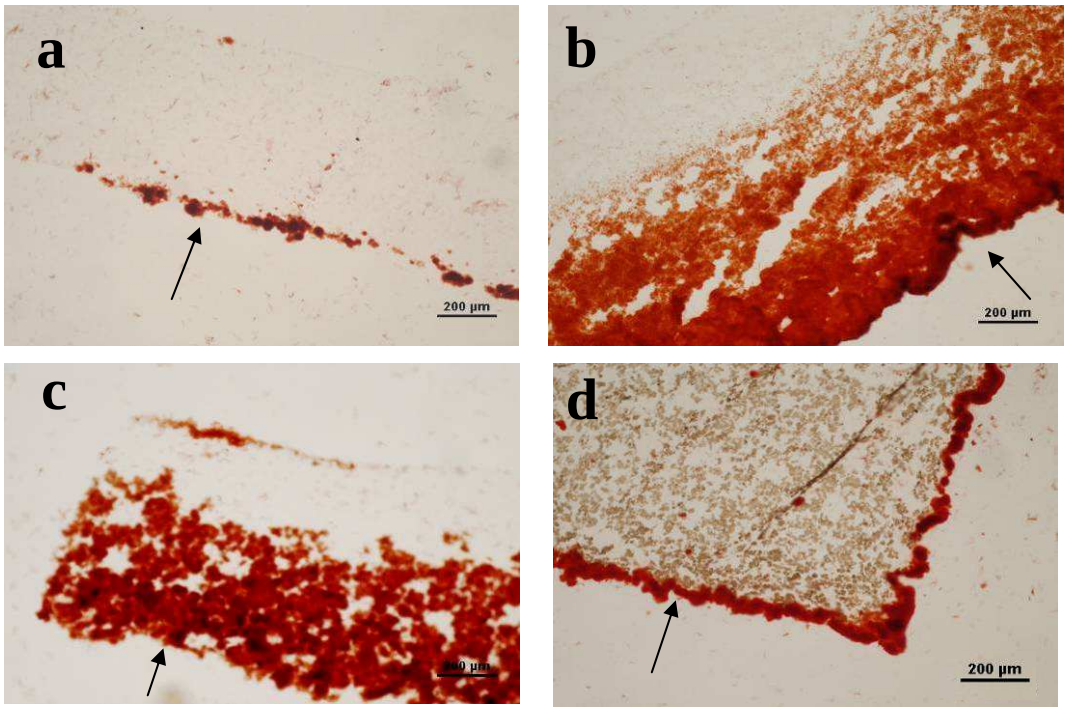

Figure 2-18 Light micrographs of (a) 20HEMA, (b) 10HEMA-7.5TiO_2, (c) 20HEMA- 7.5TiO_2, and (d) 40HEMA-7.5TiO_2 hydrogels after incubation in SBF for 28 days. The arrows indicate the top surface of the hydrogels where the CaP formation and infiltration started. The orange-red coloured areas represent the thickness of the formed CaP in each hydrogel

2.3.6. Cell Viability

A group of composite hydrogels containing 30 wt% HEMA, but with different additives (TiO_2, SiO_2, CNT) was selected to evaluate the influence of the additives on cell viability. The results are displayed in Figure 2-19. Results from 30HEMA hydrogel and a cell culture plate (TPP, Transadingen, Switzerland) are shown as the control. It was clear that no apparent cell growth had occurred after Day 1, particularly for the composite hydrogel containing CNT, whereas significant cell growth was seen at Day 3. The NIH 3T3 fibroblast cells continued growing and proliferating, and the cell numbers increased greatly for all hydrogels. This comparison of cell growth on composite hydrogels containing different additives showed that 3T3 fibroblast cells proliferate more rapidly on 30HEMA and 30HEMA-10TiO_2 hydrogel than on 30HEMA-10SiO_2 and 30HEMA-0.5CNT.

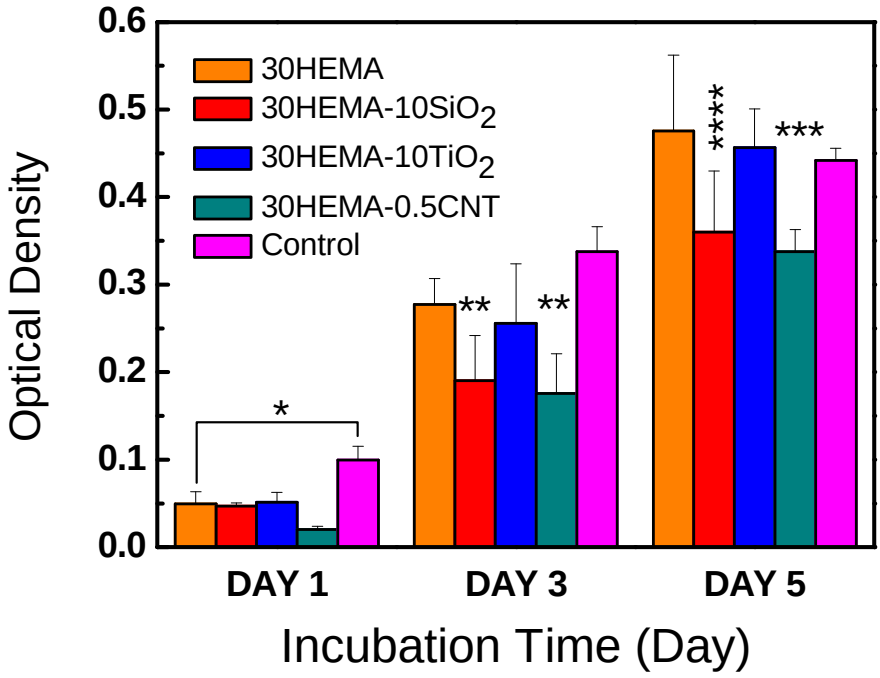

Figure 2-19 *In vitro* cell viability measured by MTT assay. The optical density values are proportional to the numbers of the living cells. (*) indicates there is no significant difference for Day 1, (**) indicates results at Day 3, where 30HEMA-10SiO_2 and 30HEMA-10CNT are significantly different from the Control at the same period of time, but not significantly different from the rest of the hydrogels, (***) shows that, at Day 5, 30HEMA-10CNT is significantly different as compared to the Control at Day 5 and the rest of the hydrogel samples, (****) shows that, at Day 5, 30HEMA-10 SiO_2 is significantly different as compared to the hydrogels including 30HEMA and 30HEMA-10TiO_2

Figure 2-20 shows the NIH 3T3 fibroblast cell viability as a function of incubation time on PHEMA-7.5TiO_2 composite hydrogels containing different concentrations of HEMA monomer. 20HEMA hydrogel is an United States of America Food and Drug Administration (FDA) approved material for ophthalmic implants (Lou, Munro, and Wang 2004; Vijayasekaran et al. 2000) and, therefore, is used as a control material. The results from the cell culture plate also are shown as a control. No significant difference among the materials was observed after Day 1, attributed to the recovery of the cells from the culture conditions. Apparent cell growth was demonstrated in all hydrogel materials on Day 3. There was no significant difference between the cell viability of the control hydrogels and that of the composite hydrogels, 10HEMA-7.5TiO_2, 20HEMA-7.5TiO_2 and 40HEMA-7.5TiO_2. A reduction of cell growth on 40HEMA-7.5TiO_2 and a significant reduction on 30HEMA-7.5TiO_2 were observed

on Day 3, which was probably due to the less porous surface structures of these two hydrogels (Figure 2-8 and Figure 2-9). The results from the cell culture plate at Day 3 showed a significant difference among all hydrogel samples.

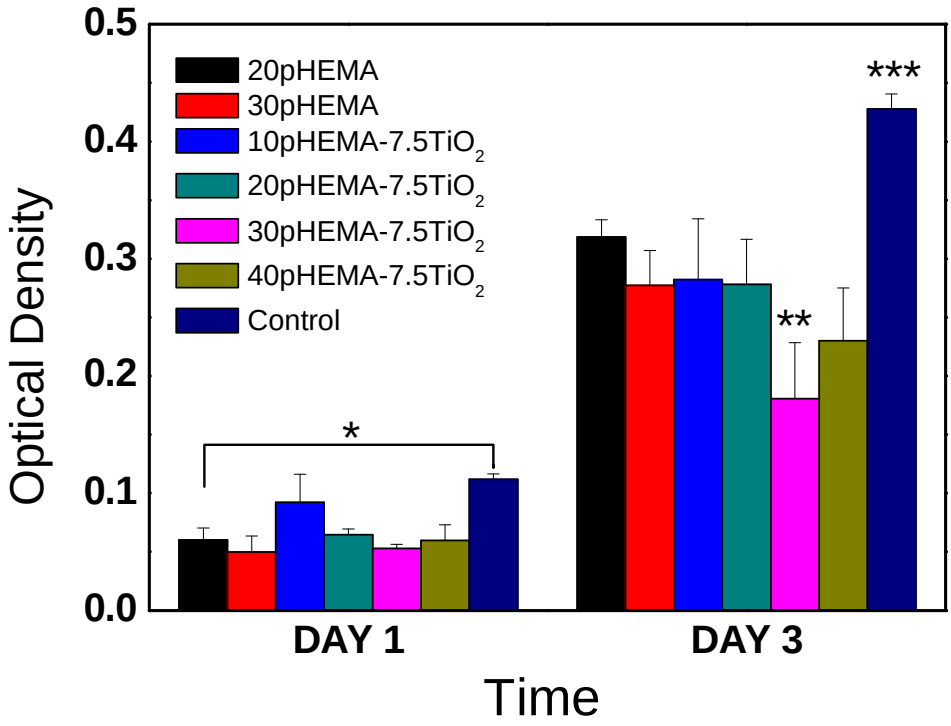

Figure 2-20 *In vitro* cell viability measured by MTT assay. The optical density values are proportional to the numbers of the cells. (*) indicates there is no significant difference for Day 1, (**) indicates, at Day 3, 30HEMA-TiO_2 is significantly different from the rest of the hydrogels, (***) shows that, at Day 3, the control sample is significantly different in cytotoxicity as compared to the hydrogel samples

2.4. Conclusions

Eighteen porous PHEMA composite hydrogels containing various amounts of nanoadditives, together with five control PHEMA hydrogels, were successfully prepared through a free radical polymerization process in the presence of water.

SEM examinations indicated the presence of macroporous structure in all hydrogels. The porous structure of the resultant hydrogels was largely dependent on the amount of water used in the polymerisation process. In general, higher water content was beneficial for a more porous structure formation. The addition of the additives had no

obvious influence on the porosity of the hydrogels containing the same amount of HEMA monomer when their concentrations were less than 30%. Therefore, the results demonstrated that the macroporous structure of the hydrogel polymers can be tuned simply by adjusting the chemical composition of the formula.

A calcification study demonstrated that the calcification capacity of porous PHEMA hydrogels can be enhanced significantly using TiO_2 nanoparticles. Changing of porosity also can improve the ability to enhance and the infiltration capacity of the calcium phosphate deposits.

MTT assay has demonstrated that most hydrogels were well tolerated by 3T3 fibroblast cells. In comparison of cell activities on composite hydrogels containing TiO_2 nanoparticles, a reduction of cell growth on 40HEMA-7.5TiO_2 and a significant reduction on 30HEMA-7.5TiO_2 were observed on Day 3, which was probably due to reduced porous surface structures of these two hydrogels after the incorporation of the nanoadditives.

Based on the above results, the TiO_2 nanoadditive has been chosen for further investigation, including mechanical responses and drug transport properties, for following chapters.

CHAPTER 3 TENSILE AND RHEOLOGICAL RESPONSES OF PHEMA AND PHEMA-TiO_2 COMPOSITE HYDROGELS

3.1. Introduction

The focus of this chapter is to evaluate the tensile and rheological responses of porous PHEMA and PHEMA-composite hydrogels. The tensile tests were conducted using fully hydrated hydrogel specimens according to a standard-D2116 from American Society for Testing and Materials (ASTM D2116). Three different modules were used in rheological measurements. These include oscillation strain sweep, oscillation amplitude sweep, and controlled creep-recovery tests. The mechanical properties of the hydrogels were correlated with the structures and the compositions of the hydrogels.

The mechanical properties of a tissue scaffold for engineering tissues are of great importance. In general, the scaffold should exhibit sufficient mechanical strength to maintain the spaces required for cell in-growth and tissue formation. It must also provide sufficient temporary mechanical support, matching the mechanical properties of the host tissue in order to bear in vivo stresses/strains. Moreover, mechanical forces play an important role in the homeostasis, remodelling, and repair of load-bearing tissues, such as bone and cartilage (Puppi et al. 2010).

A wide range of methods can be used to characterize the mechanical properties of the tissue substrates. These include tensile, compressive, and rheological testing methods which are often performed directly on bulk materials. AFM-related techniques are also used working on small volumes of tissue scaffolds (Engler et al. 2004). Tensile tests have been extensively used to characterize the tissue scaffolds, so properties including ultimate tensile stress (strain), tensile modulus, Poisson's ratio, and equilibrium relaxation modulus can be obtained. Properties such as aggregate modulus, hydraulic permeability, and young's modulus can be gained though compressive tests (Moutos, Freed, and Guilak 2007).

Rheological test is a one of the commonly used methods for the characterization of the viscoelastic properties of soft materials and/or tissues. Properties including equilibrium shear modulus, complex shear modulus, and loss angle can be obtained (Moutos, Freed, and Guilak 2007). These parameters determine the capability of materials to dissipate mechanical energy, covering a few influencing factors, including temperature, frequency and shear amplitude. In addition, most of the living tissues in the human body exhibit viscoelastic behaviour and thus comprehensive characterizations of these living tissues using rheological tests provide criteria for designing suitable tissue scaffolds.

Rheological test can be performed using different modules, such as creep, relaxation and oscillatory tests. In a creep test, a shear stress is applied onto the materials through different loading modes, resulting in a deformation measured as a function of time. A recovery segment is normally linked to the creep test, in which the shear stress is set to zero. Thus, the resultant deformation from the creep test can recover at zero stress level and the recoverable portion of the deformation can be determined based on the stress levels.

Oscillatory rheology is the most commonly used technique for understanding the structural and dynamic behaviour of materials (Macosko 1994). Two methods in the present study, including oscillation strain sweep and oscillation amplitude sweep, are based on the oscillatory mode. The principle of oscillatory rheology is to induce a sinusoidal shear deformation (γ) in the sample and measure the resultant stress (σ) response. Figure 3-1 illustrates a loaded hydrogel sample parallel-plate configuration during a test, in which a specimen is placed between two plates and a sinusoidal force is applied on the specimen. The shear deformation can then be created onto the hydrogel as the force is applied onto the hydrogel sample for a period ($t_0 \rightarrow t_1$). At a time point (t), the shear strain can be expressed by $\gamma = \gamma_0 \sin(\omega t)$, where γ_0 is the shear amplitude, ω the oscillation frequency. Simultaneously, a stress response from the soft sample can be determined by $\sigma(t) = G'(\omega)\gamma_0 \sin(\omega t) + G''(\omega)\gamma_0 \cos(\omega t)$, in which $G'(\omega)$ is the elastic modulus and $G''(\omega)$ the viscous modulus. Both moduli represent the viscoelastic properties of the material, from which the complex

modulus of the hydrogel can be derived using $G^* = G' + iG''$. The magnitude of the complex modulus | G* | can be obtained by $|G^*| = \sqrt{G'^2 + G''^2}$. The ratio of viscous and elastic modulus, $\frac{G''}{G'} = \frac{\sin(\omega t)}{\cos(\omega t)} = \tan\delta$ shows the phase shift between two modules, where δ is the phase shift. The same principle is applied for the stress controlled test. The value of δ for a soft material lies between that of solids and liquids, $0 < \delta < \pi/2$.

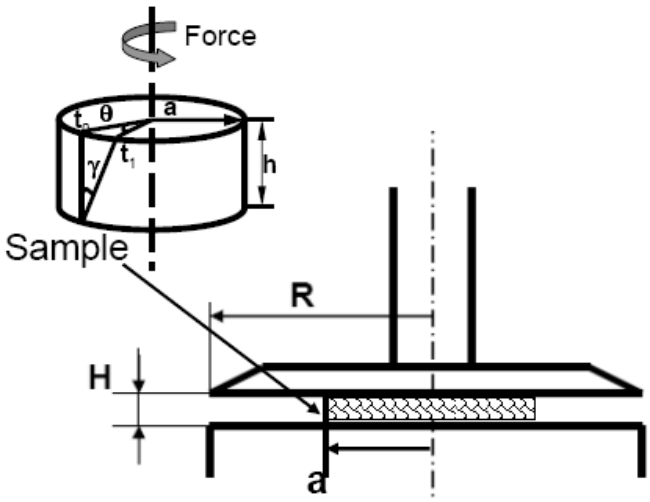

Figure 3-1 Schematic illustration of a loaded hydrogel button in the parallel-plate configuration; h is the thickness of the hydrogel, a is radius of the hydrogels, γ is the shear strain, θ is angular displacement, H is the gap size and R is the radius of the plate

The oscillation strain sweep test is employed to determine the limit of linear viscoelasticity of a material. The test is conducted at constant frequency with varying strain amplitude until a particular value, in which a critical point can be found where dynamic properties (G', G") remain steady. The values of G', G" begin to change beyond this range. Thus, this point in strain represents the limit of linear viscoelasticity. The material displays non-linear viscoelastic behaviour beyond that point.

The oscillation amplitude sweep is conducted by applying a small sinusoidal strain (within the linear viscoelastic range) at a range of frequency. The levels of G', G" and δ at a particular range of frequency are determined.

The G', G" and δ values, together with other properties including the strength, modulus and recovery, allow for correlating the dynamic mechanical behaviour of the materials with physiological requirements for tissue substitutes. Understanding of these properties is very important for the ultimate usage of the materials as tissue engineering scaffolds.

In order to fully understand the mechanical properties of porous PHEMA and PHEMA-TiO_2 composite hydrogels, the characterizations of tensile and viscoelastic properties of the hydrogels were conducted on a series of materials containing different concentrations of HEMA and TiO_2 nanoadditives.

3.2. Experimental

3.2.1. Hydrogel Selection

Hydrogel polymers selected for this study are listed in Table 3-1. Tensile tests were conducted on four composite hydrogels including 10HEMA-7.5TiO_2, 20HEMA-7.5TiO_2, 30HEMA-7.5TiO_2 and 40HEMA-7.5TiO_2. Rheological tests were conducted on five composite hydrogels including 25HEMA-3TiO_2, 25HEMA-7.5TiO_2, 25HEMA-12TiO_2, 30HEMA-7.5TiO_2 and 40HEMA-7.5TiO_2. Control PHEMA hydrogels were also tested using the same methods to investigate the influence of the TiO_2 nanoparticles on the mechanical properties.

Table 3-1 Hydrogels for tensile and rheological tests

Hydrogel codes	Tensile test	Rheological test		
		Oscillation strain sweep	Oscillation frequency sweep	Creep recovery
10HEMA	√			
10HEMA-7.5TiO_2	√			
20HEMA	√			
20HEMA-7.5TiO_2	√			
25HEMA		√	√	√
25HEMA-3TiO_2			√	√
25HEMA-7.5TiO_2		√	√	√
25HEMA-12TiO_2			√	√
30HEMA	√	√	√	√
30HEMA-7.5TiO_2	√	√	√	√
40HEMA	√	√	√	√
40HEMA-7.5TiO_2	√	√	√	√

3.2.2. Tensile Tests

Tensile testing was carried out using a SINTECH® 200/M Material Testing Workstation (MTS Systems Corporation, USA) (Figure 3-2 a). Dumb-bell shaped specimens were cut from fully hydrated hydrogel samples to the dimensions recommended by ASTM D2116 (Figure 3-2 b). The working length of the central part was 13 mm and the thicknesses of the hydrogels were measured by a digital calliper. The movement of crosshead was controlled at a speed of 0.5 mm/s until the hydrogel specimen was broken. The measurements were conducted at room temperature. The modulus, tensile strength and percentage elongation at break point were recorded and average values were taken from five measurements. Mean ± standard deviation and the P value were calculated using one-way ANOVA with OriginPro (Version 7.5) software and Turkey test. P values <0.05 were considered statistically significant.

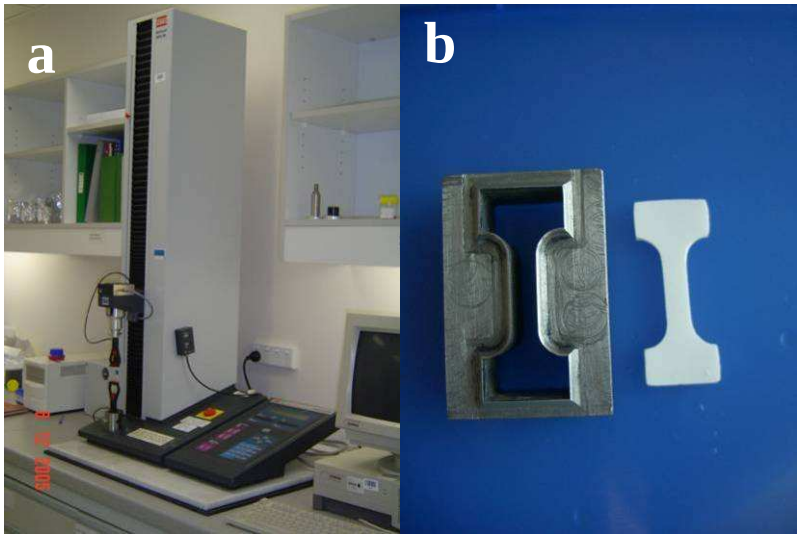

Figure 3-2 (a) SINTECH® 200/M material testing workstation and (b) a dumb-bell shaped specimen and the sample cutter

3.2.3. Rheological Characterizations

The rheological properties of the hydrogel specimens were carried out using a HAAKE MARS III Modular Advanced Rheometer System (Thermo Electron, Germany) with a stainless steel, parallel-plate geometry (Figure 3-3 a). The diameter of the plate geometry is 35 mm. Hydrogel specimens were cut from the hydrogel sheets into cylindrical disks with a diameter of 16 mm, followed by immersing in deionised (DI) water for over 12 hours for equilibrium prior to conducting the measurements (Figure 3-3 b). The thickness of the hydrogels (h) was measured using a digital calliper. The specimen was loaded onto the centre of the bottom plate of the rheometer. A gap size (H) was reached by lowering down the top plate to 0.9 h, which results in a compressive strain on hydrogel samples.

Ten percent compressive strain was used to ensure a complete torque transfer. Validation experiments were carried out to confirm that there was no interference to the testing result in such conditions (3.3.2.). This set-up was used for all rheological measurements, including strain sweep oscillation, oscillation amplitude sweep and creep-recovery tests. All tests were conducted at 25^{o}C, which was controlled by a DC 50 thermocontroller.

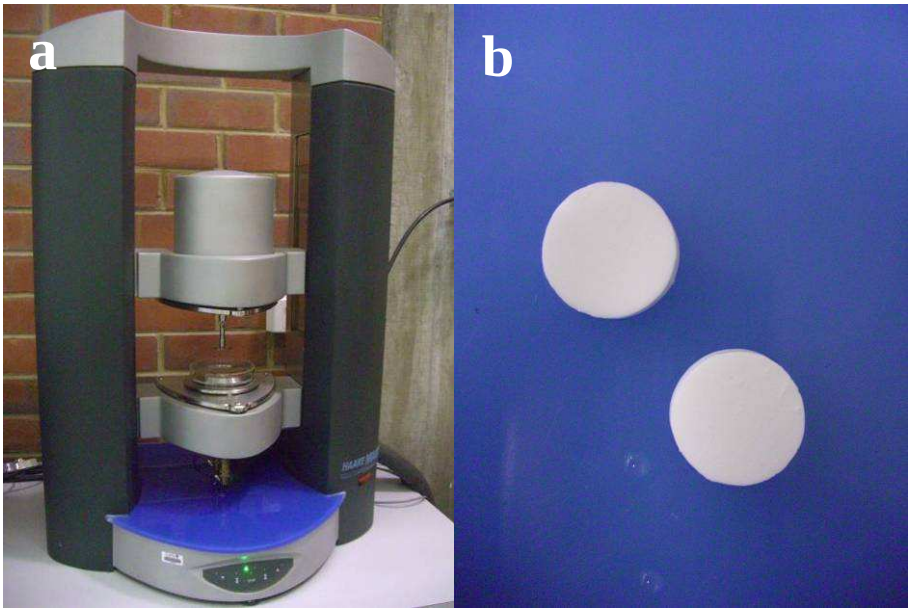

Figure 3-3 (a) HAAKE MARS III Modular Advanced Rheometer System and (b) hydrogel buttons for the rheological tests

Oscillation strain sweep

The oscillation strain sweep was conducted at a fixed frequency of 1 Hz under an increasing shear strain (γ_0), increasing from 0.05% to 50%. Elastic (G') and viscous (G″) moduli were recorded. Three measurements were conducted for each hydrogel formulation.

Oscillation frequency sweep

The hydrogels were subjected to fixed sinusoidal strain (0.35%) within the viscoelastic linear range. Elastic (G') and viscous moduli (G″) were recorded within a wide range of frequency, ranging from 0.02 to 20 Hz. Three measurements were carried out for each hydrogel formulation.

Creep-recovery test

The creep-recovery test was measured using a controlled stress method. Two different loading modes, Mode A and Mode B, were employed, shown in Figure 3-4.

In loading Mode A, a simultaneous shear stress (40, 75, 125 or 250 Pa) was applied onto a hydrogel specimen for 600 s followed by the recovery of the hydrogel that was recorded for 600 s after releasing the stress. The recoverable elastic portions were calculated. In Mode B, a stress was gradually applied from 0 to a selected value (75 Pa or 500 Pa) within 120 s and afterwards the shear stress was released. The recovery profile was recorded by shear strain γ as a function of relaxation time t.

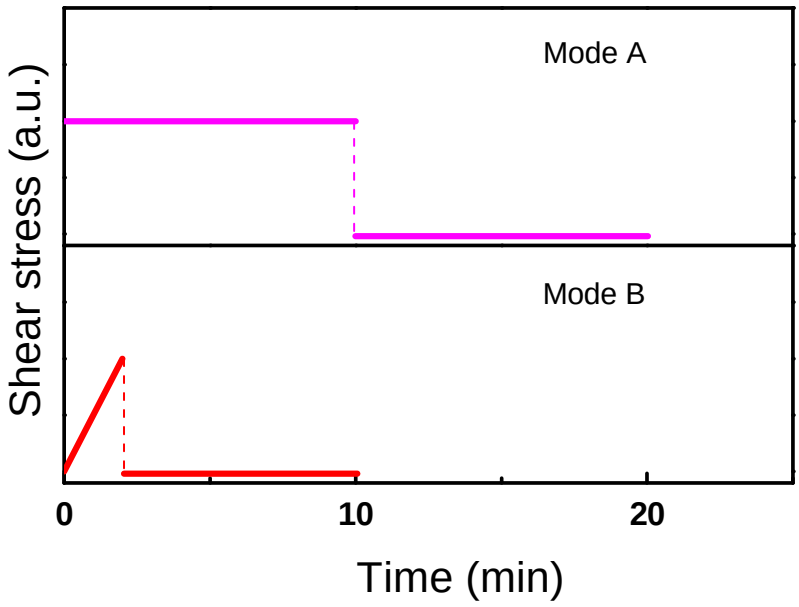

Figure 3-4 Illustration of the loading Mode A and Mode B applied in the creep-recovery test

3.2.4. Method Validation and Data Corrections

It should be noted that the values (shear strain) are based on measurements at the outer edge of the samples in the parallel plate configuration, where the strain is maximal (Instruction Manual, HAAKE MARS; Version 1.1). Since the diameter of the samples is smaller than the plate diameter R, the measured moduli are underestimated by a factor of $(R/R_{sample})^4$, where R= 17.5 mm and R_{sample}=8 mm, because the stress scales with R as $1/R^3$, while the strain is proportional to diameter. Therefore, the correction factor was 22.9 for elastic and viscous moduli and 0.46 for the strain.

3.3. Results and Discussion

3.3.1. Tensile Properties

Figure 3-5 shows (a) tensile modulus, (b) tensile strength and (c) elongation (%) of PHEMA and the composite PHEMA containing 7.5% TiO_2. Tensile modulus and strength of the composite hydrogels increased significantly with the increase in HEMA content in the monomer mixture. This is due to the decrease of porosity of the hydrogel materials (Figure 2-7 to 2-9 in Chapter 2). There was an increase in tensile strength in most composite hydrogels after the addition of TiO_2 particulates. The change became more significant in hydrogels containing higher HEMA content, such as 40HEMA-7.5TiO_2. A drastic reduction of tensile strength was observed for 20HEMA-7.5TiO_2 when compared with its control polymer 20HEMA (Figure 3-5 b). Repeated testing on the same hydrogel and those produced in different batches yielded similar results. Reasons are unknown. Change in tensile modulus by TiO_2 was insignificant and without an apparent pattern. This was probably due to the large pore sizes of the hydrogels and generally low concentration of TiO_2 particulates incorporated into the hydrogels.

PHEMA hydrogels containing a low HEMA concentration exhibited a greater elongation value. The percentage elongation was reduced when HEMA content was increased from 10 wt.% to 30 wt.% and then 40 wt.% (Figure 3-5 c). This is due to the increased density of the polymer structure that limits the capability of movement. For 10HEMA and 20HEMA, the addition of TiO_2 decreased the elongation of macroporous hydrogels. This could be due to the weakened conjunction force between hydrogel chains in the presence of the TiO_2 nanoparticles. An increase of elongation was observed for 30HEMA and 40HEMA composite hydrogels, which was attributed to their less porous structure, which was influenced after incorporating TiO_2 nanoparticles.

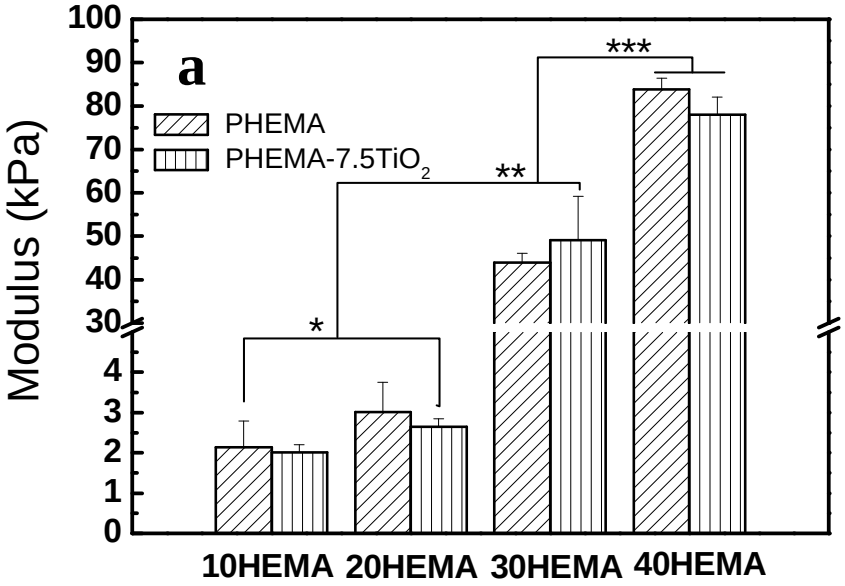
a
PHEMA
PHEMA-7.5TiO2
Modulus (kPa)
100
90
80
70
60
50
40
30
4
3
2
1
0
*
**
***
10HEMA
20HEMA
30HEMA
40HEMA

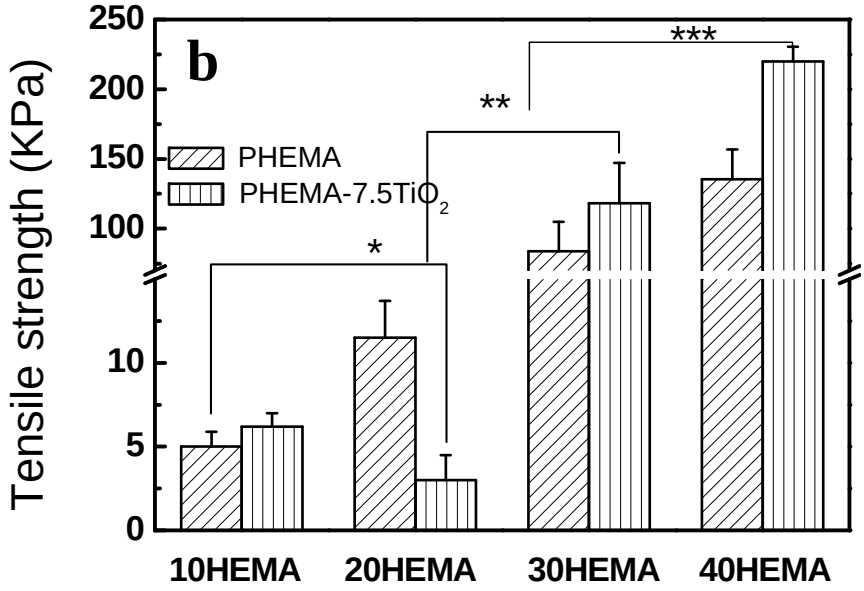
b
PHEMA
PHEMA-7.5TiO2
Tensile strength (KPa)
250
200
150
100
10
5
0
*
**
***
10HEMA
20HEMA
30HEMA
40HEMA

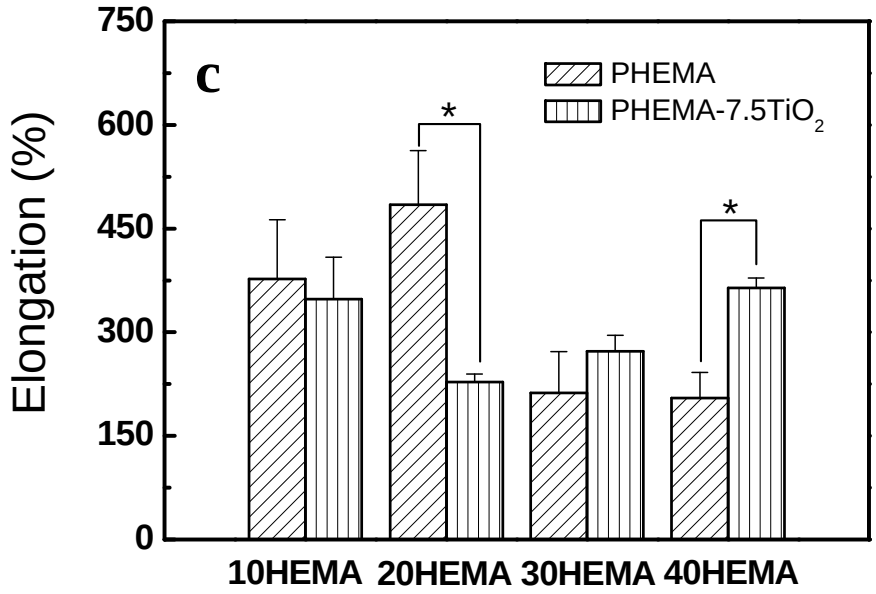

Figure 3-5 (a) Modulus, (b) tensile strength and (c) elongation of PHEMA and PHEMA-7.5TiO_2; in Figure (a) and (b): (*) indicates no significant difference among 10HEMA, 20HEMA and their composite, (**) and (***) indicate significant difference for 30HEMA, 40HEMA and their composite hydrogels; in Figure (c), (*) indicates significant difference between PHEMA and its composite hydrogel

3.3.2. Viscoelastic Properties

Shear Strain Influence

Figure 3-6 displays the elastic modulus G' and viscous modulus G″ from oscillation strain sweep on (a) PHEMA and (b) PHEMA-7.5TiO_2 composite hydrogels containing different HEMA concentrations. Hydrogels containing no TiO_2 nanoparticles (Figure 3-6 a) exhibited a linear viscoelastic dependence of up to 15-25% shear strain, whilst most composite hydrogels showed a linear dependence within a range of 1.7-10% (Figure 3-6 b). Hydrogels containing lower HEMA content, such as 25HEMA showed a wider range of linear viscoelastic dependence in comparison to that of both 30HEMA and 40HEMA hydrogels. This is true for both plain and composite hydrogels.

The increased linear viscoelasticity range observed in the hydrogels containing less HEMA was attributed to the more porous structure in these hydrogels, which ensured better material mobility and stretchability (Stavrouli, Aubry, and Tsitsilianis 2008).

The presence of TiO_2 nanoadditives can cause some defects in the hydrogels, which can be easily broken under shear forces. As a result, reduction in linear range was observed for hydrogels, especially in 30HEMA and 40HEMA.

The results also demonstrated that the moduli of the hydrogels were largely dependent on HEMA:water ratios in the hydrogels. In PHEMA hydrogels, the elastic and viscous moduli were increased from G': 19900 Pa; G″: 1900 Pa to G': 34000 Pa; G″: 3300 Pa, when HEMA content was increased from 25 wt.% to 30 wt.%. The moduli were further increased to about G':70000 Pa and G″: 7500 Pa for 40HEMA hydrogel, indicating an increasing elastic stiffness of the hydrogels as a result of increasing HEMA concentrations. The change of moduli in PHEMA-7.5TiO_2 composite hydrogels followed a similar trend as PHEMA hydrogels and there was no significant change of the values after incorporating the nanoparticles into the hydrogels. The lack of influence of TiO_2 addition on the stiffness of PHEMA hydrogels was due to the smaller size of the particles.

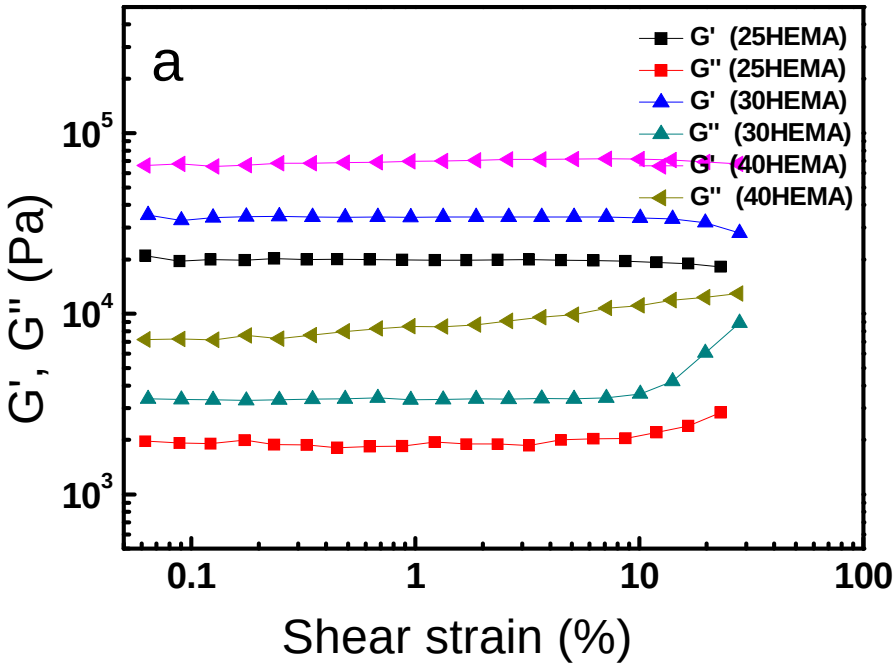

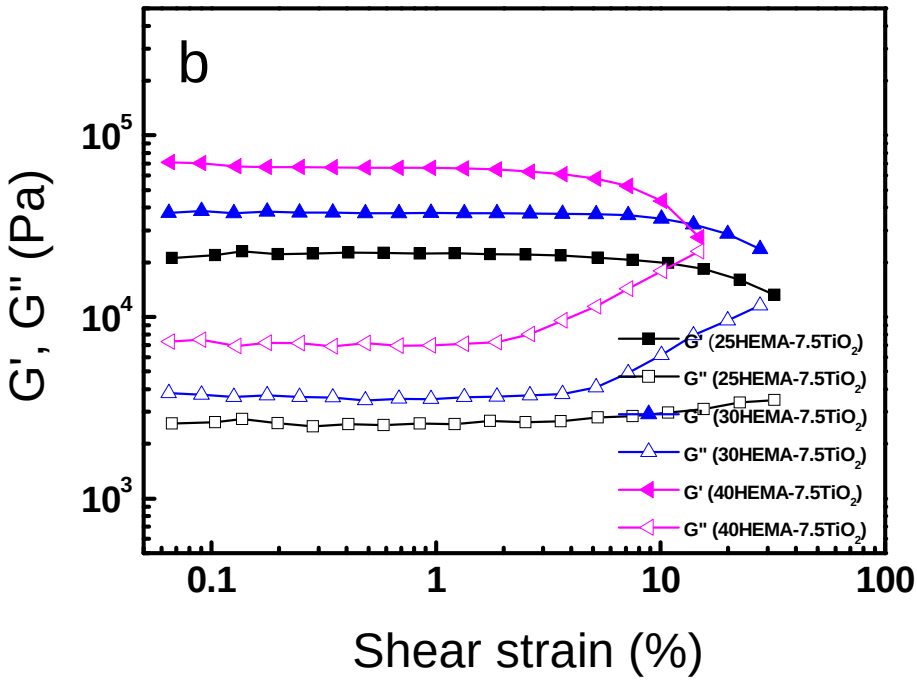

Figure 3-6 Strain sweep oscillation results of (a) PHEMA and (b) PHEMA-7.5TiO_2 hydrogels

A similar experiment was carried out on 25HEMA composite hydrogels containing CNTs. A more apparent increase in moduli in 25HEMA hydrogels containing CNTs was observed in comparison to that of blank 25HEMA (Figure 3-7 a). The values of the moduli values of the hydrogels are listed in Table 3-2. A significant increase was observed as CNTs were added into the hydrogel, while varying concentration of CNTs (0.5 and 2%) did not show a significant increase in the moduli, indicating a maximum improvement of moduli via the addition of CNTs. The increase of moduli in composite PHEMA containing CNTs was attributed to the long fibre structure (5-15 μm) of the multi-walled CNTs used in the investigations. Figure 3-7 b shows the fibre structure of the CNTs using a TEM micrograph.

Table 3-2 Elastic and viscous moduli of PHEMA hydrogels at a frequency of 1 Hz*

Sample codes	Elastic moduli (Pa)	Viscous moduli (Pa)
25HEMA	19700	2000
25HEMA-7.5TiO_2	22000	2600
25HEMA-0.5CNT	29600	4000
25HEMA-2CNT	31200	3900
30HEMA	34000	3900
30HEMA-7.5TiO_2	38000	3600
40HEMA	69000	9100
40HEMA-7.5TiO_2	68000	7100

*The results were summarised from strain sweep oscillation tests in the linear range (Figure 3-6).

It should be noted that for both the blank and composite hydrogels, elastic modulus G' maintained a higher level than viscous modulus G″ during the whole measurement range. This indicates that PHEMA and its composite hydrogels are highly elastic materials.

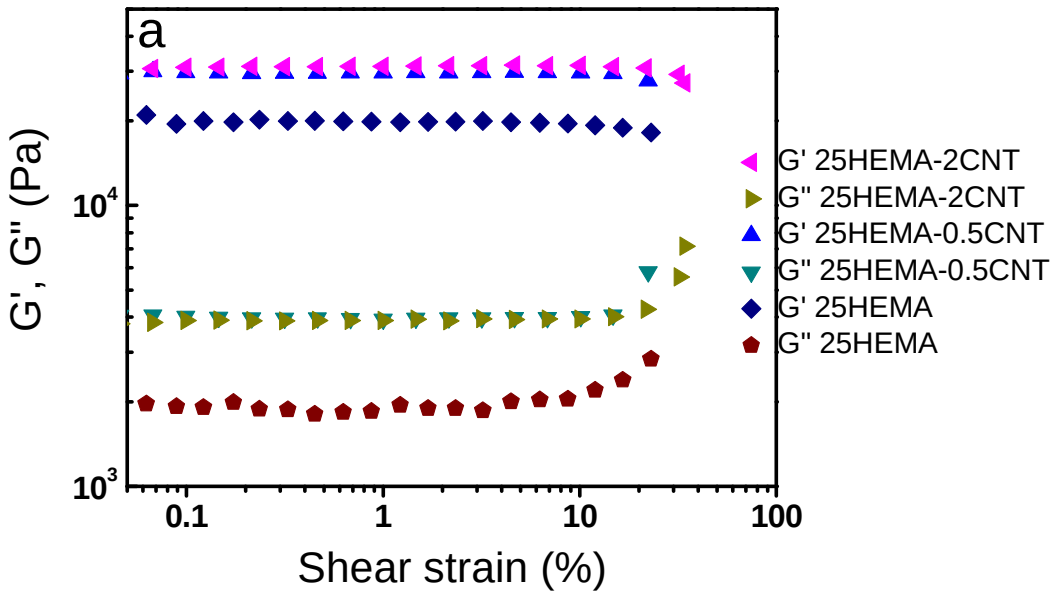

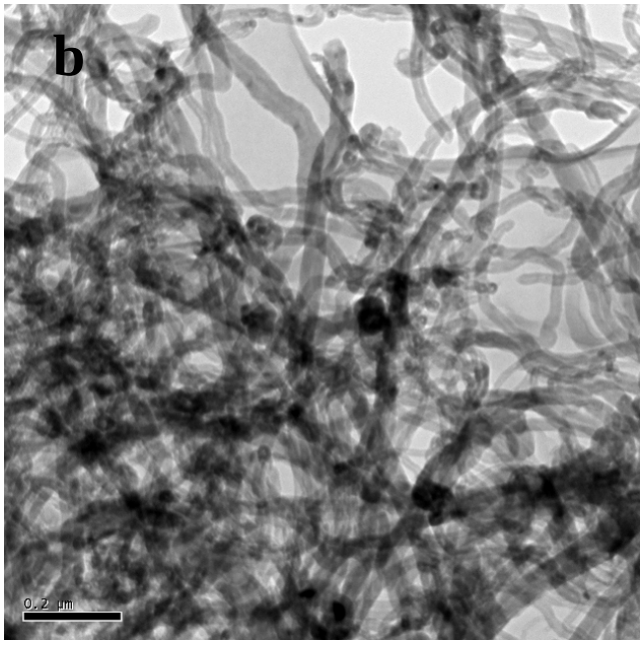

Figure 3-7 (a) Strain sweep oscillation results of PHEMA-CNT composite hydrogels and (b) a TEM micrograph of CNTs

Frequency influence

The complex modulus $|G^*|$ and the phase shift tanδ were used to investigate the effect of the oscillatory frequency on the viscoelastic properties of the composite hydrogels. As shown in Figure 3-8 a, the complex moduli of all hydrogels were frequency-dependent. Within the investigated frequency range (0.05-15 Hz), a continuous increase of complex modulus is demonstrated with an increasing frequency. This is a typical behaviour of strong gel, as described by Clark and Ross-Murphy (Clark and Ross-Murphy 1987).

The results also show that the hydrogels containing higher HEMA concentrations exhibited higher $|G^*|$ values. There was a increase in complex modulus in the composite hydrogels in comparison with the blank hydrogel polymers. However the influence of TiO_2 nanoparticles on $|G^*|$ was less prominent than that of HEMA content. When CNTs were incorporated into hydrogels, a more significant increase in the complex modulus was observed (Figure 3-9). This is again due to the size of the CNTs, which is about 5-15 μm.

The influence of frequency change on phase angle tanδ, representing the ratio of the viscous (G') and elastic (G″) portion of the viscoelastic deformation behaviour of the hydrogels, is displayed in Figure 3-8 b. It was found that the phase angle was increased with increasing frequency, indicating a more rapid increase in viscous modulus with the increase in the frequency of oscillation.

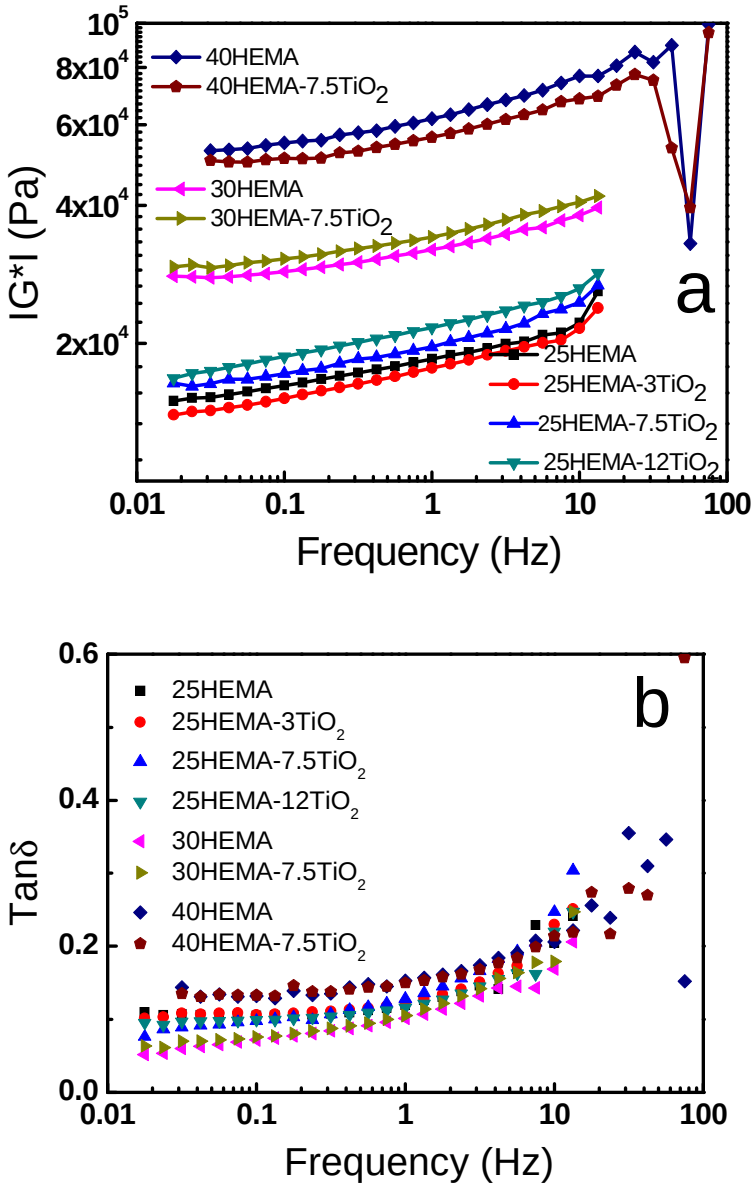

Figure 3-8 (a) Complex modulus | G* | and (b) tanδ of PHEMA and PHEMA-TiO_2 composite hydrogels under the influence of frequency

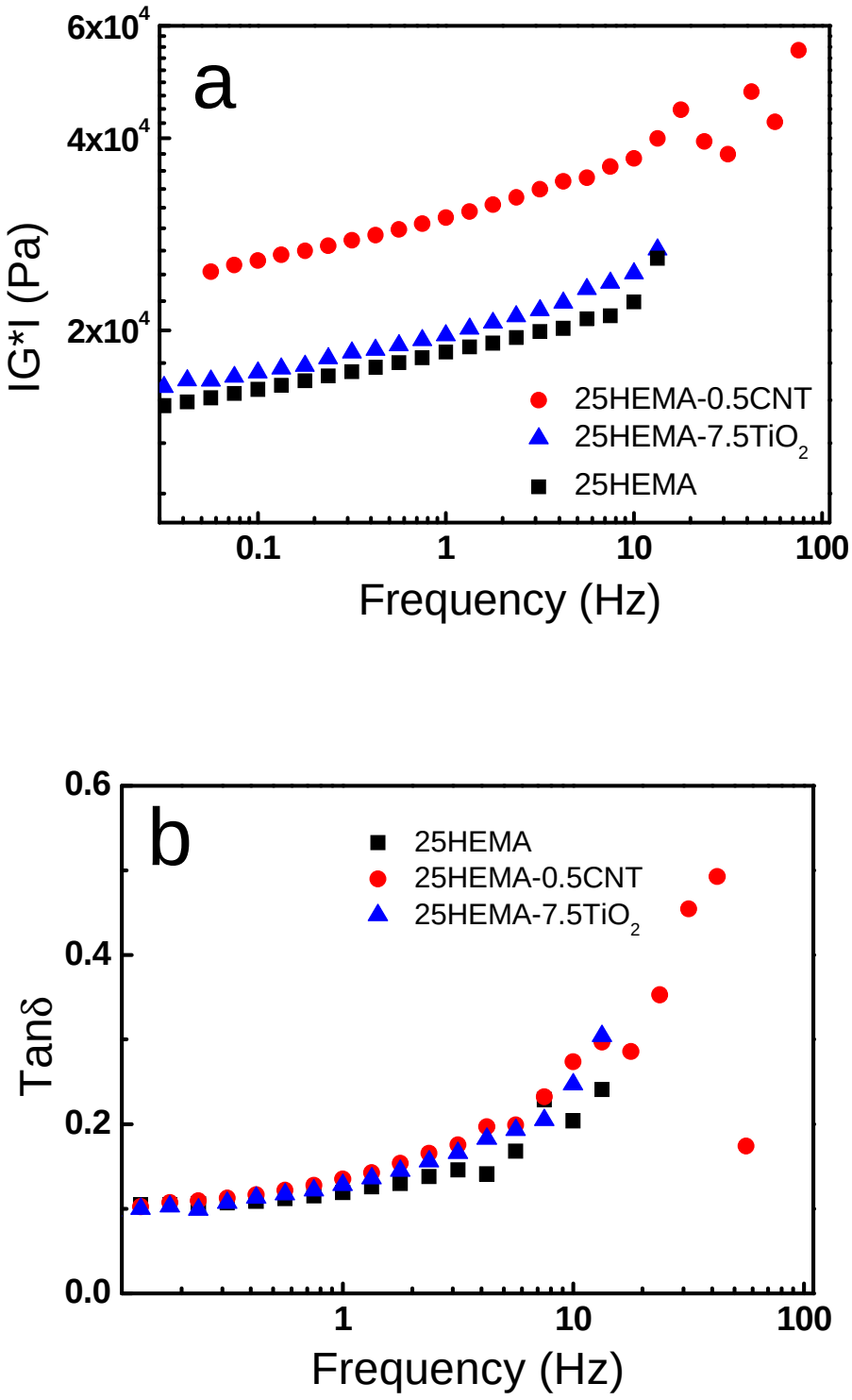

Figure 3-9 (a) Complex modulus | G* | and (b) tanδ of 25HEMA, 25HEMA-7.5TiO_2 and 25HEMA-0.5CNT hydrogels

Compressive strain influence

It should be noted that the above results were obtained at a 10% compressive strain. When a higher compressive strain (15%) was applied to the samples, similar responses were observed for the hydrogels. Figure 3-10 shows (a) the |G*| and (b) tanδ at 1 Hz and 0.35% shear amplitude, when two different shear strains were applied on the samples. There was no significant change on |G*| for majority hydrogels except 40HEMA hydrogel when the compressive strain was increased from 10% to 15%. As for tanδ, these was no significant change for all the hydrogels as different compressive strains were applied.

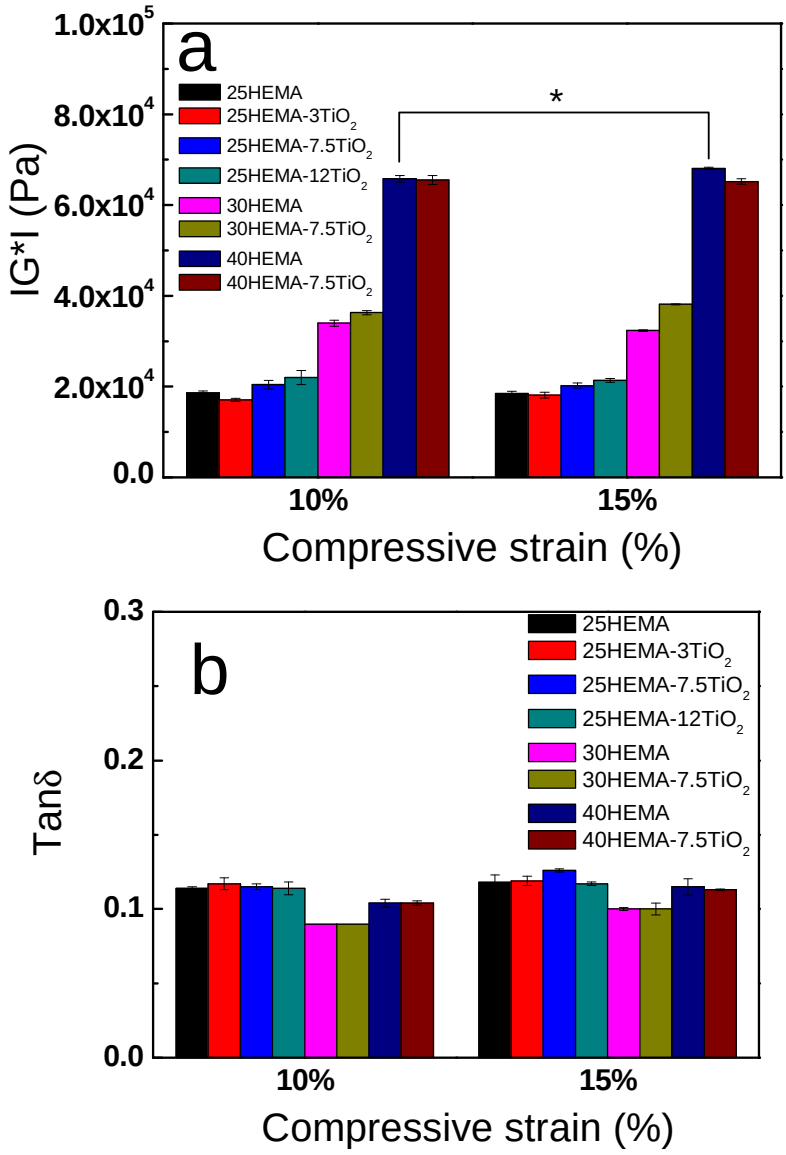

Figure 3-10 (a) Complex modulus |G*| and (b) tanδ of PHEMA and PHEMA-TiO_2 composite hydrogels under the influence of compressive strains (*) indicates the significant difference in |G*| between different compressive strains were applied on 40HEMA hydrogel

3.3.3. Creep-Recovery Properties

The creep-recovery test was conducted using two different loading modes as described in 3.2.3. Figure 3-11 represents the creep-recovery of a 25HEMA hydrogel via loading Mode A, where the selected hydrogels were tested under two different shear stresses (75 Pa and 125 Pa), resulting in different levels of deformations. The hydrogel recovered to different levels once the stress was released and the recovery ratio was dependent on the permanent damage caused by different stresses. Therefore, the recovered portion of the hydrogel after different levels of shear stress can be calculated to investigate the nonlinear rheological properties of the hydrogels, which is important for understanding the materials behaviour in an environment that experiences complex force conditions, such as a tissue scaffold.

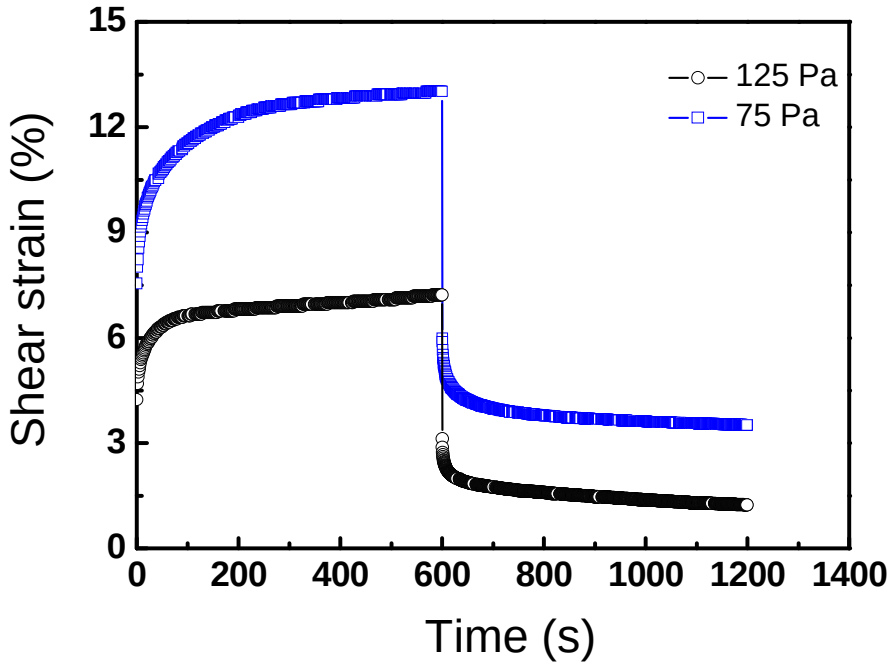

Figure 3-11 Creep-recovery of 25HEMA hydrogels with loading Mode A under different loading forces

Listed in Table 3-3 are the test results from HEMA and HEMA composite hydrogels that have been examined by the creep recovery method using the Mode A. Most hydrogels can recover fully under a small stress (40 Pa). When the stress was increased to 75 Pa, the recovery portion of 25HEMA hydrogel was 83.3%, lower than that from 25HEMA-3TiO_2 and 25HEMA-7.5TiO_2 hydrogels (87%, and 86% respectively), indicating the addition of TiO_2 nanoadditives increased the recovery

capability of the hydrogels. All other hydrogels can fully recover under this shear stress (75 Pa).

When the stress was increased to 125 Pa, the recovery portions of 25HEMA and 25HEMA-3TiO_2 hydrogel were reduced 72.9% and 77.1% respectively indicating the high nonlinear deformation of the hydrogels, while other hydrogels (25HEMA-12TiO_2, 30HEMA, 30HEMA-7.5TiO_2 and 40HEMA) were able to fully recover. A dramatic decrease in the recovery portion was seen for 40HEMA-7.5TiO_2 hydrogel, attributed to the damage of the structure from its nonuniform structure after TiO_2 nanoparticles addition.

A high shear stress, 250 Pa, was applied to 30HEMA, 30HEMA-7.5TiO_2, 40HEMA, and 40HEMA-7.5TiO_2 hydrogels. A complete recovery was only observed from 40HEMA hydrogel and other hydrogels showed different levels of permanent deformations, indicating that the porous structure of the hydrogels can be destroyed. A dramatically reduced recovery was found for hydrogels containing TiO_2 nanoparticles, which was due to the formation of defects in the polymer structure after the addition of the particles into the porous structure.

Table 3-3 Percentage recovery of PHEMA and PHEMA-TiO_2 composite hydrogels

Sample codes	Recoverable portion (%)			
	40 Pa	75 Pa	125 Pa	250 Pa
25HEMA	NA	83	73	NA
25HEMA-3TiO_2	100	87	77	NA
25HEMA-7.5TiO_2	100	86	87	NA
25HEMA-12TiO_2	100	100	100	NA
30HEMA	NA	100	100	87
30HEMA-7.5TiO_2	NA	100	100	7
40HEMA	NA	100	100	100
40HEMA-7.5TiO_2	NA	100	54	65

The test results are based on single measurement.

Figure 3-12 shows the creep-recovery of different composite hydrogels when a stress (75 Pa) was applied to the specimens via loading Mode B. Different shear strains were induced for different hydrogels under the same stress. The value of induced shear strain was 5.4% for 25HEMA-7.5TiO_2, 2.6% for 30HEMA-7.5TiO_2 and 1.5% for 40HEMA-7.5TiO_2 respectively. The difference in the reduced shear strain levels is due to the different stiffness of hydrogels. 30HEMA-7.5TiO_2 and 40HEMA-7.5TiO_2 hydrogels fully recovered after the share stress was removed, consistent with the results from oscillation strain sweep (Figure 3-6 b). 96% recovery was found for 25HEMA-7.5TiO_2 hydrogel and the loss of minimal water during the loading process was attributed to this non-fully recovery.

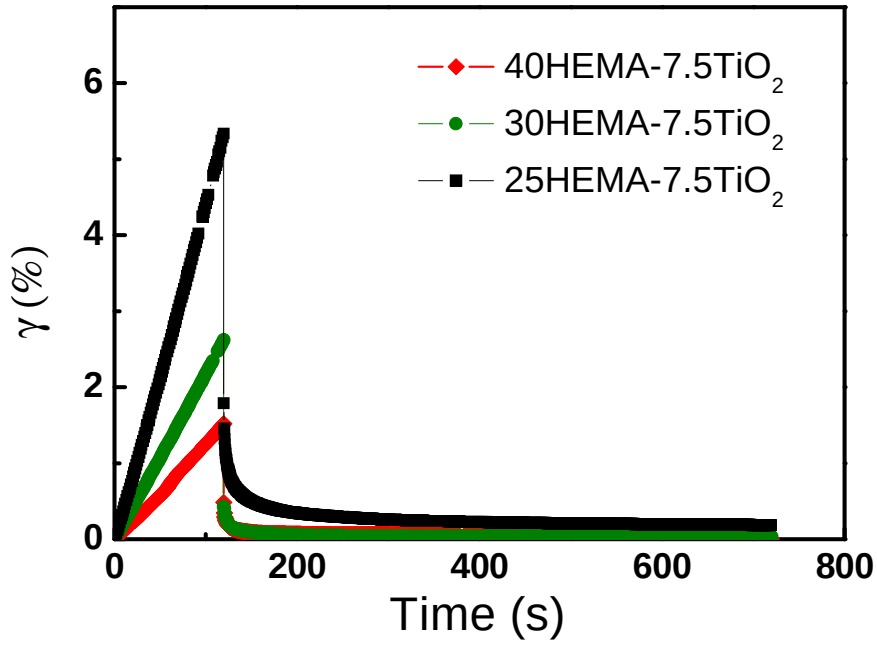

Figure 3-12 Creep-recovery of PHEMA-TiO_2 composite with loading Mode B under a stress of 75 Pa

When an increased shear stress, τ=250 Pa, was applied to 30HEMA, 30HEMA-7.5TiO_2, 40HEMA and 40HEMA-7.5TiO_2 composite hydrogels, increased shear strains were observed (Figure 3-13). About 11% shear strains were found for 30HEMA, 30HEMA-7.5TiO_2. The shear strains were about 5% for 40HEMA and 40HEMA-7.5TiO_2 hydrogels. After the stress was released, 40HEMA and 40HEMA-7.5TiO_2 hydrogels demonstrated an almost complete recovery (95%), which was attributed to the high stiffness of hydrogels containing higher HEMA concentrations. However, higher permanent deformation, 14% and 22% respectively, was found for the 30HEMA, 30HEMA-7.5TiO_2 hydrogels. The more permanent deformation that occurred on 30HEMA-7.5TiO_2 hydrogel was because of some defects caused by the addition of TiO_2 nanoparticles. These defects in the composite hydrogels can be easily damaged under the stress. Similar observations can be made for 40HEMA-7.5TiO_2 under a further increased stress (Figure 3-14).

In comparison with the results from loading Mode A, better recovery behaviours were found, particularly for hydrogels from loading Mode B. This observation was most noticeable for composite hydrogels including 30HEMA-7.5TiO_2 and 40HEMA-7.5TiO_2. In loading mode B, a slow loading was applied from the top surface of the

hydrogel and therefore the stress on the hydrogel, can be transferred down to the whole hydrogel. Thus it was assumed that the deformation of the hydrogel in Mode B was more uniform than that for hydrogel under Mode A. In this case, the defects in the hydrogels showed better resistance for the strain within. Large stress levels (Mode A) can easily destroy the porous structure of composite hydrogels.

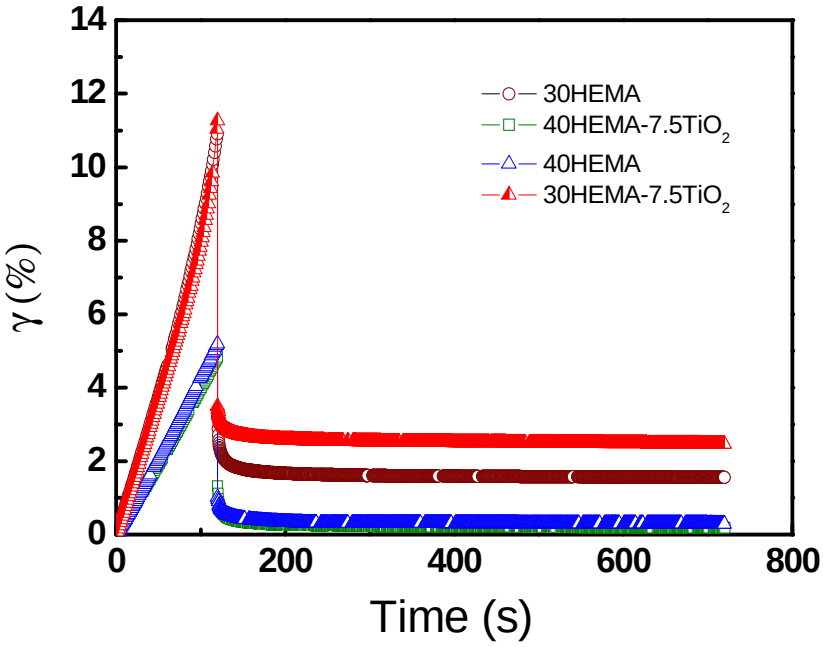

Figure 3-13 Creep-recovery of PHEMA-TiO_2 composite with loading Mode B under a stress of 250 Pa

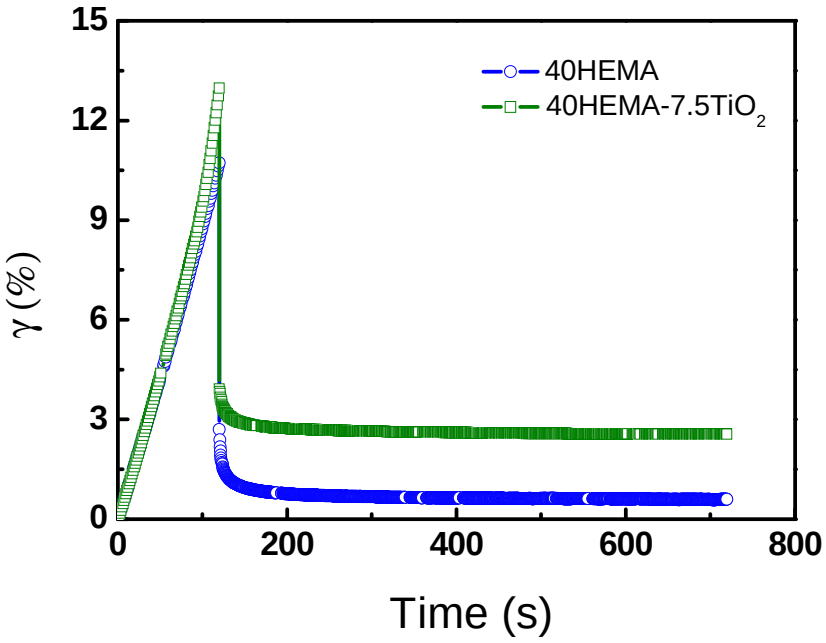

Figure 3-14 Creep-recovery of 40HEMA and 40HEMA-TiO_2 composite with loading Mode B at a stress of 500 Pa

3.3.4. Comparison of Mechanical Properties of Hydrogel Materials

Table 3-4 shows the shear moduli of a series of soft tissues and of some reported hydrogel materials for soft tissue engineering applications. The modulus values of the tissues were categorized according to their levels, ranging from very soft brain and nerve tissues (10^2-10^3 Pa), to liver and relaxed muscle tissues (10^3-10^4 Pa) and further to connective tissues (10^5-10^6 Pa). The shear modulus of cartilage tissue is reported by Moutos et al within a range from 5×10^4 to 2.5×10^5 Pa (Moutos, Freed, and Guilak 2007; Vanderhooft et al. 2009). For some soft tissue engineering applications, the desirable shear modulus ranges from 2 to 2.5×10^5 Pa (Agrawal et al. 2008).

Table 3-4 Shear moduli of different tissues and hydrogel materials

Tissues and hydrogels	Shear modulus (Pa)	Reference
Brian, nerves	10^2-10^3	(Engler et al. 2006)
Liver, fat, relaxed muscle, breast gland tissue	10^3-10^4	(Vanderhooft et al. 2009)
*Porous PHEMA and PHEMA composite hydrogels	10^4~10^5	Current study
Articular cartilage	5×10^4-2.5×10^5	(Moutos, Freed, and Guilak 2007)
Dermis, connective tissue, contracted muscle	10^5-10^6	(Vanderhooft et al. 2009)
Eepidermis, cartilage	10^7-10^8	(Vanderhooft et al. 2009)
HYAFF®11 (HA)	1.9×10^5 ~4.2×10^5	(Borzacchiello et al. 2007)

* See Table 3-2 and Figure 3-8 for details.

The shear moduli of the hydrogels produced in this study are in the range of 10^4 and 10^5Pa, depending on the HEMA concentrations and the nanoadditives in the hydrogels. One can see from Table 3-4 that the materials are very suitable for the applications as nerve and muscle tissues. In addition, the values in the PHEMA composite hydrogels are very close to the shear modulus of articular cartilage reported by the reference (Moutos, Freed, and Guilak 2007). The phase angle of PHEMA hydrogels was about 0.10-0.22, which covers the reported phase angle value for articular cartilage (~0.17) (Zhu et al. 1993).

The shear moduli of a few commercial hydrogel polymers that are commonly used in engineering these tissues are also summarized in Table 3.4. HYAFF®11 is a linear derivative of hyaluronic acid obtained by total esterification of carboxyl groups with benzyl alcohol and has been investigated for adipose tissue engineering applications. The elastic moduli of HYAFF®11 sponges are between 1.9×10^5 Pa (200-315 μm) and 4.2×10^5 Pa (400-500 μm), depending on the pore sizes (Borzacchiello et al. 2007).

Table 3-5 shows the tensile properties from current study (Figure 3-5), peer reported hydrogel materials for soft tissue regeneration and the values of a series of soft tissues. In comparison to PHEMA hydrogel fabricated via similar methods, Chirila et al. changed the polymerization procedure, resulting in an increase of tensile strength (Chirila et al. 1995). Also Liu et al. suggested having NaCl in the polymerization media, aiming for a multi-phase separation during the polymerization process. Significantly improved tensile modulus also has been seen for the produced PHEMA hydrogel (Liu et al. 2000). When photo-polymerization (5 min on each side of the mold at 365 nm and an intensity of 4 mW/cm^2) was applied to produce porous PHEMA hydrogel using poly (methyl methacrylate) (PMMA) microspheres, different pore size hydrogel structures with a range of mechanical properties can be formed (LaNasa, Hoffecker, and Bryant 2011). Similar range of tensile strength was seen comparing to the results from current study. However, significant increased tensile modulus was seen, which could stem from their low water contents. Comparing with the values of soft tissues, the tensile strength of PHEMA covers partial range of arterial tissue and the tensile modulus covers the value for skin tissue. It should be noted that the elongation of PHEMA hydrogel produced in current study is significantly higher than the reported hydrogel systems, which could be a huge advantage in the applicable area. In comparison to hydrogel materials which have been popularly applied for the application of soft tissue regeneration, PHEMA hydrogel exhibits much high tensile properties (Wang et al. 2011; Temenoff et al. 2002; Adekogbe and Ghanem 2005). The tensile properties of PHEMA and other hydrogel systems in this discussion are all low in comparison to some tissues like cartilage.

Table 3-5 Comparison of the tensile properties of various PHEMA hydrolgels, soft tissues and other hydrogel systems for soft tissue regeneration

Polymer/soft tissue	**Procedure**	**Specification (mm)**	**Water content (%)**	**Testing conditions**	***Tensile strength (kPa)***	***Elastic modulus (kPa)***	***Elongation (%)***	**Reference**
Porous PHEMA	Photo-polymerized for 5min at 365nm and an intensity of mW/cm^2	-	**37-46**	-	~60-220	~60-850*	-	(LaNasa, Hoffecker, and Bryant 2011)
	See Chapter 2, Section 2.2.2 for details	*Porous sponge*	*60-90*	*ATSM D2116 (0.5mm/s)*	*Up to 250*	*~5-220*	*~175-500*	***Present study (Figure 3-5)***
	(1) Three 10h steps heating at 30˚C, 40˚C, 50˚C or (2) Two steps heating at 30˚C (6h), followed by 50˚C (15h)	10×1×1.5 sponge (pore size>10 µm)	70	Myograph	320	-	-	(Chirila et al. 1995)
	Polymerization in a 0.3–0.7 M NaCl solution	45×6×1.5	40-60	*30 mm/min*	-	~125-250	-	(Liu et al. 2000)
Hydrogel systems /soft tissue	**Target tissue applications**	**Preparation conditions**						
Crosslinked chitosan scaffolds	Skin tissue regeneration	Non or dimethyl 3-3, dithio bis' propionimidate crosslined crosslinked	-	6 mm/min	<100	~36-110	~8-110	(Adekogbe and Ghanem 2005)
Collagen-chitosan scaffolds	-	(1) Thermally triggered fabricated scaffold; (2) GA cross-linked Col–Chi scaffold	-	10 mm/min	~85-361	-	-	(Wang et al. 2011)
Oligo(poly(ethylene glycol) fumarate)	Cartilage tissue regeneration	Develoed from different molecular weight poly(ethylene glycol)	-	ASTM D638-98 (25mm/min)	~10-25	~20-90	~36-80	(Temenoff et al. 2002)
Arterial tissue	-	-	-	-	~100-1000		-	(Ramakrishna et al. 2001)
Intraocular lens	-	-	-	-	~2,300	~5,000	-	
Skin tissue	-	-	-	-	~7600	~100		
Cartilage tissue	-	-	-	-	~27,000	~10,000	-	

**The valve shown here is aquasi-static modulus which was evaluated within the lowest 75% of the curve prior to reaching the elastic limit*

3.4. Conclusions

Comprehensive evaluation of the tensile and viscoelastic properties on PHEMA and PHEMA-TiO_2 composite hydrogels were carried out. It was found that tensile modulus and strength, and viscoelastic moduli were mainly dependent on HEMA:water concentrations in the polymerization mixtures. In general, a high HEMA:water ratio facilitated the production of high modulus hydrogels, but a less porous microstructure. A low HEMA:water ratio resulted in more porous structure that showed a greater range of linear viscoelasticity. All hydrogels exhibited a quick recovery, and the full recovery was dependent on stresses, loading modes, the addition of the nanoadditive and the porous structures of the hydrogels. Therefore, these porous hydrogels have a better adaptivity to a more complex mechanical environment. The results demonstrated that the porous PHEMA and PHEMA composite hydrogels can be tailor-made for engineering a range of soft tissues.

CHAPTER 4 DELIVERY OF BIOMOLECULES FROM POROUS HYDROGEL POLYMERS UNDER STATIC AND DYNAMIC CONDITIONS

4.1. Introduction

This chapter focuses on the studies of the biomolecule delivery properties of porous hydrogels under both static and dynamic conditions. From previous studies, it is understood that drug delivery from macroporous hydrogels in static conditions is largely dependent on the porous structure and the drug concentrations in the polymer matrices (Lou, Munro, and Wang 2004; Lou, Wang, and Tan 2007; Wang et al. 2010). Since there are no significant variations in porosity between composite hydrogels and the blank PHEMA hydrogels, the latter were used in the current investigations. The work in this Chapter is divided into two stages. First, three hydrogels, including 20HEMA, 25HEMA and 30HEMA, were selected to deliver a model drug, methylene blue (MB), under rheological stimulations, which were applied under different shear strains and frequencies. Second, based on results from the previous stage, the delivery of three biomolecules, including prednisolone 21-hemisuccinate sodium salt (PSS), caffeine (CAF) and bovine serum albumin (BSA) from 20HEMA hydrogel, was examined under static conditions. The delivery of a dual-drug system from 20HEMA and 30HEMA was also investigated. PSS and CAF were used for dual-drug delivery. In the end, the relationship between the drug release characteristics of PHEMA hydrogels and their compositions, structures and the stimulations is then discussed.

Successful delivery of biomolecules is of importance in tissue engineering applications and a controlled delivery manner is essential because tissue regeneration normally occurs over long time frames (Biondi et al. 2008; Tayalia and Mooney 2009). These biomolecules include various growth factors and antibiotics (Baldwin and Saltzman 1998; Boontheekul and Mooney 2003; Shi et al. 2009; Tessmar and Göpferich 2007). Delivery of these biomolecules in a single manner using various controlled release strategies within scaffolding materials has been extensively

reported. However, in certain circumstances, a single biomolecule is not sufficient in type and/or quantity in engineering different tissues, particular for repairing large size defects. Therefore, multiple drug delivery is essential and studies on delivery of dual-drug have been conducted in a few research groups (Lee et al. 2008; Mandal and Kundu 2009; Su et al. 2009).

Static conditions are the most commonly employed means for operating the drug delivery investigations. However, a tissue regenerating scaffold needs to adapt to habitual physical demands from the tissues within the body (such as compression in bone and cartilage, tension in muscle and tendon, and shear force in blood vessels) after implantation (Butler, Goldstein, and Guilak 2000). Therefore, the release of the biomolecules via the scaffold will be under dynamic conditions instead of static conditions. The release profiles of the biomolecules from static and dynamic conditions are believed to be different, and this eventually will affect the ultimate outcome of the regeneration process. Therefore, a study of dynamic drug release under physiological conditions is essential to correlate with that from static conditions. The relationship between them enables a complete understanding of the difference and thus facilitates the design of an ideal controlled drug delivery system for tissue regeneration.

Attention has been paid to the release of biomolecules in response to some physiological variables in either chemical (pH, proteins) or physical signals (temperature, ultrasound, magnetic field, mechanical) (Kost and Langer 2001). A compressive signal consisting of six cycles of compression for 2 min, followed by relaxation for 8 min was employed to investigate its influence on controlled drug delivery (Lee, Peters, and Mooney 2001; Lee et al. 2000). It was pointed out that the effect of mechanical stimuli on the controlled delivery was dependent on the interactions of the drug with the polymer scaffolds and the mechanical signals can actively trigger the release of interactive drugs. A contrary study investigated drug absorbance characteristics in skeletal muscle tissue under controlled dynamic loads, both static (0-20%) and cyclic (±2.5% strain, 0-20% mean, 1-3 Hz) (Wu, Minisini, and Edelman 2009; Wu and Edelman 2008). The study demonstrated that the permeability and drug transport in mechanically active tissues can be influenced by the interrelated effect of architectural configuration and functional dynamics.

Most tissues in the human body are subjected to various *in vivo* mechanical loadings with the influence of variable frequencies during normal daily activities, which make the microenvironment complicated. As a result, the release investigations from either static conditions or a simple mechanical stimulation can not represent the real drug delivery results occurring in human body once the tissue substitutes are implanted. As explained in Chapter 3, rheological testing can be performed in various modes and the stresses/strains from these dynamic forces can be used to mimic the microenvironment of the tissues in human body. Therefore, a dynamic release platform, as established in Chapter 3, can provide these kinds of mechanical stimulations and is very useful for studying the biomolecule delivery from tissue scaffolds.

4.2. Experimental

4.2.1. Drug Selections and Hydrogel Specimens

Methylene blue (MB) from Unilab (Australia) was used as the model drug in stage I. Prednisolone 21-hemissucinate sodium salt (PSS) powder, a very commonly used anti-inflammatory drug, and bovine serum albumin (BSA), a biomolecule representing large molecular weight proteins, were used for single drug delivery studies and both were from Sigma & Aldrich. Caffeine (CAF) was used in conjunction with PSS for dual-drug delivery study and was purchased from Ajax Laboratory Chemicals (Australia). A bicinchoninic acid assay kit was purchased from Sigma & Aldrich for protein assay. The chemical structures and UV-VIS spectrum properties of the used drugs are listed in Table 4-1. The evaluation of MB, PSS, and CAF was determined by measuring the absorbance at 665 nm, 247 nm, and 272 nm, respectively using UV-VIS spectrometry. These measured values are well consistent with references (Lin, Chiu, and Lee 2005; Chung and Rubner 2002; Lou, Wang, and Tan 2007). 20HEMA, 25HEMA, and 30HEMA were prepared according to the procedure explained in Chapter 2.

Table 4-1 Chemical structures and wavelengths for UV-VIS measurements

Model drug	Chemical structure	Maximum wavelength (nm)
MB (Mw= 373.90)	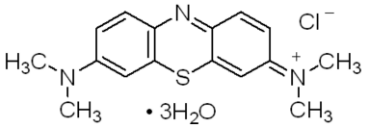	665
PSS (Mw= 482.50)	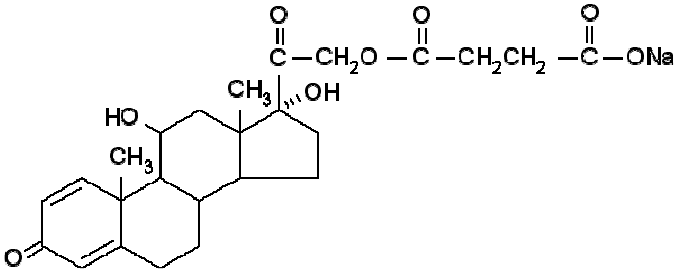	247
CAF (Mw= 194.19)	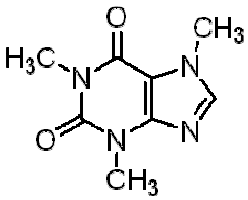	272
BSA (Mw=67000)	-	562 (BCA kit used)

4.2.2. Drug Loading and Drug Loading Level

Two different concentrations of MB solutions (20 mg/ml and 5 mg/ml), three drug solutions including PSS (10 mg/ml), CAF (10 mg/ml), and BSA (10 mg/ml), and three dual-drug solutions including PSS(10 mg/ml)-CAF(10 mg/ml), PSS(10 mg/ml)-CAF(10 mg/ml), and PSS(5 mg/ml)-CAF(5 mg/ml) were used for different delivery systems. The drug loading was conducted using freeze-dried hydrogel samples. Each hydrogel specimen was placed into a vial containing 3~5 ml drug solution, which was sufficient to allow full hydration of the hydrogel sample. The

drug loading was conducted for a minimum of 3 days at ambient temperature, ensuring a complete equilibration of the hydrogels. The drug loading level in the hydrogel samples was presented using the amounts of the drugs in the loading solution taking away the residual amounts of drugs after the loading. The method to determine the amounts of drugs in a solution is described in 4.2.4. The drug loading levels were then normalized against the weights of freeze dried samples, providing comparable values (drug uptake per unit mass) across the variety of hydrogel formulations. It should be noted that both the drug loading and drug delivery experiment are based on single measurement. The repeatability has been demonstrated in previous report and confirmed during method validation stage (Lou, Munro, and Wang 2004).

4.2.3. Drug Delivery Set-ups

Static drug release

Figure 4-1 illustrates the experimental set-up for static drug release. A drug loaded hydrogel specimen was placed in a container, after being blotted with a wet tissue to remove the excessive drug solution. A Teflon disc (Φ17.3×2.5 mm) was then put above the top surface of the hydrogel serving as an impermeable barrier. Thus drugs can only be released out of the hydrogel sample from the radical direction. Release media (11 ml) was poured into the container carefully. The release experiment was conducted in an orbital shaker (Chiltern Scientific) at a speed of 50 rpm at room temperature. Sampling (200 μl) was done at pre-designed time intervals, which were 30, 60, 120, 240, 360, 480 min.

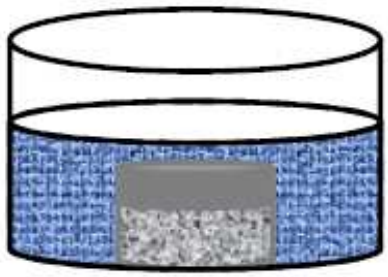

Figure 4-1 A set-up for static molecule release study

Dynamic drug release

Dynamic release experiments were conducted on a set-up schematically illustrated in Figure 4-2. The set-up was developed from a HAAKE MARS III Modular Advanced Rheometer System (Thermo Electron, Germany), from which the rheological stimulations were transmitted to the hydrogel specimen. The set-up consists of two parts, including a sample part and a circulated part. A parallel-plate geometry was employed in the sample part and the plate geometry was kept in a beaker (91 mm in diameter). The hydrogel sample was then loaded between the two plates and 50 ml of the release medium was added into the beaker. A measurement gap size (90% height of hydrogel sample thickness) was reached by lowing down the top plate. The circulated part was connected with an external magnetic stirring. The mixing process using a pump ensures the homogeneity of the solution in the test. The dynamic drug release started whist the rheological stimulation was applied. Sand paper on both plates was applied to prevent slipperiness. Sampling (200 μl) was taken every 30 min up to 420 min.

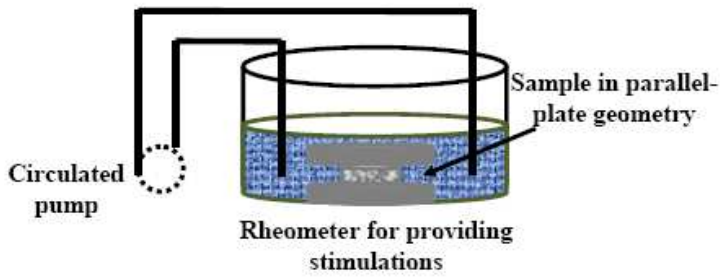

Figure 4-2 Schematic illustration of the set-up for biomolecule delivery study under dynamic stimulations

4.2.4. Drug Quantification

A GBC 916 UV-Visible (UV-Vis) Spectroscopy was used to quantify the drugs in an unknown solution which can be a sample containing released drugs or a sample from a drug loading solution. A maximum wave length was first selected depending on the drugs involved in the experiment. A calibration curve was established based on a series of known concentration solutions and the UV absorbance at the maximum wavelength. The concentration of an unknown solution was then calculated based on

its absorbance using the calibration curve. Details of drug quantification on each of the single and dual drug systems are given below.

Bovine serum albumin (BSA)

A bicinchoninic acid protein assay kit (Sigma-Aldrich) was used to evaluate the BSA release at different time intervals. The procedure of using the assay kit was according to the manufacturer's instructions. Basically, 0.1 ml BSA containing samples were mixed with 2 ml of BCA working reagent, followed by thorough mixing. The mixed samples were then incubated at 60°C for 15 min. The absorbance of the solutions was measured at the maximum wavelength of 562 nm. A UV-VIS spectrum of a BSA solution at a concentration of 600 μg/ml pre-treated with the BCA kit is shown in Figure 4-3, showing the maximum absorbance of the samples. The amount of released BSA was then determined by comparison the absorbance obtained with the standard curve prepared using a series of BSA solutions. The standard curve is shown in Figure 4-4.

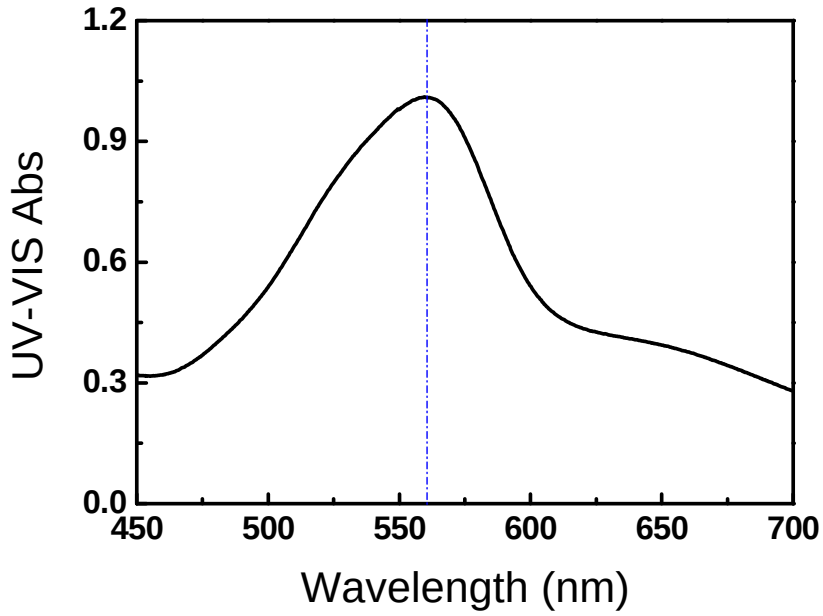

Figure 4-3 An UV-VIS spectrum of BSA solution at a concentration of 600 μg/ml pretreated with a BCA kit

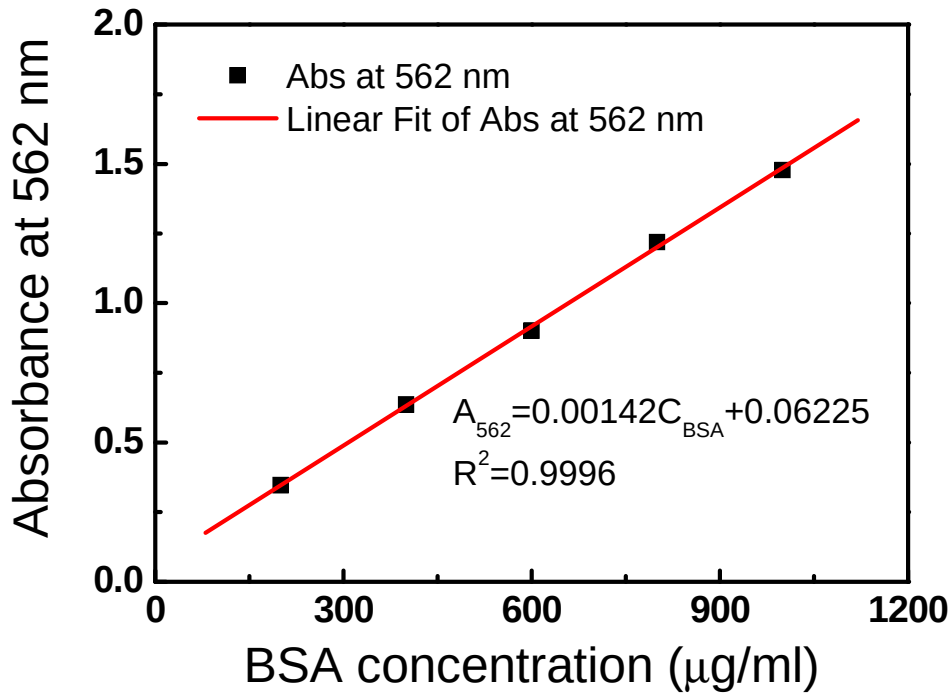

Figure 4-4 A standard curve of BSA solution at a wavelength of 562 nm

MB

The maximum wavelength used for the UV-VIS measurement of MB is 665 nm (Figure 4-5). A standard curve was established using a series of MB solutions (Figure 4-6). The retrieved sample solutions at different time points were diluted to a proper concentration and then measured using a GBC 916 UV-VIS spectroscopy. The concentration of the solution was then determined using the established standard concentration–intensity calibration curve taking into consideration the dilution factors.

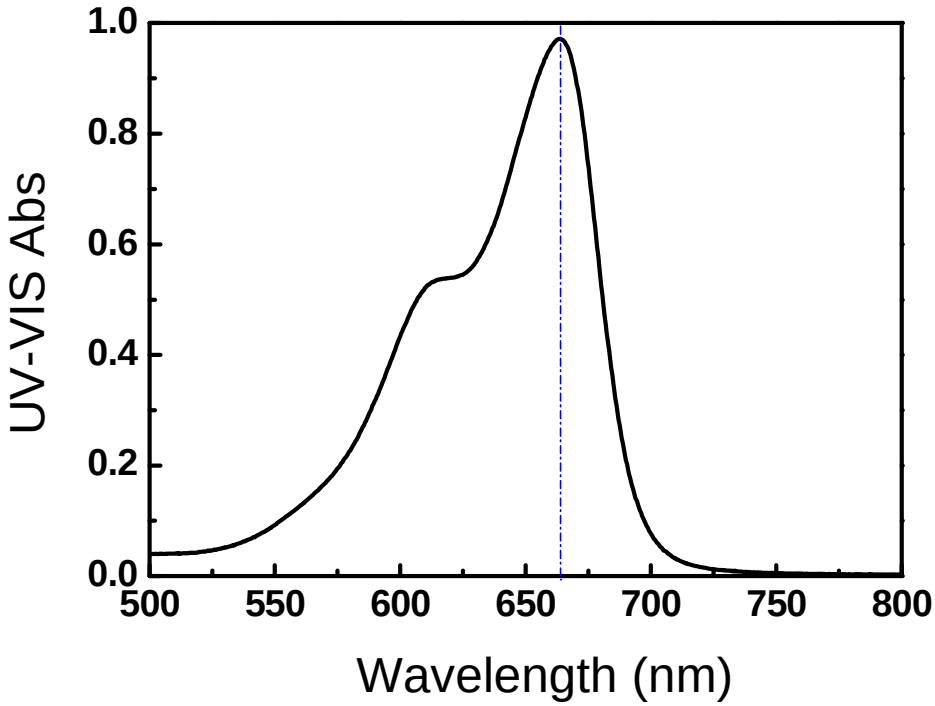

Figure 4-5 An UV-VIS spectrum of MB solution at a concentration of 5 μg/ml

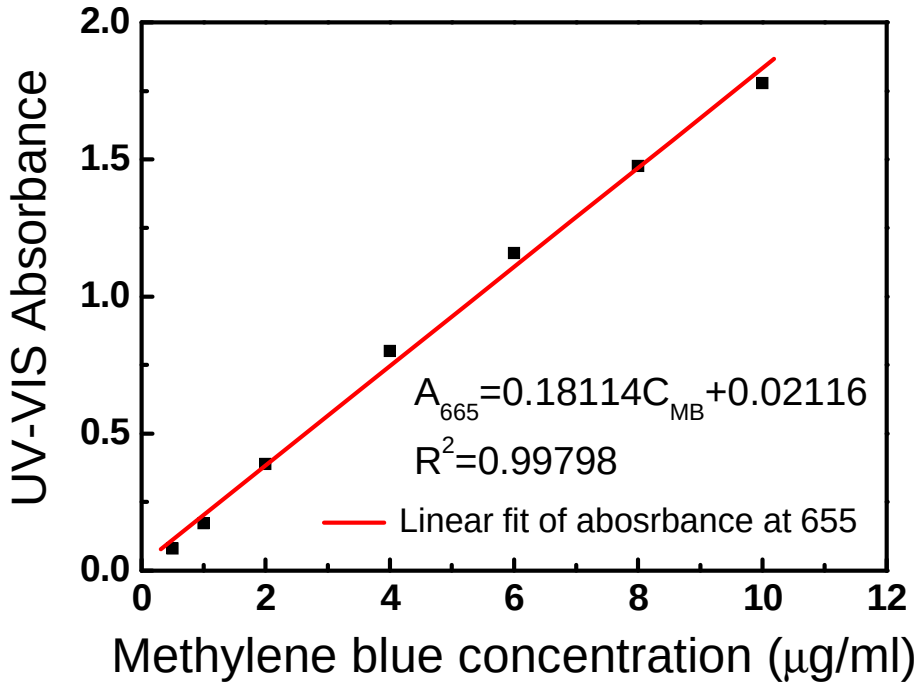

Figure 4-6 A standard curve of MB at a wavelength of 665 nm

PSS, CAF, and the combined PSS-CAF

The maximum wavelengths are 247 nm and 272 nm for PSS and CAF respectively. Standard curves were established using a series of known concentrations of PSS and CAF solutions respectively. Two standard curves at both 247 nm and 272 nm wavelengths were obtained for each drug (Figure 4-7 and Figure 4-8).

For the single release of PSS or CAF, the retrieved sample solutions at different time points were diluted to a proper concentration and then measured using a GBC 916 UV-VIS spectroscopy. The concentration of the solution was then determined using the established standard concentration–intensity standard curve taking into consideration the dilution factors. The standard curve from the maximum absorbance was used to determine the single release of PSS and CAF.

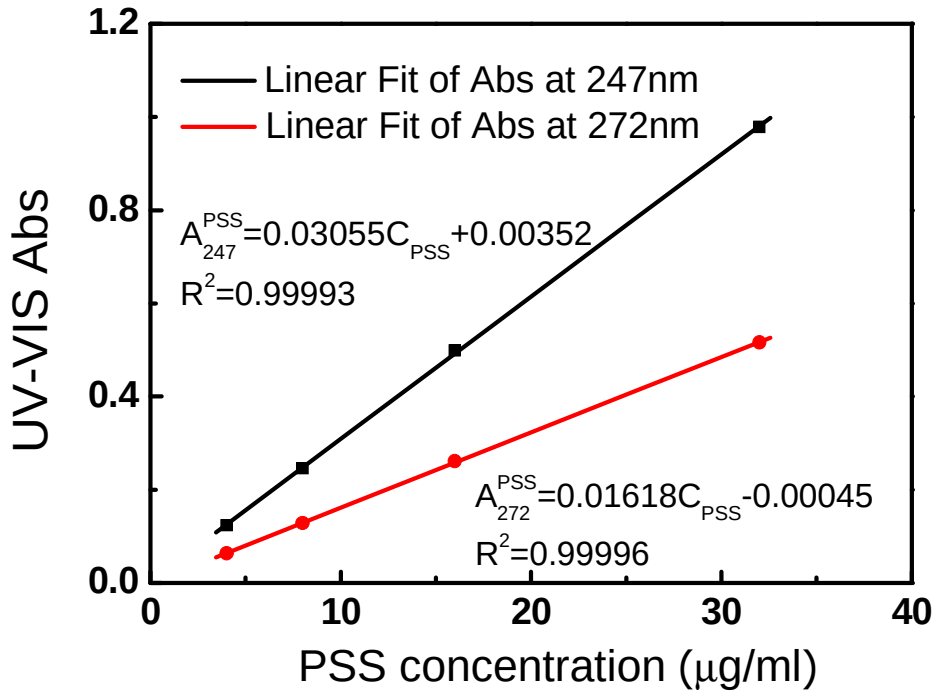

Figure 4-7 Standard curves of PSS at both 247 nm and 272 nm wavelengths

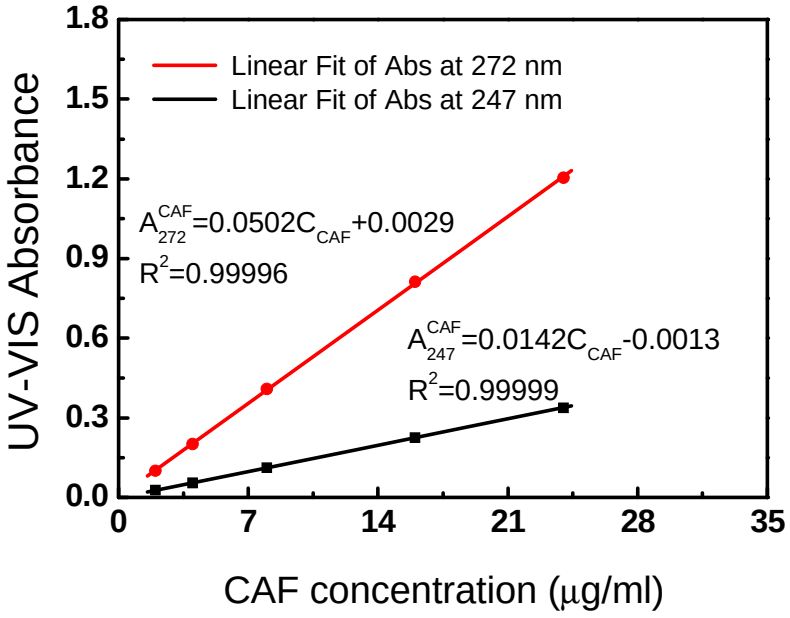

Figure 4-8 Standard curves of CAF at both 247 nm and 272 nm wavelengths

Figure 4-9 shows spectra of three solutions, including A (PSS, 10 μg/ml), B (CAF, 10 μg/ml), and a dual-drug solution C containing both PSS and CAF of the same concentration (10 μg/ml). D was an imaginative solution synergising A and B. C and D were almost the same, indicating that there was no interference between CAF and PSS at the investigated concentration.

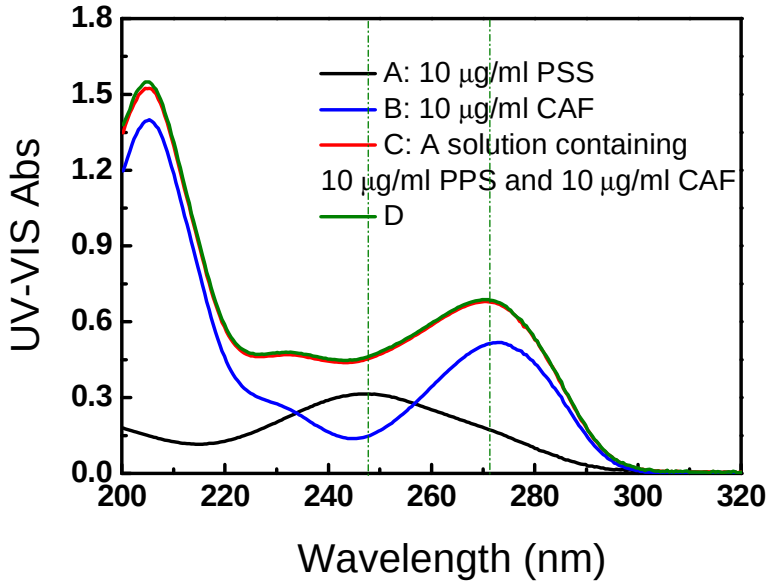

Figure 4-9 UV-VIS spectra for a dual-drug and two single drug solutions

More solutions were examined at 247 nm and 272 nm, respectively. The absorbance of the dual-drug and each of the single drug solutions are listed in Table 4-2. It can be seen clearly that the absorbance of the dual-drug solution was a simple synergic result of the absorbance of the two individual drug solutions at the same wavelength. No interference between the two drugs was observed. Therefore, the following equations can be established (Equation 4-1).

$$\begin{cases} A_{247}^{Total} = A_{247}^{PSS} + A_{247}^{CAF} \\ A_{272}^{Total} = A_{272}^{PSS} + A_{272}^{CAF} \end{cases} \quad (4\text{-}1)$$

From Figure 4-7,

$$A_{247}^{PSS} = 0.0306C_{PSS} + 0.0035 \quad (4\text{-}2)$$

$$A_{272}^{PSS} = 0.0162C_{PSS} - 0.0004 \quad (4\text{-}3)$$

From Figure 4-8,

$$A_{247}^{CAF} = 0.0142C_{CAF} - 0.0013 \quad (4\text{-}4)$$

$$A_{272}^{CAF} = 0.0502C_{CAF} + 0.0029 \quad (4\text{-}5)$$

Where A_{247}^{Total} and A_{272}^{Total} represent the absorbance of a dual drug solution at 247 nm and 272 nm respectively; A_{247}^{PSS} and A_{272}^{PSS} represent the contribution of PSS to the absorbance at the specified wavelength. Similarly, A_{247}^{CAF} and A_{272}^{CAF} represent the contribution of CAF to the absorbance at the two maximum wavelengths.

Substitute A_{247}^{PSS}, A_{272}^{PSS}, A_{247}^{CAF}, and A_{272}^{CAF} in Equation 4-1 with equations (4-2) to (4-5), Equation 4-6 is obtained, from which C_{PPS} and C_{CAF} can be determined with the measured A_{247}^{Total} and A_{272}^{Total}.

$$\begin{cases} A_{247}^{Total} = 0.0306C_{PSS} + 0.0142C_{CAF} + 0.0012 \\ A_{272}^{Total} = 0.0162C_{PSS} + 0.0502C_{CAF} + 0.025 \end{cases} \quad (4\text{-}6)$$

Table 4-2 UV-Vis absorbance of PSS, CAF, and combined PSS and CAF solution, confirming no interference from each of biomolecule

Solutions	A247	A272	Solutions	A247	A272
A1(10 μl/ml PSS)	0.3148	0.1675	A2(20 μl/ml PSS)	0.6018	0.3222
B1(10 μl/ml CAF)	0.1447	0.5169	B2(20 μl/ml CAF)	0.2829	1.0128
C1(10 μl/ml PSS, 10 μl/ml CAF)	**0.4501**	**0.6758**	C2(10 μl/ml PSS, 10 μl/ml CAF)	**0.4483**	**0.6792**
	A247	**A272**		**A247**	**A272**
A3(14 μl/ml PSS)	0.4215	0.2247	A4(6 μl/ml PSS)	0.1884	0.1010
B3(6 μl/ml CAF)	0.0872	0.3123	A4(14 μl/ml CAF)	0.2005	0.7155
C3 (14 μl/ml PSS , 6 μl/ml CAF)	**0.5070**	**0.5364**	C4(6 μl/ml PSS , 14 μl/ml CAF)	**0.3831**	**0.8118**

4.3. Results and Discussion

4.3.1. Drug Loading Level

Drug loading levels for PHEMA hydrogels are presented by the weights of drugs in the hydrogel samples and then these values were normalised against the weights of freeze dried hydrogels (Table 4-3). The influence of hydrogel formulations on the mass of drugs per unit mass of hydrogels was apparent. When a MB solution (20 mg/ml) was used for drug loading, 20HEMA had the largest quantity of MB per unit mass (93~108 mg/g) and the lowest quantity of MB per unit mass of the hydrogel was found for 30HEMA (30~42 mg/g). The significant difference for two hydrogels was due to the various porous structures, which was demonstrated in Chapter 2 using SEM micrographs and polymer volume fractions (Figure 2-6, 2-7, and 2-8; Table 2-3). The MB mass uptake per unit mass of the hydrogel can also be significantly affected by the concentrations of the drug loading solutions. When a MB solution (5 mg/ml) was used for the drug loading, a drastic decrease in the MB mass uptake per unit mass of dry 20HEMA hydrogel was noticed (20 mg/g). Similar results were

obtained when PSS and CAF were used in combination for drug loading. For example, when a dual-drug solution containing PSS (10 mg/ml) and CAF (10 mg/ml) was used, drug uptake levels (54 mg/g for both drugs) were achieved. The drug uptake level of CAF was decreased to 27 mg/g when the concentration of CAF in the solution was decreased to 5 mg/ml, whereas there was no change in the drug uptake level for PSS. The mass uptake of different drugs per unit mass of 20HEMA hydrogel, PSS (60 mg/g), CAF (53 mg/g), and BSA (49 mg/g) was attributed to the difference of their molecule weights.

Therefore, the porous structure and the polymer volume fraction of the hydrogel determine the drug uptake levels of these hydrogel materials. On the other hand, the drug loading level can be adjusted to a high degree when a high concentration drug solution was used. Finally, different drug uptake levels can be obtained when different drugs were applied.

Table 4-3 Information for biomolecule loading and delivery study

Hydrogel codes	Stock solutions for loading	Concentrations *In the stock solutions (mg/ml)*	Mass of molecules per gram of hydrogel (mg/g)				Experimental conditions for biomolecule delivery
			MB	PSS	CAF	BSA	
20HEMA	MB solutions	20	93	-	-	-	f=0Hz; γ=0%,
20HEMA		20	108	-	-	-	f=1Hz; γ=5%,
20HEMA		20	106				f=5Hz; γ=5%
20HEMA		5	20	-	-	-	f=1Hz; γ=5%
25HEMA		20	76	-	-	-	f=1Hz; γ=0.5%
25HEMA		20	66	-	-	-	f=1Hz; γ=5%
25HEMA		20	69	-	-	-	f=15Hz; γ=5%
25HEMA		20	45	-	-	-	f=0Hz; γ=0%,
30HEMA		20	30	-	-	-	f=0Hz; γ=0%,
30HEMA		20	42	-	-	-	f=1Hz; γ=5%
20HEMA	Single biomolecule solutions	CAF (10)	-	-	53	-	Static
20HEMA		PSS (10)	-	60	-	-	Static
20HEMA		BSA (10)	-	-	-	49	Static
20HEMA	Dual biomolecule solutions	PSS (10)–CAF(10)	-	54	54	-	Static
20HEMA		PSS (10)–CAF(5)	-	53	27	-	Static
30HEMA		PSS (5)–CAF(5)	-	16	17	-	Static

4.3.2. Dynamic MB Release

Hydrogel Formulation Effect

The relative MB release profiles from 20HEMA, 25HEMA, and 30HEMA hydrogels under a same rheological stimulation (f=0 Hz; γ=0%) are displayed in Figure 4-10. About 65% MB was released from 20HEMA within 420 min. In the same period of time, 43% was released from 25HEMA and only 28% released from 30HEMA hydrogel. The difference in relative release rate of these hydrogels is mainly due to variations in the pore size and polymer volume fraction of these materials, which has been reported by other researchers (Lee and Lin 2002). In addition, it has also been reported that increasing the pore size and its volume fraction of pores in the hydrogel can lead to a significant improvement of drug release (Tamagawa, Popovic, and Taya 2000; Falk, Garramone, and Shivkumar 2004). According to the results discussed in Chapter 2 (Figures 2-6, 2-7, 2-8 and Table 2-3), 20HEMA is the most porous, followed by 25HEMA and 30HEMA among these three hydrogels. Therefore, the highest relative release was observed for 20HEMA hydrogel, and the lowest relative release was seen for 30HEMA hydrogel.

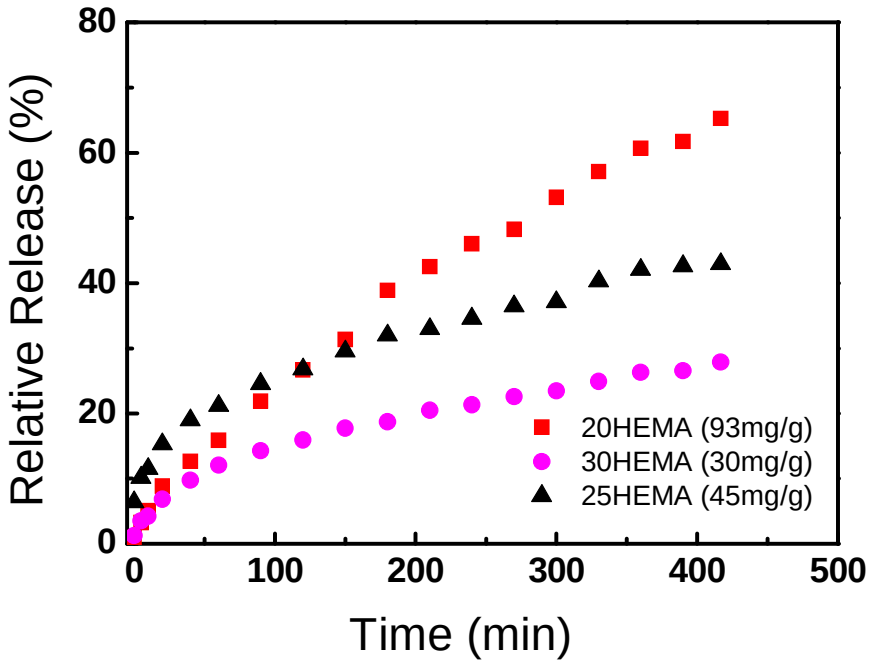

Figure 4-10 Relative MB release from PHEMA hydrogels at f=0 Hz; γ=0%

Figure 4-11 shows (a) the relative MB release and (b) the released amount of MB from three hydrogels, including 20HEMA, 25HEMA, and 30HEMA, under the same rheological stimulation (f=1 Hz; γ=5%). 20HEMA and 25HEMA hydrogels showed similar release profiles during the whole release procedure, and eventually about 41% MB was released from both hydrogels. 30% relative release was observed for 30HEMA hydrogel. The similar relative release of MB from 20HEMA and 25HEMA hydrogels was attributed to the similar porous structure (Figure 2-6a and 2-7 a). The dramatic decrease in pore size of 30HEMA hydrogel resulted in a slow relative release of MB via 30HEMA hydrogel. In comparison to the release with no stimulation, the relative release of MB from 20HEMA under the rheological stimulation was dramatically reduced, while no significant change was observed for both 25HEMA and 30HEMA hydrogels. The reduced relative release in 20HEMA hydrogel was probably caused by reabsorption of MB into the porous structure under the stimulation.

The released amounts of MB from three hydrogels are displayed in Figure 4-11 b. Large amounts of MB were released from 20HEMA and 25HEMA hydrogels in comparison to that of 30HEMA hydrogel, which showed the lowest released amount of MB. The amount from 20HEMA hydrogel was higher than that from 25HEMA. This difference was caused by the different relative release in addition to the loading level difference when a certain concentration of MB solution was selected.

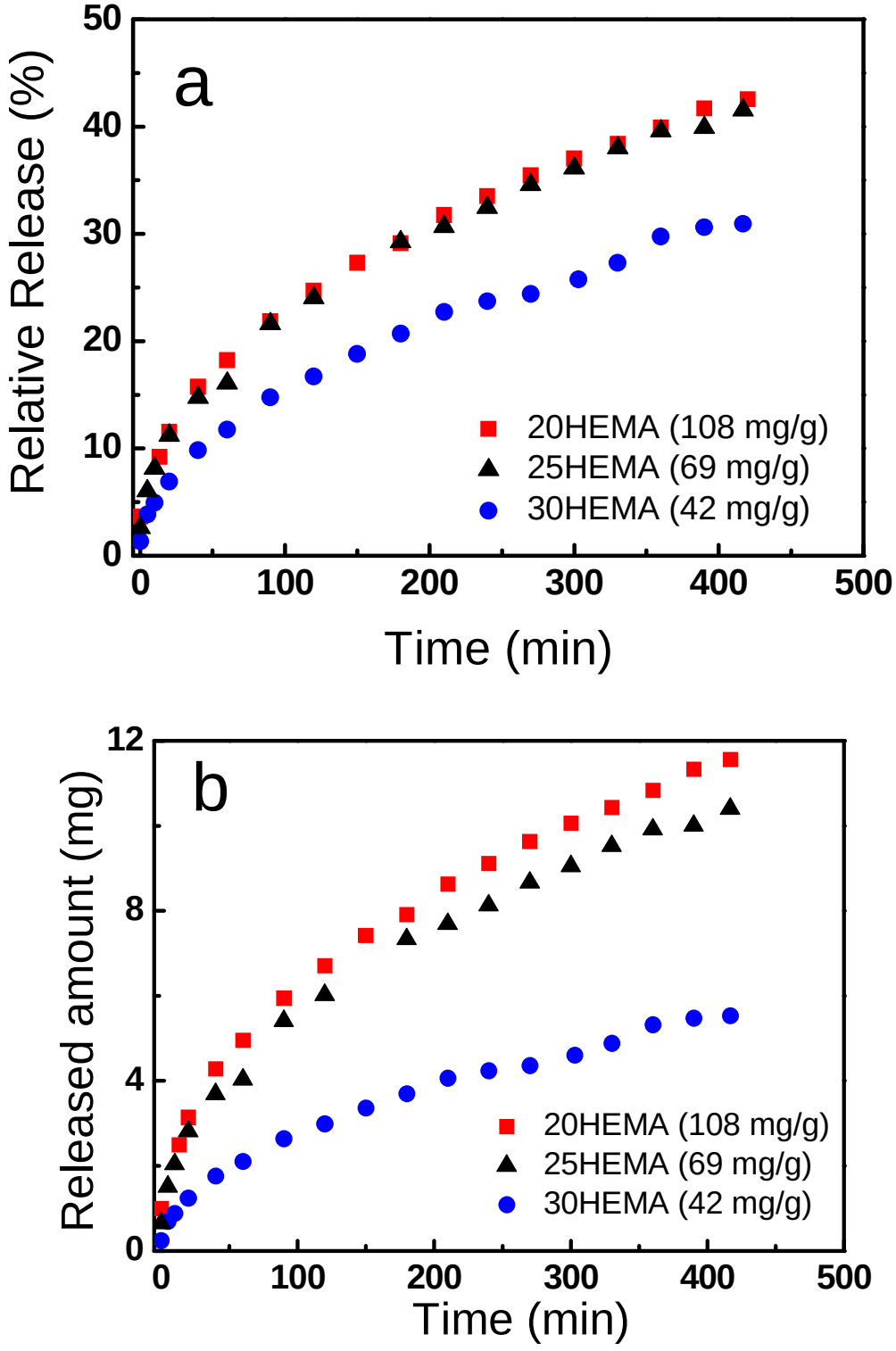

Figure 4-11 Dynamic release of MB from PHEMA hydrogels at f=1 Hz; γ=5%. The figures show (a) relative MB release and (b) released MB amount at various time points

Drug loading level effect

Figure 4-12 shows (a) the relative MB release and (b) the released amount through 20HEMA hydrogels under a rheological stimulation (f=1 Hz; γ=5%). 20HEMA hydrogels were previously loaded using 5 mg/ml and 20 mg/ml MB stock solutions, resulting in different MB uptake per unit mass of hydrogel (20 mg/g and 108 mg/g), respectively. Similar relative release profiles were observed for both hydrogels (Figure 4-12a). However, the released amounts of drugs from the two discs were dramatically different (Figure 4-12b). This indicates that the relative release system is independent of the amounts of the drugs in the hydrogels, which were obtained using different concentrations of MB stock solutions. A similar conclusion was also obtained for other hydrogel delivery systems (Gayet and Fortier 1996). In this case, the amounts of the drugs can be adjusted by the concentrations of the loading solutions to meet the requirements for different therapeutic purposes.

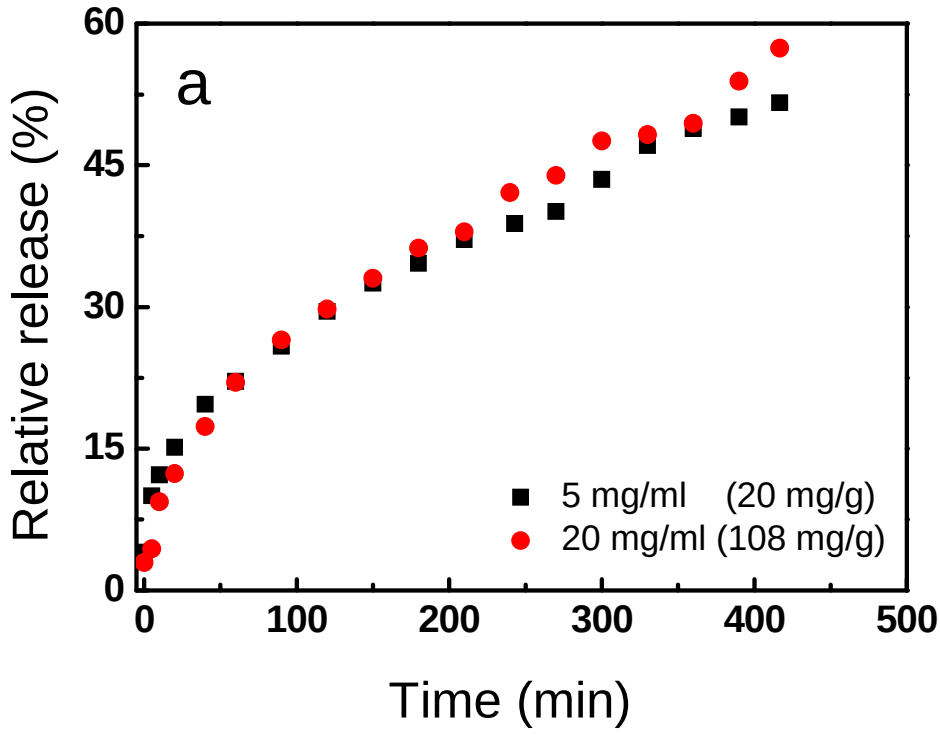

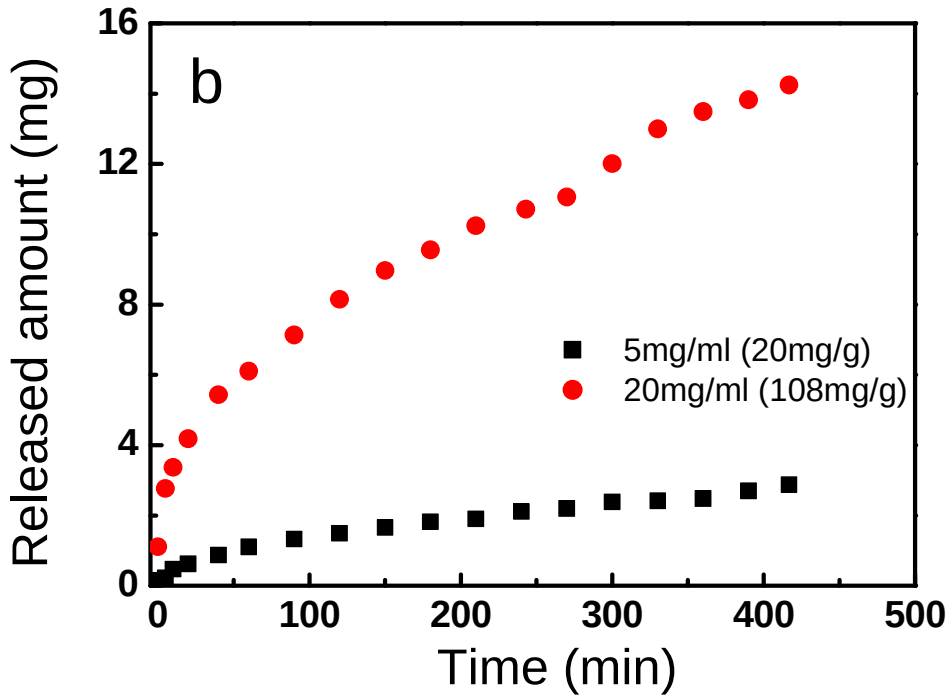

Figure 4-12 Dynamic release of MB from 20HEMA hydrogels at f=1 Hz; γ=5% loaded with different concentrations of MB solutions. The figures show (a) relative MB release and (b) released MB amount at various time points

Effect of shear strain

Figure 4-13 shows the relative MB release through 25HEMA hydrogel under two different shear strains, including 0.5% and 5%. The static release profile is included in the figure for comparison. The relative MB release consisted of an initial eluting release, followed by a slow release. Similar release behaviours were seen for both strains in the initial release within 150 min and then a higher relative MB release was observed under 5% stimulation. After 420 min, 35% MB was released from 25HEMA hydrogel at 0.5% shear strain, which was increased to 42% at 5% shear strain. A higher relative release was found under the static condition than for those from dynamic conditions due to the reabsorption of MB into the hydrogel. However, the release profile became very similar to that of the static condition when the dynamic conditions became vigorous.

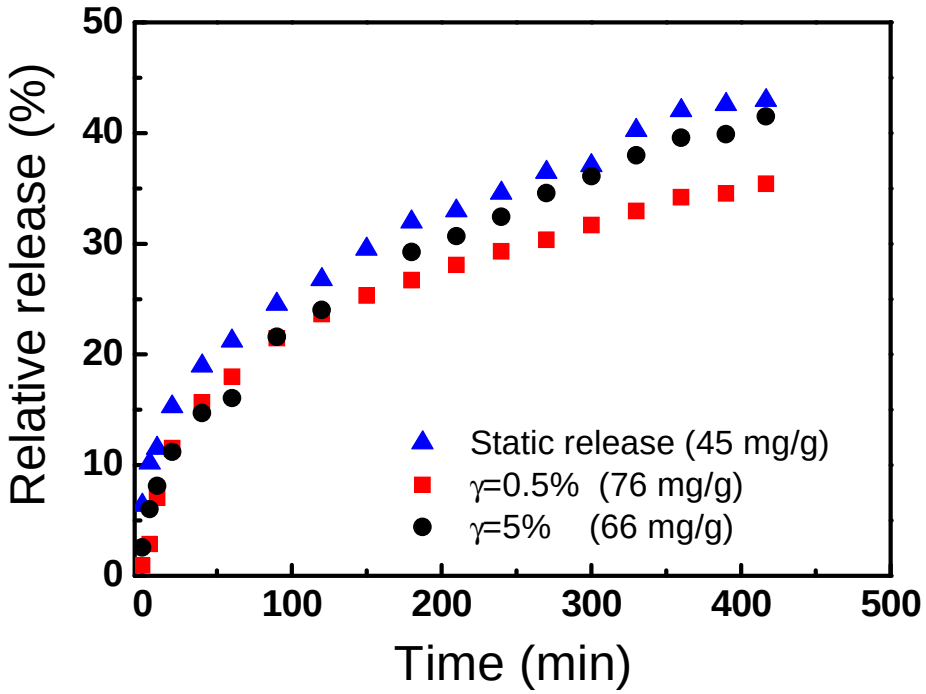

Figure 4-13 Dynamic MB release from 25HEMA hydrogel at f=1 Hz under different shear strains. The static release profile was used for comparison

Effect of frequency

The influence of frequencies on the relative release of MB from 25HEMA (1, 15 Hz) and 20HEMA (1, 5 Hz) hydrogel at a shear strain of 5% is displayed in Figure 4-14 and 4-15. Higher relative release was noticed under the higher frequency for both hydrogels. However, the impact of the frequency change on the relative release was greater to 20HEMA than to 25HEMA. Again reabsorption of MB into the hydrogel resulted in lower relative release of MB from the hydrogel under a mild dynamic condition. The relative release was increased as the dynamic condition became vigorous. The reabsorption was quicker for 20HEMA hydrogel due to its more porous structure. Thus, the relative release for 20HEMA under both dynamic conditions was much lower than that of static conditions.

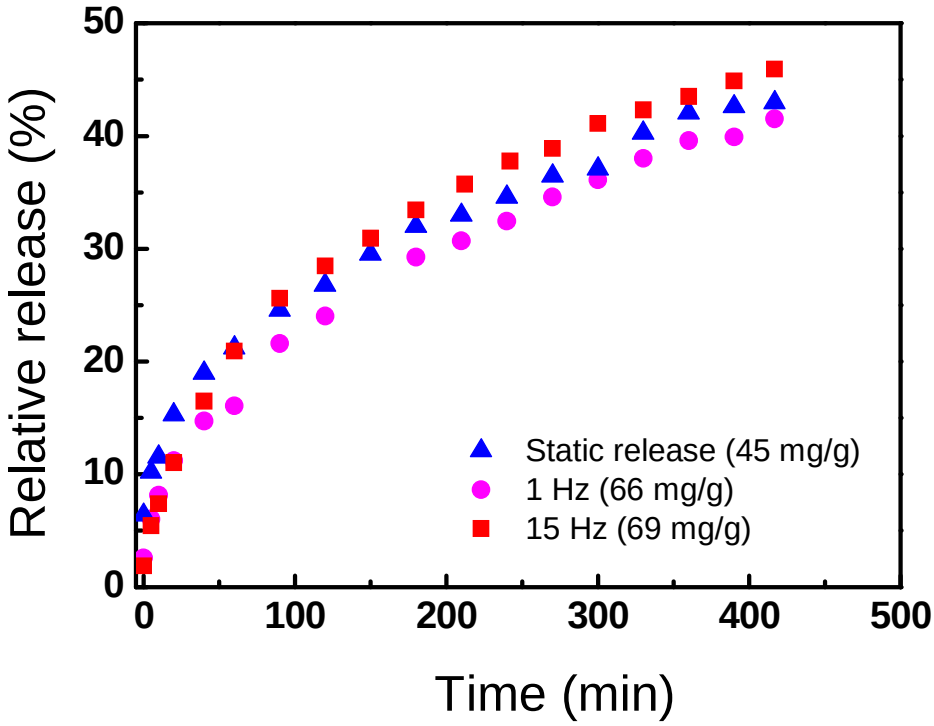

Figure 4-14 Dynamic MB relative from 25HEMA hydrogels at γ=5% under different frequencies. The static release profile was used for comparison

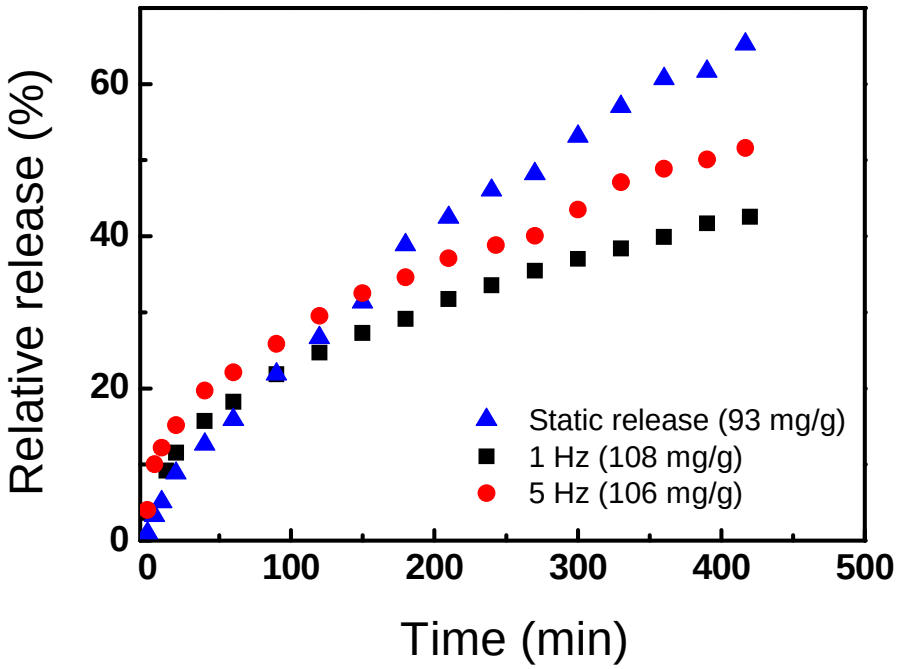

Figure 4-15 Dynamic MB relative from 20HEMA hydrogels at γ=5% under different frequencies. The static release profile was included for comparison

4.3.3. Release Profiles of Various Biomolecules

When various biomolecules were used, the release profile changed significantly depending on molecule weights of the biomolecules and the drug type. Figure 4-16 shows the relative release of PSS, CAF, and BSA from 20HEMA hydrogel under static release conditions. At 480 min, the released biomolecules are 63%, 56% and 41%, respectively, although the drug uptake levels are similar for all of them. The drug uptake levels were 60 mg/g (PSS), 53 mg/g (CAF), and 49 mg/g (BSA).

The release of the drugs through 20HEMA hydrogel is diffusion-controlled, and therefore the concentration gradient is the driving force for the release of the three drugs (Wang et al. 2010). A few factors, including pore volume fraction, pore size of the hydrogel, molecule weight of the biomolecules, and the type and strength of interactions of the drug with the polymer chains that make up the hydrogel network, are generally believed to influence the release of a biomolecule from a hydrogel sample (Fu and Kao 2010; Brazel and Peppas 1999). Since the hydrogel matrix is the same for all the biomolecules, the release rates of these molecules are largely determined by the molecular size, drug types, and the interactions between drug and the hydrogel matrix. From the perspective view of molecule size, the slowest release rate is found for BSA (Mw=67,000), followed by PSS (Mw=482.50) and then CAF (Mw=194.19). Given the similar molecular size of PSS and CAF, higher release level found in CAF could be due to the hydrophobic character of CAF and less solubilisation within the hydrophilic PHEMA gel matrix, which has been also been found in delivery of different drugs using PHEMA hydrogel (Hong et al. 2010; Ei-Arini and Leuenberger 1995; Lee and Lin 2002). In addition, larger interaction between PSS with PHEMA hydrogel chains than that between the CAF and PHEMA chains can result in difference in the relative release (Lee and Lin 2002).

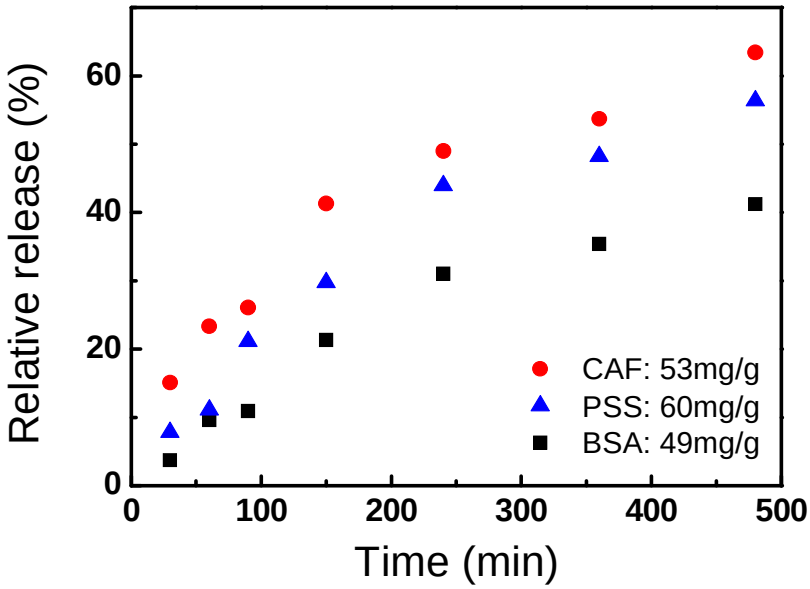

Figure 4-16 Relative release of PSS, CAF, and BSA from 20HEMA hydrogels under static conditions

A dual drug system containing PSS (54 mg/g) and CAF (54 mg/g) was investigated using 20HEMA hydrogel. The release profile of each compound is shown in Figure 4-17. The relative release of each compound was 61% for CAF and 57% for PSS after 480 min and there was small range of difference in the relative release percentages as compared with those from single drug delivery systems (Figure 4-16). This lack of difference in the relative release of PSS and CAF in the dual-drug delivery system is due to the macroporous structure of 20HEMA hydrogel. In addition, lack of intermolecular interactions between the two drugs also led to the appearance of this release characteristic. A similar measurement was conducted using 20HEMA hydrogel loaded with PSS (53 mg/g) and CAF (27 mg/g). Similar relative release profiles for both drugs were observed in this case (data not shown); whilst the released amounts of two single drugs at different time points were significantly different due to low loading level of CAF in the hydrogel (Figure 4-18). 7.2 mg PSS and 4 mg CAF were released from 20HEMA hydrogel after 480 min. Therefore, the amounts of drugs released at a particular time can be properly controlled by the amount of drugs loaded in the matrix. This is particularly useful in a delivery system where various therapeutic levels are required for different drugs.

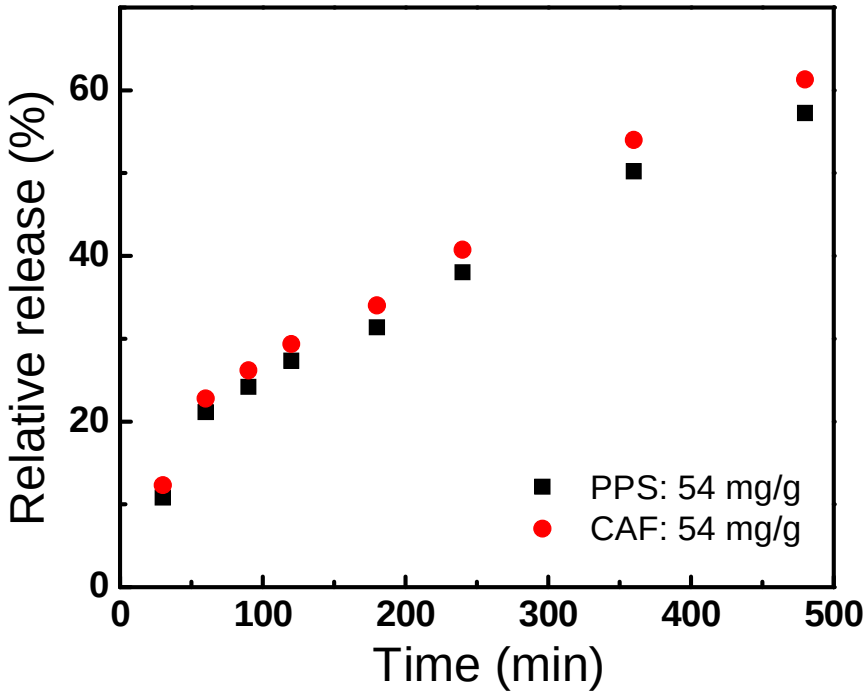

Figure 4-17 Relative releases of PSS and CAF from 20HEMA hydrogel in a dual biomolecule system under static conditions

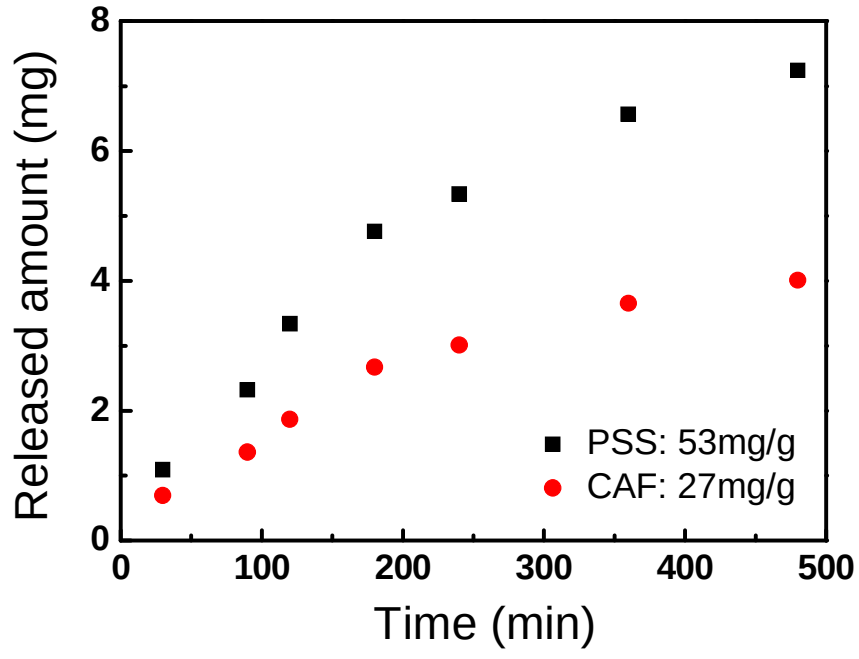

Figure 4-18 Released amounts of PSS and CAF from 20HEMA hydrogel in a dual biomolecule system under static conditions

It has been demonstrated that the relative release of PSS and CAF from a macroporous structure hydrogel (20HEMA) did not show significant difference in their single and dual-drug release systems. 30HEMA, a much less porous hydrogel, was then used to investigate the release of the same two drugs. 30HEMA hydrogel was loaded with PSS (16 mg/g) and CAF (17 mg/g) and the relative release of the drugs is presented (Figure 4-19). It was found that the relative release CAF was much higher than that of PSS during the whole release period, which can be attributed the small size of CAF, its hydrophobic and less solubilisation characteristics, and its week interaction between PHEMA hydrogel (Lee and Lin 2002). As such, a high amount of CAF was released from the hydrogel during the period due to its high transportable capability and high loading level (Figure 4-20).

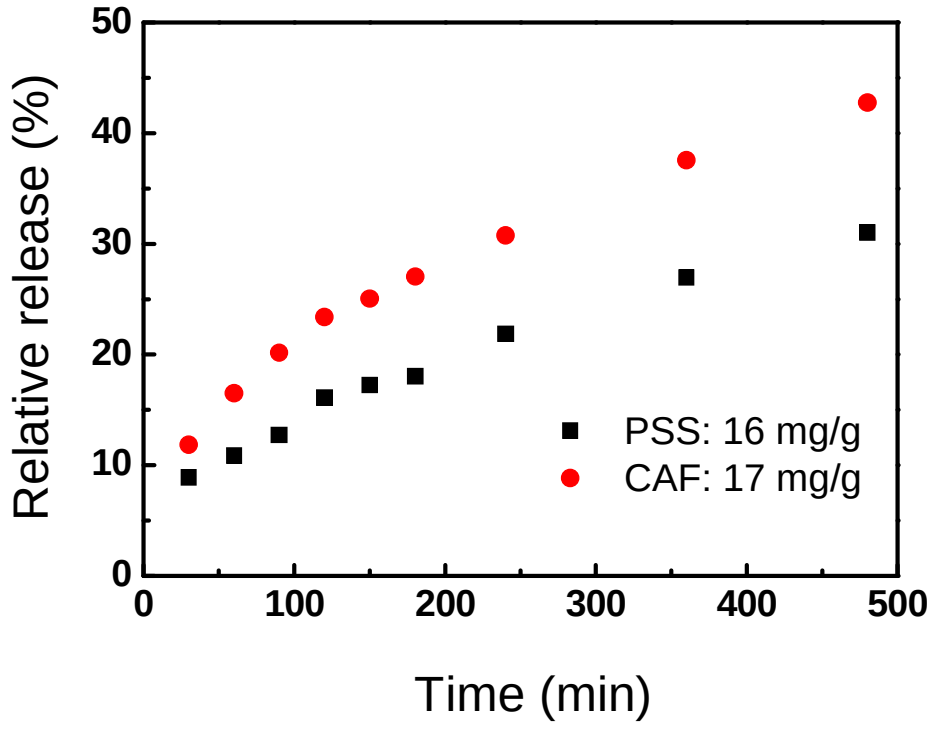

Figure 4-19 Relative release of PSS and CAF from 30HEMA hydrogel in a dual biomolecule system under static conditions

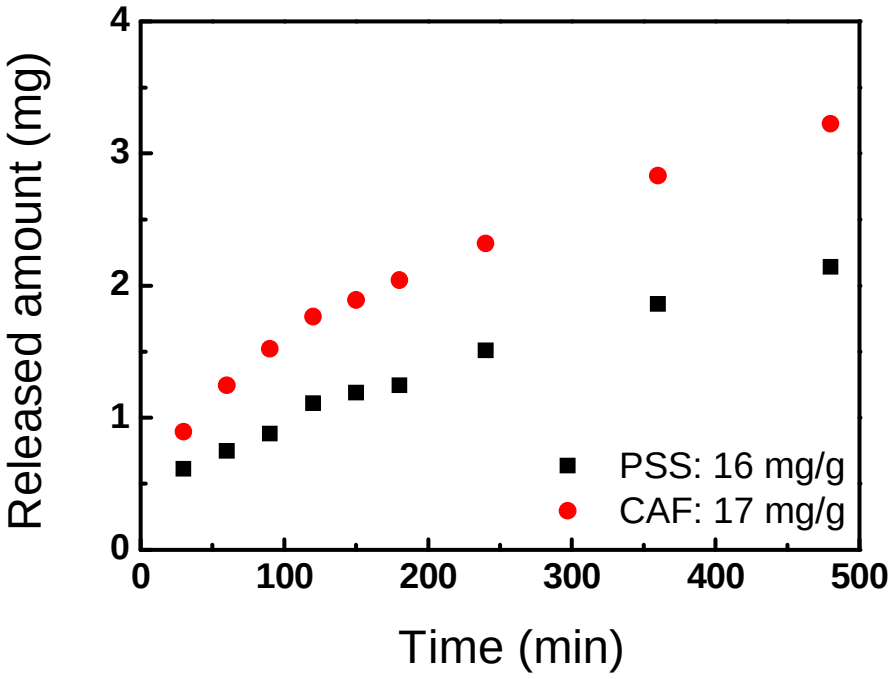

Figure 4-20 Released amounts of PSS and CAF from 30HEMA hydrogel in a dual biomolecule system under static conditions

4.3.4. Release mechanism studies

In order to understand the release mechanism of different PHEMA hydrogels, power law, developed by Ritger and Peppas et al. (Equation 4-7) is used to analyse the results from current study (Siepmann and Peppas 2001; Peppas et al. 2000 ; Ritger and Peppas 1987). It is reported that the molecular diffusion in a matrix can be significant influenced by a mechanical force and its impact on transport kinetics could be much beyond molecular diffusion alone (McCarthy, Soong, and Edelman 1984). Thus, this data analysis is carried out on the static release experiments from the current work (Section 4.3.3. in Chapter 4). The principle has been extensively used by other researchers for such a purpose and the materials include PHEMA hydrogel and other macroporous hydrogel materials (De La Torre, Torrado, and Torrado 2003; Lu and Anseth 1999).

$$M_t / M_\infty = kt^n \qquad (4\text{-}7)$$

Here, Mt and M∞ are the absolute cumulative amount (%) of the drug release at time t (min) and at infinite time. n is a diffusional exponent, indicating the mechanism of the hydrogels. k is the apparent release rate (%/min) and it is a

constant incorporating structural and geometric characteristics of the delivery devices. For a cylinder geometry sample, when the exponent n=0.89 in Equation 4-7, the drug release rate is independent of time. This corresponds to zero-order release. When the exponent n=0.45 in Equation 4-7, it corresponds to Fickian diffusion release. The n values between 0.45 and 0.89 indicate non-Fickian diffusion. This equation is applicable for M_t/M_∞ <0.6.

Figure 4-21 shows the plots of ln(Mt/M∞) against lnt for different drugs release from 20HEMA hydrogel. This data analysis were done based on the data shown in Figure 4-16. It can be seen that a good linearity is shown for each release, indicating that the power law equation is applicable to current release systems. As can be seen, the diffusional exponents (n), shown in Table 4-4 for all the molecules delivery were greater 0.45, indicating the release of these three molecules from 20HEMA followed non-Fickian behavior. In addition, the diffusional exponent shows an increasing trend as the molecule size increases, showing a consistent result from other report (Brazel and Peppas 1999). The diffusional exponent increased from 0.52 (CAF: M_w=194.19) to 0.86 (BSA: M_w=67000). No significant difference of diffusional exponent between small molecules (CAF and PSS) and large molecule (BSA) can be attributed to solute convection during the diffusional release process from macroporous 20HEMA hydrogel (Peppas and Lustig 1986; Lou, Munro, and Wang 2004). The power law has also been applied for dual-drug delivery systems (Ma, Tu, and Zhang 2010; Wei et al. 2009). Thus, the dual-drug delivery results of release exponent (n), rate constant (k), and correlation coefficient (R^2) following linear regression from Figure 4-17, Figure 18 (Only released amounts results are reported in the thesis) and Figure 4-19 were evaluated using the equation and the results also are displayed in Table 4-4. When 20HEMA hydrogel was used for the dual-drug delivery, the diffusional exponents for both drugs were greater than 0.45, indicating non-Fickian behavior. In addition, as the drug loading level was reduced (PSS (53 mg/g) and CAF (27 mg/g)), the PSS release rate was decreased from 1.83 to 0.75 (PSS) and CAF release rate was decreased from 2.16 to 1.1. This deduction in the release rates indicates a less control of the release kinetics from drug diffusion for 20HEMA hydrogel. It has been observed previously (Kim 1998). However, as the pore size dramatically decreased seen for 30HEMA

hydrogel, the diffusional exponents for both drug were 0.46 and 0.47 respectively, indicating a non-Fickian diffusion release. But the values were close to the 0.45, which corresponds to Fickian diffusion. In comparison of the release rate constant, k for different conditions, it is noticed that CAF experienced a much higher release rate than that of PSS and BSA, which can be attributed to hydrophobic, weak interactions with PHEMA hydrogel and less solubilisation characteristics of CAF as discussed before (Hong et al. 2010).

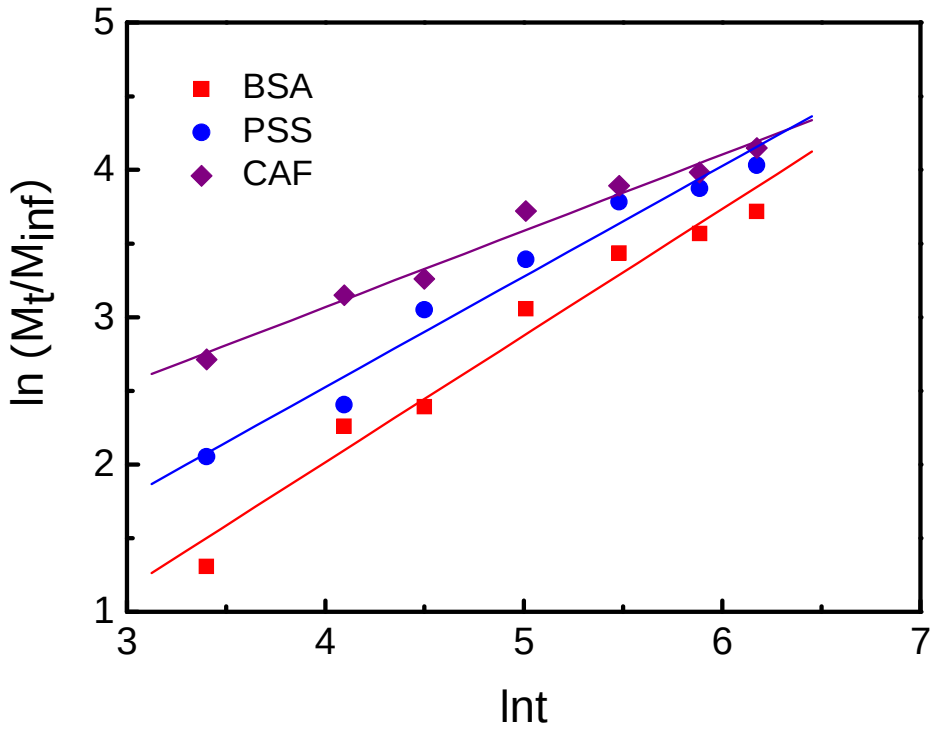

Figure 4-21 Plots of ln(M_t/M_∞) against lnt for different drugs release from 20HEMA hydrogel

Table 4-4 Release exponent (n), rate constant (k), and correlation coefficient (R^2) following linear regression for static drug delivery experiments

Release type	Hydrogel code	Drug	Drug uptake level (mg/g)	Release exponent, n	Rate constant, k	Correlation coefficient (R^2)
Single drug release	20HEMA	BSA	49	0.86	0.24	0.97
	20HEMA	PSS	60	0.75	0.62	0.97
	20HEMA	CAF	53	0.52	2.71	0.98
Dual-drug release	20HEMA	PSS	54	0.56	1.83	0.97
		CAF	54	0.54	2.16	0.98
	20HEMA	PSS	53	0.71	0.75	0.98
		CAF	27	0.66	1.1	0.98
	30HEMA	PSS	16	0.47	1.67	0.99
		CAF	17	0.46	2.53	1.00

4.4. Conclusions

The delivery of a model biomolecule, MB, and three different biomolecules, including PSS, CAF, and BSA, from porous hydrogels was investigated under static and dynamic conditions. Delivery of single and dual biomolecule was investigated.

In the single biomolecule release, increasing the frequency and the shear strain of the stimulations enhanced the relative release of the biomolecule. However, the relative release of the biomolecule was slowed by the application of mechanical stimulations due to the reabsorption of the biomolecule into the hydrogel matrix in comparison to that seen for static conditions. The release profiles of the biomolecule were significantly affected by the porous structure of the hydrogels, molecule weights of the biomolecules, and the character of the biomolecule. In general, a more porous hydrogel demonstrated a higher relative release profile than that seen for a less porous hydrogel. A higher relative release was found for biomolecules with smaller molecule weights. A quicker release of CAF in comparison to PSS was attributed to its hydrophobic and less solubilisation characteristics. Analysis of the data obtained

from static conditions showed that the release the various biomolecules from 20HEMA follows non-Fickian diffusion.

PSS and CAF were used for a dual biomolecule delivery system. It was found that the delivery profiles of each of the biomolecules were the same as the single biomolecule delivery profile. No significant difference was found in the relative release profiles of PSS and CAF from macroporous 20HEMA hydrogels containing different loading levels of each component. However, the released amounts of the each component (PSS or CAF) were significantly dependent on its loading level. For example, the relative release of PSS and CAF was observed similar for two different loading levels-(PSS: 54 mg/g; CAF: 54 mg/g) and (PSS: 53 mg/g; CAF: 27 mg/g), while the released amount of CAF in the latter drug loading level was significantly deducted from 8.7 mg to 4 mg. The relative release of an individual biomolecule from a dual biomolecule delivery system was also affected by the pore structures of the hydrogels, the molecule weights of the biomolecules, and the interactions between the molecule and hydrogel. Analysis of the data obtained from dual biomolecule release showed that the drug release from 20HEMA behaviours non-Fickian, and that from less porous 30HEMA is close to Fickian diffusion. It should be noted that the loading level of each biomolecule can be adjusted simply by changing the concentration of the component in the solutions. Therefore, adjusting the concentrations of each biomolecule can be used to administer proper amounts in order to reach clinical levels for the regeneration of tissues.

CHAPTER 5 CELL ACTIVITIES IN PHEMA AND PHEMA-TiO_2 COMPOSITE HYDROGEL SCAFFOLDS

5.1. Introduction

The focus of this chapter is to investigate the cell activities in PHEMA and PHEMA-TiO_2 composite hydrogels after the hydrogels were modified using an OVICOLL® | CLEAR collagen solution. From the cell viability assay results in Chapter 2, we know that: (1) both PHEMA and PHEMA-TiO_2 composite hydrogels are not toxic to the mouse 3T3 fibroblast cells; (2) the cell growth on hydrogels containing more porous structures, such as 10HEMA and 20HEMA, is more rapid than less porous structures; and (3) the addition of nanoadditives to the porous PHEMA hydrogels has little influence on the cell adhesion or growth. However, in comparison to the cell growth on the tissue culture plates (TPP, Trasadingen, Switzerland), the cell growth on both PHEMA and PHEMA composite hydrogels is relatively slow (Figure 2-19 & Figure 2-20). For tissue engineering applications, improvement of cell activities is essential for these materials. Therefore, collagen was used to modify the existing hydrogels in order to increase the bioactivity of the hydrogels. The modification was completed by immersing the hydrogels in the OVICOLL® | CLEAR collagen solution, followed by a crosslinking process using a glutaraldehyde solution. The hydrogels selected for this study included 10HEMA, 10HEMA-7.5TiO_2, 20HEMA, and 20HEMA-7.5TiO_2. The presence of collagen in the hydrogels was examined using SEM, UV-VIS, and a FTIR. The cell activities in these scaffolds were investigated using three different cell types: green fluorescent protein (GFP)-transfected Swiss 3T3 mouse cells (GFP-3T3), green fluorescent protein (GFP)-transfected 253 human melanoma cells (GFP-MM253), and human mesenchymal stem cells (hMSCs). A laser scanning confocal microscope (LSCM) and a fluorescent microscope were used to monitor the cell adhesion and growth. In addition, a MTT assay was used to study quantitatively the proliferation of hSMCs on 20HEMA and Col20HEMA hydrogels. The influence of hydrogel composition, pore structure, and the presence of collagen in the hydrogels to the cell growth and proliferation is discussed.

Collagen is a major protein comprising the native extracellular matrix (ECM), which provides both the physical support for cells, as well as functions for cell adhesion and regulates cellular growth in human body (Järveläinen et al. 2009; Lutolf and Hubbell 2005). Collagen has been extensively used to improve the bioactivities and cellular functions of synthetic and/or hydrogel scaffolds that are typically bioinert and lack the binding sides or functions that an ECM can provide (Heinemann et al. 2008; Ma et al. 2002; Brynda et al. 2009). Collagen molecules can be incorporated into tissue scaffolds by physical entrapment and blending methods (Lee et al. 2006), dipping/crosslinking methods (Heinemann et al. 2008), or covalent attachment (Bax et al. 2010). Modification from a contacting solution, followed by a further treatment (crosslinking or drying), is a convenient and quick route. In addition, this method has less influence on the porous structures and mechanical properties of the scaffolds (Heinemann et al. 2008; Ragetly, Griffon, and Chung 2010; Shi et al. 2010). Apart from collagen, other biomolecules, such as gelatin, heparin, hyaluronic acid, short peptide sequences originating from cell adhesive proteins such as the Arg-Gly-Asp (RGD) or Tyr-Ile-Gly-Ser-Arg (YIGSR), can also be used to modify tissue scaffolds (Chung and Park 2007; Hersel, Dahmen, and Kessler 2003; Järveläinen et al. 2009; Lutolf and Hubbell 2005).

PHEMA hydrogels are synthetic polymers that do not process supporting lignands for cellular recognition. Researchers have attempted to modify PHEMA hydrogels for better cellular responses (Zainuddin et al. 2008). Studies have been carried out to improve the bioactivities on both non-porous and porous bulk PHEMA-based hydrogels using various biomolecules. In one study, type I collagen has been deposited on non porous poly(2-hydroxyethyl methacralate-co-methacrylic acid) (p(HEMA/MA)) hydrogels. The resultant hydrogels showed improved mesenchymal stromal cell adhesion and growth (Brynda et al. 2009). In other studies, osteopontin, an ECM protein for regulating inflammatory responses, was immobilized onto non-porous PHEMA hydrogels through an iodine monochloride immobilisation method (Martin et al. 2003). The presence of osteopontin on the surface of PHEMA hydrogels enhanced the adhesion of endothelial cells. Moreover, laminin, another ECM protein, and fibronectin/laminin (1:1) were tethered onto the surface of poly(methacryethyl mechacrylate-co-methacrylic acid) (p(HEMA-MMA)). The results indicated that the tethered surface enhanced the corneal epithelial cell

adhesion and growth in comparison to that seen from fibronectin or laminin-coated or plain p(HEMA-MMA) hydrogel surfaces (Jacob et al. 2005). In a different study, RGD was covalently coupled to the surface of PHEMA hydrogels through tresyl chloride immobilization method, which relies on the hydroxyethyl groups on the surface of PHEMA hydrogels. The modified PHEMA hydrogels showed an increase of 3T3 fibroblast cells adhesion by three orders of magnitude (Massia and Hubbell 1990).

For porous PHEMA hydrogels, the modification of hydrogels using collagen type I with the immobilization method was reported. The resultant hydrogels have shown significantly improved C2C12 skeletal myoblast cell spreading (Bryant et al. 2007). YIGSR and Ser-Ile-Lys-Val-Ala-Val (SIKVAV), two laminin-derived oligopeptides, have been covalently coupled to p(2-hydroxylethyl methacrylate-co-2-aminoethyl methacrylate) (p(HEMA-co-AEMA)) hydrogels. The resultant hydrogels promoted cell adhesion and neurite outgrowth (Yu and Shoichet 2005). The efforts of modification of porous PHEMA-based hydrogels have been demonstrated by another group (Kubinová et al. 2010; Kubinová, Horák, and Syková 2009). This research group has reported the cell activities on porous poly(2-hydroxyethyl methacrylate-co-cholesterol methacrylate), PHEMA-CHLMA, when the laminin was used to modify the hydrogels. Desirable cell adhesion, spreading and proliferation are achieved on both unmodified and laminin-modified porous p(HEMA-CHLMA) (Kubinová, Horák, and Syková 2009). In a latest study, SIKVAV was immobilized on porous poly(2-hydroxyethyl methacrylate-co-2-aminoethyl methacrylate), p(HEMA-AEMA), hydrogels. The results demonstrated that the presence of the peptide sequence on porous p(HEMA-AEMA) hydrogels significantly increased numbers of rat mesenchymal stem cells adhesion and their growth area in the absence of serum in the culture medium. Also, it was found that the immobilized peptides supported human fetal neural stem cell attachment, proliferation and differentiation (Kubinová et al. 2010).

In the present study, a mixture of collagen type I and III (OVICOLL® | CLEAR collagen, 10 mg/ml) was used to modify PHEMA and PHEMA-7.5TiO_2 hydrogels via a dipping method, followed by the crosslinking of collagen using a glutaraldehyde solution (0.25%). Cell activities (adhesion, spreading, and

proliferation) on these modified hydrogel were evaluated using three different cell lines, including GFP-3T3, GFP-MM253, and hMSCs. The purpose of using different cell lines is for a board screening.

5.2. Experimental

5.2.1. Chemicals

Cell culture medium, Dulbecco's Modified Eagle's Medium (DMEM) high glucose without phenol red, for GFP-3T3 cells and GFP-MM253 cells was from Logan (Utah, USA). Mesenchymal stem cell growth medium (MSCGM) was from Lonza, USA. Fetal bovine serum (FBS) was from HyClone. L-glutamine, HEPES, sodium pyruvate and 0.05trypsin-EDTA were obtained from Invitrogen (Carlsbad, California, USA). RPMI-1640 medium was obtained from Signa-Aldrich (St Louis, Missouri, USA). 3-[4,5-dimethylthiazolyl-2]-2,5-diphenyl tetrazolium bromide (MTT), dimethyl sulfoxide (DMSO), Calcein AM, ethidium homodimer-1 and glutaraldehyde (50% in H_2O) were purchased from Sigma-Aldrich. An OVICOLL® | CLEAR collagen solution (10 mg/ml) was received from CollTech Australia Ltd, Australia. The OVICOLL® | CLEAR collagen was a type I and III collagen combination and the ratio is approximately 80:20 (type I: type III). All other chemicals were of analytical grade, and used as-received.

5.2.2. Modification of Hydrogels with Collagen

Freeze dried hydrogels were first gently polished using a sand paper in order to allow the opening of the surface pores that might have been closed in the manufacture process due to the skin effect (Lou et al. 2005). The hydrogel samples were then placed in 2.5 ml centrifugation tubes separately, and 100 µl OVICOLL® | CLEAR collagen solution (10 mg/ml) was added into each tube. The incubation was carried out in an orbital shaker (50 rpm) for 24 hours, followed by removing the collagen residual solution from each tube. 100 µl glutaraldehyde solutions (0.25 wt.%) were added into each tube for crosslinking and the samples were treated at 60ºC for 10 minutes. The crosslinking process was further conducted at 5ºC for overnight. After the crosslinking process, they were treated at 60ºC for 10 minutes again. All hydrogel samples were removed from the container and put into Milli-Q water after

keeping them at room temperature for 2 hours. The residual chemicals including unattached collagen were extracted by water exchange twice per day for over 7 days.

5.2.3. Characterization of the Modified Hydrogels

Morphological analysis was conducted using SEM (Philips XL30 and Zeiss, NEON 40EsB, Germany). The same procedure was used to prepare SEM samples (Chapter 2.2.4).

A PerkinElmer FTIR spectrometer (PerkinElmer, Spectrum 100 Series, USA) was used to verify the presence of OVICOLL® | CLEAR collagen in PHEMA hydrogel. The test was conducted from 4000 to 1000 cm^{-1} using a resolution of 2 cm^{-1}. Twenty measurements were repeated for each test.

A GBC 916 UV-Vis spectrometer (GBC Scientific Equipment, Australia) also was used to verify the presence of collagen in PHEMA hydrogel (Alina 2001). A piece of Col20HEMA was cut into small pieces, followed by heating up to 60°C in 0.5 ml water. The clear solution was measured using the UV-VIS. Control 20HEMA and an OVICOLL® | CLEAR collagen solution (20 μg/ml) also were evaluated with UV-VIS using the same procedure.

5.2.4. Cellular Activities

(1) Human mesenchymal stem cells (hMSCs)

hMSCs were cultured in mesenchymal stem cell growth medium (MSCGM) (Lonza, U.S.A.) and incubated at 37°C in a humidified 5% CO_2 incubator. The medium was refreshed every three days. The cells were harvested with PBS containing 0.025 % trypsin and 0.01% EDTA, followed by centrifuged and subcultured to passage 4 in the MSCGM medium. 30 μl of hMSCs suspension (1×10^5 cells/ml) were added on the top of PHEMA hydrogels (surface area: 0.2 cm^2), which were placed in a 96-well culture plate. Three samples were used for each hydrogel formulation. At the desired time intervals (Day 1, 3, 6 or 7), 150 μl fresh MTT solution (5mg/ml in PBS) were added to each well and the culture plates were incubated for 4 hours. The formed purple formazan was dissolved with 200 μl DMSO. 100 μl of DMSO solution were

transferred to a fresh 96-well plate and measured with a spectrophotometer at 550 nm with background subtraction at 690 nm. In addition, the imaging was conducted at the designated time intervals.

(2) Green fluorescent protein (GFP)-transfected Swiss 3T3 mouse cells (GFP-3T3)

Green fluorescent protein (GFP)-transfected Swiss 3T3 mouse (GFP-3T3) cells were cultured in a phenol red free Dulbecco's Modified Eagle's Medium (DMEM) supplemented with 2 mM L-glutamine, 10mM HEPES, 1mM sodium pyruvate and 10% fetal bovine serum (FCS) at 37°C in a humidified 5% CO_2 incubator. Hydrogel disks (surface area: 0.33cm^2) were sterilized (autoclave: 121°C, 15 min) prior to the pre-culture with DMEM media in 24-well cell culture plates for 2 hours. 5 μl of cell suspension with a density of 3.3×10^5 cells/ml were added to each of the hydrogels after the pre-culture media was aspirated. After 5 min, 5 μl of the same cell suspension were added again. 400 μl of fresh media were carefully added after 40 min. The hydrogels were continuous cultured at 37°C in a humidified 5% CO_2 incubator until they were processed at time intervals (Day 3). The culture medium was refreshed every other day.

(3) (GFP)-transfected MM253 human melanoma cells (GFP-MM253)

Same culture protocol for GFP-3T3 mouse cells was used for GFP-MM253. The cell density in the cell suspension solution was 5×10^5 cells/ml. The hydrogels were continuous cultured at 37°C in a humidified 5% CO_2 incubator until they were processed at time intervals (Day 1 and Day 4). The culture medium was refreshed every other day.

The growth of the hMSCs was monitored and photographed using a confocal laser scanning microscope (CLSM; Olympus FV300, Japan). Live/dead staining assay was used for CLSM imaging. Briefly, cells cultured on the surfaces of hydrogels in chambered coverglass (NUNC, Denmark) were washed with PBS and incubated in 0.5 ml of PBS containing calcein AM (2 μM; labelling live cells) and ethidium homodimer-1 (2 μM; labelling dead cells) for 30 min, and then visualized by CLSM at excitation wavelengths of 488 nm and 532 nm. The growth of GFP-3T3 and GFP-

MM253 cells was monitored using a fluorescent microscope (Carl Zeiss). After the culture time has been reached, the hydrogel was placed on a glass slide and coved using a coverslip. The hydrogel was viewed under the fluorescent microscope and a Spot Pursuit^{TM} 4MP digital camera was used to take images. Mean ± standard deviation and the P value were calculated using one-way ANOVA with OriginPro (Version 7.5) software and Turkey test. P values <0.05 were considered statistically significant.

5.3. Results and Discussion

5.3.1. Confirmation of Collagen in Hydrogels

Figure 5-1 shows the FTIR spectra of Col20HEMA and 20HEMA hydrogel and the FTIR spectrum from as-received OVICOLL® | CLEAR collagen. Typical peaks including ~3380 cm^{-1} (O-H stretching vibrations), 1720 cm^{-1} (C=O stretching vibrations), 1650 cm^{-1} (H-O-H bending vibrations), and 1079 cm^{-1} (C-O-C bending vibrations), were attributed to wet 20HEMA hydrogel, and all these typical peaks were found in the spectrum of Col20HEMA hydrogel (Perova, Vij, and Xu 1997). A peak from the spectrum of Col20HEMA was seen at 1544 cm^{-1} after the hydrogel was modified using OVICOLL® | CLEAR collagen. This peak was attributed to amide II group for amide N-H bending vibrations coupled with C-N stretching in collagen. In addition, the relative intensity of 1656 cm^{-1} was also found enhanced. This is due to the presence of the Amide I: C=O stretching vibrations, coupled with O-H in collagen. These findings indicate the presence of collagen in Col20HEMA hydrogel. Other typical peaks, including 3310 cm^{-1} (Amide A: N-H stretching vibrations coupled with O-H, and 1243 cm^{-1} (Amide III: N-H bending vibrations), were found for collagen.

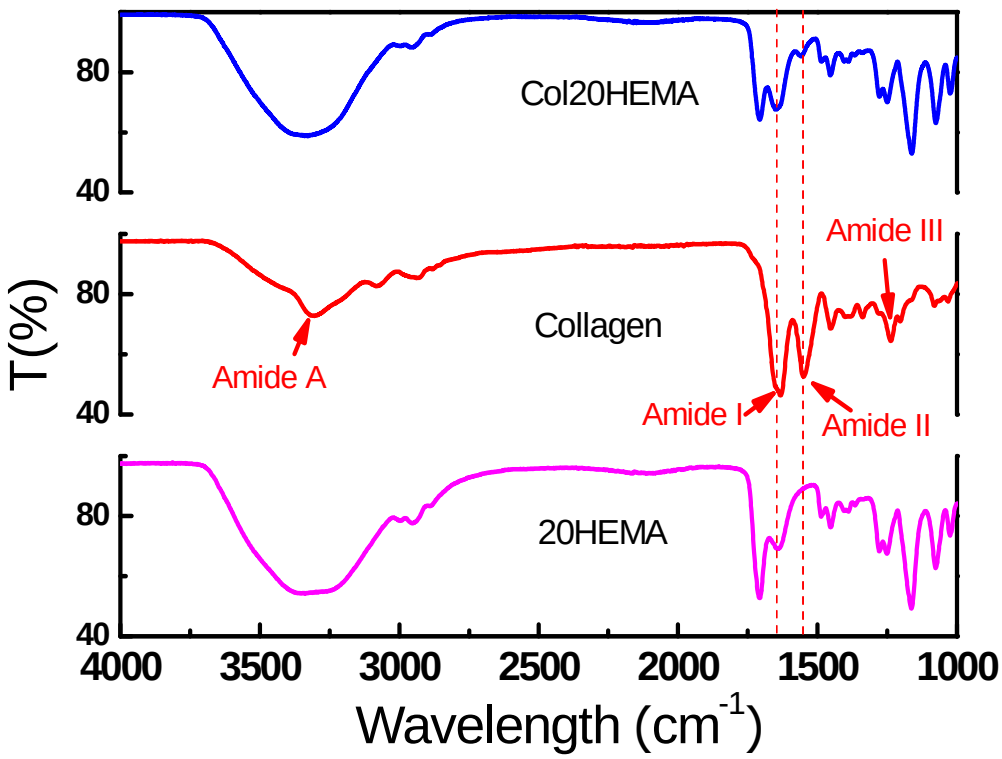

Figure 5-1 FTIR spectra of collagen, 20HEMA, and Col20HEMA

UV-VIS spectra from extracted solutions of Col20HEMA and 20HEMA, and an OVICOLL® | CLEAR collagen solution (20 μg/ml), are displayed in Figure 5-2. Absorbance ranging from 250 nm to 280 nm was observed from the solution of Col20HEMA hydrogel and this absorbance range was in accordance with that from the OVICOLL® | CLEAR collagen solution. In this range, there was no absorbance from the solution of 20HEMA hydrogel. Therefore, the presence of collagen in Col20HEMA hydrogel was verified again.

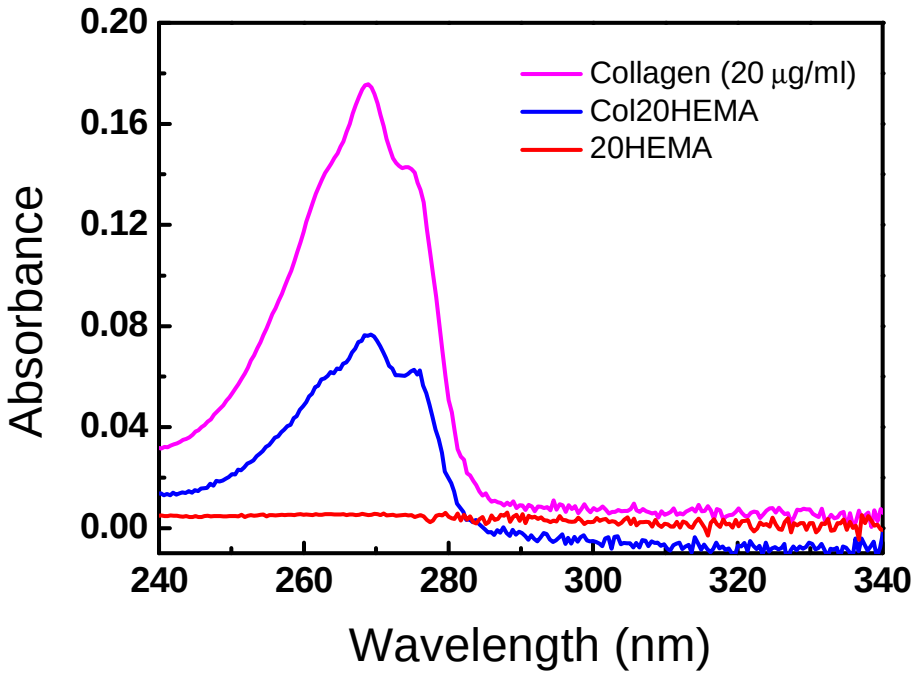

Figure 5-2 UV-VIS spectra of the aqueous extracts from Col20HEMA and 20HEMA hydrogels; Spectrum from an OVICOLL® | CLEAR collagen solution (20 μg/ml) was used for comparison

5.3.2. Morphological Analysis

Figure 5-3 shows the morphology of the hydrogels including 10HEMA, 10HEMA-7.5TiO_2, 20HEMA, and 20HEMA-7.5TiO_2 before and after the modification using OVICOLL® | CLEAR collagen. There was a change in morphology between the treated and untreated 10HEMA and 10HEMA-TiO_2 hydrogels which was probably due to the freeze drying process applied to the samples prior to the SEM examination. There was no apparent changes in the treated for 20HEMA and 20HEMA-7.5TiO_2 hydrogels. This is understandable as 20HEMA hydrogels are generally harder and have less water content than 10HEMA and 10HEMA-TiO_2, therefore, the effect of freeze drying on these two hydrogels was less effective. Fibrous networks were found on the surface of the hydrogels of Col10HEMA, Col10HEMA-7.5TiO_2, Col20HEMA, and Col20HEMA-7.5TiO_2 (Figure 5-3 b, d, f, and h). These structures were very apparent on the surface of Col10HEMA and Col20HEMA hydrogels. A high magnification of SEM was taken from Col10HEMA (Figure 5-4 a) which displays a reassembling of collagen structure that has been shown by other researchers (Han 2006) (Figure 5-4 b).

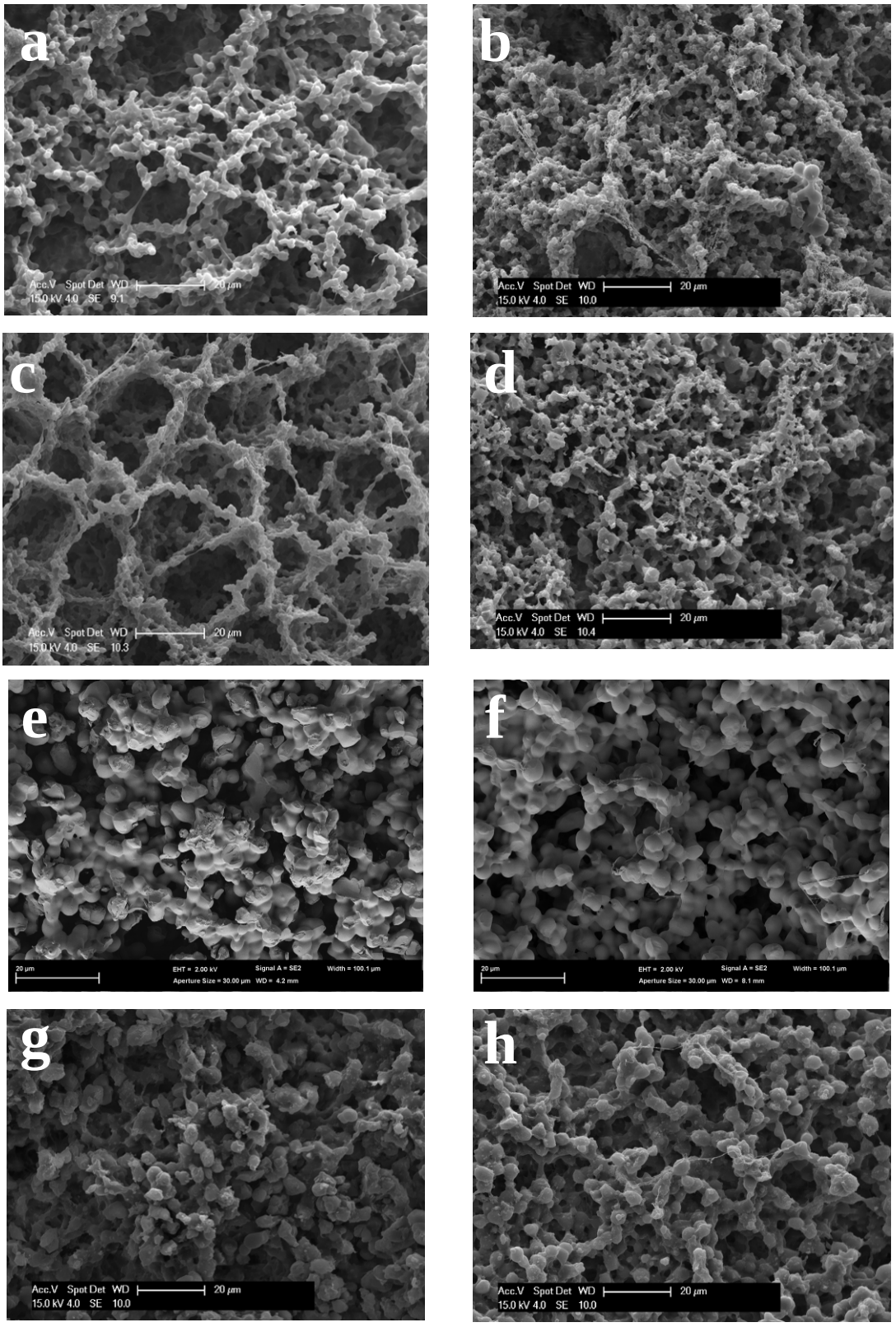

Figure 5-3 SEM micrographs of hydrogels (a) 10HEMA, (b)Col10HEMA, (c) 10HEMA-7.5TiO_2, (d) Col10HEMA-7.5TiO_2, (e) 20HEMA, (f) Col20HEMA, (g) 20HEMA-7.5TiO_2, and (h) Col20HEMA-7.5TiO_2

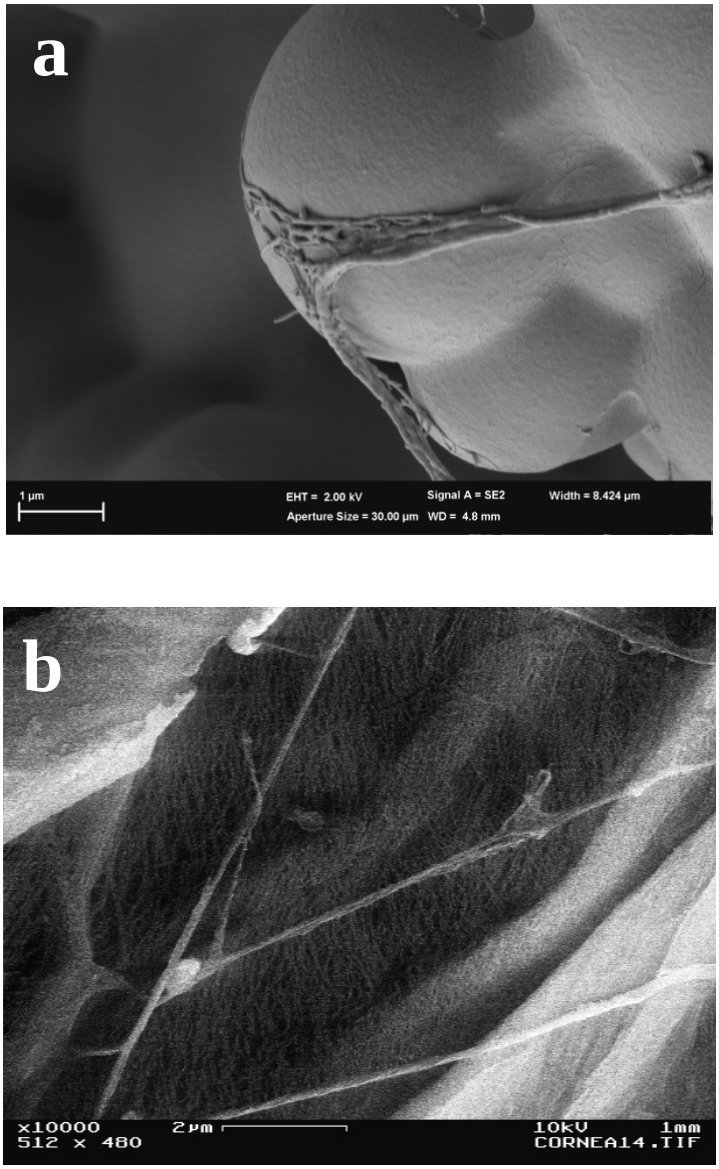

Figure 5-4 (a) SEM micrograph of Col10HEMA hydrogel, and (b) collagen fibrils making up the rat cornea (Han 2006)

5.3.3. Cell Activities in the Porous Hydrogel Surfaces

Figure 5-5 shows the growth of GFP-3T3 cells on (a) 20HEMA, (b) Col20HEMA and (c) Col20HEMA-7.5TiO_2. Cellular adhesion was observed for all hydrogels. However, significantly high GFP-3T3 cell densities were found on Col20HEMA and Col20HEMA-7.5TiO_2 hydrogels compared to that on 20HEMA after Day 3. This finding suggests that the presence of OVICOLL® | CLEAR collagen on the hydrogels

enhanced the cell adhesion after seeding and their growth. In addition, GFP-3T3 cells were not well spread on the 20HEMA hydrogel and they were mainly aggregated instead of adhering onto the surface of 20HEMA hydrogel. The GFP-3T3 cells were adhered, well spreaded and proliferated on hydrogels after modification using OVICOLL® | CLEAR collagen, which confirmed the presence of collagen was also able to enhance GFP-3T3 cell spreading and stimulate GFP-3T3 cell growth. A higher magnification of GFP-3T3 cells on Col20HEMA hydrogel is inserted in Figure 5-5 (b). No significant influence from TiO_2 addition on the cell growth was observed after a comparison that between Col20HEMA and Col20HEMA-7.5TiO_2 hydrogels (Figure 5-5 b and c).

The growth of GFP-MM253 cells was also studied after Day 1 and 4 and the results are displayed in Figure 5-6. After Day 1, GFP-MM253 cells can be found on Col10HEMA and Col20HEMA hydrogels and there were no apparent cells on 2-HEMA hydrogel. GFP-MM253 cells on Col10HEMA and Col20HEMA hydrogels were significantly increased after Day 3. The number of cells on 20HEMA after Day 3 was still significantly low. This finding again suggests that the presence of collagen fibres on the hydrogel improved the cell adhesion and the following proliferation of GFP-MM253 cells. No significant difference in cell responses was found between Col10HEMA and Col20HEMA hydrogels (Figure 5-6 b and d). In comparison to cellular activities seen for GFP-3T3, it was observed that GFP-MM253 cells had less capability of spreading on the modified hydrogels.

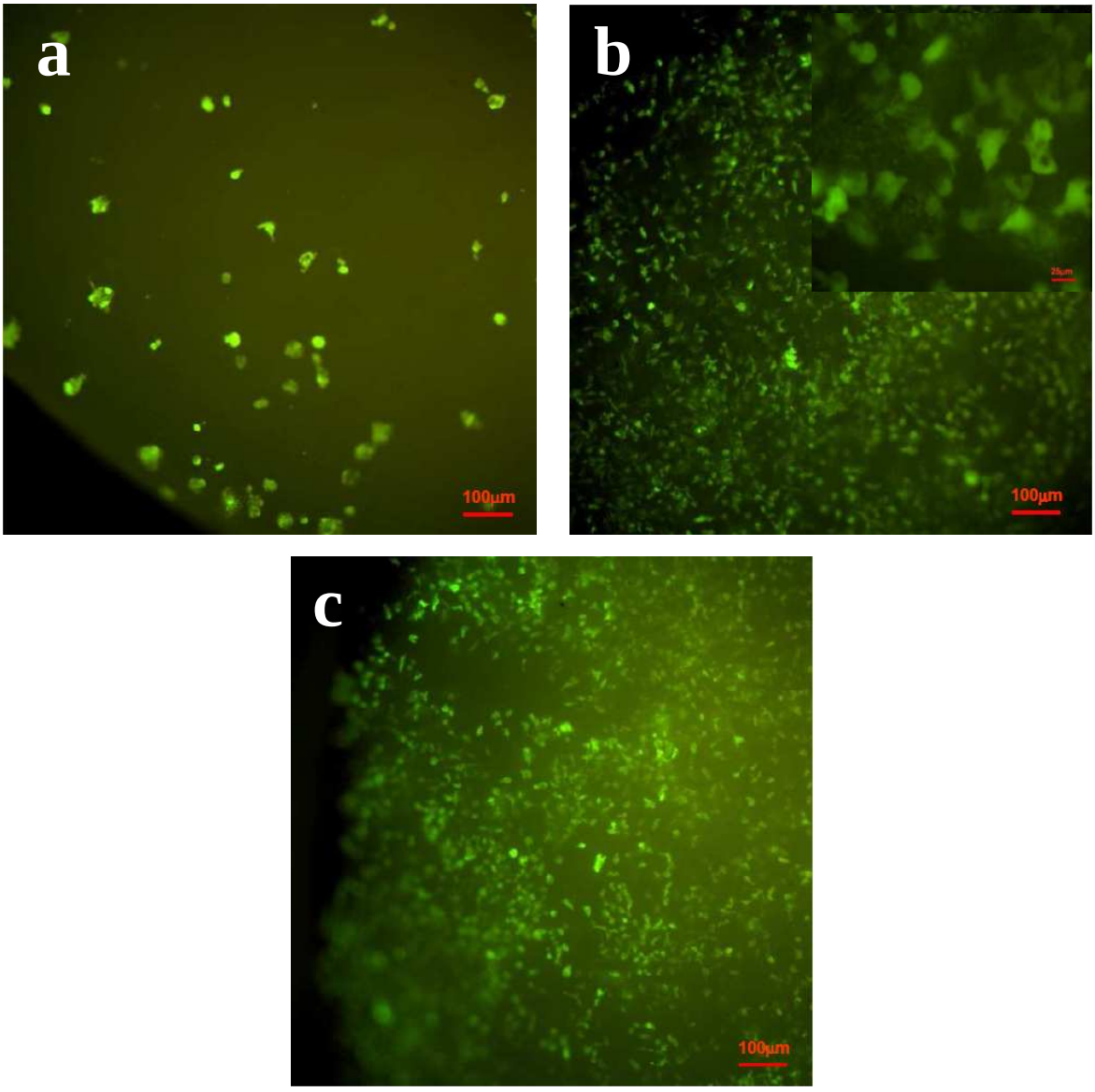

Figure 5-5 Fluorescent micrographs showing the growth of GFP-3T3 cells on the surface of (a) 20HEMA, (b) Col20HEMA and (c) Col20HEMA-7.5TiO_2 hydrogels after Day 3

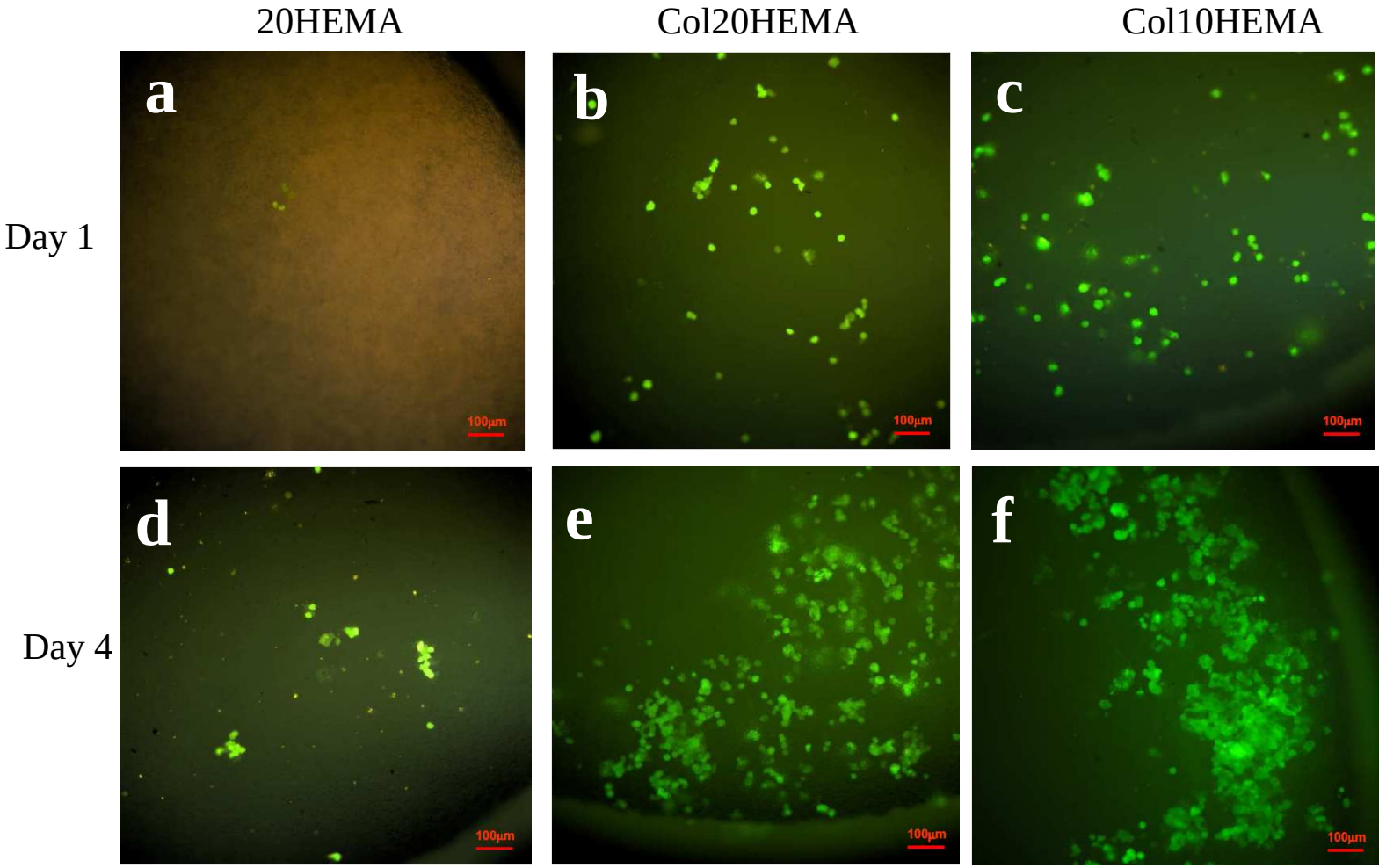

Figure 5-6 Fluorescent micrographs showing the growth of GFP-MM253 cells on the surface of (a, d) 20HEMA, (b, e) Col20HEMA, and (c, f) Col10HEMA hydrogels after Day 1 and Day 4

Figure 5-7 shows of the growth of hMSCs on 20HEMA and Col20HEMA after Day 1, 3, and Day 7. Similar results of the cell activities were observed. Very limited numbers of hMSCs were seen on the surface of control 20HEMA hydrogel, while the numbers of hMSCs on Col20HEMA were increased greatly, attributed to the presence of collagen in the hydrogel. In addition, when the cell culture incubation was increased until Day 7, the cells on Col20HEMA showed good spreading and signs of apparent proliferation. However, the cells on 20HEMA hydrogel did not show a good spreading and no apparent sign for cell proliferation was seen. This further demonstrates that not only cell attachment but also cell growth capability were enhanced after the modification using OVICOLL® | CLEAR collagen. Furthermore, a cross-sectional image for investigating the growth of hMSCs within Col20HEMA after Day 7 is shown in Figure 5-8, from which hMSCs were observed. It indicates that hMSCs were capable of growing into Col20HEMA hydrogel. This in-growth characteristic can be beneficial greatly for regenerating tissues. From the top surface of the hydrogel indicated by an arrow in the image, hMSCs have, overall, penetrated downwards the macroporous structure about 0.6 mm. It was seen that aggregates of the hMSCs were located separately within the hydrogel. This distribution probably was attributed to the pore structure and the amounts of the collagen in the places where cells were found.

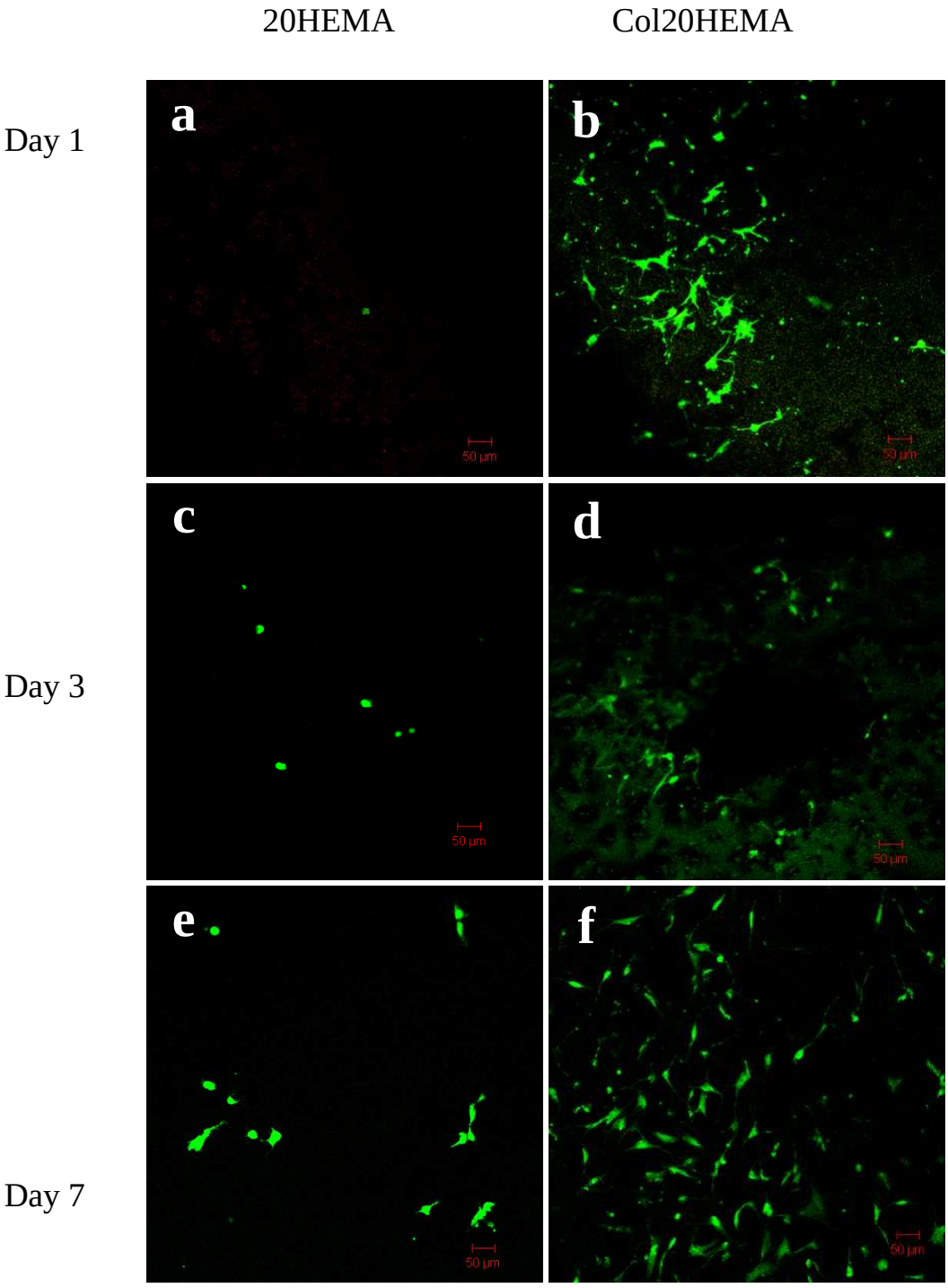

Figure 5-7 LSCM micrographs showing the growth of hMSCs on the surface of (a, c, and e) 20HEMA and (b, d, and f) Col20HEMA after Day 1, 3, and 7

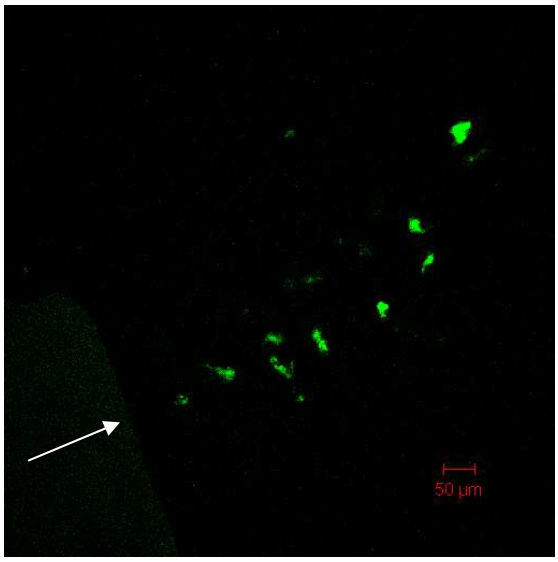

Figure 5-8 Cross-section analysis of hMSC in Col20HEMA after Day 7 using a LSCM (arrow shows the top surface of the hydrogel)

Figure 5-9 shows the optical density, which is proportional to the cell density of hMSCs, of 20HEMA and Col20HEMA hydrogels. Overall, increased viable hMSCs on both hydrogels was seen as the incubation time was increased. The relatively low absorbance at Day 1 was attributed to the recovery of the cells from the culture conditions. Increased cell growth was noticed at Day 3 and Day 7. At Day 7, significant increase of cell numbers were found in Col20HEMA hydrogels, indicating that the modified hydrogels were more preferable for cell adhesion and cell growth. This finding indicates that the treatment of the hydrogels with OVICOLL® | CLEAR collagen had a positive impact on the cell proliferation.

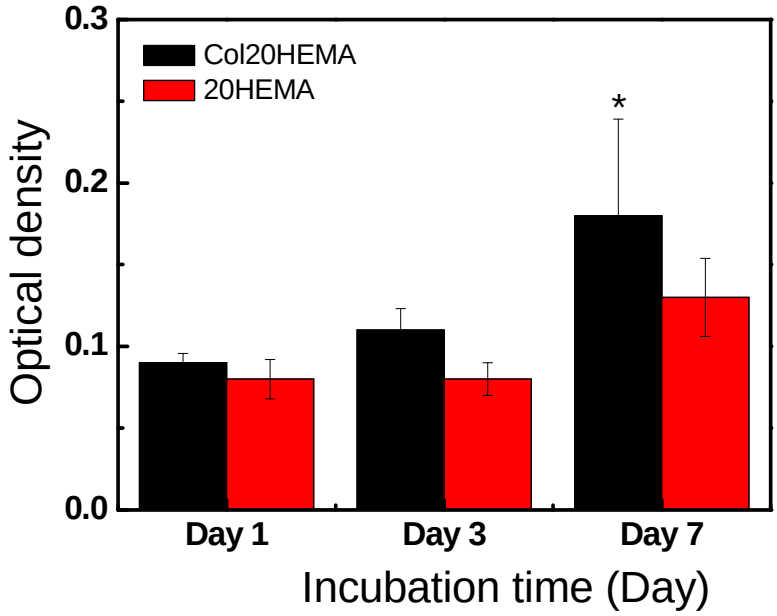

Figure 5-9 The hMSCs growth measured by the MTT assay. The optical density values are proportional to the numbers of the living hMSCs. (*) indicates the significant different in optical density in comparison to that from Day 1 Day 3 for Col20HEMA

5.4. Conclusions

Four hydrogels, including 10HEMA, 20HEMA, 10HEMA-7.5TiO_2, and 20HEMA-7.5TiO_2, were successfully modified with OVICOLL® | CLEAR collagen. The presence of collagen in the hydrogels was confirmed using FTIR, UV-VIS and morphological analysis. Fibrous networks of collagen were found on the cross-section of the modified hydrogels. The presence of collagen in hydrogels enhanced significantly the cellular adhesion and spreading for three cell lines, including GFP-3T3 cells, GFP-MM253 cells, and hMSCs. Accelerated proliferation of GFP-MM253 cells and hMSCs was also observed for hydrogels modified with collagen along the incubation time.

CHAPTER 6 CONCLUSIONS

Eighteen porous PHEMA composite hydrogels containing TiO_2, multi-walled CNTs and SiO_2, and five plain PHEMA hydrogels were successfully synthesized and evaluated for applications as soft tissue regeneration scaffolds. Four of these hydrogels were further modified with an OVICOLL® | CLEAR collagen, a mixture of type I and type III collagen, for the improvement of cell activities.

Both PHEMA and PHEMA composite hydrogels appeared opaque and exhibited macroporous structures. The porous structures were largely dependent on the HEMA:water concentrations in the polymerization mixtures. In general, a lower HEMA:water concentration ratio resulted in a more porous structure, whist a higher HEMA:water ratio facilitated the production of a less porous structure hydrogel. The addition of the nanoadditives showed some minor impact on the porous structures of the less porous hydrogels, i.e., the hydrogels contained high HEMA concentrations. This finding is very useful for the production of tissue scaffolds with incorporation of essential biomolecules for the regeneration of specific tissues without varying the pore structures of the scaffold.

The porous structure in hydrogel polymers had significant impacts on their mechanical properties. In general, higher tensile and elastic moduli were seen for hydrogels with less porous structures. Conversely, lower tensile and elastic moduli were seen for more porous structured hydrogels. The addition of TiO_2 particulates did not show significant influence on tensile and elastic moduli. However, the addition of CNTs increased the viscoelastic moduli of PHEMA hydrogels, attributed to their fibre characteristics. Both PHEMA and PHEMA-TiO_2 composite hydrogels showed a moderate shear elastic modulus in the range of 10^4~10^5 Pa, which is comparable for the liver, muscle, and nucleus pulpous tissues. The value was also within the range for native cartilaginous tissue (0.7×10^3-1×10^6 Pa) (Söntjens et al. 2005; Vanderhooft et al. 2009). In comparison with another hydrogel, poly (ethylene glycol) diacrylate, that have been evaluated for human adipose tissue regeneration (Patel, Smith, and Patrick 2005), PHEMA and PHEMA-TiO_2 hydrogels produced in this study have showed a greater range of linear viscoelasticity (2~25%), dependent

on the macroporous structures and the presence of the TiO_2 nanoadditives. In addition, the tensile properties of the investigated hydrogels are within the range of a few soft tissues. Moreover, PHEMA and PHEMA-TiO_2 composite hydroegls demonstrate excellent elongation properties, which is truly an advantage when this property becomes a factor for tissue regeneration. These indicate that macroporous PHEMA and its composite hydrogels have a better adaptivity and can be tuned to accommodate more complex mechanical environments, which enable them to become a potential scaffolding materials for engineering such tissues as nerves, muscles, and cartilaginous tissues such as articular cartilage.

The delivery of biomolecules from the selected PHEMA hydrogels was also investigated. Four different biomolecules were investigated using both single and dual molecule modes at both static and dynamic conditions. For the dynamic delivery, increasing the frequencies and the shear strains of the rheological stimulations accelerated the relative release of these biomolecules from PHEMA hydrogels. In comparison with results from the release without stimulation, significant difference in the relative release was found only when the frequency and strain of the rheological stimulations were relative low. When these parameters were increased, the delivery properties became similar to those in the static conditions. This finding can assist the researches to consider the dosing amount of different biomolecules in such a dynamic release circumstance. The relative release of the biomolecules was affected by the concentration and molecular weights of the biomolecules, the biomolecule type, the interaction between the biomolecule and the hydrogel, as well as the porous structure of the hydrogels. In general, a more porous PHEMA hydrogel showed a higher relative release under both static and dynamic conditions. A quicker relative release was seen for the biomolecules with a smaller molecule weight or a higher concentration. When dual biomolecules were used in the system, the delivery profiles of each of the biomolecules were the same as the single biomolecule delivery profile. The relative release was dependent on the molecule weights and the porous structures. It should be noted that loading level of each biomolecule could be easily adjusted by using various concentrations of the biomolecule, resulting in different released amounts of the biomolecule (Lou, Munro, and Wang 2004; Wang et al. 2010). Therefore, it becomes possible to regulate accurately the amount and time

period of biomolecule release for regenerative processes. This is a great benefit for the tissue engineering scaffolds.

Finally, bioactivity of the PHEMA and PHEMA composite hydrogels were evaluated though a calcification study and cell activities study. At low HEMA concentrations, the composite hydrogels contain more pores and more suitable surface properties and are favourable to the formation and infiltration of CaP. The addition of TiO_2 nanoparticles can significantly enhance the formation of CaP in hydrogel polymers. However, no significant effect can be seen from composite hydrogels containing SiO_2 and CNTs. For the cell activity studies, no significant impact has been seen from the incorporation of nanoadditives in this study. However, when small amounts of collagen molecules were added into the hydrogels, the cell activities were significantly enhanced. This is true for both PHEMA and PHEMA-TiO_2 composite hydrogels.

Overall, the macroporous structures, the mechanical properties, and biomolecule transportation and delivery properties of PHEMA and PHEMA-composite hydrogel polymers can be tailor-made to meet specifications required by various applications. Moreover, the cellular responses of PHEMA and PHEMA-TiO_2 hydrogels can be further improved using collagen, an ECM protein. Therefore, these preliminary investigations of PHEMA and PHEMA composite hydrogel have demonstrated their great potential for such applications as liver, muscle, nucleus pulpous, and articular cartilage.

REFERENCES

Abouna, G. M. 2001. The humanitarian aspects of organ transplantation. Transplant International 14 (2): 117-123.

Adekogbe, I., and Ghanem, A. 2005. Fabrication and characterization of DTBP-crosslinked chitosan scaffolds for skin tissue engineering. Biomaterials 26: 7241-7250.

Agrawal, S. K., Sanabria-DeLong, N., Tew, G. N., and Bhatia, S. R. 2008. Nanoparticle-reinforced associative network hydrogels. Langmuir 24 (22): 13148-13154.

Aimoli, C. G., Torres, M. A., and Beppu, M. M. 2006. Investigations into the early stages of "in vitro" calcification on chitosan films. Materials Science and Engineering: C 26 (1): 78-86.

Alina, S. 2001. The influence of glutathione on the photochemical stability of collagen. Polymer Degradation and Stability 73 (1): 107-112.

Altman, G., H. , Diaz, F., Jakuba, C., Calabro, T., Horan, R., L. , Chen, J., Lu, H., Richmond, J., and Kaplan, D., L. . 2003. Silk-based biomaterials. Biomaterials 24: 401-416.

Andac, M., Plieva, F. M., Denizli, A., Galaev, I. Y., and Mattiasson, B. 2008. Poly(hydroxyethyl methacrylate)-Based Macroporous Hydrogels with Disulfide Cross-Linker. Macromolecular Chemistry and Physics 209 (6): 577-584.

Andrews, K. D., Hunt, J. A., and Black, R. A. 2007. Effects of sterilisation method on surface topography and in-vitro cell behaviour of electrostatically spun scaffolds. Biomaterials 28 (6): 1014-1026.

Arima, Y., and Iwata, H. 2007. Effect of wettability and surface functional groups on protein adsorption and cell adhesion using well-defined mixed self-assembled monolayers. Biomaterials 28 (20): 3074-3082.

Atala, A., Bauer, S. B., Soker, S., Yoo, J. J., and Retik, A. B. 2006. Tissue-engineered autologous bladders for patients needing cystoplasty. The Lancet 367 (9518): 1241-1246.

Atzet, S., Curtin, S., Trinh, P., Bryant, S., and Ratner, B. 2008. Degradable Poly(2-hydroxyethyl methacrylate)-co-polycaprolactone Hydrogels for Tissue Engineering Scaffolds. Biomacromolecules 9 (12): 3370-3377.

Baldwin, S. P., and Saltzman, W. M. 1998. Materials for protein delivery in tissue engineering. Advanced Drug Delivery Reviews 33 (1-2): 71-86.

Barik, T., Sahu, B., and Swain, V. 2008. Nanosilica—from medicine to pest control. Parasitology Research 103 (2): 253-258.

Bavaresco, V. P., Zavaglia, C. A. C., Reis, M. C., and Gomes, J. R. 2008. Study on the tribological properties of pHEMA hydrogels for use in artificial articular cartilage. Wear 265 (3-4): 269-277.

Bax, D. V., McKenzie, D. R., Weiss, A. S., and Bilek, M. M. M. 2010. The linker-free covalent attachment of collagen to plasma immersion ion implantation treated polytetrafluoroethylene and subsequent cell-binding activity. Biomaterials 31 (9): 2526-2534.

Bennett, D. J., Burford, R. P., Davis, T. P., and Tilley, H. J. 1995. Synthesis of porous hydrogel structures by polymerizing the continuous phase of a microemulsion. Polymer International 36 (3): 219-226.

Bhattacharyya, S., Guillot, S., Dabboue, H., Tranchant, J.-F., and Salvetat, J.-P. 2008. Carbon nanotubes as structural nanofibers for hyaluronic acid hydrogel scaffolds. Biomacromolecules 9 (2): 505-509.

Bianco, P., and Robey, P. G. 2001. Stem cells in tissue engineering. Nature 414: 118-121.

Biondi, M., Ungaro, F., Quaglia, F., and Netti, P. A. 2008. Controlled drug delivery in tissue engineering. Advanced Drug Delivery Reviews 60 (2): 229-242.

Bisson, I., Kosinski, M., Ruault, S., Gupta, B., Hilborn, J., Wurm, F., and Frey, P. 2002. Acrylic acid grafting and collagen immobilization on poly(ethylene terephthalate) surfaces for adherence and growth of human bladder smooth muscle cells. Biomaterials 23 (15): 3149-3158.

Boccaccini, A. R., Erol, M., Stark, W. J., Mohn, D., Hong, Z., and Mano, J. F. 2010. Polymer/bioactive glass nanocomposites for biomedical applications. A Review. Composites Science and Technology DOI: 10.1016/j.compscitech.2010.06.002.

Bock, A. K., Ibarreta, D., and Rodriguez-Cerezo, E. 2003. Human tissue-engineered products-Today's market and future prospects. Brussels: European Commission.

Boontheekul, T., and Mooney, D. J. 2003. Protein-based signaling systems in tissue engineering. Current Opinion in Biotechnology 14 (5): 559-565.

Borzacchiello, A., Mayol, L., Ramires, P. A., Pastorello, A., Bartolo, C. D., Ambrosio, L., and Milella, E. 2007. Structural and rheological characterization of hyaluronic acid-based scaffolds for adipose tissue engineering. Biomaterials 28 (30): 4399-4408.

Brandon, V. S., Shahana, S. K., Omar, Z. F., Ali, K., and Nicholas, A. P. 2009. Hydrogels in regenerative medicine. Advanced Materials 21 (32-33): 3307-3329.

Brazel, C. S., and Peppas, N. A. 1999. Mechanisms of solute and drug transport in relaxing, swellable, hydrophilic glassy polymers. Polymer 40 (12): 3383-3398.

Bryant, S. J., Cuy, J. L., Hauch, K. D., and Ratner, B. D. 2007. Photo-patterning of porous hydrogels for tissue engineering. Biomaterials 28 (19): 2978-2986.

Brynda, E., Houska, M., Kysilka, J., Přádný, M., Lesný, P., Jendelová, P., Michálek, J., and Syková, E. 2009. Surface modification of hydrogels based on poly(2-hydroxyethyl methacrylate) with extracellular matrix proteins. Journal of Materials Science: Materials in Medicine 20 (4): 909-915.

Brynda, E., Štol, M., Chytrý, V., and Cífková, I. 1985. The removal of residuals and oligomers from poly(2-hydroxyethylmethacrylate). Journal of Biomedical Materials Research 19 (9): 1169-1179.

Butler, D., L. , Goldstein, S., A. , and Guilak, F. 2000. Functional tissue engineering: The role of biomechanics. Journal of Biomechanical Engineering 122 (6): 570-575.

Cabañas, M. V., Peña, J., Román, J., and Vallet-Regí, M. 2009. Tailoring vancomycin release from β-TCP/agarose scaffolds. European Journal of Pharmaceutical Sciences 37 (3-4): 249-256.

Cao, H., and Kuboyama, N. 2010. A biodegradable porous composite scaffold of PGA/β-TCP for bone tissue engineering. Bone 46 (2): 386-395.

Carbone, R., Marangi, I., Zanardi, A., Giorgetti, L., Chierici, E., Berlanda, G., Podestà, A., Fiorentini, F., Bongiorno, G., Piseri, P., Pelicci, P. G., and

Milani, P. 2006. Biocompatibility of cluster-assembled nanostructured TiO_2 with primary and cancer cells. Biomaterials 27 (17): 3221-3229.

Carone, T. W., and Hasenwinkel, J. M. 2006. Mechanical and morphological characterization of homogeneous and bilayered poly(2-hydroxyethyl methacrylate) scaffolds for use in CNS nerve regeneration. Journal of Biomedical Materials Research Part B: Applied Biomaterials 78B (2): 274-282.

Casadio, Y. S., Brown, D. H., Chirila, T. V., Kraatz, H.-B., and Baker, M. V. 2010. Biodegradation of Poly(2-hydroxyethyl methacrylate) (PHEMA) and Poly{(2-hydroxyethyl methacrylate)-co-[poly(ethylene glycol) methyl ether methacrylate]} Hydrogels Containing Peptide-Based Cross-Linking Agents. Biomacromolecules 11 (11): 2949-2959.

Castro-Concha, L. A., Escobedo, R. M., and Miranda-Ham, M. L. 2006. Measurement of cell viability in in vitro cultures. In Methods in Molecular Biology Plant Cell Culture Protocols, ed. V. M. Loyola-Vargas and F. Vázquez-Flota, 71-76. Humana Press.

Ceballos, D., Navarro, X., Dubey, N., Wendelschafer-Crabb, G., Kennedy, W. R., and Tranquillo, R. T. 1999. Magnetically aligned collagen gel filling a collagen nerve guide improves peripheral nerve regeneration. Experimental Neurology 158 (2): 290-300.

Chalal, M., Ehrburger-Dolle, F., Morfin, I., Vial, J.-C., Aguilar de Armas, M.-R., San Roman, J., Bolgen, N., Piskin, E., Ziane, O., and Casalegno, R. 2009. Imaging the Structure of Macroporous Hydrogels by Two-Photon Fluorescence Microscopy. Macromolecules 42 (7): 2749-2755.

Chen, F.-M., Zhang, M., and Wu, Z.-F. 2010. Toward delivery of multiple growth factors in tissue engineering. Biomaterials 31 (24): 6279-6308.

Chen, Q. Z., Thompson, I. D., and Boccaccini, A. R. 2006. 45S5 Bioglass®-derived glass-ceramic scaffolds for bone tissue engineering. Biomaterials 27 (11): 2414-2425.

Chen, X., Tam, U. C., Czlapinski, J. L., Lee, G. S., Rabuka, D., Zettl, A., and Bertozzi, C. R. 2006. Interfacing carbon nanotubes with living cells. Journal of the American Chemical Society 128 (19): 6292-6293.

Cheung, H.-Y., Lau, K.-T., Lu, T.-P., and Hui, D. 2007. A critical review on polymer-based bio-engineered materials for scaffold development. Composites Part B: Engineering 38 (3): 291-300.

Chin, S. S., Chiang, K., and Fane, A. G. 2006. The stability of polymeric membranes in a TiO_2 photocatalysis process. Journal of Membrane Science 275 (1-2): 202-211.

Chirila, T. V., Chen, Y.-C., Griffin, B. J., and Constable, I. J. 1993. Hydrophilic sponges based on 2-hydroxymethyl methacrylate. I. Effect of monomer mixture composition on the pore size. Polymer International 32 (3): 221-232.

Chirila, T. V., Constable, I. J., Crawford, G. J., Vijayasekaran, S., Thompson, D. E., Chen, Y.-C., Fletcher, W. A., and Griffin, B. J. 1993. Poly(2-hydroxyethyl methacrylate) sponges as implant materials: in vivo and in vitro evaluation of cellular invasion. Biomaterials 14 (1): 26-38.

Chirila, T. V., Hicks, C. R., Dalton, P. D., Vijayasekaran, S., Lou, X., Hong, Y., Clayton, A. B., Ziegelaar, B. W., Fitton, J. H., Platten, S., Crawford, G. J., and Constable, I. J. 1998. Artificial cornea. Progress in Polymer Science 23 (3): 447-473.

Chirila, T. V., Yu, D.-Y., Chen, Y.-C., and Crawford, G. J. 1995. Enhancement of mechanical strength of poly(2-hydroxyethyl methacrylate) sponges. Journal of Biomedical Materials Research 29 (8): 1029-1032.

Chlopek, J., Czajkowska, B., Szaraniec, B., Frackowiak, E., Szostak, K., and Béguin, F. 2006. In vitro studies of carbon nanotubes biocompatibility. Carbon 44 (6): 1106-1111.

Choi, Y. J., Kim, M. S., Kang, H. K., Park, H. S., Noh, I., and Park, K. D. 2008. Evaluation of porous poly(lactide-co-glycolide) scaffold surface-modified by irradiation of nitrogen ion beams. Surface and Coatings Technology 202 (22-23): 5713-5717.

Chung, A. J., and Rubner, M. F. 2002. Methods of Loading and Releasing Low Molecular Weight Cationic Molecules in Weak Polyelectrolyte Multilayer Films. Langmuir 18 (4): 1176-1183.

Chung, C. J., Chiang, C. C., Chen, C. H., Hsiao, C. H., Lin, H. I., Hsieh, P. Y., and He, J. L. 2008. Photocatalytic TiO_2 on copper alloy for antimicrobial purposes. Applied Catalysis B: Environmental 85 (1-2): 103-108.

Chung, H. J., and Park, T. G. 2007. Surface engineered and drug releasing pre-fabricated scaffolds for tissue engineering. Advanced Drug Delivery Reviews 59 (4-5): 249-262.

Ciapetti, G., Granchi, D., Verri, E., Savarino, L., Cavedagna, D., and Pizzoferrato, A. 1996. Application of a combination of neutral red and amido black staining for rapid, reliable cytotoxicity testing of biomaterials. Biomaterials 17 (13): 1259-1264.

Clark, A. H., and Ross-Murphy, S. B. 1987. Structural and mechnical properties of biopolymer gels. Advances in Polymer Science 83: 57.

Clayton, A. B., Chirila, T. V., and Lou, X. 1997. Hydrophilic sponges based on 2-hydroxyethyl methacrylate. V. effect of crosslinking agent reactivity on mechanical properties. Polymer International 44 (2): 201-207.

Correa-Duarte, M. A., Wagner, N., Rojas-Chapana, J., Morsczeck, C., Thie, M., and Giersig, M. 2004. Fabrication and biocompatibility of carbon nanotube-based 3D networks as scaffolds for cell seeding and growth. Nano Letters 4 (11): 2233-2236.

Costa, R., Pereira, M., Lameiras, F., and Vasconcelos, W. 2005. Apatite formation on poly(2-hydroxyethyl methacrylate)-silica hybrids prepared by sol-gel process. Journal of Materials Science: Materials in Medicine 16 (10): 927-932.

Coutu, D. L., Yousefi, A.-M., and Galipeau, J. 2009. Three-dimensional porous scaffolds at the crossroads of tissue engineering and cell-based gene therapy. Journal of Cellular Biochemistry 108 (3): 537-546.

Crawford, G. J., Hicks, C. R., Lou, X., Vijayasekaran, S., Tan, D., Mulholland, B., Chirila, T. V., and Constable, I. J. 2002. The Chirila Keratoprosthesis: phase I human clinical trial. Ophthalmology 109 (5): 883-889.

Cui, D., Tian, F., Ozkan, C. S., Wang, M., and Gao, H. 2005. Effect of single wall carbon nanotubes on human HEK293 cells. Toxicology Letters 155 (1): 73-85.

Cui, H.-F., Vashist, S. K., Al-Rubeaan, K., Luong, J. H. T., and Sheu, F.-S. 2010. Interfacing carbon nanotubes with living mammalian cells and cytotoxicity issues. Chemical Research in Toxicology.

Curtis, A. 2004. Tutorial on the biology of nanotopography. NanoBioscience, IEEE Transactions on 3 (4): 293-295.

Dado, D., and Levenberg, S. 2009. Cell-scaffold mechanical interplay within engineered tissue. Seminars in Cell & Developmental Biology 20 (6): 656-664.

Dames, J. E., Causton, B., Bovell, Y., Davy, K., and Sturt, C. S. 1986. The migration of osteoblasts over substrata of discrete surface charge. Biomaterials 7 (3): 231-233.

Dang, J. M., and Leong, K. W. 2006. Natural polymers for gene delivery and tissue engineering. Advanced Drug Delivery Reviews 58 (4): 487-499.

Davis, M. W., and Vacanti, J. P. 1996. Toward development of an implantable tissue engineered liver. Biomaterials 17: 365-372.

Day, R. M., Boccaccini, A. R., Shurey, S., Roether, J. A., Forbes, A., Hench, L. L., and Gabe, S. M. 2004. Assessment of polyglycolic acid mesh and bioactive glass for soft-tissue engineering scaffolds. Biomaterials 25 (27): 5857-5866.

De La Torre, P. M., Torrado, S., and Torrado, S. 2003. Interpolymer complexes of poly(acrylic acid) and chitosan: influence of the ionic hydrogel-forming medium. Biomaterials 24 (8): 1459-1468.

Dekker, R. J., de Bruijn, J. D., Stigter, M., Barrere, F., Layrolle, P., and van Blitterswijk, C. A. 2005. Bone tissue engineering on amorphous carbonated apatite and crystalline octacalcium phosphate-coated titanium discs. Biomaterials 26 (25): 5231-5239.

DePhillips, P., and Lenhoff, A. M. 2000. Pore size distributions of cation-exchange adsorbents determined by inverse size-exclusion chromatography. Journal of Chromatography A 883 (1-2): 39-54.

Drury, J. L., and Mooney, D. J. 2003. Hydrogels for tissue engineering: scaffold design variables and applications. Biomaterials 24 (24): 4337-4351.

Ducheyne, P., and Qiu, Q. 1999. Bioactive ceramics: the effect of surface reactivity on bone formation and bone cell function. Biomaterials 20 (23-24): 2287-2303.

Dumortier, H., Lacotte, S., Pastorin, G., Marega, R., Wu, W., Bonifazi, D., Briand, J.-P., Prato, M., Muller, S., and Bianco, A. 2006. Functionalized carbon nanotubes are non-cytotoxic and preserve the functionality of primary immune cells. Nano Letters 6 (7): 1522-1528.

Dusek, K. I. i. b. c. i. t. c. o. c. c., in Polymer Networks: Structure and Mechanical Properties. Edited by E. A. J. C. S. Newman. New York: Plenum Press. 1971. Inhomogeneities induced by crosslinking in the course of crosslinking copolymerization. In Polymer Networks: Structure and Mechanical Properties, ed. A. J. Chompff and S. Newman, 245-260. New York: Plenum Press.

Dziubla, T. D., Torjman, M. C., Joseph, J. I., Murphy-Tatum, M., and Lowman, A. M. 2001. Evaluation of porous networks of poly(2-hydroxyethyl methacrylate) as interfacial drug delivery devices. Biomaterials 22 (21): 2893-2899.

Ei-Arini, S. K., and Leuenberger, H. 1995. Modelling of drug release from polymer matrices: Effect of drug loading. International Journal of Pharmaceutics 121 (2): 141-148.

Engler, A. J., Griffin, M. A., Sen, S., Bonnemann, C. G., Sweeney, H. L., and Discher, D. E. 2004. Myotubes differentiate optimally on substrates with tissue-like stiffness: pathological implications for soft or stiff microenvironments. The Journal of Cell Biology 166 (6): 877-887.

Engler, A. J., Sen, S., Sweeney, H. L., and Discher, D. E. 2006. Matrix elasticity directs stem cell lineage specification. Cell 126 (4): 677-689.

Ennett, A. B., Kaigler, D., and Mooney, D. J. 2006. Temporally regulated delivery of VEGF in vitro and in vivo. Journal of Biomedical Materials Research Part A 79A (1): 176-184.

Eun, J. K., Kang, I.-K., Moon, K. J., and Yong, B. P. 1998. Preparation of insulin-immobilized polyurethanes and their interaction with human fibroblasts. Biomaterials 19 (1-3): 239-249.

Falk, B., Garramone, S., and Shivkumar, S. 2004. Diffusion coefficient of paracetamol in a chitosan hydrogel. Materials Letters 58 (26): 3261-3265.

Ferrari, M., Fornasiero, M. C., and Isetta, A. M. 1990. MTT colorimetric assay for testing macrophage cytotoxic activity in vitro. Journal of Immunological Methods 131 (2): 165-172.

Firkowska, I., Olek, M., Pazos-Peréz, N., Rojas-Chapana, J., and Giersig, M. 2006. Highly ordered MWNT-based matrixes: Topography at the nanoscale conceived for tissue engineering. Langmuir 22 (12): 5427-5434.

Firme Iii, C. P., and Bandaru, P. R. 2010. Toxicity issues in the application of carbon nanotubes to biological systems. Nanomedicine: Nanotechnology, Biology and Medicine 6 (2): 245-256.

Flahaut, E., Durrieu, M. C., Remy-Zolghadri, M., Bareille, R., and Baquey, C. 2006. Investigation of the cytotoxicity of CCVD carbon nanotubes towards human umbilical vein endothelial cells. Carbon 44 (6): 1093-1099.

Flynn, L., Dalton, P. D., and Shoichet, M. S. 2003. Fiber templating of poly(2-hydroxyethyl methacrylate) for neural tissue engineering. Biomaterials 24 (23): 4265-4272.

Fong, P., Shin' oka, T., Lopez-Soler, R. I., and Breuer, C. 2006. The use of polymer based scaffolds in tissue-engineered heart valves. Progress in Pediatric Cardiology 21: 193-199.

Francis, L., Meng, D., Knowles, J. C., Roy, I., and Boccaccini, A. R. 2010. Multi-functional P(3HB) microsphere/45S5 Bioglass®-based composite scaffolds for bone tissue engineering. Acta Biomaterialia 6 (7): 2773-2786.

Francis Suh, J. K., and Matthew, H. W. T. 2000. Application of chitosan-based polysaccharide biomaterials in cartilage tissue engineering: a review. Biomaterials 21 (24): 2589-2598.

Frosch, K. H., Sondergeld, I., Dresing, K., Rudy, T., Lohmann, C. H., Rabba, J., Schild, D., Breme, J., and Stuermer, K. M. 2003. Autologous osteoblasts enhance osseointegration of porous titanium implants. Journal of Orthopaedic Research 21 (2): 213-223.

Fu, Y., and Kao, W. J. 2010. Drug release kinetics and transport mechanisms of non-degradable and degradable polymeric delivery systems. Expert Opinion on Drug Delivery 7 (4): 429-444.

Fuchs, E., and Segre, J. A. 2000. Stem cells: A new lease on life. Cell 100 (1): 143-155.

Gan, T., Zhang, Y., and Guan, Y. 2009. In situ gelation of P(NIPAM-HEMA) microgel dispersion and Its applications as injectable 3D cell scaffold. Biomacromolecules 10 (6): 1410-1415.

Gayet, J. C., and Fortier, G. 1996. High water content BSA-PEG hydrogel for controlled release device: Evaluation of the drug release properties. Journal of Controlled Release 38 (2-3): 177-184.

Gelse, K., Pöschl, E., and Aigner, T. 2003. Collagens--structure, function, and biosynthesis. Advanced Drug Delivery Reviews 55 (12): 1531-1546.

George, J. H. 2009. Engineering of fibrous scaffolds for use in regenerative medicine, Department of Materials, Imperial College London, London

Gerhardt, L. C., Jell, G., and Boccaccini, A. 2007. Titanium dioxide (TiO_2) nanoparticles filled poly($_{D,L}$ lactid acid) (PDLLA) matrix composites for bone tissue engineering. Journal of Materials Science: Materials in Medicine 18 (7): 1287-1298.

Ghosh, K., and Ingber, D. E. 2007. Micromechanical control of cell and tissue development: Implications for tissue engineering. Advanced Drug Delivery Reviews 59 (13): 1306-1318.

Gouda, J. H., Povodator, K., Warren, T. C., and Prins, W. 1970. Evidence for a micro-mesomorphic structure in poly (2-hydroxyethyl methacrylate) hydrogels. Journal of Polymer Science Part B: Polymer Letters 8 (4): 225-229.

Griffith, L. G., and Naughton, G. 2002. Tissue engineering--current challenges and expanding opportunities. Science 295 (5557): 1009-1014.

Gurdon, J. B., and Bourillot, P. Y. 2001. Morphogen gradient interpretation. Nature 413 (6858): 797-803.

Guyot, A., and Bartholin, M. 1982. Design and properties of polymers as materials for fine chemistry. Progress in Polymer Science 8 (3): 277-331.

Haldon, R. A., and Lee, B. E. 1972. Structure and permeability of porous films of poly(hydroxy ethyl methacrylate). British Polymer Journal 4 (6): 491-501.

Hallab, N. J., Bundy, K. J., O'Connor, K., Moses, R. L., and Jacobs, J. J. 2001. Evaluation of metallic and polymeric biomaterial surface energy and surface roughness characteristics for directed cell adhesion. Tissue Engineering 7 (1): 55-71.

Han, X. 2006. Electron Microscope Observation of Collagen fibers. http://www.optics.rochester.edu/workgroups/cml/opt307/spr06/xiaoxing/Xiaoxing.html (accessed 14 June, 2010).

Harrison, B. S., and Atala, A. 2007. Carbon nanotube applications for tissue engineering. Biomaterials 28 (2): 344-353.

Hasa, J., and Janáček, J. 1967. Effect of diluent content during polymerization on equilibrium deformational behavior and structural parameters of polymer network. Journal of Polymer Science Part C: Polymer Symposia 16 (1): 317-328.

Heath, C. A. 2000. Cells for tissue engineering. Trends in Biotechnology 18 (1): 17-19.

Heinemann, C., Heinemann, S., Bernhardt, A., Worch, H., and Hanke, T. 2008. Novel textile chitosan scaffolds promote spreading, proliferation, and differentiation of osteoblasts. Biomacromolecules 9 (10): 2913-2920.

Hejcl, A., Urdzikova, L., Sedy, J., Lesny, P., Pradny, M., Michalek, J., Burian, M., Hajek, M., Zamecnik, J., Jendelova, P., and Sykova, E. 2008. Acute and delayed implantation of positively charged 2-hydroxyethyl methacrylate scaffolds in spinal cord injury in the rat. Journal of Neurosurgery: Spine 8 (1): 67-73.

Hench, L. L. 1991. Bioceramics: from concept to clinic. Journal of the American Ceramic Society 74 (7): 1487-1510.

Hench, L. L. 1997. Sol-gel materials for bioceramic applications. Current Opinion in Solid State and Materials Science 2 (5): 604-610.

Hersel, U., Dahmen, C., and Kessler, H. 2003. RGD modified polymers: biomaterials for stimulated cell adhesion and beyond. Biomaterials 24 (24): 4385-4415.

Hicks, C., Clayton, A., Chirila, T., Crawford, G., Constable, I., and Fitton, J. 2002. Ocular socket prosthesis AU US 6346121B1, filed Aug. 14 1997, and issued Feb. 12 2002.

Hicks, C. R., Fitton, J. H., Chirila, T. V., Crawford, G. J., and Constable, I. J. 1997. Keratoprostheses: Advancing toward a true artificial cornea. Survey of Ophthalmology 42 (2): 175-189.

Hicks, C. R., Morris, I. T., Vijayasekaran, S., Fallon, M. J., McAllister, J., Clayton, A. B., Chirila, T. V., Crawford, G. J., and Constable, I. J. 1999. Correlation of histological findings with gadolinium enhanced MRI scans during healing of a PHEMA orbital implant in rabbits. British Journal of Ophthalmology 83 (5): 616-621.

Hicks, C. R., Morrison, D., Lou, X., Crawford, G. J., Gadjatsy, A., and Constable, I. J. 2006. Orbital implants: potential new directions. Expert Review of Medical Devices 3 (6): 805-815.

Holy, C. E., Cheng, C., Davies, J. E., and Shoichet, M. S. 2001. Optimizing the sterilization of PLGA scaffolds for use in tissue engineering. Biomaterials 22 (1): 25-31.

Hong, K., Jeon, Y.-S., Chung, D., and Kim, J.-H. 2010. Drug release characteristics of modified PHEMA hydrogel containing thermo-responsive pluronic copolymer. Macromolecular Research 18 (2): 204-207.

Horák, D., Lednick, F., and Bleha, M. 1996. Effect of inert components on the porous structure of 2-hydroxyethyl methacrylate-ethylene dimethacrylate copolymers. Polymer 37 (19): 4243-4249.

Hsu, S.-h., Whu, S. W., Hsieh, S.-C., Tsai, C.-L., Chen, D. C., and Tan, T.-S. 2004. Evaluation of Chitosan-alginate-hyaluronate Complexes Modified by an RGD-containing Protein as Tissue-engineering Scaffolds for Cartilage Regeneration. Artificial Organs 28 (8): 693-703.

Huang, S.-L., Chin, W.-K., and Yang, W. P. 2004. Viscosity, particle size distribution, and structural investigation of tetramethyloxysilane/2-hydroxyethyl methacrylate sols during the sol–gel process with acid and base catalysts. Journal of Polymer Science Part B: Polymer Physics 42 (18): 3476-3486.

Huang, S.-L., Chin, W.-K., and Yang, W. P. 2005. Structural characteristics and properties of silica/poly(2-hydroxyethyl methacrylate) (PHEMA) nanocomposites prepared by mixing colloidal silica or tetraethyloxysilane (TEOS) with PHEMA. Polymer 46 (6): 1865-1877.

Hutmacher, D. W. 2000. Scaffolds in tissue engineering bone and cartilage. Biomaterials 21 (24): 2529-2543.

Hutmacher, D. W. 2006. Functional bone tissue engineering. Journal of Biomechanics 39 (Supplement 1): S215-S215.

Ignatius, A. A., and Claes, L. E. 1996. In vitro biocompatibility of bioresorbable polymers: poly(, -lactide) and poly(-lactide-co-glycolide). Biomaterials 17 (8): 831-839.

Jacob, J. T., Rochefort, J. R., Bi, J., and Gebhardt, B. M. 2005. Corneal epithelial cell growth over tethered-protein/peptide surface-modified hydrogels. Journal of Biomedical Materials Research 72B (1): 198-205.

Jansen, E. J. P., Sladek, R. E. J., Bahar, H., Yaffe, A., Gijbels, M. J., Kuijer, R., Bulstra, S. K., Guldemond, N. A., Binderman, I., and Koole, L. H. 2005.

Hydrophobicity as a design criterion for polymer scaffolds in bone tissue engineering. Biomaterials 26 (21): 4423-4431.

Järveläinen, H., Sainio, A., Koulu, M., Wight, T. N., and Penttinen, R. 2009. Extracellular matrix molecules: Potential targets in pharmacotherapy. Pharmacological Reviews 61 (2): 198-223.

Jen, A. C., Wake, M. C., and Mikos, A. G. 1996. Review: Hydrogels for cell immobilization. Biotechnology and Bioengineering 50 (4): 357-364.

Ji, X.-L., Jiang, S.-C., Qiu, X.-P., Dong, D.-W., Yu, D.-H., and Jiang, B.-Z. 2003. Structure and properties of hybrid poly(2-hydroxyethyl methacrylate)/SiO2 monoliths. Journal of Applied Polymer Science 88 (14): 3168-3175.

Jia, G., Wang, H., Yan, L., Wang, X., Pei, R., Yan, T., Zhao, Y., and Guo, X. 2005. Cytotoxicity of carbon nanomaterials: Single-wall nanotube, multi-wall nanotube, and fullerene. Environmental Science & Technology 39 (5): 1378-1383.

Jones, J. R., Ehrenfried, L. M., and Hench, L. L. 2006. Optimising bioactive glass scaffolds for bone tissue engineering. Biomaterials 27 (7): 964-973.

Jones, J. R., Tsigkou, O., Coates, E. E., Stevens, M. M., Polak, J. M., and Hench, L. L. 2007. Extracellular matrix formation and mineralization on a phosphate-free porous bioactive glass scaffold using primary human osteoblast (HOB) cells. Biomaterials 28 (9): 1653-1663.

Karageorgiou, V., and Kaplan, D. 2005. Porosity of 3D biomaterial scaffolds and osteogenesis. Biomaterials 26: 5474-5491.

Karlsson, K. H., Fröberg, K., and Ringbom, T. 1989. A structural approach to bone adhering of bioactive glasses. Journal of Non-Crystalline Solids 112 (1-3): 69-72.

Kim, B.-S., and Mooney, D. J. 1998. Development of biocompatible synthetic extracellular matrices for tissue engineering. Trends in Biotechnology 16 (5): 224-230.

Kim, C.-J. 1998. Effects of Drug Solubility, Drug Loading, and Polymer Molecular Weight on Drug Release from Polyox® Tablets. Drug Development and Industrial Pharmacy 24 (7): 645-651.

Kim, S.-S., Sun Park, M., Jeon, O., Yong Choi, C., and Kim, B.-S. 2006. Poly(lactide-co-glycolide)/hydroxyapatite composite scaffolds for bone tissue engineering. Biomaterials 27 (8): 1399-1409.

Kishen, A., George, S., and Kumar, R. 2006. Enterococcus faecalis-mediated biomineralized biofilm formation on root canal dentine in vitro. Journal of Biomedical Materials Research Part A 77A (2): 406-415.

Kofron, M. D., Opsitnick, N. C., Attawia, M. A., and Laurencin, C. T. 2003. Cryopreservation of tissue engineered constructs for bone. Journal of Orthopaedic Research 21 (6): 1005-1010.

Kommireddy, D. S., Patel, A. A., Shutava, T. G., Mills, D. K., and Lvov, Y. M. 2005. Layer-by-Layer assembly of TiO_2 nanoparticles for stable hydrophilic biocompatible coatings. Journal of Nanoscience and Nanotechnology 5: 1081-1087.

Kommireddy, D. S., Sriram, S. M., Lvov, Y. M., and Mills, D. K. 2006. Stem cell attachment to layer-by-layer assembled TiO_2 nanoparticle thin films. Biomaterials 27 (24): 4296-4303.

Kopeek, J., and Yang, J. 2007. Hydrogels as smart biomaterials. Polymer International 56 (9): 1078-1098.

Kose, G. T., Korkusuz, F., Korkusuz, P., Purali, N., Ozkul, A., and Hasirci, V. 2003. Bone generation on PHBV matrices: an in vitro study. Biomaterials 24 (27): 4999-5007.

Kost, J., and Langer, R. 2001. Responsive polymeric delivery systems. Advanced Drug Delivery Reviews 46 (1-3): 125-148.

Krauch, C. H., and Sanner, A. 1968. Polymerisation auf kristalliner Matrix. Naturwissenschaften 55 (11): 539-540.

Kroupová, J., Horák, D., Pacherník, J., Dvořák, P., and Šlouf, M. 2006. Functional polymer hydrogels for embryonic stem cell support. Journal of Biomedical Materials Research Part B: Applied Biomaterials 76B (2): 315-325.

Kubinová, S., Horák, D., Kozubenko, N., Vanecek, V., Proks, V., Price, J., Cocks, G., and Syková, E. 2010. The use of superporous Ac-CGGASIKVAVS-OH-modified PHEMA scaffolds to promote cell adhesion and the differentiation of human fetal neural precursors. Biomaterials 31 (23): 5966-5975.

Kubinová, S., Horák, D., and Syková, E. 2009. Cholesterol-modified superporous poly(2-hydroxyethyl methacrylate) scaffolds for tissue engineering. Biomaterials 30 (27): 4601-4609.

Kuhl, P. R., and Griffith-Cima, L. G. 1996. Tethered epidermal growth factor as a paradigm for growth factor-induced stimulation from the solid phase. Nature Medicine 2 (9): 1022-1027.

Kwok, C. S., Mourad, P. D., Crum, L. A., and Ratner, B. D. 2001. Self-assembled molecular structures as ultrasonically-responsive barrier membranes for pulsatile drug delivery. Journal of Biomedical Materials Research 57 (2): 151-164.

LaNasa, S. M., Hoffecker, I. T., and Bryant, S. J. 2011. Presence of pores and hydrogel composition influence tensile properties of scaffolds fabricated from well-defined sphere templates. Journal of Biomedical Materials Research Part B: Applied Biomaterials 96B (2): 294-302.

Langer, R., and Vacanti, J. P. 1993. Tissue engineering. Science 260: 920-926.

Laurencin, C. T., Ambrosio, A. M. A., Borden, M. D., and Cooper, J. A. 1999. Tissue engineering: Orthopedic applications. Annual Review of Biomedical Engineering 1: 19-46.

Lee, C. H., Singla, A., and Lee, Y. 2001. Biomedical applications of collagen. International Journal of Pharmaceutics 221 (1-2): 1-22.

Lee, J. S., Bae, J. W., Joung, Y. K., Lee, S. J., Han, D. K., and Park, K. D. 2008. Controlled dual release of basic fibroblast growth factor and indomethacin from heparin-conjugated polymeric micelle. International Journal of Pharmaceutics 346 (1-2): 57-63.

Lee, K. Y., and Mooney, D. J. 2001. Hydrogels for tissue engineering. Chemical Reviews 101 (7): 1869-1880.

Lee, K. Y., Peters, M. C., Anderson, K. W., and Mooney, D. J. 2000. Controlled growth factor release from synthetic extracellular matrices. Nature 408 (6815): 998-1000.

Lee, K. Y., Peters, M. C., and Mooney, D. J. 2001. Controlled drug delivery from polymers by mechanical signals. Advanced Materials 13 (11): 837-839.

Lee, S. J., Lim, G. J., Lee, J.-W., Atala, A., and Yoo, J. J. 2006. In vitro evaluation of a poly(lactide-co-glycolide)-collagen composite scaffold for bone regeneration. Biomaterials 27 (18): 3466-3472.

Lee, W.-F., and Lin, W.-J. 2002. Preparation and Gel Properties of Poly[hydroxyethylmethacrylate-co-poly(ethylene glycol) methacrylate]

Copolymeric Hydrogels by Photopolymerization. Journal of Polymer Research 9 (1): 23-29.

Li, C., Zheng, Y.-F., and Lou, X. 2009. Calcification capacity of porous pHEMA–TiO_2 composite hydrogels. Journal of Materials Science: Materials in Medicine 20 (11): 2215-2222.

Li, P., Ohtsuki, C., Kokubo, T., Nakanishi, K., Soga, N., and de Groot, K. 1994. The role of hydrated silica, titania, and alumina in inducing apatite on implants. Journal of Biomedical Materials Research 28 (1): 7-15.

Li, W.-J., Cooper Jr, J. A., Mauck, R. L., and Tuan, R. S. 2006. Fabrication and characterization of six electrospun poly(α-hydroxy ester)-based fibrous scaffolds for tissue engineering applications. Acta Biomaterialia 2 (4): 377-385.

Lichtenfeld, M. 2010. Regenerative medicine: The best ways to play this fast-growing market. http://www.investmentu.com/2010/June/investing-in-regenerative-medicine.html (accessed June 15, 2010).

Lin, C.-L., Chiu, W.-Y., and Lee, C.-F. 2005. Preparation of thermoresponsive core–shell copolymer latex with potential use in drug targeting. Journal of Colloid and Interface Science 290 (2): 397-405.

Linnes, M. P., Ratner, B. D., and Giachelli, C. M. 2007. A fibrinogen-based precision microporous scaffold for tissue engineering. Biomaterials 28 (35): 5298-5306.

Liu, H., Slamovich, E., B. , and Webster, T., J. . 2006. Increased osteoblast functions among nanophase titania/poly(lactide-co-glycolide) composites of the highest nanometer surface roughness. Journal of Biomedical Materials Research Part A 78A (4): 798-807.

Liu, Q., Hedberg, E. L., Liu, Z., Bahulekar, R., Meszlenyi, R. K., and Mikos, A. G. 2000. Preparation of macroporous poly(2-hydroxyethyl methacrylate) hydrogels by enhanced phase separation. Biomaterials 21 (21): 2163-2169.

Liu, X., and Ma, P. X. 2004. Polymeric scaffolds for bone tissue engineering. Annals of Biomedical Engineering 32 (3): 477-486.

Liu, X., and Ma, P. X. 2009. Phase separation, pore structure, and properties of nanofibrous gelatin scaffolds. Biomaterials 30 (25): 4094-4103.

Liu, X., Tao, S., and Ding, C. 2002. Bioactivity of plasma sprayed dicalcium silicate coatings. Biomaterials 23 (3): 963-968.

Lopez-Heredia, M. A., Sohier, J., Gaillard, C., Quillard, S., Dorget, M., and Layrolle, P. 2008. Rapid prototyped porous titanium coated with calcium phosphate as a scaffold for bone tissue engineering. Biomaterials 29 (17): 2608-2615.

Lou, X., Dalton, P. D., and Chirila, T. V. 2000. Hydrophilic sponges based on 2-hydroxyethyl methacrylate Part VII: Modulation of sponge characteristics by changes in reactivity and hydrophilicity of crosslinking agents. Journal of Materials Science: Materials in Medicine 11 (5): 319-325.

Lou, X., Munro, S., and Wang, S. 2004. Drug release characteristics of phase separation pHEMA sponge materials. Biomaterials 25 (20): 5071-5080.

Lou, X., Vijayasekaran, S., Chirila, T. V., Maley, M. A. L., Hicks, C. R., and Constable, I. J. 1999. Synthesis, physical characterization, and biological performance of sequential homointerpenetrating polymer network sponges based on poly(2-hydroxyethyl methacrylate). Journal of Biomedical Materials Research 47 (3): 404-411.

Lou, X., Vijayasekaran, S., Sugiharti, R., and Robertson, T. 2005. Morphological and topographic effects on calcification tendency of pHEMA hydrogels. Biomaterials 26 (29): 5808-5817.

Lou, X., Wang, S., and Tan, S. Y. 2007. Mathematics-aided quantitative analysis of diffusion characteristics of pHEMA sponge hydrogels. Asia-Pacific Journal of Chemical Engineering 2 (6): 609-617.

Lu, S., and Anseth, K. S. 1999. Photopolymerization of multilaminated poly(HEMA) hydrogels for controlled release. Journal of Controlled Release 57 (3): 291-300.

Lutolf, M. P., and Hubbell, J. A. 2005. Synthetic biomaterials as instructive extracellular microenvironments for morphogenesis in tissue engineering. Nature Biotechnology 23 (1): 47-55.

Ma, D., Tu, K., and Zhang, L.-M. 2010. Bioactive Supramolecular Hydrogel with Controlled Dual Drug Release Characteristics. Biomacromolecules 11 (9): 2204-2212.

Ma, P. X. 2004. Scaffolds for tissue engineering. Materials Today: 30-40.

Ma, P. X., and Zhang, R. 1999. Synthetic nano-scale fibrous extracellular matrix. Journal of Biomedical Materials Research 46 (1): 60-72.

Ma, Z., Gao, C., Gong, Y., Ji, J., and Shen, J. 2002. Immobilization of natural macromolecules on poly-L-lactic acid membrane surface in order to improve its cytocompatibility. Journal of Biomedical Materials Research 63 (6): 838-847.

Ma, Z., Gao, C., Gong, Y., and Shen, J. 2005. Cartilage tissue engineering PLLA scaffold with surface immobilized collagen and basic fibroblast growth factor. Biomaterials 26 (11): 1253-1259.

MacDonald, R. A., Laurenzi, B. F., Viswanathan, G., Ajayan, P. M., and Stegemann, J. P. 2005. Collagen-carbon nanotube composite materials as scaffolds in tissue engineering. Journal of Biomedical Materials Research Part A 74A (3): 489-496.

Macosko, C. W. 1994. Rheology: Principles, Measurements, and Applications (Advances in Interfacial Engineering) New York: Wiley-VCH.

Madhumathi, K., Sudheesh Kumar, P. T., Kavya, K. C., Furuike, T., Tamura, H., Nair, S. V., and Jayakumar, R. 2009. Novel chitin/nanosilica composite scaffolds for bone tissue engineering applications. International Journal of Biological Macromolecules 45 (3): 289-292.

Mahoney, M. J., and Saltzman, W. M. 1996. Controlled release of proteins to tissue transplants for the treatment of neurodegenerative disorders. Journal of Pharmaceutical Sciences 85 (12): 1276-1281.

Malafaya, P. B., Silva, G. A., Baran, E. T., and Reis, R. L. 2002. Drug delivery therapies II.: Strategies for delivering bone regenerating factors. Current Opinion in Solid State and Materials Science 6 (4): 297-312.

Malafaya, P. B., Silva, G. A., and Reis, R. L. 2007. Natural-origin polymers as carriers and scaffolds for biomolecules and cell delivery in tissue engineering applications. Advanced Drug Delivery Reviews 59 (4-5): 207-233.

Malda, J., Woodfield, T. B. F., van der Vloodt, F., Kooy, F. K., Martens, D. E., Tramper, J., Blitterswijk, C. A. v., and Riesle, J. 2004. The effect of PEGT/PBT scaffold architecture on oxygen gradients in tissue engineered cartilaginous constructs. Biomaterials 25 (26): 5773-5780.

Mandal, B. B., and Kundu, S. C. 2009. Calcium alginate beads embedded in silk fibroin as 3D dual drug releasing scaffolds. Biomaterials 30 (28): 5170-5177.

Mann, B. K., Schmedlen, R. H., and West, J. L. 2001. Tethered-TGF-β increases extracellular matrix production of vascular smooth muscle cells. Biomaterials 22: 439-444.

Mano, J. F., Silva, G. A., Azevedo, H. S., Malafaya, P. B., Sousa, R. A., Silva, S. S., Boesel, L. F., Oliveira, J. M., Santos, T. C., Marques, A. P., Neves, N. M., and Reis, R. L. 2007. Natural origin biodegradable systems in tissue engineering and regenerative medicine: present status and some moving trends. Journal of the Royal Society Interface 4 (17): 999-1030.

Martin, C., Winet, H., and Bao, J. Y. 1996. Acidity near eroding polylactide-polyglycolide in vitro and in vivo in rabbit tibial bone chambers. Biomaterials 17 (24): 2373-2380.

Martin, S. M., Ganapathy, R., Kim, T. K., Leach-Scampavia, D., Giachelli, C. M., and Ratner, B. D. 2003. Characterization and analysis of osteopontin-immobilized poly(2-hydroxyethyl methacrylate) surfaces. Journal of Biomedical Materials Research Part A 67A (1): 334-343.

Martys, N. S., Torquato, S., and Bentz, D. P. 1994. Universal scaling of fluid permeability for sphere packings. Physical Review E 50 (1): 403.

Masami, T., Takeshi, Y., Tadashi, K., Masahiko, M., Takeaki, M., Takashi, N., and Takao, Y. 1994. Apatite coating on organic polymers by a biomimetic process. Journal of the American Ceramic Society 77 (11): 2805-2808.

Massia, S. P., and Hubbell, J. A. 1990. Covalently attached GRGD on polymer surfaces promotes biospecific adhesion of mammalian cells. Annals of the New York Academy of Sciences 589 (Biochemical Engineering): 261-270.

Matsusue, Y., Yamamuro, T., Oka, M., Shikinami, Y., Hyon, S.-H., and Ikada, Y. 1992. In vitro and in vivo studies on bioabsorbable ultra-high-strength poly(L-lactide) rods. Journal of Biomedical Materials Research 26 (12): 1553-1567.

Mayer, J., Karamuk, E., Akaike, T., and Wintermantel, E. 2000. Matrices for tissue engineering-scaffold structure for a bioartificial liver support system. Journal of Controlled Release 64: 81-90.

McCarthy, M. J., Soong, D. S., and Edelman, E. R. 1984. Control of drug release from polymer matrices impregnated with magnetic beads - A proposed mechanism and model for enhanced release. Journal of Controlled Release 1 (2): 143-147.

McIntosh, I., Bellus, G., and Jab, E. W. 2000. The pleiotropic effects of fibroblast growth factor receptors in mammalian development. Cell Structure and Function 25 (2): 85-96.

Mikos, A. G., Bao, Y., Cima, L. G., Ingber, D. E., Vacanti, J. P., and Langer, R. 1993. Preparation of poly(glycolic acid) bonded fiber structures for cell attachment and transplantation. Journal of Biomedical Materials Research 27 (2): 183-189.

Minamiguchi, S., Takechi, M., Yuasa, T., Momota, Y., Tatehara, S., Takano, H., Miyamoto, Y., Satomura, K., and Nagayama, M. 2008. Basic research on aw-AC/PLGA composite scaffolds for bone tissue engineering. Journal of Materials Science: Materials in Medicine 19 (3): 1165-1172.

Mitragotri, S., and Lahann, J. 2009. Physical approaches to biomaterial design. Nat Mater 8 (1): 15-23.

Miyazaki, T., Kim, H.-M., Kokubo, T., Ohtsuki, C., Kato, H., and Nakamura, T. 2002. Mechanism of bonelike apatite formation on bioactive tantalum metal in a simulated body fluid. Biomaterials 23 (3): 827-832.

Monteiro-Riviere, N. A., Nemanich, R. J., Inman, A. O., Wang, Y. Y., and Riviere, J. E. 2005. Multi-walled carbon nanotube interactions with human epidermal keratinocytes. Toxicology Letters 155 (3): 377-384.

Moore, M. J., Jabbari, E., Ritman, E. L., Lu, L., Currier, B. L., Windebank, A. J., and Yaszemski, M. J. 2004. Quantitative analysis of interconnectivity of porous biodegradable scaffolds with micro-computed tomography. Journal of Biomedical Materials Research Part A 71A (2): 258-267.

Mor, G. K., Varghese, O. K., Paulose, M., Shankar, K., and Grimes, C. A. 2006. A review on highly ordered, vertically oriented TiO2 nanotube arrays: Fabrication, material properties, and solar energy applications. Solar Energy Materials and Solar Cells 90 (14): 2011-2075.

Mosmann, T. 1983. Rapid colorimetric assay for cellular growth and survival: Application to proliferation and cytotoxicity assays. Journal of Immunological Methods 65 (1-2): 55-63.

Moutos, F. T., Freed, L. E., and Guilak, F. 2007. A biomimetic three-dimensional woven composite scaffold for functional tissue engineering of cartilage. Nature Materials 6 (2): 162-167.

Müller, F. A., Müller, L., Hofmann, I., Greil, P., Wenzel, M. M., and Staudenmaier, R. 2006. Cellulose-based scaffold materials for cartilage tissue engineering. Biomaterials 27: 3955-3963.

Müller, R., Abke, J., Schnell, E., Macionczyk, F., Gbureck, U., Mehrl, R., Ruszczak, Z., Kujat, R., Englert, C., Nerlich, M., and Angele, P. 2005. Surface engineering of stainless steel materials by covalent collagen immobilization to improve implant biocompatibility. Biomaterials 26 (34): 6962-6972.

Müller, R., Abke, J., Schnell, E., Scharnweber, D., Kujat, R., Englert, C., Taheri, D., Nerlich, M., and Angele, P. 2006. Influence of surface pretreatment of titanium- and cobalt-based biomaterials on covalent immobilization of fibrillar collagen. Biomaterials 27 (22): 4059-4068.

Murphy, S. M., Skelly, P. J., and Tighe, B. J. 1992. Synthetic hydrogels: Part 9 - Preparation and characterisation of macroporous hydrophilic matrices. Journal of Materials Chemistry 2 (10): 1007-1013.

Murugan, R., and Ramakrishna, S. 2005. Development of nanocomposites for bone grafting. Composites Science and Technology 65 (15-16): 2385-2406.

Muschler, G. F., Nakamoto, C., and Griffith, L. G. 2004. Engineering principles of clinical cell-based tissue engineering. The Journal of Bone and Joint Surgery 86: 1541-1558.

Myllyharju, J., and Kivirikko, K. I. 2004. Collagens, modifying enzymes and their mutations in humans, flies and worms. Trends in Genetics 20 (1): 33-43.

Nakano, T., Kaibara, K., Tabata, Y., Nagata, N., Enomoto, S., Marukawa, E., and Umakoshi, Y. 2002. Unique alignment and texture of biological apatite crystallites in typical calcified tissues analyzed by microbeam x-ray diffractometer system. Bone 31 (4): 479-487.

Nguyen, V. H., Haldorai, Y., Pham, Q. L., and Shim, J.-J. 2011. Supercritical fluid mediated synthesis of poly(2-hydroxyethyl methacrylate)/Fe3O4 hybrid nanocomposite. Materials Science and Engineering: B 176 (10): 773-778.

Ni, S. Y., Chang, J., and Chou, L. 2006. A novel bioactive porous $CaSiO_3$ scaffold for bone tissue engineering. Journal of Biomedical Materials Research Part A 76A (1): 196-205.

Niall, M., Ryan, G. B., and O'Brien, B. M. 1982. The effect of epidermal growth factor on wound healing in mice. Journal of Surgical Research 33 (2): 164-169.

Nof, M., and Shea, L. D. 2002. Drug-releasing scaffolds fabricated from drug-loaded microspheres. Journal of Biomedical Materials Research 59 (2): 349-356.

Oh, S. H., Kang, S. G., Kim, E. S., Cho, S. H., and Lee, J. H. 2003. Fabrication and characterization of hydrophilic poly(lactic-co-glycolic acid)/poly(vinyl alcohol) blend cell scaffolds by melt-molding particulate-leaching method. Biomaterials 24 (22): 4011-4021.

Okay, O. 2000. Macroporous copolymer networks. Progress in Polymer Science 25 (6): 711-779.

Park, E. J., and Park, K. 2009. Oxidative stress and pro-inflammatory responses induced by silica nanoparticles in vivo and in vitro. Toxicology Letters 184 (1): 18-25.

Park, T. G., and Hoffman, A. S. 1994. Estimation of temperature-dependent pore size in poly(N-isopropylacrylamide) hydrogel beads. Biotechnology Progress 10 (1): 82-86.

Patel, P. N., Smith, C. K., and Patrick, C. W. J. 2005. Rheological and recovery properties of poly(ethylene glycol) diacrylate hydrogels and human adipose tissue. Journal of Biomedical Materials Research Part A 73A (3): 313-319.

Pattison, M. A., Wurster, S., Webster, T. J., and Haberstroh, K. M. 2005. Three-dimensional, nano-structured PLGAscaffolds for bladder tissue replacement applications. Biomaterials 26: 2491-2500.

Peppas, N. A., Bures, P., Leobandung, W., and Ichikawa, H. 2000. Hydrogels in pharmaceutical formulations. European Journal of Pharmaceutics and Biopharmaceutics 50 (1): 27-46.

Peppas, N. A., and Khare, A. R. 1993. Preparation, structure and diffusional behavior of hydrogels in controlled release. Advanced Drug Delivery Reviews 11 (1-2): 1-35.

Peppas, N. A., and Lustig, S. R., eds. 1986. Solute diffusion in hydrophilic network structure. Edited by N. A. Peppas. Vol. I, Hydrogels in Medicine and Pharmacy, Volume I Fundamentals. Boca Raton: CRC Press.

Pereira, M. M., Clark, A. E., and Hench, L. L. 1995. Effect of Texture on the Rate of Hydroxyapatite Formation on Gel-Silica Surface. Journal of the American Ceramic Society 78 (9): 2463-2468.

Perova, T., Vij, J., and Xu, H. 1997. Fourier transform infrared study of poly (2-hydroxyethyl methacrylate) PHEMA. Colloid & Polymer Science 275 (4): 323-332.

Peterson, D. A., Kimura, H., and Schubert, D. 1997. Mechanism of cellular 3-(4,5-Dimethylthiazol-2-yl)-2,5-diphenyltetrazolium bromide (MTT) reduction. Journal of Neurochemistry 69 (2): 581-593.

Phillips, J. E., Gersbach, C. A., and Garcia, A. J. 2007. Virus-based gene therapy strategies for bone regeneration. Biomaterials 28 (2): 211-229.

Pittenger, M. F., Mackay, A. M., Beck, S. C., Jaiswal, R. K., Douglas, R., Mosca, J. D., Moorman, M. A., Simonetti, D. W., Craig, S., and Marshak, D. R. 1999. Multilineage potential of adult human mesenchymal stem cells. Science 284 (5411): 143-147.

Place, E. S., Evans, N. D., and Stevens, M. M. 2009. Complexity in biomaterials for tissue engineering. Nature Materials 8 (6): 457-470.

Place, E. S., George, J. H., Williams, C. K., and Stevens, M. M. 2009. Synthetic polymer scaffolds for tissue engineering. Chemical Society Reviews 38 (4): 1139-1151.

Plant, G. W., Chirila, T. V., and Harvey, A. R. 1998. Implantation of Collagen IV/Poly(2-hydroxyethyl methacrylate) Hydrogels Containing Schwann Cells Into the Lesioned Rat Optic Tract. Cell Transplantation 7 (4): 381-391.

Plant, G. W., Harvey, A. R., and Chirila, T. V. 1995. Axonal growth within poly (2-hydroxyethyl methacrylate) sponges infiltrated with Schwann cells and implanted into the lesioned rat optic tract. Brain Research 671 (1): 119-130.

Plieva, F. M., Galaev, I. Y., and Mattiasson, B. 2007. Macroporous gels prepared at subzero temperatures as novel materials for chromatography of particulate-containing fluids and cell culture applications. Journal of Separation Science 30 (11): 1657-1671.

Plieva, F. M., Karlsson, M., Aguilar, M.-R., Gomez, D., Mikhalovsky, S., and Galaev, I. Y. 2005. Pore structure in supermacroporous polyacrylamide based cryogels. Soft Matter 1 (4): 303-309.

Ponsonnet, L., Reybier, K., Jaffrezic, N., Comte, V., Lagneau, C., Lissac, M., and Martelet, C. 2003. Relationship between surface properties (roughness, wettability) of titanium and titanium alloys and cell behaviour. Materials Science and Engineering: C 23 (4): 551-560.

Puppi, D., Chiellini, F., Piras, A. M., and Chiellini, E. 2010. Polymeric materials for bone and cartilage repair. Progress in Polymer Science 35 (4): 403-440.

Quaglia, F. 2008. Bioinspired tissue engineering: The great promise of protein delivery technologies. International Journal of Pharmaceutics 364 (2): 281-297.

Radin, S. R., and Ducheyne, P. 1992. Plasma spraying induced changes of calcium phosphate ceramic characteristics and the effect on<i>in vitro</i> stability. Journal of Materials Science: Materials in Medicine 3 (1): 33-42.

Ragetly, G., Griffon, D. J., and Chung, Y. S. 2010. The effect of type II collagen coating of chitosan fibrous scaffolds on mesenchymal stem cell adhesion and chondrogenesis. Acta Biomaterialia doi:10.1016/j.actbio.2010.05.016.

Ramakrishna, S., Mayer, J., Wintermantel, E., and Leong, K. W. 2001. Biomedical applications of polymer-composite materials: a review. Composites Science and Technology 61 (9): 1189-1224.

Ranella, A., Barberoglou, M., Bakogianni, S., Fotakis, C., and Stratakis, E. 2010. Tuning cell adhesion by controlling the roughness and wettability of 3D micro/nano silicon structures. Acta Biomaterialia 6 (7): 2711-2720.

Ratner, B. D., Hoffman, A. S., Schoen, F. J., and Lemons, J. E. 2004. Biomaterials science, second edition: An introduction to materials in medicine. 2 edition ed. San Diego, CA: Academic Press.

Rezwan, K., Chen, Q. Z., Blaker, J. J., and Boccaccini, A. R. 2006. Biodegradable and bioactive porous polymer/inorganic composite scaffolds for bone tissue engineering. Biomaterials 27 (18): 3413-3431.

Rich, J., Jaakkola, T., Tirri, T., Närhi, T., Yli-Urpo, A., and Seppälä, J. 2002. In vitro evaluation of poly(ε-caprolactone-co-DL-lactide)/bioactive glass composites Biomaterials 23 (10): 2143-2150.

Ritger, P. L., and Peppas, N. A. 1987. A simple equation for description of solute release I. Fickian and non-fickian release from non-swellable devices in the form of slabs, spheres, cylinders or discs. Journal of Controlled Release 5 (1): 23-36.

Rosenberg, M., Bartl, P., and Leško, J. 1960. Water-soluble methacrylate as an embedding medium for the preparation of ultrathin sections. Journal of Ultrasructure Research 4 (3-4): 298-303.

Salvay, D. M., and Shea, L. D. 2006. Inductive tissue engineering with protein and DNA-releasing scaffolds. Molecular BioSystems 2 (1): 36-48.

Sarkar, S., Lee, G., Y. , Wong, J., Y. , and Desai, T., A. . 2006. Development and characterization of a porous micro-patterned scaffold for vascular tissue engineering applications. Biomaterials 27: 4775-4782.

Savaiano, J. K., and Webster, T. J. 2004. Altered responses of chondrocytes to nanophase PLGA/nanophase titania composites. Biomaterials 25 (7-8): 1205-1213.

Savina, I. N., Cnudde, V., D'Hollander, S., Van Hoorebeke, L., Mattiasson, B., Galaev, I. Y., and Du Prez, F. 2007. Cryogels from poly(2-hydroxyethyl methacrylate): macroporous, interconnected materials with potential as cell scaffolds. Soft Matter 3 (9): 1176-1184.

Savina, I. N., Gun'ko, V. M., Turov, V. V., Dainiak, M., Phillips, G. J., Galaev, I. Y., and Mikhalovsky, S. V. 2011. Porous structure and water state in cross-linked polymer and protein cryo-hydrogels. Soft Matter 7 (9): 4276-4283.

Sayil, C., and Okay, O. 2001. Macroporous poly(N-isopropyl)acrylamide networks: formation conditions. Polymer 42 (18): 7639-7652.

Seidl, J., Malinsky, J., Dusek, K., and Heitz, W. 1967. Macroporose styrol-divinylbenzol copolymere und ihre anwendung in der chromatographie und zur darstellung von ionenaustauschern. Advanced polymer science 5: 113-213.

Shelton, R. M., Rasmussen, A. C., and Davies, J. E. 1988. Protein adsorption at the interface between charged polymer substrata and migrating osteoblasts. Biomaterials 9 (1): 24-29.

Shi, J., Wang, L., Zhang, F., Li, H., Lei, L., Liu, L., and Chen, Y. 2010. Incorporating protein gradient into electrospun nanofibers as scaffolds for tissue engineering. ACS Applied Materials & Interfaces 2 (4): 1025-1030.

Shi, Q. H., Wang, J. F., Zhang, J. P., Fan, J., and Stucky, G. D. 2006. Rapid-Setting, Mesoporous, Bioactive Glass Cements that Induce Accelerated In Vitro Apatite Formation. Advanced Materials 18 (8): 1038-1042.

Shi, X., Wang, Y., Ren, L., Zhao, N., Gong, Y., and Wang, D.-A. 2009. Novel mesoporous silica-based antibiotic releasing scaffold for bone repair. Acta Biomaterialia 5 (5): 1697-1707.

Shvedova, A., Castranova, V., Kisin, E., Schwegler-Berry, D., Murray, A., Gandelsman, V., Maynard, A., and Baron, P. 2003. Exposure to carbon nanotube material: Assessment of nanotube cytotoxicity using human keratinocyte cells. Journal of Toxicology and Environmental Health, Part A: Current Issues 66 (20): 1909 - 1926.

Siepmann, J., and Peppas, N. A. 2001. Modeling of drug release from delivery systems based on hydroxypropyl methylcellulose (HPMC). Advanced Drug Delivery Reviews 48 (2-3): 139-157.

Sill, T. J., and von Recum, H. A. 2008. Electrospinning: Applications in drug delivery and tissue engineering. Biomaterials 29 (13): 1989-2006.

Silva, A. K. A., Richard, C., Bessodes, M., Scherman, D., and Merten, O.-W. 2009. Growth factor delivery approaches in hydrogels. Biomacromolecules 10 (1): 9-18.

Silvestri, B., Luciani, G., Costantini, A., Tescione, F., Branda, F., and Pezzella, A. 2009. In-situ sol-gel synthesis and characterization of bioactive pHEMA/SiO2 blend hybrids. Journal of Biomedical Materials Research Part B: Applied Biomaterials 89B (2): 369-378.

Simon, P., Kasimir, M. T., Rieder, E., and Weigel, G. 2006. Tissue engineering of heart valves—Immunologic and inflammatory challenges of the allograft scaffold. Progress in Pediatric Cardiology 21: 161-165.

Sinha, V. R., and Trehan, A. 2003. Biodegradable microspheres for protein delivery. Journal of Controlled Release 90 (3): 261-280.

Song, J., Malathong, V., and Bertozzi, C. R. 2005. Mineralization of synthetic polymer scaffolds: A bottom-up approach for the development of artificial bone. Journal of the American Chemical Society 127 (10): 3366-3372.

Song, J., Saiz, E., and Bertozzi, C. R. 2003. Preparation of pHEMA-CP composites with high interfacial adhesion via template-driven mineralization. Journal of the European Ceramic Society 23 (15): 2905-2919.

Söntjens, S. H. M., Nettles, D. L., Carnahan, M. A., Setton, L. A., and Grinstaff, M. W. 2005. Biodendrimer-based hydrogel scaffolds for cartilage tissue repair. Biomacromolecules 7 (1): 310-316.

Spiller, K. L., Laurencin, S. J., Charlton, D., Maher, S. A., and Lowman, A. M. 2008. Superporous hydrogels for cartilage repair: Evaluation of the morphological and mechanical properties. Acta Biomaterialia 4 (1): 17-25.

Spoerke, E. D., Murray, N. G., Li, H., Brinson, L. C., Dunand, D. C., and Stupp, S. I. 2005. A bioactive titanium foam scaffold for bone repair. Acta Biomaterialia 1 (5): 523-533.

Stancu, I. C., Layrolle, P., Libouban, H., Filmon, R., Legeay, G., Cincu, C., Baslé, M. F., and Chappard, D. 2007. Preparation of macroporous poly (2-hydroxyethyl) methacrylate with interconnected porosity. JOURNAL OF OPTOELECTRONICS AND ADVANCED MATERIALS 9 (7): 2125-2129.

Stappenbeck, T. S., and Miyoshi, H. 2009. The role of stromal stem cells in tissue regeneration and wound repair. Science 324 (5935): 1666-1669.

Stavrouli, N., Aubry, T., and Tsitsilianis, C. 2008. Rheological properties of ABA telechelic polyelectrolyte and ABA polyampholyte reversible hydrogels: A comparative study. Polymer 49 (5): 1249-1256.

Stevens, M. M., and George, J. H. 2005. Exploring and engineering the cell surface interface. Science 310 (5751): 1135-1138.

Su, Y., Li, X. Q., P., L. S., Mo, X. M., and Seeram, R. 2009. Controlled release of dual drugs from emulsion electrospun nanofibrous mats. Colloids and Surfaces B: Biointerfaces 73 (2): 376-381.

Suh, H., Hwang, Y.-S., Lee, J.-E., Han, C. D., and Park, J.-C. 2001. Behavior of osteoblasts on a type I atelocollagen grafted ozone oxidized poly--lactic acid membrane. Biomaterials 22 (3): 219-230.

Supronowicz, P. R., Ajayan, P. M., Ullmann, K. R., Arulanandam, B. P., Metzger, D. W., and Bizios, R. 2002. Novel current-conducting composite substrates for exposing osteoblasts to alternating current stimulation. Journal of Biomedical Materials Research 59 (3): 499-506.

Tabata, Y. 2000. The importance of drug delivery systems in tissue engineering. Pharmaceutical Science & Technology Today 3: 80-89.

Tabata, Y. 2003. Tissue regeneration based on growth factor release. Tissue Engineering 9 (supplement 1): 5-15.

Takebe, J., Itoh, S., Okada, J., and Ishibashi, K. 2000. Anodic oxidation and hydrothermal treatment of titanium results in a surface that causes increased attachment and altered cytoskeletal morphology of rat bone marrow stromal cells in vitro. Journal of Biomedical Materials Research 51 (3): 398-407.

Tamagawa, H., Popovic, S., and Taya, M. 2000. Pores and diffusion characteristics of porous gels. Polymer 41 (19): 7201-7207.

Tambralli, A., Blakeney, B., Anderson, J., Kushwaha, M., Andukuri, A., Dean, D., and Jun, H.-W. 2009. A hybrid biomimetic scaffold composed of electrospun polycaprolactone nanofibers and self-assembled peptide amphiphile nanofibers. Biofabrication 1 (2): 025001.

Tayalia, P., and Mooney, D. J. 2009. Controlled growth factor delivery for tissue engineering. Advanced Materials 21 (32-33): 3269-3285.

Taylor, M. S., Daniels, A. U., Andriano, K. P., and Heller, J. 1994. Six bioabsorbable polymers: In vitro acute toxicity of accumulated degradation products. Journal of Applied Biomaterials 5 (2): 151-157.

Taylor, P. M., Cass, A. E. G., and Yacoub, M. H. 2006. Extracellular matrix scaffolds for tissue engineering heart valves. Progress in Pediatric Cardiology 21: 219-225.

Temenoff, J. S., Athanasiou, K. A., Lebaron, R. G., and Mikos, A. G. 2002. Effect of poly(ethylene glycol) molecular weight on tensile and swelling properties of oligo(poly(ethylene glycol) fumarate) hydrogels for cartilage tissue engineering. Journal of Biomedical Materials Research 59 (3): 429-437.

Tessmar, J. K., and Göpferich, A. M. 2007. Matrices and scaffolds for protein delivery in tissue engineering. Advanced Drug Delivery Reviews 59 (4-5): 274-291.

Tong, H.-W., and Wang, M. 2011. Electrospinning of poly(hydroxybutyrate-co-hydroxyvalerate) fibrous tissue engineering scaffolds in two different electric fields. Polymer Engineering & Science 51 (7): 1325-1338.

Torres, F. G., Nazhat, S. N., Sheikh Md Fadzullah, S. H., Maquet, V., and Boccaccini, A. R. 2007. Mechanical properties and bioactivity of porous PLGA/TiO_2 nanoparticle-filled composites for tissue engineering scaffolds. Composites Science and Technology 67 (6): 1139-1147.

Valentin, J. E., Freytes, D. O., Grasman, J. M., Pesyna, C., Freund, J., Gilbert, T. W., and Badylak, S. F. 2009. Oxygen diffusivity of biologic and synthetic scaffold materials for tissue engineering. Journal of Biomedical Materials Research Part A 91A (4): 1010-1017.

Vanderhooft, J. L., Alcoutlabi, M., Magda, J. J., and Prestwich, G. D. 2009. Rheological properties of cross-linked hyaluronan-gelatin hydrogels for tissue engineering. Macromolecular Bioscience 9 (1): 20-28.

Vijayasekaran, S., V.Chirila, T., Robertson, T. A., Lou, X., Fitton, J. H., Hicks, C. R., and Constable, I. J. 2000. Calcification of poly(2-hydroxyethyl methacrylate) hydrogel sponges implanted in the rabbit cornea: A 3-month study. Journal of Biomaterials Science, Polymer Edition 11: 599-615.

Viola, J., Lal, B., and Grad, O. 2003. The emergence of tissue engineering as a research field. Cambridge, MA

Wang, S., Mahali, S., McGuiness, A., and Lou, X. 2010. Mathematical models for estimating effective diffusion parameters of spherical drug delivery devices.

Theoretical Chemistry Accounts: Theory, Computation, and Modeling (Theoretica Chimica Acta) 125 (3): 659-669.

Wang, X., Sang, L., Luo, D., and Li, X. 2011. From collagen-chitosan blends to three-dimensional scaffolds: The influences of chitosan on collagen nanofibrillar structure and mechanical property. Colloids and Surfaces B: Biointerfaces 82 (1): 233-240.

Wang, Z., and Chen, Y. 2007. Supramolecular hydrogels hybridized with single-walled carbon nanotubes. Macromolecules 40 (9): 3402-3407.

Warren, T. C., and Prins, W. 1972. Polymer-diluent interaction in cross-linked gels of poly(2-hydroxyethyl methacrylate). Macromolecules 5 (4): 506-512.

Wei, L., Cai, C., Lin, J., and Chen, T. 2009. Dual-drug delivery system based on hydrogel/micelle composites. Biomaterials 30 (13): 2606-2613.

Weinand, C., Pomerantseva, I., Neville, C. M., Gupta, R., Weinberg, E., Madisch, I., Shapiro, F., Abukawa, H., Troulis, M. J., and Vacanti, J. P. 2006. Hydrogel-β-TCP scaffolds and stem cells for tissue engineering bone. Bone 38 (4): 555-563.

Wichterle, O., and Lim, D. 1960. Hydrophilic gels for biological use. Nature 185 (4706): 117-118.

Williams, D. F. 2008. On the mechanisms of biocompatibility. Biomaterials 29 (20): 2941-2953.

Witte, F., Reifenrath, J., Müller, P. P., Crostack, H. A., Nellesen, J., Bach, F. W., Bormann, D., and Rudert, M. 2006. Cartilage repair on magnesium scaffolds used as a subchondral bone replacement. Materialwissenschaft und Werkstofftechnik 37 (6): 504-508.

Wu, P. I., Minisini, S., and Edelman, E. R. 2009. Intramuscular drug transport under mechanical loading: Resonance between tissue function and uptake. Journal of Controlled Release 136 (2): 99-109.

Wu, P. I. K., and Edelman, E. R. 2008. Structural biomechanics modulate intramuscular distribution of locally delivered drugs. Journal of Biomechanics 41 (13): 2884-2891.

Yang, J., Wan, Y., Yang, J., Bei, J., and Wang, S. 2003. Plasma-treated, collagen-anchored polylactone: Its cell affinity evaluation under shear or shear-free conditions. Journal of Biomedical Materials Research Part A 67A (4): 1139-1147.

Yang, S. F., Leong, K. F., Du, Z. H., and Chua, C. K. 2001. The design of scaffolds for use in tissue engineering. Part I. traditional factors. Tissue Engineering 7 (6): 679-689.

Yang, X. B., Roach, H. I., Clarke, N. M. P., Howdle, S. M., Quirk, R., Shakesheff, K. M., and Oreffo, R. O. C. 2001. Human osteoprogenitor growth and differentiation on synthetic biodegradable structures after surface modification. Bone 29 (6): 523-531.

Yannas, I. V. 1992. Tissue regeneration by use of collagen-glycosaminoglycan copolymers. Clinical Materials 9 (3-4): 179-187.

Yao, Y., and Lenhoff, A. M. 2004. Determination of pore size distributions of porous chromatographic adsorbents by inverse size-exclusion chromatography. Journal of Chromatography A 1037 (1-2): 273-282.

Yasuda, H., Gochin, M., and Stone, J. W. 1966. Hydrogels of poly(hydroxyethyl methacrylate) and hydroxyethyl methacrylate - glycerol monomethacry-late copolymers. Journal of Polymer Science Part A-1: Polymer Chemistry 4 (12): 2913-2927.

Yin, L., Fei, L., Cui, F., Tang, C., and Yin, C. 2007. Superporous hydrogels containing poly(acrylic acid-co-acrylamide)/O-carboxymethyl chitosan interpenetrating polymer networks. Biomaterials 28 (6): 1258-1266.

Yokogawa, Y., Paz Reyes, J., Mucalo, M. R., Toriyama, M., Kawamoto, Y., Suzuki, T., Nishizawa, K., Nagata, F., and Kamayama, T. 1997. Growth of calcium phosphate on phosphorylated chitin fibres. Journal of Materials Science: Materials in Medicine 8 (7): 407-412.

Yoshii, S., Oka, M., Shima, M., Taniguchi, A., and Akagi, M. 2002. 30 mm regeneration of rat sciatic nerve along collagen filaments. Brain Research 949 (1-2): 202-208.

Yu, T. T., and Shoichet, M. S. 2005. Guided cell adhesion and outgrowth in peptide-modified channels for neural tissue engineering. Biomaterials 26 (13): 1507-1514.

Zainuddin, Barnard, Z., Keen, I., Hill, D. J. T., Chirila, T. V., and Harkin, D. G. 2008. PHEMA hydrogels modified through the grafting of phosphate groups by ATRP support the attachment and growth of human corneal epithelial cells. Journal of Biomaterials Applications 23 (2): 147-168.

Zainuddin, Hill, D., Whittaker, A., and Chirila, T. 2006. <i>In-vitro</i> study of the spontaneous calcification of PHEMA-based hydrogels in simulated body fluid. Journal of Materials Science: Materials in Medicine 17 (12): 1245-1254.

Zhang, H., Li, C., Guo, J., Zang, L., and Luo, J. 2012. In Situ Synthesis of Poly(methyl methacrylate)/SiO_2 Hybrid Nanocomposites via "Grafting Onto" Strategy Based on UV Irradiation in the Presence of Iron Aqueous Solution. Journal of Nanomaterials 2012.

Zhang, H., Liu, J., Yao, Z., Yang, J., Pan, L., and Chen, Z. 2009. Biomimetic mineralization of electrospun poly(lactic-co-glycolic acid)/multi-walled carbon nanotubes composite scaffolds in vitro. Materials Letters 63 (27): 2313-2316.

Zhang, L. W., Zeng, L., Barron, A. R., and Monteiro-Riviere, N. A. 2007. Biological interactions of functionalized single-wall carbon nanotubes in human epidermal keratinocytes. International Journal of Toxicology 26 (2): 103-113.

Zhao, L., and Chang, J. 2004. Preparation and characterization of macroporous chitosan/wollastonite composite scaffolds for tissue engineering. Journal of Materials Science: Materials in Medicine 15 (5): 625-629.

Zheng, L. Y., Xu, M. X., and Xu, T. X. 2000. TiO_2-x thin films as oxygen sensor. Sensors and Actuators B: Chemical 66 (1-3): 28-30.

Zhu, W. B., Mow, V. C., Koob, T. J., and Eyre, D. R. 1993. Viscoelastic shear properties of articular cartilage and the effects of glycosidase treatments. Journal of Orthopaedic Research 11 (6): 771-781.

Zisch, A. H., Lutolf, M. P., and Hubbell, J. A. 2003. Biopolymeric delivery matrices for angiogenic growth factors. Cardiovascular Pathology 12: 295-310.